2013

Risk-Based Approach for Life-Cycle Assessment and Management of Bridges and Ship Structures

Alberto Deco
Lehigh University

Risk-Based Approach for Life-Cycle Assessment and Management of Bridges and Ship Structures

by

Alberto Decò

Presented to the Graduate and Research Committee
of Lehigh University
in Candidacy for the Degree of
Doctor of Philosophy

in

Structural Engineering

Lehigh University

September 2013

Approved and recommended for acceptance as a dissertation in partial fulfillment of the requirements for the degree of Doctor of Philosophy

_____
Date

_____
Dr. Dan M. Frangopol
Dissertation Advisor
Professor of Civil and
Environmental Engineering
Lehigh University

_____
Acceptance Date

Committee Members:

_____
Dr. John L. Wilson
Committee Chairperson
Professor of Civil and
Environmental Engineering
Lehigh University

_____
Dr. Richard Sause
Member
Professor of Civil and
Environmental Engineering
Lehigh University

_____
Dr. James M. Ricles
Member
Professor of Civil and
Environmental Engineering
Lehigh University

_____
Dr. Joan R. Casas
External Member
Professor of Civil Engineering
UPC-BARCELONATECH

ACKNOWLEDGEMENTS

First of all, I would like to acknowledge my research advisor Prof. Dan M. Frangopol for giving me the great opportunity of studying at Lehigh University and conducting research at the Advanced Technology for Large Structural Systems (ATLSS) Engineering Research Center under his supervision. Prof. Frangopol has continuously supported me both morally and financially throughout my Ph.D. program and has provided me with his precious time, guidance, and assistance. Without his help I would not be in the position of developing and presenting this study.

I would also like to extend my sincere gratitude to all members of my Ph.D. Thesis committee, including Prof. John L. Wilson, who guided my course work as academic advisor and served as Chairperson of my Ph.D. committee, Prof Dan M. Frangopol as supervisor of my research work, Prof. Richard Sause, Prof. James M. Ricles, and Prof. Joan R. Casas.

I gratefully acknowledge the support from the research sponsors, including (a) the National Science Foundation through grant CMS-0639428, (b) the U.S. Federal Highway Administration Cooperative Agreement Award DTFH61-07-H-00040, and (c) the U.S. Office of Naval Research through contracts N-00014-08-0188, and N 00014-12-1- 0023 (Structural Reliability Program, Director Dr. Paul E. Hess III, ONR).

I would also like to sincerely thank the former visiting scholars in the research team of my research advisor, including Dr. Giorgio Barone, Dr. Paolo Bocchini, Dr.

Andrè D. Orcesi, and Dr. Alfred Strauss, former Ph.D. students Dr. Sunyong Kim, Dr. Kihyon Kwon, and Dr. Nader M. Okasha, and current Ph.D. candidates You Dong, Duygu Saydam, Mohamed Soliman, and Benjin Zhu for the constructive discussion and friendship shared over the past five years. Among them, I especially thank Nader M. Okasha for his collaboration at the early stage of my Ph.D. program in developing part of the computational platform used for ship structures, Benjin Zhu for her contribution in some of the computations, and Paolo Bocchini for contributing on the part of my study dealing with resilient structures by providing useful insights and computational assistance. Also, I would like to thank Peter Bryan, the IT Manager of ATLSS, for his genuine help and assistance in providing me with the needed technological support.

Finally and most importantly, I would like to infinitely thank my wife Ilaria Sacchini with whom I am awaiting the arrival of a little baby girl. Ilaria followed me through this difficult life path by providing me with her love, understanding, and patience, and by being such a good model to follow. Special thanks go to my parents Amedeo Decò and Daniela Zanella for their continuous encouragement and for being so close, although so far away from me.

TABLE OF CONTENTS

LIST OF TABLES

LIST OF FIGURES

ABSTRACT

Existing civil and marine structures and infrastructures have to maintain their serviceability and safety under the effects induced by “normal events” and to withstand the effects of “extreme events”. Although the quantification of the performance of a structural system is usually conducted considering only structural aspects, in this study consequences arising from the occurrence of potential disruption of service due to failure/malfunction of structural components are also considered, leading to risk assessment.

Uncertainties are unavoidable in planning, design, and maintenance of structural systems. Advanced probabilistic methods, such as Monte Carlo simulations based on Latin Hypercube sampling, finite element and response surfaces analyses are used in this study in order to account for uncertainties and their propagation over time.

The main focus of this study is to develop a risk-based approach for the life-cycle assessment and management of civil and marine structures with emphasis on single highway bridges, groups of bridges, and ship structures. Risk is assessed for highway bridges under the effects of multiple hazards, including traffic, environmental attacks, scour, and earthquakes, whereas the effects of traffic and earthquake are accounted for groups of bridges. Other performance indicators, including reliability, redundancy, and resilience to disasters, are also investigated. For ship structures, a novel approach is developed for the evaluation of time-variant reliability, redundancy, and risk

accounting for different limit states of the ship hull, potential effects induced by corrosion, and considering different ship operational conditions over time.

Risk is assessed based on reliability analysis by accounting several limit states and quantifying the associated potential monetary losses for a spectrum of consequences, including operating costs and accident costs.

A novel approach for near real-time multi-criteria optimal ship routing, integrating risk and structural health monitoring data is developed considering different damage scenarios and generic operational conditions.

The developed approaches are applied to several structures, including a highway bridge crossing the Wisconsin River in Wausau, WI, a highway bridge carrying a segment of the northbound I-15 crossing the Temescal Wash located close to the city of Corona, CA, a group of existing bridges located north of the San Diego metropolitan area, and a NAVY's Joint High-Speed Sealift.

CHAPTER 1

INTRODUCTION

Background, Objectives and Contributions

1.1 OVERVIEW

During the last century remarkable progress in design and construction of new structures and infrastructures has been achieved. As a consequence, structures have been built in a more economical and challenging way than ever before but, unfortunately, most of these new structures have a much shorter expected lifetime than those previously built. For instance, antique structures such as Egyptian temples and Roman aqueducts, among others, have been withstanding the effects of aging and extreme events, thus surviving over centuries.

Civil infrastructure and marine structural systems are exposed to the effects of the environment and therefore they may be subjected to the decay of their structural performances. Although aging phenomena and degradation processes generally reduce structural safety. Natural hazards and man-made disasters may induce progressive and sudden deterioration of the performance of structures.

For the case of highway bridges, environmental processes along with other natural and man-made hazards are responsible for the occurrence of partial and total collapses. However, in most cases, bridges may slowly deteriorate while in service and their

performance may potentially down-cross critical thresholds. Therefore, in order to evaluate the status of existing highway bridges, every year the Federal Highway Administration (FHWA) provides data summarizing the condition of the bridges for each State and the whole United States (FHWA 2011a) through the National Bridge Inventory (NBI) database. For instance, Table 1.1 summarizes the condition of bridges in the states of New Jersey, New York, Pennsylvania and the whole United States. Generally, every two years the condition of several bridge components is assessed trough an evaluation process that involves condition and appraisal rating. Condition rating quantifies the degree of deterioration or damage of bridge components, whereas appraisal rating estimates relevant features for their effect on the safety and serviceability of the bridge and its approaches (FHWA 2011b). Bridges are defined structurally deficient (SD) when their condition rating and appraisal rating are 4 or less and 2 or less, respectively, for the relevant bridge item categories, including deck, superstructure, substructure, and waterway adequacy (FHWA 2011b). Bridges are defined functionally obsolete (FO) when appraisal rating of other item categories, including deck geometry, underclearances, and approach roadway alignment, among others, is 3 or less (FHWA 2011b). Based on FHWA (2011a), Figure 1.1 shows the condition of the bridges in terms of percentage with respect to the total number of bridges for the states of (a) New Jersey, (b) New York, (c) Pennsylvania, and (d) for the whole United States. It can be noted that for New Jersey and New York the percentage of functionally obsolete bridges is significantly above the whole US average, whereas for Pennsylvania the percentage of both structural deficient and functional obsolete bridges is above the whole US average.

Other developed countries share a similar situation. For instance, in Italy the problem of bridge safety is becoming very important. The majority of Italian highways have been built in the period of the maximum economic expansion during the 1960s and 1970s (Das and Pardi 2001). Therefore, most of these bridges are more than 40 years old. Figure 1.2 shows the bridges per year of construction and material type (reinforced concrete in situ, post-tensioned, pretensioned, steel-composite, and others) managed by 'Autostrade per l'Italia', the Italian major highway company.

Civil structures are not the only ones subjected to these degradation processes. Generally, all types of fixed and movable structures exposed to environmental hazards experience progressive or sudden drops in their structural performance over time. For instance, also marine structures such as ship structures are subjected to several hazards that determine potential loss of safety, such as the weather condition, grounding, fire/explosion, collision, hull damage, machinery (Wang *et al.* 2009, IUMI 2012). Based on the data provided by the International Union of Marine Insurance (IUMI) (2012), Figure 1.3 shows the world fleet statistics for vessels with cargo carrying capacity greater than 500 GT (gross tonnage). Figure 1.3(a) reports the number of incidents to vessels that suffered total loss, serious loss, and their grand total within the period 1995–2011, where incidents are categorized based on specific parameters (e.g. number of death and value of damage to property). Although the total number of incidents increased, the number of vessels that suffered total loss tends to slightly decrease over time due to improved management. For the case of total loss, Figure 1.3(b) shows the frequencies associated with the different loss causes within the period 1997–2011. It is clear that weather condition has the greatest impact. The weather

conditions and hull damage are responsible for more than 40% of the total number of incidents. These two causes are investigated in this study.

Therefore, it is obvious that existing structural systems including single and groups of structures need to be preserved against excessive degradation of their performance over time. In this context, although different structures share different issues, their proper management is crucial in order to avoid critical situations that may result in the loss of serviceability, or even worse, failure/collapse of the whole structure. The decrease in structural performance is generally due to both progressive deterioration processes (e.g. the effects of corrosion on structural members and fatigue phenomena) and the effects of extreme events (e.g. earthquakes, floods, strong winds, fire, and explosions). The main goal of managing authorities and organizations is trying to maintain these structures in good condition, by providing a sufficient degree of reliability with an efficient planning of maintenance, rehabilitation, and retrofit actions.

According to Frangopol (2011), the proper management of structures includes the following four stages:

1. Quantification of structural performance that can be conducted by developing deterministic or probabilistic approaches. The probabilistic approach is to be preferred because it includes the uncertainty deriving from the intrinsic nature of the involved phenomena and from the quality of the used prediction models.
2. Prediction of structural performance by accounting for the potential deterioration effects and/or considering specific events, that can belong to both “normal” and “extreme” situations.

3. Development of optimal strategies through decision making, based on potential investigated outcomes that guarantee that the structure will survive and will be serviceable under certain limits over time.
4. Update the decision making process by integrating the initial prediction with site data through inspections, and/or by using structural health monitoring (SHM) systems able to collect useful observations of selected parameters.

Time-variant structural performance indicators, including reliability, redundancy, condition index, robustness, have been used as the main indicators for decision makers (Frangopol 2011). However, only in the recent years, the assessment of structural safety with respect to common failure modes has been associated with the quantification of the relevant generated consequences. Potential failures or malfunctions of structural elements, or even of whole systems, may cause a large spectrum of consequences that are different in type and magnitude. The proper quantification of their associated economic impact elevates the safety problem to a new level, leading to risk analysis (CIB 2001, Ellingwood 2001, Ellingwood 2005, JCSS 2008). Based on this, the management approach evolves into a risk-informed decision making process.

The assessment and prediction of structural performance is a process fraught with uncertainties associated with structural geometry, material properties, loading effects, and damage processes. Uncertainties are always present; some of them can be reduced by improving the knowledge or the quality of the prediction model (epistemic uncertainties), others cannot be reduced because of the intrinsic nature of the randomness (aleatory uncertainties) (Ang and de Leon 2005). The treatment of such

uncertainties in modeling/predicting the time-dependent performance of single bridges, bridge networks, and ship structures requires the use of probabilistic and statistical techniques.

Life-cycle assessment (LCA) of structures includes the investigation and the evaluation of the impacts that external factors can produce during the structure overall life span. LCA is performed by evaluating key performance indicators, considering design specifications and integrating further information when available. The evaluation of the costs associated with operation activities and maintenance actions needed for the rehabilitation of deficient members/systems represent part of the life-cycle cost (LCC). Nowadays, the optimal allocation of funds for the assessment of maintenance, retrofit, and recovery plans is becoming an aspect of crucial relevance. The current socio-political situation requires that optimal decisions must be made in order to follow a cost-saving-oriented economic policy. When limited funds are allocated, this analysis also implies an investigation considering the consequence of delaying the application of maintenance/recovery actions. Despite some life-cycle management frameworks available in the literature, methods that incorporate risk are very sparse and far from being fully exploited. Therefore, the development of a general risk-informed management framework is required. Moreover, depending on the type of considered hazard, investigating resilience to disaster, which is easily coupled with risk assessment, can improve the decision making process.

The role of inspection and monitoring campaigns is crucial. In fact, through the collection of new data, a better knowledge of the condition of structures can be provided. Structural management teams have the opportunity to take advantage of this

new information by integrating the collected data into the prediction models in order to better assess the condition and the remaining lifetime of structural systems.

1.2 LIFE-CYCLE MANAGEMENT CONCEPTS OF BRIDGES AND SHIP STRUCTURES

Nowadays, life-cycle management of single bridges, groups of bridges within transportation networks, and ship structures has become an issue of critical relevance worldwide. Proper structural management is required in order to maintain structural performance above acceptable levels. Decision frameworks are necessary in order to capture the economic impact generated by potential structural failures or malfunctions. Proper management strategies must be planned in order to reduce structural vulnerability and mitigate negative effects.

Although useful information is obtained by assessing structural performance such as reliability, redundancy, robustness, and condition index, among others, the assessment of structural safety with respect to common failure modes can also be associated with the quantification of the relevant generated consequences. Therefore, risk assessment is necessary for the proper management of structural systems. The occurrence and the effects due to different types of events induced by multiple hazards can be included into risk analysis (Adey, Hajdin and Brühwiler 2003, Akiyama, Frangopol and Matsuzaki 2011, Skjong and Bitner-Gregersen 2002).

1.2.1 BRIDGE STRUCTURES

In life-cycle analysis of highway bridges, performance indicators, such as reliability, redundancy, and condition have been widely accepted and used. Frangopol, Kallen and van Noortwijk (2004) introduced the combined use of reliability index with condition index, while Decò and Frangopol (2010) reported on the correlation between these indices. The assessment and prediction of structural reliability and redundancy are risk-related topics that have been extensively studied over the last decades using time-invariant (Frangopol and Curley 1987, Frangopol and Nakib 1991, Ghosn, Moses and Frangopol 2010) and time-variant (Okasha and Frangopol 2010a) approaches. However, in many studies, the evaluation of the structural performance and the decision making process do not consider social issues emerging from the local economy of the region in which the structure is located. As indicated by Ellingwood (2005) and Frangopol (2011), the inclusion of risk into the management of structures and infrastructures should be seen as crucial for the development of the so-called "risk-informed decision making process". Therefore, risk can be treated as a performance indicator being part of a generic framework. In order to maximize its contribution as a useful performance indicator, it is convenient to combine risk with other structural performance indicators to finally provide the decision maker with an enhanced decision space. Qualitative risk assessment, including single or multiple hazards, is a topic previously investigated (Blockley 1999, Bea 2001, Adey, Hajdin and Brühwiler 2003). However, only few studies provide indications on the quantitative assessment of risk, usually focusing on a single hazard and without

considering the risk time-dependency (Stein *et al.* 1999, Ang and de Leon 2005, Ellingwood and Wen 2005). Therefore, research effort is needed for the development of a comprehensive and flexible approach for risk assessment that accounts for time-dependency considering multiple hazards. This is the first objective of this study.

Risk assessment for single bridges has been mostly studied with respect to single hazard and sporadically for multiple hazards. Stein *et al.* (1999) developed a practical approach to estimate risk due to the effects induced by scour (single hazard), whereas Adey, Hajdin and Brühwiler (2003) investigated the potential consequences due to traffic hazard and scour in order to schedule optimal interventions over time (multiple hazards). On the other hand, risk assessment of groups of bridges needs to be further developed. Recently, different aspects concerning performance of transportation networks have been extensively investigated (Golroo, Mohaymany. and Mesbah 2010, Frangopol 2011, Frangopol and Bocchini 2012, Bocchini and Frangopol 2011a). For instance, life-cycle analyses of a bridge network located within the Denver metropolitan area have been performed, mostly focusing on the assessment of network performance and on the optimization of maintenance interventions (Liu and Frangopol 2005, Liu and Frangopol 2006, Frangopol and Liu 2007, Bocchini and Frangopol 2013). A predominant part of the research activity focused on the performance of transportation networks subjected to seismic ground motion considering bridge spatial distribution. Risk has often been included in such analyses (Chang, Shinozuka and Moore 2000, Jones, Middelmann and Corby 2005, Padgett, DesRoches and Nilsson 2010). Although these studies fully cover seismic-related aspects, most of the analyses focus on risk induced only by a single hazard. So far, few studies focused on the

inclusion of traffic hazards as part of the identified predominant hazards for risk assessment. Furthermore, except for a few studies (such as Adey, Hajdin and Brühwiler 2003), the research lacks in assessing time-dependent risk of bridges. The time-dependency of risk of groups of bridges subjected to multiple hazards requires to be investigated and is the second objectives of this study.

Another important aspect to be considered for bridge management is resilience to disaster that is worth exploring when bridges are located within hazard-prone regions, in which sudden important events may occur. The concept of resilient structural systems, which is very closely related to risk, is recently catching the attention of practitioners and the scientific community (Bruneau *et al.* 2003, Chang and Shinozuka 2004, Rose 2004, Miles and Chang 2006, Cimellaro, Reinhorn and Bruneau 2010, Bocchini and Frangopol 2012a, Bocchini and Frangopol 2012b). When extreme events occur, such as strong earthquakes, transportation infrastructures require to be protected against sudden unserviceability. An extended time of interrupted service of transportation facilities and networks may lead to large impact in terms of economic losses. If structures and, more generally, communities are resilient, the consequences of catastrophic events may be mitigated. The proper quantification of resilience of transportation networks is one of the key aspects for the development of management/retrofit strategies and for reaching the desired level of network serviceability in a reasonable time after the strike of an earthquake. In the past, some progress has been achieved by the introduction of analytical deterministic definitions of resilience (Bruneau *et al.* 2003, Frangopol and Bocchini 2011, Bocchini and Frangopol 2012a, Bocchini and Frangopol 2012b), many of them focusing on post-

event recovery analysis. Further developments (Bruneau and Reinhorn 2007, Xu *et al.* 2007 Cimellaro, Reinhorn and Bruneau 2010, Chang *et al.* 2012) opened the path for the probabilistic treatment of resilience. Recently, deterministic evaluation of resilience has been provided for complex bridge networks (Bocchini and Frangopol 2012b). However, a probabilistic approach for the prediction of seismic resilience of single and groups of bridges is missing. Therefore, a contribution to the development of a probabilistic approach to bridge resilience is necessary. This is the third objective of this study. The performance of the transportation entire network, necessary for the evaluation of resilience, can be obtained by considering the performance of each single bridge and accounting for the interconnections among the investigated routes (Bocchini and Frangopol 2011a).

1.2.2 SHIP STRUCTURES

The assessment of performance indicators that characterize structural safety (such as reliability and redundancy) is crucial (Frangopol *et al.* 2011a, Frangopol *et al.* 2011b, Frangopol *et al.* 2012), especially if adverse sea conditions are expected to be encountered. Preventing the safety of ship structures under operation from down-cross predefined thresholds leads to avoid potential failures that may cause economic losses and loss of lives.

The assessment of the ultimate flexural capacity of the hull midship section, usually considered as the most critical one, has been the subject of numerous studies dealing also with the progressive collapse mechanisms of plates and stiffeners (Paik and Frieze 2001, Paik *et al.* 2002). Moreover, in the last decades, several methods for

the evaluation of reliability associated with the ultimate flexural capacity of ship structures (Mansour and Hovem 1994, Mansour 1997, Paik, Kim and Lee 1998, Paik *et al.* 1998, Guedes Soares and Garbatov 1999, Ayyub, Assakkaf and Atua 2000, Guedes Soares and Teixeira 2000, Akpan *et al.* 2002, Lua and Hess 2003, Hørte, Wang and White 2007) and fatigue failure criteria (Hu, Cui and Pedersen 2004, Kim and Frangopol 2011, Kwon and Frangopol 2012, Kwon, Frangopol and Kim 2013) have been developed with the purpose of assessing the safety level or to estimate the residual life of ships. Reliability has also been evaluated with respect to specific ship limit states for the case of sudden damage such as grounding or collision (Hussein and Guedes Soares 2009, Luís, Teixeira and Guedes Soares 2009). Moreover, ship reliability has been investigated also with respect to the flexural capacity associated with the failure of the first element (stiffened plate) within a ship cross-section (Lua and Hess 2006). However, research in the field of redundancy of ship structures has not advanced significantly. Therefore, in this study a computational efficient approach will be developed for this purpose. This is the fourth objective of this study.

Ship safety may be evaluated by considering reliability analysis that does not account for any type of consequences. However, the inclusion of economic losses due to potential structural failures or malfunctions plays a central role in the decision analysis leading to risk assessment. Risk analysis of ship structures has been conducted in the past focusing on both qualitative (Akpan *et al.* 2002, Ayyub *et al.* 2002) and quantitative (Skjong 2002, Skjong and Bitner-Gregersen 2002) assessments, including the effects of different types of events. Moreover, important guidelines regarding formal safety assessment for estimating risk under shipping activities (IMO

1997) and regarding the development of ship construction standards based on risk assessment (IMO 2006) have been recently developed. However, a comprehensive approach for the time-dependent risk assessment of ship structures is not found in the current literature. This is the fifth objective of this study.

Routing of ships is an important and interesting part of ship management that involves decision making under uncertainty and includes the assessment of performance indicators affecting the selection of an optimal route. Routing optimization strategies have been developed mainly accounting for minimization of ship movements (i.e. maximum traveling comfort), minimization of fuel consumption (depending on wave resistance), and other operating costs (e.g. shipowners' costs, and cargo costs) (Journée and Meijers 1980, Brown, Graves and Ronen 1987, Fagerholt, Laporte and Norstad 2010, Papatzanakis, Papanikolaou and Liu 2012). The minimization of the estimated time of arrival of a ship trip has also been recently investigated (Hinnenthal 2008, Dolinskaya *et al.* 2009). However a risk-based approach that specifically includes structural performance, the quantification of potential losses, weather prediction aspects, and integrating SHM data is missing. The integration of SHM data into risk assessment and the development of an approach for optimal ship routing based on risk are the last two objectives of this study.

1.3 OBJECTIVES

The following are the main objectives of this study:

1. Develop an approach for the quantification of risk of single bridges by considering multi-hazard, and including the effects induced by aging processes and extreme events.
2. Extend the approach developed for a single bridge to a group of bridges.
3. Contribute to the development of a probabilistic approach for the prediction of seismic resilience of highway bridges based on an extension of an existing deterministic model.
4. Assess time-variant redundancy of ship structures using a computational efficient approach.
5. Develop a comprehensive computational platform for the assessment of time-variant risk of aging ship structures under different operational conditions.
6. Develop a closed-form approach for integrating SHM data into risk assessment of ship structures in order to obtain updated risk profiles.
7. Propose an approach for optimal ship routing based on risk and considering different damage scenarios and operational conditions.

1.4 SUMMARY OF THE APPROACH

In this study, the application of life-cycle concepts and decision making under uncertainty, including optimization techniques, are applied to (a) single bridges and bridge groups, and (b) ship structures.

The purpose of this research is to develop a rational framework as a support tool for decision makers to manage aging structural and infrastructural systems, including single bridges, bridge groups and ship structures. Figure 1.4 shows the proposed

framework, which incorporates probabilistic, statistical, and decision making tools used for the management of structures under uncertainty. Four blocks, denoted (1), (2), (3), and (4), representing the main phases and objectives of this study, and the type of investigated applications (civil and marine structures), are shown in Figure 1.4.

Block (1) performs the assessment and prediction of life-cycle system performance including structural and social indicators. The structural indicators are those accounting for the assessment of component/system load effects and strength, whereas the social indicators are those that additionally account for the potential consequences caused by structural unserviceability and failure (risk) and for the effort to recover from damage and activity disruptions caused by an extreme event (resilience). The evaluation of strength and load effects of structural components and systems requires the use of advanced tools, such as nonlinear incremental finite element analysis simulation based on Latin-Hypercube sampling, second order response surfaces, and second order reliability analysis. The prediction over time of these performance indicators is achieved by including the effects of processes that may decrease the performance, such as aging and corrosion phenomena, and/or the effects induced by selected scenarios. Uncertainties associated with structural geometry, material properties, and loading effects are considered in this block.

Block (2) in Figure 1.4 performs risk assessment with respect to selected or random events for characterizing the effects of different types of hazards. The main aspects to be considered and modeled are the quantification of the effects induced by the selected hazards, the assessment of the induced structural vulnerability based on reliability analysis, and the evaluation of a spectrum of caused consequences.

Additional uncertainties associated with the quantification of direct and indirect losses are accounted for.

Block (3) introduces the risk-informed management of structures under uncertainty based on the use of decision techniques, such as event tree and multi-criteria optimization. The considered criteria upon which decisions can be made are the levels of structural safety and risk, direct investments based on the quantified level of structural damage, and the limitation of the caused indirect consequences. Depending on the considered structure and on the investigated hazard, different management activities are developed in this study. Decision making associated with the recovery of single bridges and bridge groups from the effects of extreme seismic events, and risk-informed optimal ship routing considering different damage scenarios and operational conditions are investigated.

Finally, block (4) introduces the option of including further data collected by making use of SHM in order to improve the assessment and prediction of the structural performance. By using Bayesian statistics, the initially assessed performance, herein called prior information, can be updated, thus obtaining a more accurate (posterior) performance by including the collected SHM data. The integration of SHM concepts and technologies into structural management allows the improvement of performance prediction by reducing the uncertainties.

Figure 1.5 describes in detail how risk (presented in block (2) of Figure 1.4) is assessed for bridges and ship structures. Although these two types of structures are highly different, for risk assessment they share common aspects, as shown in Figure 1.5. The first step towards risk assessment is the identification of the most critical

hazards (Figure 1.5-Step (a)) that affect the component/structure under analysis, depending on the level of modeling detail that a specific risk assessment requires. Each hazard is modeled by investigating the effects generated by relevant events. The second step is the evaluation of structural vulnerability of specific components/structures with respect to selected failure modes (Figure 1.5-Step (b)). The proper selection of limit states that account for the evaluation of different failure probabilities is a key aspect for risk assessment. Structural vulnerability is estimated by performing reliability analysis based on the statistical properties of load effects and strength (or displacement and deformations, among others). The third and final step towards the assessment of risk is the quantification of the consequences associated with the occurrence of specific levels of damage/serviceability (Figure 1.5-Step (c)). Risk assessment usually requires the evaluation of direct and indirect consequences (losses) caused by potential structural damage (or partial and full unserviceability), or even structural failure (or full unserviceability).

Practically, the entire research of this study is developed by using self-developed, commercial and freeware programs, including (a) MATLAB (The MathWorks 2011) codes for managing the necessary calculation, connecting other software, and extrapolating and presenting the results, (b) Finite Element (FE) software for the modeling of structural strength, such as SAP2000 (CSI 2009) and ABAQUS (Dassault Systèmes Simulia 2011), (c) the reliability programs RELSYS (Estes and Frangopol 1998) and CALREL (Liu, Lin and Der Kiureghian 1989), (d) the program PDSTRIP (2006) performing computing seakeeping analysis, and (e) the surface modeling software FREE!ship (2006).

1.5 OUTLINE

This study is composed of two parts. Part I involves single bridges and bridge groups, whereas Part II deals with ship structures. Part I develops a risk-informed life-cycle management approach for single bridges and bridge groups. Although risk assessment is the backbone of the proposed decision approach for both bridges and ship structures, for the case of single bridges and bridge groups (Part I) resilience to disasters is also accounted for. Part II proposes a framework that includes an optimality-based approach for the management of aging ship structures considering reliability, redundancy, and risk of ships under different operational conditions, and integrating SHM. For each topic treated within each chapter, a case study is investigated in order to show the applicability of the proposed approach.

The remainder of the thesis is organized as follows:

Part I – Life-Cycle Management of Single Bridges and Bridge Groups based on Risk

- **Chapter 2** presents a comprehensive overview on risk assessment and proposes a framework for the quantification of the time-dependent risk of highway bridges, estimating the effects of multiple common hazards, such as abnormal traffic loads, environmental attacks, scour, and earthquakes. Time-dependent failure probabilities, hazard functions, and probability density functions (PDF) of the time-to-failure are also obtained for each hazard. Direct and indirect consequences are quantified in terms of monetary losses.

- **Chapter 3** develops a rational framework for the quantitative assessment of life-cycle risk of bridges within a transportation network. Bridge vulnerability is evaluated with respect to seismic and abnormal traffic hazards. The effects induced by seismic hazard are investigated by means of fragility analysis. Random earthquakes are generated using Latin Hypercube sampling technique, and probabilities of exceeding specific structural damage states are computed for each specific seismic scenario. Traffic hazard is assessed considering Weibull distributed time-to-failure of the bridge superstructure.
- **Chapter 4** extend the deterministic model, proposed by several researchers in the field of resilience of structures, to a probabilistic approach for the pre-event assessment of seismic resilience of bridges, including uncertainties associated with expected damage, restoration process, and rebuilding/rehabilitation costs. Depending on the level of regional seismic hazard, the level of performance that decision makers plan to achieve, the allowable economic impact, and the available budget for post-event rehabilitation activities, a wide spectrum of scenarios are investigated.

Part II – Optimality-Based Approach for the Management of Aging Ship Structures considering Reliability, Redundancy, and Risk of Ships under Different Operational Conditions and Integrating Structural Health Monitoring

- **Chapter 5** proposes a framework for the assessment of structural safety of ship hulls under different operational conditions by evaluating performance indicators such as reliability and redundancy. Reliability and redundancy are based upon the

evaluation of the flexural capacities associated with the ultimate hull failure and the failure of the first stiffened panel within a selected cross-section. Furthermore, aging effects due to corrosion phenomena are investigated. Polar representations of reliability and redundancy are obtained for different encountered sea states, ship speeds and headings, covering a large spectrum of operational conditions. Uncertainties associated with structural geometry, material properties, and loading are accounted for.

- **Chapter 6** develops a risk-informed decision tool for optimal routing of ships considering different damage scenarios and operational conditions. The strength of the hull is investigated by modeling the midship section with finite elements, and by analyzing different damage levels depending on the propagation of plastification throughout the section. Vertical and horizontal flexural interaction is investigated. Uncertainties associated with geometry and material properties are accounted for by means of the implementation of the response surface method. Risk is assessed by including the direct losses associated with five investigated damage states. The effects of corrosion on aged ships are included in the proposed approach. The optimal routing of ships is obtained by minimizing both the estimated time of arrival and the expected direct risk, which are clearly conflicting objectives.
- **Chapter 7** proposes a novel approach for near real-time multi-criteria optimal ship routing integrating risk and SHM. The inclusion of collected SHM data into the developed decision support tool provides useful information to be used during the real-time decision process. Wave-induced effects represent the prior information to

be updated by using the Bayesian statistics. A closed-form solution and a simulation-based technique are proposed for Bayesian updating. Also, weather forecasts, associated with different time frames, are included within the developed framework. The optimal routing of ships is found by solving a three-objective optimization problem, required to minimize the estimated time of arrival, mean total risk, and fuel cost, given the assumed sea weather maps and the origin and destination points.

- **Chapter 8** provides the conclusions from this study and the recommendations for future work.
- **Appendix 1** provides a review of performance indicators, probabilistic methods, and optimization techniques used in this study.
- **Appendix 2** contains the developed **c**omputational framework for the assessment of structural performance and management of aging ship structures used in Chapters 5, 6, and 7.
- **Appendix 3** contains the list of the notations used in this study.

1.6 CONTRIBUTIONS

The main contribution of this study is the development of a quantitative general approach that explicitly incorporates risk, by combing the structural and social aspects of the performance, into a management framework for structures and infrastructures with emphasis on highway bridges and ship structures, including:

- Development of a framework for the assessment of risk for single bridges subjected to multiple hazards, including traffic loads, environmental attacks, scour, and earthquakes.
- Extension of the framework for single bridges to bridge groups and spatially distributed bridges.
- Contributions to the development of a probabilistic approach for the quantification of resilience to disaster of single bridges and bridge groups based on the extension of an existing deterministic model.
- Development of an efficient approach for the evaluation of time-variant reliability and redundancy indices of aging ship structures subjected to different operational conditions.
- Development of a novel management framework for the near real-time multi-criteria optimal ship routing integrating risk, weather prediction, and SHM data by means of Bayesian updating.
- Development of a comprehensive computational platform for the evaluation of time-dependent reliability, redundancy, and risk of aging ship structures integrating finite element - response surfaces analyses, hydrodynamic response analysis, effects of aging phenomenon, SHM data, and optimality-based ship routing as management tool.

Table 1.1 Structurally deficient and functionally obsolete bridges in terms of number of bridges and deck area within the states of New Jersey, New York, Pennsylvania and whole United States (FHWA 2011a).

State	Number of bridges	Number of SD bridges	Number of FO bridges	Number of Def. bridges	Deck area	SD deck area	FO deck area	Def deck area
New Jersey	6,514	656	1,632	2,288	6,588,208	665,412	1,823,572	2,488,984
New York	17,384	2,092	4,337	6,429	12,670,592	1,756,243	5,218,944	6,975,187
Pennsylvania	22,320	5,563	3,749	9,312	12,400,088	2,057,870	2,883,705	4,941,575
Total (whole US)	605,086	67,526	76,363	143,889	355,047,700	29,702,170	60,155,959	89,858,130

Deck area is in m^2
SD = Structurally deficient
FO = Functionally obsolete
Def = Deficient

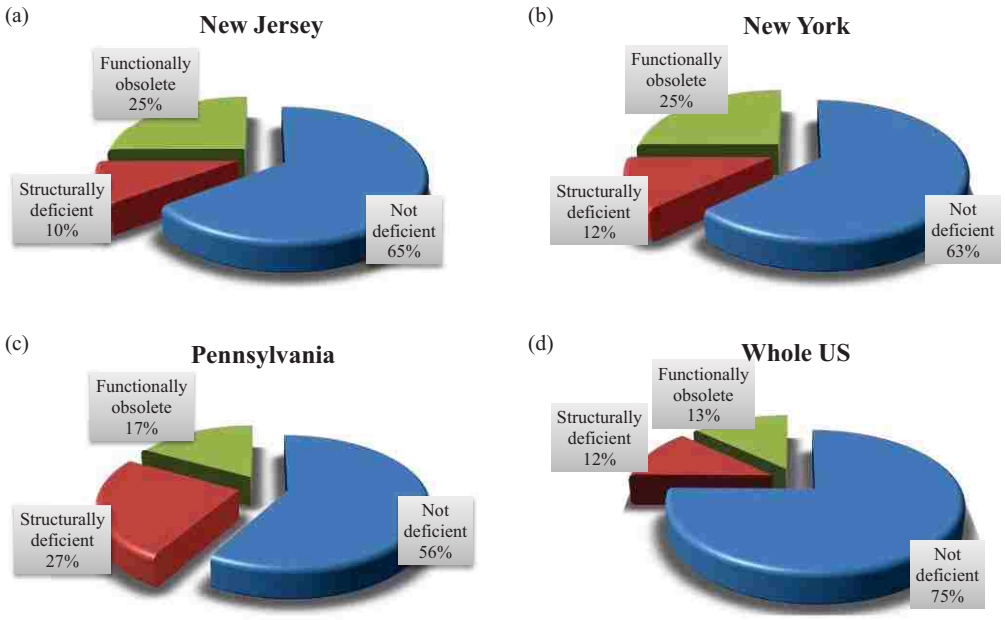

Figure 1.1 Percentage of bridges classified as structurally deficient, functionally obsolete, and not deficient with respect to the total number of bridges for the states of (a) New Jersey, (b) New York, (c) Pennsylvania and (d) for the whole United States (data from FHWA 2011a).

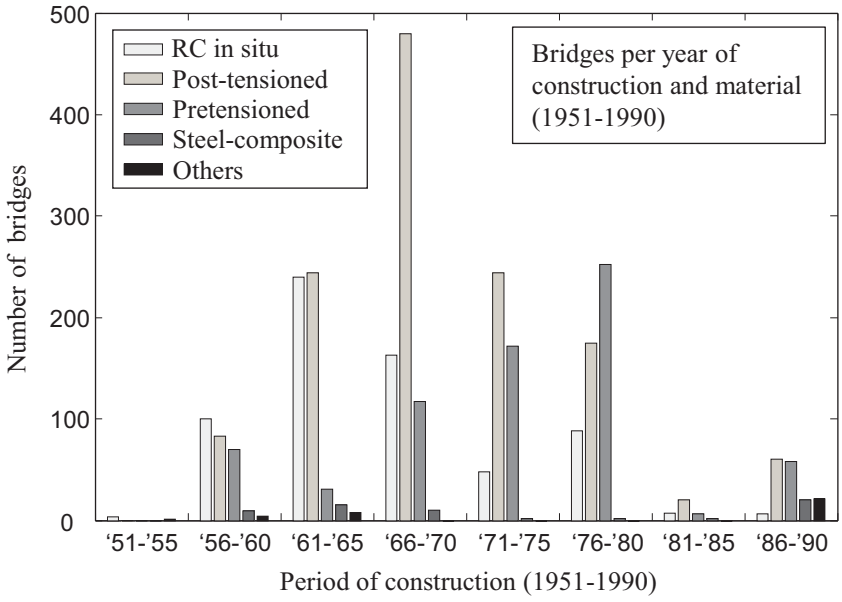

Figure 1.2 Bridges per year of construction and material type (reinforced concrete in situ, post-tensioned, pretensioned, steel-composite, and others) managed by 'Autostrade per l'Italia', the Italian major highway company (data from Das and Pardi 2001).

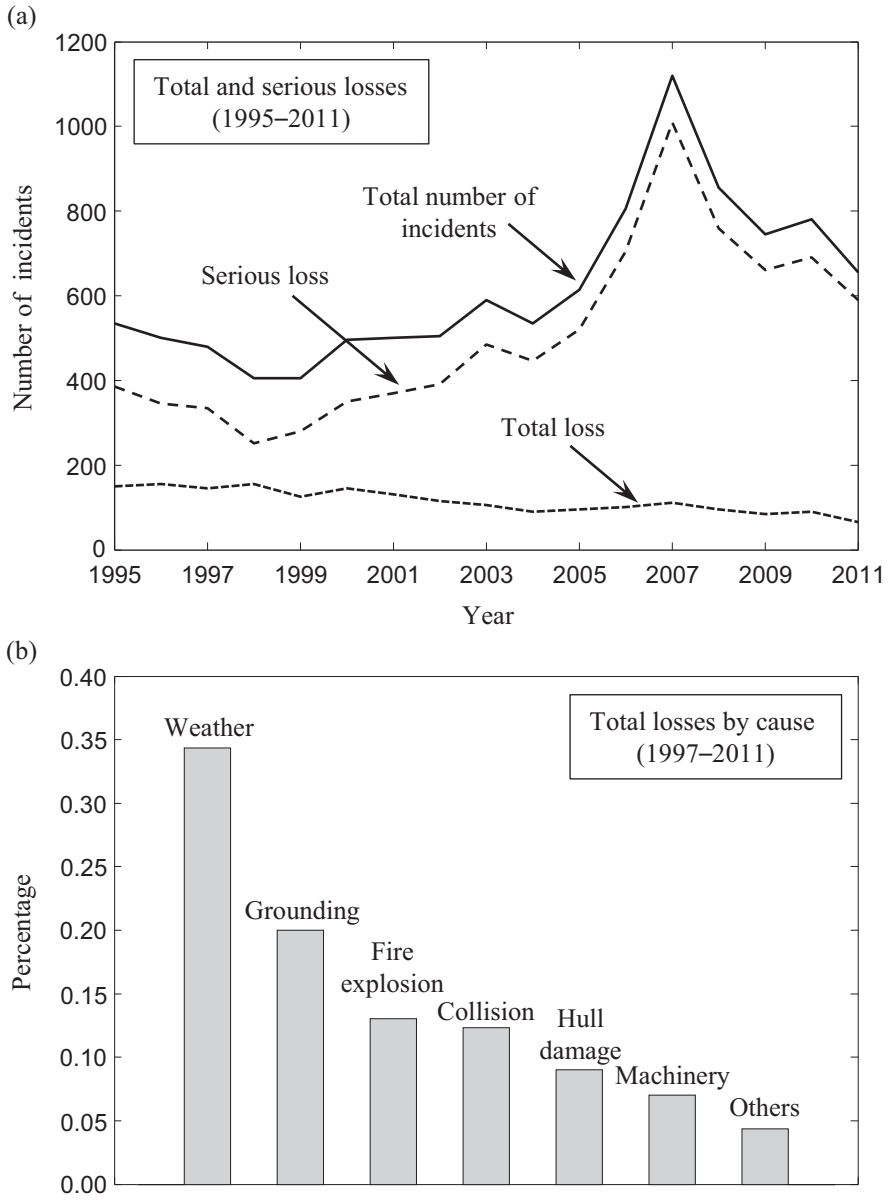

Figure 1.3 World fleet statistics for vessels with cargo carrying capacity greater than 500 GT in terms of (a) number of incidents to vessels that suffered total loss, serious loss, and their grand total within the period 1995–2011 and (b) percentages associated with different total loss causes within the period 1997–2011 (data from IUMI 2012).

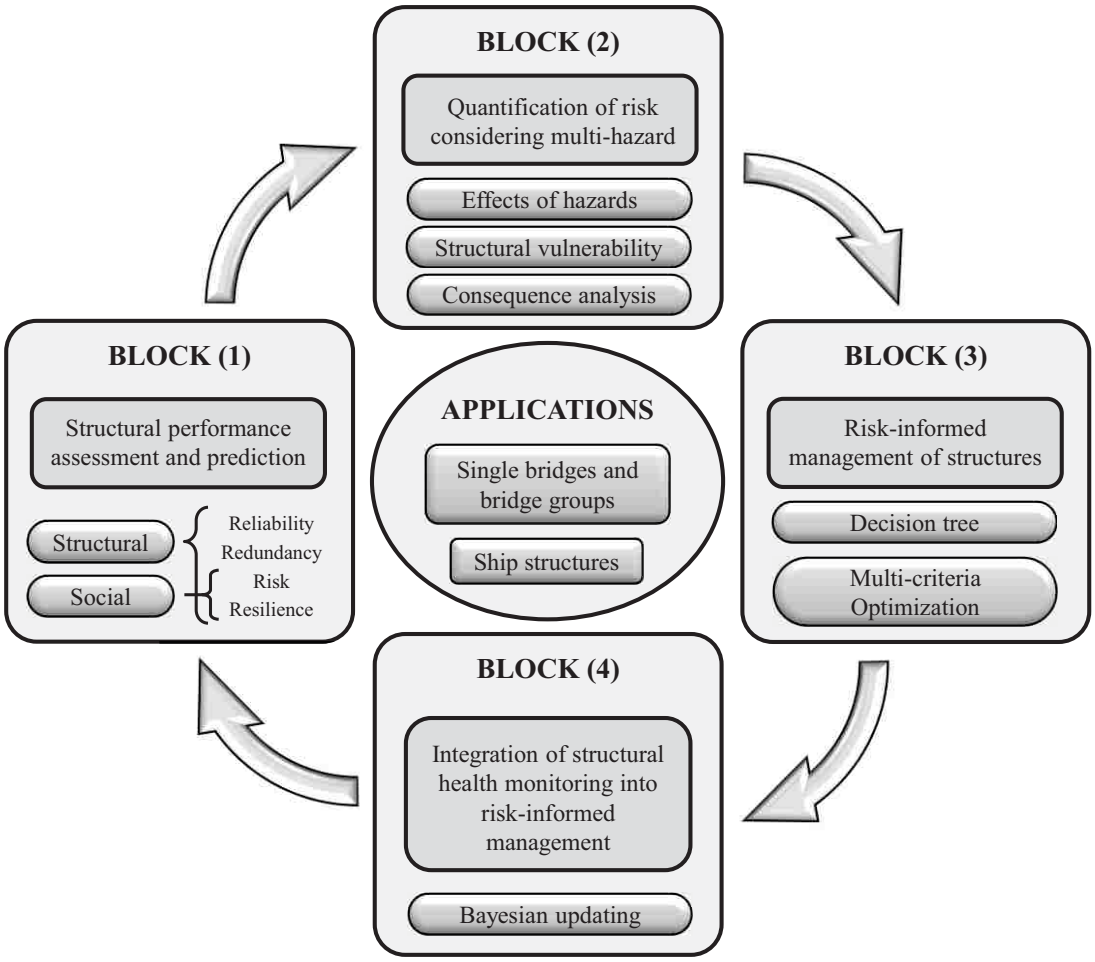

Figure 1.4 Proposed life-cycle management framework which incorporates probabilistic, statistical, and decision making tools included into four blocks representing the main phases and objectives of this study. This framework is applied to civil and marine structures.

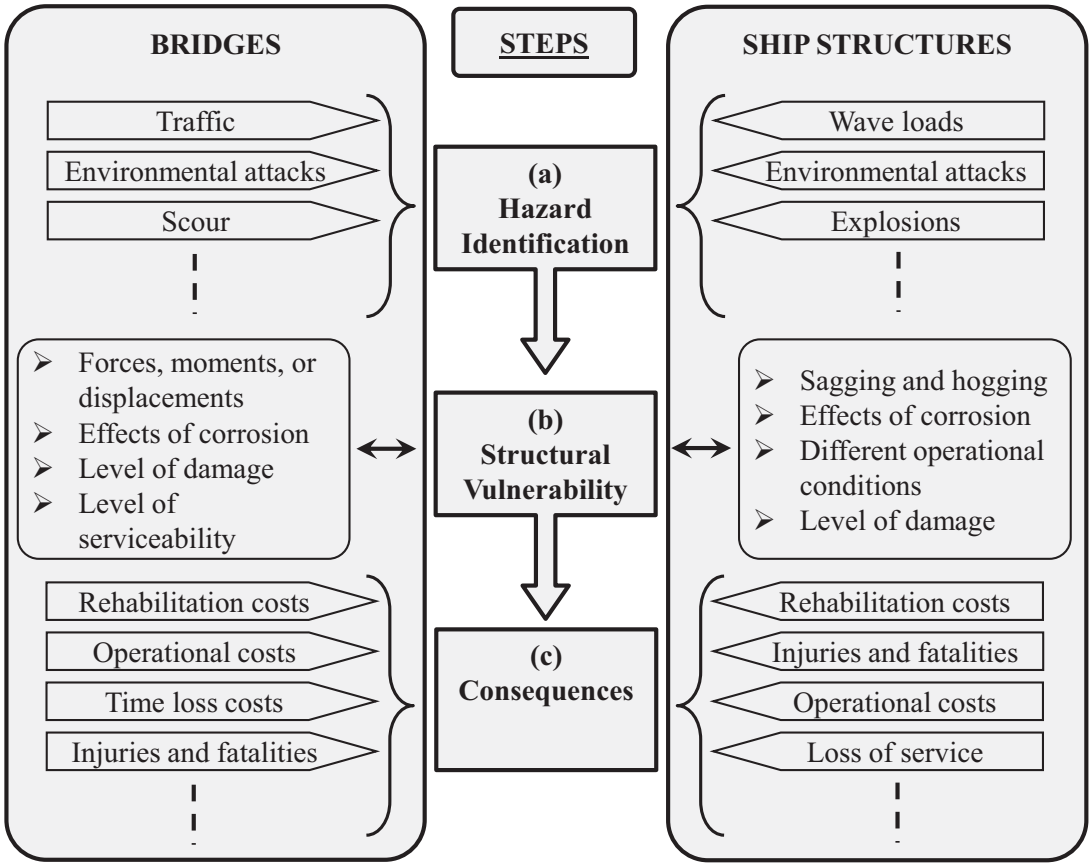

Figure 1.5 Framework showing the main steps towards risk assessment and the comparison between the main aspects involved in the risk assessment of bridges and ships.

PART I

LIFE-CYCLE MANAGEMENT OF SINGLE BRIDGES AND BRIDGE GROUPS BASED ON RISK

CHAPTER 2

RISK ASSESSMENT OF HIGHWAY BRIDGES UNDER MULTIPLE HAZARDS

2.1 INTRODUCTION

The deterioration of structural performance, the load increase, and the possible occurrence of extreme events could generate major safety concerns for existing structures and infrastructures. Effective maintenance of structural systems is crucial in preventing excessive deterioration of their performance over time. Maintenance and repair actions are intended to enhance the capability of these systems to withstand the effects of potential hazards during their designed life spans. In this context, life-cycle assessment of structural systems, combined with quantitative risk assessment, is the basis for the development of a rational management tool that can help in preventing or minimizing possible malfunctions of structural systems.

Uncertainties affect the design, construction, assessment, maintenance, and management of structures and infrastructures. Quantitative risk assessment of structural systems is also highly affected by uncertainties: structural performance evaluation, analysis of the probability of occurrence of different types of hazards, and evaluation of the associated consequences due to the inadequacy of the structural system. In this chapter, both epistemic and aleatory uncertainties are accounted for.

A key point is the communication of risk between the parts involved in the decision process and the society (Ellingwood 2001). For instance, a decision maker with perfect knowledge of the actual risk associated with a structure makes the right decisions with a high level of confidence. Miscommunications among decision makers, stakeholders, authorities, and users can occur. In these cases, the decision makers may adopt solutions leading to increasing the indirect risk and resulting in a higher exposure for the entire society (CIB 2001, JCSS 2008). Structural system redundancy as defined in Frangopol and Nakib (1991) is associated to risk assessment; a high level of redundancy may contribute to the mitigation of the effects produced by hazard-induced events. In fact, if an extreme event produces a critical damage, a high level of structural system redundancy will be crucial in limiting the potential increase of risk due to miscommunication among the parts.

The aim of this study, which is based on Decò and Frangopol (2011), is to provide a general, rational, and flexible framework, able to evaluate the quantitative time-dependent risk of highway bridges in a multi-hazard environment. The proposed risk approach can be used to rank the structures under investigation and prioritize interventions. The introduced framework accounts for direct and indirect consequences leading to the evaluation of direct and indirect risk, respectively. The annual failure probabilities associated with common hazards (traffic loads, environmental attacks, scour, and earthquakes) are evaluated making use of: (a) existing databases including the National Bridge Inventory (NBI) database (FHWA 2009) and U.S. Geological Survey (USGS) water data (USGS 2010); (b) on-line tool (2009 Earthquake Probability Mapping) provided by USGS (2009); and (c) computer

programs such as RELSYS (Estes and Frangopol 1998), HAZUS (FEMA 2009a), SAP2000 (CSI 2009), and MATLAB (The MathWorks 2011). Furthermore, the profiles of the failure probability, hazard rate, and probability density functions (PDFs) of the time-to-failure for different types of hazard are developed, analyzed, and compared. The evaluation of the monetary consequences due to the occurrence of failure takes into account rebuilding costs, running costs, and time loss costs based on the data contained in AASHTO (2003).

This chapter develops a comprehensive framework for the quantification of the time-dependent risk of single highway bridges. Section 2.2 introduces the models for the evaluation of the probability of failure, associated reliability index, time-dependent reliability, hazard function, survivor function, and redundancy index. Section 2.3 discusses the developed framework for risk assessment of bridges subjected to the effects induced by traffic, scour, and earthquakes. Moreover, concepts related to risk communication and consequence analysis are also introduced in this section. In Section 2.4, the proposed approach is applied to an existing highway bridge crossing the Wisconsin River in Wausau, WI, USA. Finally, Section 2.5 provides the conclusions of this chapter, which is based on a published paper (Decò and Frangopol 2011).

2.2 STRUCTURAL PERFORMANCE

Based on the concepts reviewed in Appendix A the following subsections develop the models for several performance indicators that are specifically used in this chapter.

2.2.1 PROBABILITY OF FAILURE AND RELIABILITY INDEX

Reliability is defined as the ability of a component or system to perform and maintain its intended performance. In structural engineering, the performance of a component is usually related to its capacity to withstand the applied loads.

The instantaneous indication of the performance governing the problem of supply and demand considering multiple failure modes (i = 1,2,…,N) is defined by introducing the instantaneous performance functions $g_i(t)$ with respect to time t as follows

$$g_i(t) = C_i(t) - S_i(t) \tag{2.1}$$

where $C_i(t)$ and $S_i(t)$ are the instantaneous capacity and load effect associated with failure mode i, respectively. The system probability of failure $P_{f,sys}$, accounting for the occurrence of all potential failure modes, is given by (Ang and Tang 1984)

$$P_{f,sys} = \int\int ... \int f_{\mathbf{X}}(x_1,...,x_j,...,x_m)dx_1...dx_j...dx_m \tag{2.2}$$

where $f_{\mathbf{X}}(\mathbf{x})$ is the joint PDF of the vector $\mathbf{X} = \{X_1,\ldots,X_j,\ldots,X_m\}$ containing the random variables X_j. The reliability index β_{sys} associated with the system probability of failure is assumed to be

$$\beta_{sys} = \Phi^{-1}(1 - P_{f,sys}) \tag{2.3}$$

where $\Phi^{-1}(\cdot)$ is the inverse standard normal cumulative distribution function (CDF).

2.2.2 TIME-DEPENDENT RELIABILITY, HAZARD FUNCTION, AND SURVIVOR FUNCTION

When considering the instantaneous (point-in-time) probability of failure to describe the performance of a structure, the analysis is quite limited. The observation that the structure has survived until the time of assessment is an important information about its actual capacity and reliability. In other words, by using this information, the analysis will account for the lifetime of the structure by updating its point-in-time reliability. This updating process is used in the development of lifetime functions and is accomplished by considering time-dependent reliability estimates. Considering a discrete time interval of one year, the time-dependent failure probability $TDP_f(t)$ is

$$TDP_f(t) = \sum_{i=1}^{t} \left(P_{f,i} \prod_{j=1}^{i} \left(1 - P_{f,j-1}\right) \right) \tag{2.4}$$

where P_f is the annual failure probability and i and j are indices representing the time (years). The time-dependent failure probability (cumulative with time) is also defined as the CDF of the time-to-failure. Once the associated PDF of the time-to-failure $f_{ttf}(t)$ is obtained, the hazard function $h(t)$ can be expressed as (Leemis 1995)

$$h(t) = \frac{f_{ttf}(t)}{1 - TDP_f(t)} \tag{2.5}$$

In order to obtain a closed-form performance profile, the time-dependent probability (CDF of the time-to-failure) may be fitted by using the CDF of the Weibull distribution F^* (which is commonly used in survival analysis), defined as (Leemis 1995)

$$F^*(t) = 1 - e^{-(\lambda t)^{\kappa}} \qquad t \geq 0 \tag{2.6}$$

where κ is the shape parameter and λ is the scale parameter. By using the method of the least squares, the fitting process determines the parameters (κ, λ) of the vector that minimizes the function (Bucher 2009)

$$s = \sum_k \left[TDP_{f,sys}(t_k) - F^*(t_k, \kappa, \lambda) \right]^2 \tag{2.7}$$

The PDF of the fitted Weibull distribution (also PDF of the time-to-failure) is (Leemis 1995)

$$f^*(t) = \lambda\kappa(\lambda t)^{(\kappa-1)} e^{-(\lambda t)^{\kappa}} \qquad t \geq 0 \tag{2.8}$$

2.2.3 STRUCTURAL REDUNDANCY INDEX

Redundancy is a useful performance indicator that provides warning associated with local damage, partial failure, or total collapse. If a structural system is redundant, its capacity to withstand the applied load is enough even when one of its components fails. A redundant structural system will collapse only if the failure pattern propagates throughout multiple components.

Among several definitions of redundancy (Appendix A), the definition proposed in Frangopol and Okasha (2008) is adopted in this chapter

$$RI(t) = \frac{P_{y,sys}(t) - P_{f,sys}(t)}{P_{f,sys}(t)} \tag{2.9}$$

where $P_{f,sys}(t)$ and $P_{y,sys}(t)$ are the annual failure probabilities associated with the system failure and the exceedance of the yielding limit state (first yielding), respectively.

2.3 RISK ASSESSMENT

The management of structures of great importance requires the evaluation of total risk associated with identified hazards in order to account for the consequences of a potential structural failure or malfunction (damage state). It is now recognized that the inclusion of risk as an additional indicator improves the quality of the decision making process (Frangopol and Liu 2007). Unfortunately, the evaluation of risk is a process fraught with uncertainties. Risk was only qualitatively defined in most of the previous studies. These uncertainties are treated with special attention in order to evaluate risk with a higher confidence level. According to Ang and de Leon (2005), uncertainties are divided in two types: epistemic, which can generally be reduced by improving our knowledge or through the enhancement of the prediction models, and aleatory, which cannot be reduced because of their intrinsic randomness. The proposed framework for the quantitative risk assessment includes both types of uncertainties.

Risk assessment consists of two main steps: identification and evaluation. This chapter focuses on the identification of common hazards affecting highway bridges and on the quantitative evaluation of the associated risk. Figure 2.1 shows the developed general framework.

There are many possible types of hazards and they can generally be classified as follows:

1. Natural hazards: induced by natural processes. In the case of bridge risk assessment, examples of such natural hazards are floods, earthquakes, landslides, strong winds (hurricanes, tornadoes), tsunamis, and environmental attacks.
2. Man-made hazards: induced by humans. Bridges can be affected by either abnormal traffic conditions (overloading), accidents, human negligence (for instance inadequate inspection), fires, explosions, and terrorist attacks.

In this chapter, the quantitative assessment of bridge-related risk is performed based on hazards due to traffic loads, environmental attacks, scour, and earthquakes (Stage 0 in Figure 2.1). Following the identification stage, the proposed framework for the evaluation of the time-dependent total risk requires further steps (Stages 1–6 in Figure 2.1) as follows:

Stage 1: Evaluation of the annual probabilities of occurrence of selected hazard-induced events.

Stage 2: Evaluation of the annual probabilities of occurrence of different limit states including first yield and failure.

Stage 3: Evaluation of the annual redundancy index (Equation (2.9)), which may affect risk assessment.

Stage 4: Probabilistic evaluation of the annual direct and indirect consequences taking into consideration traffic conditions and economic aspects related to the location of the structure.

Stage 5 Evaluation of time-dependent failure probabilities (Equation (2.4)), hazard functions (Equation (2.5)), and fitted PDFs of the time-to-failure (Equation (2.8)) for each considered hazard.

Stage 6: Probabilistic assessment of time-dependent total risk due to identified hazards.

Although the planning of maintenance strategies is not the purpose of this chapter, it is essential to recall that the prioritization of maintenance actions for preventing failures and mitigating their consequences can be developed based on the quantitative analysis of risk. Accordingly, the following actions have to be performed:

1. Risk-based ranking of bridges provides a prioritization strategy that may be implemented.
2. Based on the PDFs of the time-to-failure associated with each hazard, the identification of the most critical hazard affecting the structures under consideration may help reducing their vulnerability by planning an appropriate mitigation strategy.

As reviewed in Appendix A, risk R is defined by CIB (2001) as

$$R = \int\int ... \int \delta\left(x_1,...,x_j,...,x_m\right) \times f_{\mathbf{X}}\left(x_1,...,x_j,...,x_m\right) dx_1 ... dx_j ... dx_m \tag{2.10}$$

where δ represents the consequences and $f_X(x)$ is the joint PDF containing the random variables $\mathbf{X} = \{X_1,\ldots,X_j,\ldots,X_m\}$. The quantification of the consequences is provided by a monetary value. The solution of the above-multiple integral is not obvious and in most cases it cannot be solved numerically. Using the assumption that the hazards are mutually exclusive and collectively exhaustive, a simpler equation for the evaluation of the instantaneous total risk R is (Ellingwood 2001)

$$R = \sum_{i=1}^{n} C_c \times P\left[F \mid H_i\right] \times P\left[H_i\right] \tag{2.11}$$

in which $P[H_i]$ is the probability of occurrence of an event due to hazard H_i, $P[F|H_i]$ is its associated conditional failure probability, C_c represents the monetary value associated with the consequences of failure, and n is the number of the considered hazards.

Risk assessment includes the evaluation of direct and indirect consequences of damage/failure. Direct consequences are the ones associated with damage or failure itself (Baker, Schubert and Faber 2008), while the indirect consequences are those related to system failure or malfunctions that induce external monetary losses. Hence, the instantaneous total risk R becomes

$$R = R_D + R_{ID} \tag{2.12}$$

in which R_D and R_{ID} are the instantaneous direct and indirect risks, respectively.

2.3.1 ANNUAL FAILURE PROBABILITIES

When estimating the probability of damage occurrence and/or failure of components or structures, a specific procedure must be undertaken. Accordingly, the required degree of accuracy depends on the level of completeness of the analysis and the importance of the considered hazard. Hazards are assumed to be mutually exclusive, thus different types of hazard-induced events can be analyzed separately.

2.3.1.1 Live loads

The structural performance associated with a specific limit state varies with respect to time due to the increasing live load effects (caused, e.g., by the growing demand of increasing traffic volume) and the progressive deterioration of the mechanical

properties (caused, e.g., by corrosion). The investigated flexural failure modes are those related to the bridge superstructure members (deck and girders). AASHTO (2007) specifications are adopted for the estimation of the load effects and capacities at each critical section. If a multi-span continuous steel girder bridge is considered, the limit state equations for the flexure of bridge deck and girders are

$$N_{FC} M_{n,i}(t) - N_S \left[M_{DL,i} + M_{LL,i}(t) \right] = 0 \tag{2.13}$$

$$N_{FC} M_{u,ij}(t) - N_S \left[M_{DL,ij} + \alpha D_{fm,j} \times M_{LL,ij}(t) \right] = 0 \tag{2.14}$$

$$N_{FC} M_{y,ij}(t) - N_S \left[M_{DL,ij} + \alpha D_{fm,j} \times M_{LL,ij}(t) \right] = 0 \tag{2.15}$$

where N_{FC} and N_S are the epistemic uncertainty coefficients associated with the flexural moment capacities and applied moments, respectively, M_n is the flexural moment capacity of the reinforced concrete (RC) deck and M_u and M_y are the ultimate and yielding girder moment capacities, respectively, M_{DL} and M_{LL} are the dead and live load applied moments, respectively, α is the dynamic allowance, D_{fm} is the distribution factor for moments, i and j are the identification numbers of each critical section and girder, respectively, and t is the time. For the girders, the critical sections are located at the intermediate supports and at mid-spans, while for the deck, they are located where positive and negative transversal moments are maxima. Assuming one year interval for the evaluation of load effects and capacities over time, the abovementioned limit state equations provide annual failure probability associated with the failure of deck and girders (Equations (2.13) and (2.14), respectively), and yielding (Equation (2.15)).

The increase over time of the live load moments is predicted considering traffic data, such as the average daily truck traffic (ADTT), and by applying the statistics of extremes (Akgül 2002). Furthermore, the deterioration of the flexural capacities over time is induced by corrosion. The corrosion process is caused by salted water exposure and atmospheric aggression in the case of girders (it is assumed that corrosion attacks the top and the sides of the bottom flanges and each side of the webs), and it is induced by chloride penetration in the case of RC deck (this generates section loss of steel reinforcement). The assumed corrosion models applied to steel girders (Equation (2.16)) and RC deck (Equation (17)) are based on studies provided by Albrecht and Naeemi (1984) and Thoft-Christensen (1998), respectively. The loss functions are defined as follows

$$C_p(t) = At^B \tag{2.16}$$

$$A_S(t) = \begin{cases} n_b \dfrac{\pi D_0^{\,2}}{4} & for \le t \le T_i \\ n_b \dfrac{\pi\left[D_0 - C_{corr} i_{corr}(t - T_i)\right]^2}{4} & for \;\; t > T_i \end{cases} \tag{2.17}$$

where t is time (years), $C_p(t)$ is the corrosion penetration (μm), A (μm) and B represent parameters based on the environment aggressivity, $A_s(t)$ is the time-variant top transversal tensile steel reinforcement area (mm^2), n_b is the number of top transversal steel bars, D_0 is the initial top reinforcement diameter (mm), i_{corr} is the corrosion parameter (mA/cm^2), C_{corr} is a corrosion coefficient, and T_i is the corrosion initiation time (years) evaluated according to Estes (1997).

The inclusion of random variables describing geometrical and material properties, and load effects (e.g., yielding stress, width and thickness of webs and flanges, elastic modulus of steel and concrete, dead and live load moments) leads to the probabilistic evaluation of the above-mentioned flexural moment capacities and acting bending moments.

Finally, the annual system failure probability of a continuous multi-span steel girder bridge (modeled as a series-parallel system) is investigated considering the most significant failure mechanisms. The occurrence of a specific collapse mechanism (i.e., plastic hinges in multiple locations) is modeled considering that the performance functions associated with the specified critical sections are in parallel, and the occurrence of overall system plastic collapse is modeled considering the possible collapse mechanisms in series. The sectional capacities and load effects are simulated by using a Latin Hypercube sampling (McKay, Conover and. Beckman 1979) (reviewed in Appendix A), and the annual system probability of collapse and first yielding are computed by using the reliability program RELSYS (Estes and Frangopol 1998).

2.3.1.2 Scour

The typical effect produced by flood-induced events on bridges crossing water streams is the scour of piers and/or abutments. According to Kattell and Eriksson (1998), scour is defined as the erosion or removal of streambed or bank material from bridge foundations due to flowing water. Scour has also been identified as the most common cause of highway bridge failures in the United States (Kattell and Eriksson 1998).

In this study, the risk associated with the scour of highway bridge foundations is evaluated using the method proposed by Stein *et al.* (1999). The method consists in characterizing the actual hydrological properties of the water stream at the bridge location, the dimensionless depth describing the height of the water flow, the typology and topology of the bridge, its waterway adequacy, its scour vulnerability, its substructure condition, and the channel protection. This methodology requires the collection of some bridge data obtained by the NBI (FHWA 2009). Based on Stein *et al.* (1999), the calculation of the annual failure probability is performed by the following steps:

1. Record the necessary NBI items (FHWA 2009) and refer to FHWA (1995) for their interpretation.
2. Evaluate the flood discharge associated with the considered river and location at the selected recurrence interval Q_{100}, by using the USGS regression equations (USGS 2003 for the case study).
3. Assess the annual probabilities of the river being in specific dimensionless depth ranges by using the available data related to the water stream and provided by USGS (2010). The dimensionless depths associated with specific discharges are (Stein *et al.* 1999) as follows

$$\frac{D}{D_f} = \left(\frac{Q}{Q_f} \right)^{0.6} \tag{2.18}$$

where D and Q are the depth and the discharge, respectively, and f refers to the full flow.

4. Determine the scour vulnerability (NBI item 113 of FHWA 2009). If not already assessed, consider the substructure condition and the channel protection (NBI items 60 and 61 of FHWA 2009).
5. Evaluate the annual failure probability $P_{f,SC}$, given the scour vulnerability and the dimensionless depth by applying the following equation (based on Stein *et al.* 1999):

$$P_{f,SC} = \sum_{DD} P[F \mid SV \text{ and } DD] \times P[SV \text{ and } DD] \tag{2.19}$$

where F is the failure, SV is the scour vulnerability, and DD represents the dimensionless depth ranges of the stream.

Furthermore, depending on the number of annual records available in the NBI database, the probability of failure can be computed for a given time period and a trend can be estimated in order to predict future values (e.g., over a lifetime of 80 years).

2.3.1.3 Earthquakes

A crucial exposure is represented by the seismic hazard, which is obviously a major concern for those regions that often have to allocate resources to face the consequences of earthquakes of great magnitude. However, especially when risk is assessed, another matter of concern arises for those regions that have low probability of occurrence of strong earthquakes, but have to deal with abnormal consequences so called low-probability/high-consequence events (Ellingwood and Wen 2005).

A methodology that, after identifying a limited set of deterministic earthquake scenarios, assesses their associated hazard-consistent probabilities was developed in order to evaluate the seismic hazard of a region (Chang, Shinozuka and Moore 2000). Wang (2007) investigated the regional seismicity by making use of the Earthquake Probability Mapping provided by USGS. In order to provide a general flexible approach, updated seismicity maps (USGS 2009) are used as a valuable tool able to estimate the probability of occurrence of an earthquake in the contiguous United States given the geographical location, the area under investigation, the desired time interval, and the magnitude. These maps are derived from seismic hazard curves calculated on a grid of sites across the United States and describing the frequency of exceeding a set of ground motions. One of the main advantages of the 2009 Earthquake Probability Mapping (USGS 2009) is its flexibility and its user friendly interface. Through this tool and by setting one year interval, the annual probability of occurrence of the *i*-th seismic scenario $P(SS_i)$ associated with the *i*-th earthquake is given as follows

$$P(SS_i) = P[HQ_i \mid XY_i, \rho_i, TS_i, and\ M_i] \tag{2.20}$$

where *HQ* is a seismic event, *XY* refers to the latitude and longitude of the epicenter, ρ is the radius of the considered region area, *TS* is the considered time span (one year), and *M* is the earthquake magnitude.

Given the occurrence of an earthquake scenario, the risk assessment requires the evaluation of the conditional failure probability (vulnerability) of a structure. This issue has been extensively studied in the past (Ellingwood and Wen 2005). The failure

probability can be evaluated by means of fragility analysis. The program HAZUS (FEMA 2009a) is used for this purpose. HAZUS is a GIS-based software tool in use in the United States. The analysis consists of defining earthquake scenarios by setting their magnitudes and locations. The results obtained are based on the development of curves describing the probability of exceeding a specific damage state (none, slight, moderate, extensive, and complete) after defining a specific seismic scenario. For highway bridges, according to FEMA (2009b) and Mander (1999), these fragility curves are expressed by a log-normal cumulative distribution probability function as follows

$$P\left[DS \mid PSA_i\right] = \Phi\left[\frac{1}{\beta_c}\ln\left(\frac{PSA_i}{A_{DS}}\right)\right] \tag{2.21}$$

where $P[DS|PSA_i]$ is the probability of occurrence of a specific damage state DS given that PSA_i is the spectral acceleration amplitude for a period of 1 sec associated with the i-th seismic scenario, β_c is the normalized composite log-normal standard deviation, A_{DS} is the median spectral acceleration associated with the occurrence of the damage state DS, and Φ is the standard normal CDF. Moreover, based on Ghosh and Padgett (2010), the effect of corrosion (exposure to chlorides from deicing salts) on the substructure may affect the seismic response of a bridge. Accordingly, the bridge fragility (see Equation (2.21)) varies with time as follows

$$P\left[DS \mid PSA_i\right](t) = \Phi\left[\frac{1}{\beta_c(t)}\ln\left(\frac{PSA_i}{A_{DS}(t)}\right)\right] \tag{2.22}$$

where t is the time.

Unfortunately, general approaches considering multiple categories of bridges based on different typologies and geometries (such as the categories included in HAZUS) and subjected to the effect of pier corrosion are still missing.

Finally, the annual probability of structural failure $P_{CD,i}(t)$ (which is defined as the probability of complete damage) is

$$P_{CD,i}(t) = P[CD \mid PSA_i](t) \times P[PSA_i \mid SS_i] \times P(SS_i) \tag{2.23}$$

where $P[CD|PSA_i]$ is the probability of having structural failure (complete damage) given a specific PSA_i, and $P[PSA_i|SS_i]$ is the probability of having a specific PSA_i given the occurrence of seismic scenario SS_i. Given a specific seismic scenario, HAZUS evaluates the probability of having structural damage by means of a set of attenuation functions accounting for the bridge typology and its minimum distance between the earthquake rupture and the bridge.

The identification of seismic scenarios to be considered depends on the desired accuracy level for the analysis. However, for those areas in which it is widely known that the risk level is low, the benefit from more detailed analysis is negligible (Seville and Metcalfe 2005).

2.3.2 RISK COMMUNICATION AND STRUCTURAL REDUNDANCY

Quantitative risk assessment requires a further estimation of potential risks arising from malfunctions in communication among different risk managing parts (CIB 2001). In fact, when it is recognized that, due to one hazard-induced event, a malfunction or

even the partial failure of a structure occurs, the communication of the updated risk becomes a crucial aspect to be considered in order to guarantee the protection and the safety of the public.

It is widely known that the main goal of having a high level of redundancy in a structural system yields a greater chance to provide warning of failure before collapse. Therefore, the implementation of redundancy into risk assessment is fully justified. According to AASHTO (2007), multiple-load path and continuous structures should be used unless there are compelling reasons not to use them. Moreover, AASHTO (2007) recognized the importance of redundancy (referring to Frangopol and Nakib 1991) by implementing a load modifier coefficient η_R which is intended to change the intensity of the load effects for each specific limit state.

If a structure is under partial failure or malfunction, the redundancy level of the structural system becomes crucial in reducing the risk associated with a potential sudden collapse. In fact, the optimal communication of the actual risk may prevent the increase of potential consequences (e.g., losses of lives and additional structural damage). For this reason, the risk modifier coefficient $RMC(t)$ is introduced in order to relate a high level of redundancy in a structure with a limitation of risk arising from potential miscommunication among the parts managing and/or using the structure. Table 2.1 shows the values of such coefficients associated with different ranges of annual reliability and redundancy indices. It is assumed that the maximum decrement of risk (20%) is reached only if the system is highly redundant ($RI > 1250$) and its reliability index is at least 3.5. Conversely, the maximum increment of risk (20%) is only reached when the level of redundancy is very low ($RI \leq 10$). The associated

ranges for the annual reliability and redundancy indices are defined based on engineering judgment and safety considerations. However, if further studies are developed and validated (for instance, by means of collecting field data, which are usually unavailable for long-term predictions), these values could be calibrated and implemented in the proposed approach.

The definition expressed by Equation (2.9) is the one used for the annual redundancy associated with the assessment of risk due to live loads. Moreover, according to Stein *et al.* (1999), a risk adjustment factor is introduced when assessing risk due to scour. This coefficient quantifies the effect of redundancy in case of scour with respect to the typology of the superstructure (simple span or continuous girder) and foundation.

2.3.3 EVALUATION OF THE CONSEQUENCES

The consequences associated with the failure or malfunction of a bridge can be dramatically high. The rebuilding of a structure is, in general, very expensive, but the loss of functionality that can affect the surrounding area in terms of damage to the quality of the environment and economic losses, among others, may yield much higher costs.

If the consequences are evaluated in terms of monetary values, the forecast of future risk must consider the dependency of future monetary losses on the present value of consequences. Starting from the year of construction, the value of consequences for each specific year t can be calculated as follows

$$FV(t) = PV(1+r)^t \tag{2.24}$$

where $FV(t)$ is the future monetary value referred to year t, PV is the present monetary value, and r represents the annual discount rate of money. The discount rate is assumed to be a random variable. Using Equation (2.24), the obtained values of the consequences are associated with the specific year for which risk needs to be evaluated.

Among other factors (some of them not easily quantifiable), and based on Stein *et al.* (1999), the most common costs associated with a bridge failure for a specific year t are:

1. Rebuilding costs $C_{Reb}(t)$: related to the cost of the bridge per square meter of deck surface

$$C_{Reb}(t) = c_{Reb} WL(1+r)^t \tag{2.25}$$

where c_{Reb} is the rebuilding cost per square meter (USD/m^2), W is the bridge width (m), and L represents the bridge length (m).

2. Running costs $C_{Run}(t)$: based on the length of the detour that users are forced to follow in the case of bridge closure. A general approach considering different types of vehicles is (Stein *et al.* 1999)

$$C_{Run}(t) = \left[c_{Run,car}\left(1 - \frac{T}{100}\right) + c_{Run,truck}\frac{T}{100} \right] D_l A(t) d(1+r)^t \tag{2.26}$$

in which $c_{Run,car}$ and $c_{Run,truck}$ are the average costs for running cars and trucks per kilometer (USD/km), respectively, D_l is the net length of the detour (km), $A(t)$ is

the average daily traffic (ADT) referred to year t, d is the duration of the detour (days), and T represents the ADTT (%). The duration of the detour is estimated upon considering that in regions where the implication of economic loss is high the repair time is shorter. The time needed to restore the bridge functionality is assumed to be: 36 months for ADT ≤ 100; 24 months for 100 < ADT ≤ 500; 18 months for 500 < ADT ≤ 1,000; 12 months for 1,000 < ADT ≤ 5,000; and 6 months for ADT > 5,000. Given that the ADT is increasing over time, costs are expected to grow over time.

3. Time loss costs $C_{TL}(t)$: associated with time loss for users and goods traveling through the detour (based on Stein *et al.* 1999)

$$C_{TL}(t) = \left[c_{AW} O_{Car} \left(1 - \frac{T}{100} \right) + \left(c_{ATC} O_{Truck} + c_{goods} \right) \frac{T}{100} \right] \frac{D_l A(t) d}{Sp} (1+r)^t \qquad (2.27)$$

where c_{AW} is the average wage per hour (USD/h), c_{ATC} is the average total compensation per hour (USD/h), c_{goods} is the time value of the goods transported in a cargo (USD/h), O_{Car} and O_{Truck} are the average vehicle occupancies for cars and trucks, respectively, and Sp represents the average detour speed (km/h). AASHTO (2003) provides a detailed estimation of the value of time loss associated with cars and trucks.

The accounted direct consequences are given by the rebuilding costs, while indirect consequences include the running costs and the time loss costs. Other types of indirect consequences, such as loss of jobs or money loss in local economy, may be quantified and accounted for in risk assessment. However, in this chapter, only the

consequences listed above are included and general guidelines applicable to more complex scenarios are provided. In order to perform a probabilistic evaluation, economic consequences are treated as random variables.

2.3.4 TIME-DEPENDENT TOTAL RISK

The proposed definition of time-dependent total risk is based on time-dependent probability profiles for multi-hazard analysis and includes the effects of structural redundancy considering epistemic and aleatory uncertainties.

Usual practice, adopted for the assessment of total risk induced by multi-hazard effects (Seville and Metcalfe 2005, among others), considers the summation of the individual risks associated with different exposures. Therefore, the time-dependent total direct $R_D(t)$ and indirect $R_{ID}(t)$ risks for a specific year t are

$$R_D(t) = \sum_{j=1}^{t}\left[\sum_{i=1}^{n}\left\{\left[N_C \times C_{D,ij}\right]\times RMC_{ij} \times f_{ttf,ij}\right\}\right] \tag{2.28}$$

$$R_{ID}(t) = \sum_{j=1}^{t}\left[\sum_{i=1}^{n}\left\{\left[N_C \times C_{ID,ij}\right]\times RMC_{ij} \times f_{ttf,ij}\right\}\right] \tag{2.29}$$

where N_C is the epistemic uncertainty coefficient referring to the consequences, C_D and C_{ID} are the monetary values associated with direct and indirect consequences (USD), respectively, *RMC* is the risk modifier coefficient, which is given by Table 2.1 when considering live loads, and by the risk adjustment factor (Stein *et al.* 1999) for scour, f_{ttf} represents the PDF of the time-dependent failure probabilities, i is the potential hazard type, and j is the time (years).

Finally, the time-dependent total risk $R(t)$ for a specific year t is given by

$$R(t) = R_D(t) + R_{ID}(t) \tag{2.30}$$

The influence of indirect risk on total risk provides indications on the socio-economic importance of the bridge under investigation. In order to investigate such importance, the normalized indirect risk index ($NR_{ID}(t)$) is introduced as follows (see Baker *et al.* 2008)

$$NR_{ID}(t) = \frac{R_{ID}(t)}{R_D(t) + R_{ID}(t)} \tag{2.31}$$

A high value of $NR_{ID}(t)$ means that a potential bridge closure can cause high indirect consequences, even higher than direct ones.

Once vulnerabilities, redundancy indices, and consequences are evaluated, a simulation based on a Latin Hypercube (McKay, Conover and Beckman 1979) sampling is executed by the software MATLAB (The MathWorks 2011). This simulation also accounts for the calculation of the consequences in order to obtain the profiles of the time-dependent total risk (Equation (2.30)) and of the normalized indirect risk index (Equation (2.31)).

2.4 CASE STUDY: AN EXISTING HIGHWAY BRIDGE

The proposed framework for the assessment of risk is applied to an existing highway bridge located near Wausau (Wisconsin, USA), crossing the Wisconsin River and carrying the northbound of US-51 and I-39. This bridge is a five-span continuous steel girder with RC deck (Figure 2.2(a,b)). It is symmetrical about the third mid-span and

has a total length of 195 m, the maximum span is 42.66 m and the distance between the girders is 2.74 m. The girders are composite with the deck and have compact sections (the dimensions of the critical cross-sections are shown in Figure 2.2(c)). The description and the monitoring data of this bridge are provided in Mahmoud, Connor and Bowman (2005).

Time-dependent direct, indirect, and total risks are computed including aleatory and epistemic uncertainties in a multi-hazard context. The highway bridge under investigation is assumed to be subjected to hazards associated with live loads, environmental attacks, scour, and earthquakes. All the profiles are obtained assuming that retrofit or maintenance actions have never been taken during the considered time horizon of 80 years.

The software MATLAB (The MathWorks 2011) provides the backbone of the computational platform and it is used for the required simulations for evaluating the time-dependent total risk. The computational platform includes three other programs: SAP2000 (CSI 2009), RELSYS (Estes and Frangopol 1998), and HAZUS (FEMA 2009a).

2.4.1 ANNUAL FAILURE PROBABILITY EVALUATION

2.4.1.1 Live loads

For the considered highway bridge, which is subjected to live loads and corrosion, the proposed procedure for the evaluation of the annual failure probabilities associated with the system failure and the exceedance of the yielding limit state (first yielding) in the superstructure as part of risk assessment, as shown in Figure 2.3(a).

Hazard given by live loads combined with the presence of corrosion affecting the deck steel reinforcement and the steel girders is modeled and investigated. Typical girder cross-sections are of three types: S 1-1 at mid-span of first and fifth spans; S 2-2 at supports; and S 3-3 at mid-span of second, third, and fourth spans, as shown in Figure 2.2(b,c). The flexural failure mode for each critical cross-section of the steel girders is investigated by making use of limit state functions of Equations (2.14) and (2.15). Similarly, the flexural failure mode of the deck for negative bending moment (which is the most critical failure mode) is investigated by Equation (2.13).

The probabilistic evaluation of the capacities (ultimate $M_{u,ij}$ and yielding moment $M_{y,ij}$) of the three cross-section types has been performed for internal and external girders. The involved random variables are listed in Table 2.1. A finite element analysis has been carried out by using the program SAP2000 (CSI 2009) in order to obtain the envelop of the bending moments affecting internal and external continuous steel girders and by following the guidelines provided by AASHTO (2007). The dependency of loads and capacities on time is provided by the application of the corrosion and the live load model (Type I largest extreme value probability distribution). For each year of the assumed bridge lifetime (80 years), mean values and standard deviations of capacities and acting bending moments (due to dead and live loads), and their correlations at each critical cross-section are obtained by fitting (with a log-normal PDF) the simulated Latin Hypercube sampling (50,000 trials). Besides, given the above and including the epistemic uncertainties, the annual system reliability can be evaluated assuming that the collapse of any girder is reached only when any of the failure mechanisms (i.e., failure of any span) of Figure 2.4(a) occurs. The collapse

of a girder is provided by the series-parallel system (System I) shown in Figure 2.4 (b) considering different limit state equations for each plastic hinge and their correlations. Meanwhile, the collapse of the bridge superstructure is assumed to occur when any two adjacent girders collapse or when the deck fails (System II in Figure 2.4(c)). Furthermore, the probability of exceeding the yielding limit state (first yielding) in the system is modeled as a series system in which the limit states of all the 36 critical cross-sections of the four girders are considered as a series system. The model used for redundancy is based on failure of any two adjacent girders (System III of Figure 2.4(d)). These annual system probabilities (failure and occurrence of first yielding) are evaluated by the reliability program RELSYS (Estes and Frangopol 1998). Figure 2.5 shows the profiles of annual reliability associated with bridge superstructure failure $\beta_{f,sys}$ (see Figure 2.5 (a)); four-girder system failure $\beta_{f,4g}$, exceedance of the yielding limit state (first yielding) $\beta_{y,4g}$, and deck failure β_{deck} (see Figure 2.5(b)); and the profiles of annual failure probability associated with bridge failure $P_{f,sys}$ (see Figure 2.5(c)); four-girder system failure $P_{f,4g}$, deck failure P_{deck}, and exceedance of the yielding limit state (first yielding) $P_{y,4g}$ (see Figure 2.5(d)). Figure 2.5(a,c) shows the separate effects on reliability and probability profiles obtained by considering only the variation of live loads $(\beta_{f,sys})_{LL}$, $(P_{f,sys})_{LL}$ (variation over time of the live loads plus dead loads) and the effect of corrosion on reliability and probability profiles associated with the initial value of the live loads $(\beta_{f,sys})_{CORR}$, $(P_{f,sys})_{CORR}$. Point A (Year 50) represents the time after which the effects due only to corrosion become more significant than those due only to the variation of live loads over time. This is explained by the fact

that corrosion effects are delayed until the time of corrosion initiation of the deck (see Equation (2.17)).

2.4.1.2 Scour

Flood-induced events may affect the highway bridge under investigation by means of scour of the piers and severely affect the integrity of the structure. The general approach used for the assessment of risk due to scour is shown in Figure 2.3(b).

The first step is to download the NBA text file (FHWA 2009) and identify the necessary information for the considered bridge. Such information is obtained by reading and decoding the NBI items (26, 27, 42, 43, 49, 52, 71, and 113) according to FHWA (1995). Table 2.3 summarizes the selected NBI items to be used for this assessment and their explanations. The second step is the characterization of the crossed river based on the USGS (2003), which reports the characteristics of the streams of Wisconsin. By selecting the Wisconsin River at the station of Rothschild (which is the closest site to the bridge), the discharge at the selected flood frequency Q_{100} (58,400 ft^3/sec) is evaluated by using the USGS regression equations (USGS 2003). The third step consists of the evaluation of the probabilities of the river being in specific dimensionless depth ranges. USGS (2010) provides the necessary water data such as the daily mean and median discharge (evaluated over the period 1944–2008) of the Wisconsin River at the station of Rothschild, which are 3,490 ft^3/sec and 2,818 ft^3/sec, respectively. Assuming that Q_{100} is equal to the discharge at full flow, the dimensionless depths are associated with the dimensionless discharges by using Equation (2.18). Furthermore, assuming that the river discharge is log-normally

distributed, the annual probabilities of the river being in specific dimensionless depth ranges are obtained by the evaluation of specific percentiles for each dimensionless depth range (see Table 2.4). The fourth step consists in the evaluation of the scour vulnerability of the bridge for specific dimensionless depths ($P[SV$ and $DD]$ of Equation (2.19)). NBI item 113 indicates category 5 (FHWA 1995), therefore 'bridge foundations are determined to be stable for calculated scour conditions; scour within limits of footing or piles.' The annual failure probabilities ($P[F|SV$ and $DD]$ of Equation (2.19)) associated with scour vulnerability and dimensionless depth ranges are empirically provided by Stein *et al.* (1999) and shown in Table 2.4. Finally, the fifth step is the evaluation of the annual failure probability $P_{f,SC}$ of the bridge, given the scour vulnerability for each dimensionless depth range by using Equation (2.19). As FHWA (2009) provides bridge data for all the years since 1992, in order to estimate the annual failure probabilities for an overall period of 80 years (the assumed lifetime of the bridge), predictions on the failure probabilities associated with years before 1992 and after 2009 are required. Hence, Table 2.4 shows also the assumed annual failure probabilities associated with the dimensionless depth ranges in the case of having scour vulnerability of category 6 (for time interval 1961–1991) and 4 (for time interval between 2010 and the end of the lifetime).

Such annual failure probabilities are considered as log-normally distributed random variables with an assumed coefficient of variation equal to 20% in order to account for epistemic uncertainties. Figure 2.6(a) shows the profiles of the annual failure probability (mean $\mu(P_{f,SC})$ and mean plus one standard deviation $\mu(P_{f,SC})+\sigma(P_{f,SC})$). It can be noted that the annual failure probability is known for the

interval time between 1992 and 2009; for years before 1992 and after 2009 the profiles are predicted.

2.4.1.3 Earthquakes

The effects due to earthquakes combined with the presence of corrosion affecting the substructure are investigated by means of the combined use of the 2009 Earthquake Probability Mapping (USGS 2009) and the software HAZUS (FEMA 2009a). The flowchart of the developed method is shown in Figure 2.3(c).

In order to characterize the seismic vulnerability of the region in which the bridge is located, a discretization of such region in sub-regions is introduced. The proposed approach quantifies the seismic vulnerability of the bridge by investigating the effects of a limited set of scenarios for each defined sub-region. The bridge seismic vulnerability is then obtained by evaluating the mean and standard deviation of the effects induced by each scenario (associated with each sub-region) on the bridge. As shown in Figure 2.7, a grid defined by 49 points discretizes the region in square sub-regions of 900 km^2. The highway bridge is located at the center of this grid. By making use of the 2009 Earthquake Probability Mapping (USGS 2009), for each circular area (which has a radius of 17 km) associated with each point of the grid, the annual probability of occurrence of a seismic scenario ($P(SS_i)$ of Equation (2.20)) is evaluated for each of the considered magnitudes (discrete magnitudes 6, 6.5, and 7 have been selected for this analysis). According to the US seismicity map for the state of Wisconsin, the occurrence probabilities of the selected seismic scenarios are extremely low. Next, for each point and for a specific year, different runs of HAZUS

associated with magnitudes 6, 6.5, and 7 are performed, and the results recorded. Afterwards, by using Eq (2.23), the annual probabilities of having complete damage are evaluated considering all the scenarios for each sub-region. Finally, by calculating the mean and standard deviation of the annual probability of having complete damage, the seismic vulnerability of the highway bridge for a specific year is obtained.

Given that this region has a homogeneous seismicity hazard, the above-introduced method guarantees acceptable approximate results. If the distance between different points of the grid was smaller, the results would become more accurate. However, in case of regions in which one or more important faults determine discontinuity on the maps, the applied method can provide acceptable results only if the number of simulated earthquakes increases significantly.

As reported by Ghosh and Padgett (2010), due to corrosion of the steel reinforcement of the piers and of the anchor bolts fixing the bearings, the mechanical properties of the substructure deteriorate over time. According to Ghosh and Padgett (2010), it is possible to account for such variation making use of fragility curves, by changing the mean and the dispersion of the system fragility parameters for the four damage states considered and for different points in time. Therefore, the default fragility curve parameters implemented in the program HAZUS are adjusted in order to perform different analyses over time. HAZUS default fragility parameters are used while assessing the bridge vulnerability at Year 0. When assessing vulnerability for years 20, 40, and 80, HAZUS default fragility parameters are scaled based on the variations found by Ghosh and Padgett (2010).

By fitting the evaluated mean values and standard deviations of the annual probabilities (at years 0, 20, 40, 60, and 80) with a third order polynomial equation, the associated prediction profiles can be obtained. Figure 2.6(b) shows the profiles of the mean $\mu(P_{CD})$ and the mean plus one standard deviation $\mu(P_{CD})+\sigma(P_{CD})$ of the probability of having complete damage.

2.4.2 REDUNDANCY, HAZARD FUNCTION AND TIME-DEPENDENT PROBABILITIES

The hazard function profiles (Equation (2.5)) and the annual redundancy index *RI* profiles associated with the flexural capacity (Equation (2.9)) of the superstructure are computed (Figure 2.8(a,b), respectively) based on the annual bridge vulnerability. It can be noticed that the hazard function of scour is always greater than that associated with live loads. The hazard function associated with earthquakes is almost constant with respect to time and much lower than those associated with the other two hazards. As shown in Figure 2.8(b), the redundancy profile associated with flexural failure mode (due to live load effects) is decreasing over time.

The profiles of the time-dependent failure probability associated with hazard induced by live loads $TDP_{f,sys}$ (Figure 2.9(a)), scour $TDP_{f,SC}$ (Figure 2.9(b)), and earthquakes TDP_{CD} (Figure 2.9(c)) are obtained by applying Equation (2.4). Accordingly, it is shown that the most critical effects are associated with scour.

By using the least squares method (Equation (2.7)), each time-dependent probability profile (cumulative) may be fitted with the CDF of the Weibull function. This procedure is justified by the fact that the obtained sum of squared residuals is

very low (i.e., less than 10−3), thus the fitting process is acceptable. Figure 2.9(d) shows the PDFs of the Weibull functions associated with each type of hazard. It can be noticed that these PDFs provide an estimation of the time-to-failure probability associated with each type of hazard. Moreover, Figure 2.9(d) shows that, without the implementation of the consequences, the most critical hazard is scour, because it reveals that the mode of the time-to-failure of the bridge is at year 38, which is less than those of the other two considered hazards.

2.4.3 EVALUATION OF CONSEQUENCES

Direct and indirect consequences due to a potential structural failure are evaluated according to Equations (2.25), (2.26), and (2.27). The inclusion of the ADT changing with time as indicated by Mahmoud, Connor and Bowman (2005) and of the annual discount rate lead to the evaluation of consequences that vary over time. A stochastic assessment of such consequences is conducted based on the assumed random parameters shown in Table 2.5. The costs in Table 2.5 refer to the year 2010, which corresponds to the 49^{th} year of life of the bridge. The cost, for the years preceding 2010 are provided by Equation (2.24) by setting a negative time interval *t*, while the cost values for the years following 2010 are obtained by considering the future cost, using a positive time interval t in Equation (2.24).

2.4.4 EVALUATION OF TIME-DEPENDENT TOTAL RISK

Once time-dependent profiles, redundancy profiles, and direct and indirect consequences are computed, the time-dependent total risk can finally be assessed

(Equation 30). In order to account for the randomness associated with consequences and structural vulnerability, a final simulation is required to evaluate consequences and risk for each type of hazard and then the time-dependent total risk is provided. Latin Hypercube (McKay, Conover and Beckman 1979) sampling is selected to simulate 50,000 trials. Although a higher number of trials leads to a more accurate estimate, it has been observed that 50,000 trials converge to an acceptable result. The profiles of the mean value (μ) and the mean value plus one standard deviation ($\mu + \sigma$) are obtained for direct and indirect time-dependent risks associated with live loads $R_{D,LL}$, $R_{I,LL}$ (Figure 2.10(a)), scour $R_{D,SC}$, $R_{I,SC}$ (Figure 2.10(b)), and earthquakes $R_{D,EQ}$, $R_{I,EQ}$ (Figure 2.10(c)). The time-dependent profile for total risk R, and total risks due to live loads $R_{T,LL}$, scour $R_{T,SC}$, and earthquakes $R_{T,EQ}$ are shown in Figure 2.10(d). Moreover, from Figure 2.10(a,b,c), it can be noted that after about 12 years indirect total time-dependent risk becomes greater than the direct one for each considered hazard. This is the consequence of greater indirect costs associated with the increase of ADT over time. The time-dependent total risk is in the order of USD millions. It can be noted that according to the high level of scour bridge vulnerability, risk due to scour always exceeds the risk associated with live loads and corrosion. Obviously, for the Wisconsin region, the seismic risk is negligible. As shown in Figure 2.11(a), it can be noticed that the standard deviation of the time-dependent total risk grows over time due to the increase of uncertainties associated with the prediction of future risk. Finally, Figure 2.11(b) shows the profiles of the mean (μ) and mean plus ($\mu + \sigma$) and minus ($\mu - \sigma$) one standard deviation of the normalized indirect risk index. As indicated, this index increases over time mainly due to increase of the ADT that

induces a potential greater impact of the indirect losses with respect to the direct ones. It also can be noted that the dispersion of the obtained samples (at years 20, 40, 60, and 80) reduces over time, due to the fact that the mean value of the NR_{ID} is reaching values approaching unity. The plateau between years 13 and 22 is due to the variation of the duration of the detour depending on the ADT for the evaluation of running costs (Equation (2.26)) and time loss costs (Equation (2.27)).

2.5 CONCLUSIONS

Risk, redundancy, and reliability are excellent performance indicators to be included in decision-making platforms.

In this chapter, which is based on Decò and Frangopol (2011), a flexible computational approach for assessing the time-dependent total risk as an indicator of the life-cycle performance and as an estimation of the consequences of potential failures has been presented. The computation is managed by using the software MATLAB, which collects the results obtained by other programs (such as RELSYS, HAZUS, and SAP2000), online tools, and databases (such as, the 2009 Earthquake Probability Mapping, NBI database, and the USGS water data). The effects, in terms of failure probabilities and occurrence of consequences of most common hazards (live loads, environmental attacks, scour, and earthquakes) have been investigated. Furthermore, structural redundancy, which can mitigate undesirable effects due to a malfunctioning risk communication process, has been modeled and implemented by introducing a risk modifier coefficient. A high level of system redundancy corresponds to high possibilities of providing warnings of partial or complete failure.

Accordingly, the proposed risk modifier coefficient will reduce and increase risk for redundant and non-redundant structures, respectively.

The following conclusions can be drawn:

1. Using the proposed methodology, the time-dependent total risk of a bridge under multiple hazards, such as, live loads, corrosion, scour, and earthquakes can be reasonably predicted.
2. The interpretation of the results given by the PDFs of the time-to-failure associated with each considered hazard represents a valuable tool for the identification of the most dangerous hazards affecting the bridge under investigation. In the specific case study considered, the hazard associated with scour is the most critical (Figure 2.9(d)).
3. While assessing risk, the level of detail in modeling the effects of a potential hazard must fit the importance of such hazard with respect to total risk. A highly detailed model is needed only for those hazards with significant contributions to the total risk. For instance, in the investigated case study, it has numerically been proven that risk due to earthquakes is negligible (Figure 2.10(d)), therefore for this bridge a low level of detail in modeling the earthquake effects is fully justified.
4. Bridge risk assessment is a process that carries significant epistemic and aleatory uncertainties generated by multiple sources such as the assessment of the bridge vulnerability and the consequences associated with bridge failure or malfunction. The treatment of such uncertainties in modeling the bridge performance over time requires exceptional care. Figure 2.11(a) shows that the dispersion of the time-

dependent total risk increases over time. This is mainly due to the presence of uncertainties that increase over time.

5. The investigation on the normalized indirect risk index provides useful information about the importance of the considered bridge. The effect of a potential failure may have great impact on the economy of the surrounding areas, causing indirect losses to be much greater than the direct ones over time (as shown in Figure 2.11(b)).

The implementation of risk profiles into a life-cycle framework for the optimal maintenance planning is a topic of major interest. Furthermore, decision makers must base their judgments according to the level of risk, and rank different structures for the optimal allocation of funds. Lastly, the implementation of the proposed framework for quantitative risk assessment may also be used for studies on transportation networks.

Table 2.1 Risk modifier coefficient given the annual system reliability and redundancy indices.

Annual redundancy index	Annual system reliability index				
	<2.0	2.0 to 3.5	3.5 to 4.5	4.5 to 6.0	> 6.0
< 10	1.2	1.2	1.2	1.2	1.2
10 to 50	1.1	1.1	1.1	1.1	1.1
50 to 250	1.0	1.0	1.0	1.0	1.0
250 to 1250	1.0	1.0	0.9	0.9	0.9
> 1,250	1.0	1.0	0.8	0.8	0.8

Table 2.2 Parameters of the assumed random variables associated with geometrical and material properties, loads, and corrosion effects for the considered bridge superstructure.

Random variables	Mean	COV	Distribution type	Ref.
Bottom flange yielding stress	345 *MPa*	0.12	LN	COV based on Estes (1997)
Concrete compressive strength	27.6 *MPa*	0.18	LN	COV based on Estes (1997)
Concrete deck thickness	191 *mm*	0.0405	LN	COV based on Estes (1997)
Concrete elastic modulus	26435 *MPa*	0.05	LN	COV assumed
Corrosion initiation time (for top steel reinforcement)	19.07 years	0.273	LN	Estes (1997)
Deck dead load moment	varies (*Nm*)	0.1	LN	COV based on Estes (1997)
Epistemic uncertainty coefficient for load	1	0.11	LN	Ang and de Leon (2005)
Epistemic uncertainty coefficient for resistance	1	0.06	LN	Ang and de Leon (2005)
Girder load moment	varies (*Nm*)	0.08	LN	COV based on Estes (1997)
Live load moment	varies (*Nm*)	varies	Type I Largest	Akgül (2002)
Longitudinal bar diameter	15.88 *mm*	0.015	LN	COV based on Estes (1997)
Railing load moment	varies (*Nm*)	0.1	LN	COV based on Estes (1997)
Steel bar corrosion coefficient	0.0203	0.03	LN	Thoft-Christensen (1998)
Steel bar yielding stress	414 *MPa*	0.11	LN	COV based on Estes (1997)
Steel elastic modulus	210000 *MPa*	0.05	LN	COV assumed
Steel girder corrosion coefficient A	80.2 μm	0.42	LN	Albrecht and Naeemi (1984)
Steel girder corrosion coefficient B	0.593	0.405	LN	Albrecht and Naeemi (1984)
Steel plate thickness	varies (*mm*)	0.015	LN	COV assumed
Steel plate width	varies (*mm*)	0.015	LN	COV assumed
Top flange yielding stress	345 *MPa*	0.12	LN	COV based on Estes (1997)
Transversal bar diameter	19.05 mm^2	0.015	LN	COV based on Estes (1997)
Wearing surface load moment	varies (*Nm*)	0.25	LN	COV based on Estes (1997)
Web yielding stress	345 *MPa*	0.12	LN	COV based on Estes (1997)
	Min.	Max.		
Steel bar corrosion parameter	2 mA/cm^2	3 mA/cm^2	Uniform	Thoft-Christensen (1998)

Note: LN = log-normal distribution; COV = coefficient of variation.

Table 2.3 NBI items used for the assessment of scour effects at year 2009 (FHWA 2009).

NBI Item No.	Description	Value	Meaning given by FHWA (1995)
26	Functional classification of inventory route	11	Principal Arterial - Other Freeways or Expressways
27	Year built	1961	
42A	Type of Service on bridge	1	Highway
42B	Type of Service under bridge	5	Waterway
43A	Kind of Material/Design	4	Steel continuous
43B	Type of Design/Construction	02	Stringer/Multi-beam or Girder
49	Structure length (*m*)	196	
52	Deck width, out-to-out (*m*)	10.7	
71	Waterway adequacy	8	Bridge deck above roadway approaches. Slight chance of overtopping roadway approaches.
113	Scour critical bridges	5	Bridge foundations determined to be stable for calculated scour conditions; scour within limits of footing or piles.

Table 2.4 Annual probabilities of the river being in specific dimensionless depth ranges and annual failure probabilities associated with the dimensionless depth ranges (based on Stein *et al.* 1999).

Annual probabilities	Dimensionless depth ranges				
	0 to 0.25	0.25 to 0.50	0.50 to 0.75	0.75 to 1.00	>1.00
Annual probabilities of the river being in specific dimensionless depth ranges	0.86457	0.13531	0.000122	6.47E-07	7.16E-09
Annual failure probabilities (scour vulnerability = 4)	0.06	0.1	0.15	0.26	0.41
Annual failure probabilities (scour vulnerability = 5)	0.01	0.04	0.08	0.16	0.27
Annual failure probabilities (scour vulnerability = 6)	0.002	0.01	0.03	0.08	0.16

Table 2.5 Statistical parameters of the assumed random variables used for the evaluation of the consequences (all the COV are assumed). The costs refer to their values at year 2010, which corresponds to the 49th year after construction (1961).

Random variables	Mean	COV	Distribution type	References
ADT	732 - 33411	0.20	LN	Mahmoud, Connor and Bowman (2005)
ADTT/ADT ratio	0.12	0.20	LN	Mahmoud, Connor and Bowman (2005)
Average compensation (truck drivers)	26.97 USD/*hour*	0.15	LN	AASHTO (2003)
Average detour speed	50 *km*/*hour*	0.15	LN	Assumed
Average vehicle occupancies for cars	1.5	0.15	LN	Assumed
Average vehicle occupancies for trucks	1.05	0.15	LN	Assumed
Average wage (car drivers)	22.82 USD/*hour*	0.15	LN	AASHTO (2003)
Discount rate	3%	0.15	LN	Assumed
Epistemic uncertainty coefficient for consequences	1	0.15	LN	Assumed
Length of detour	2.9 k*m*	NA	NA	Based on the transportation network
Rebuilding costs	894 USD/m^2	0.20	LN	Stein *et al.* (1999)
Running costs for cars	0.08 USD/k*m*	0.20	LN	Assumed
Running costs for trucks	0.375 USD/k*m*	0.20	LN	Assumed
Time value of a cargo	4 USD/*hour*	0.20	LN	Assumed

Note: LN = log-normal distribution; COV = coefficient of variation; NA = not available.

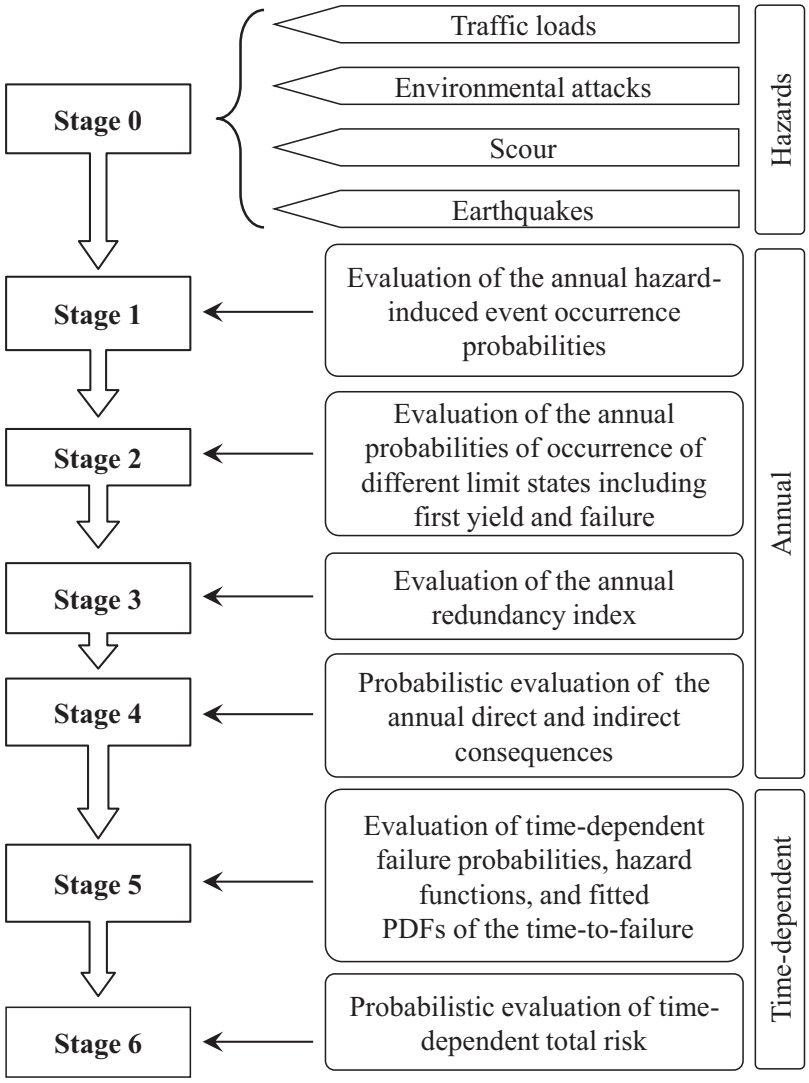

Figure 2.1 General framework for the quantitative assessment of bridge-related risk in a multi-hazard context.

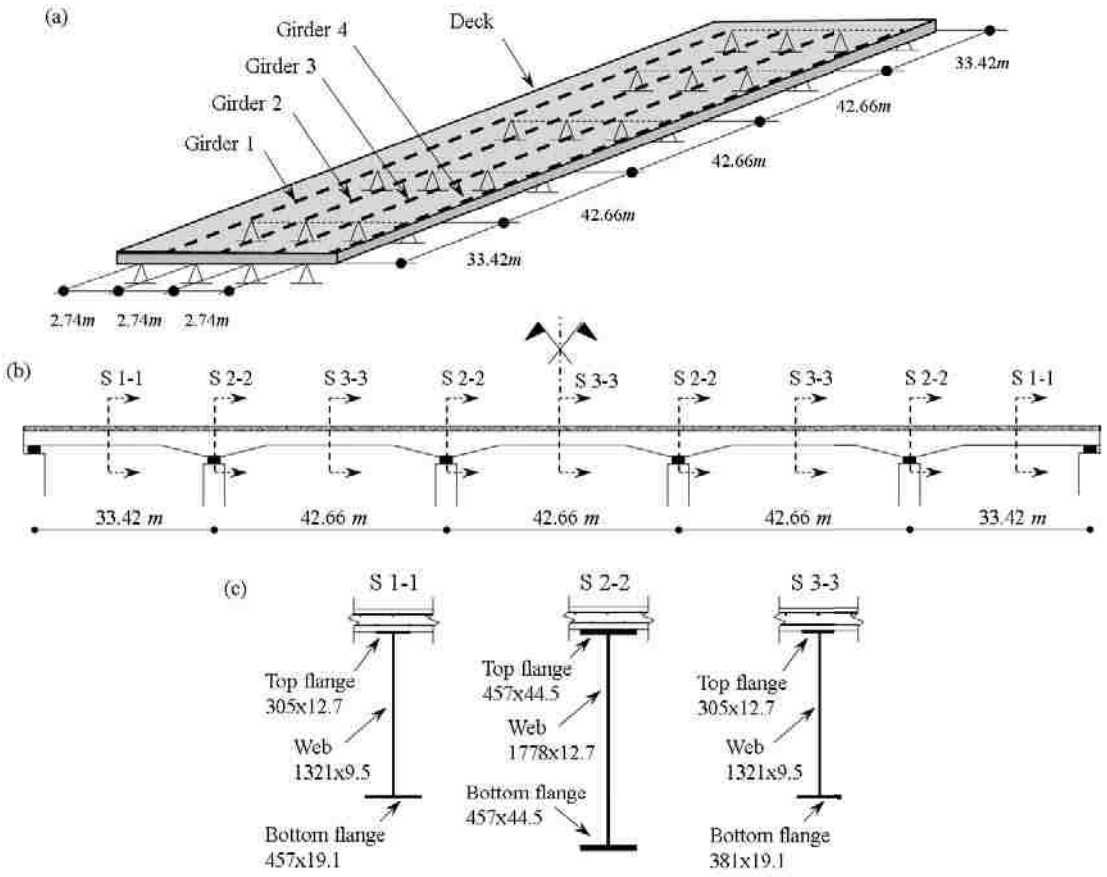

Figure 2.2 Highway bridge: (a) deck and girders, (b) longitudinal cross-section, and (c) three critical cross-sections of the girders with dimensions in mm.

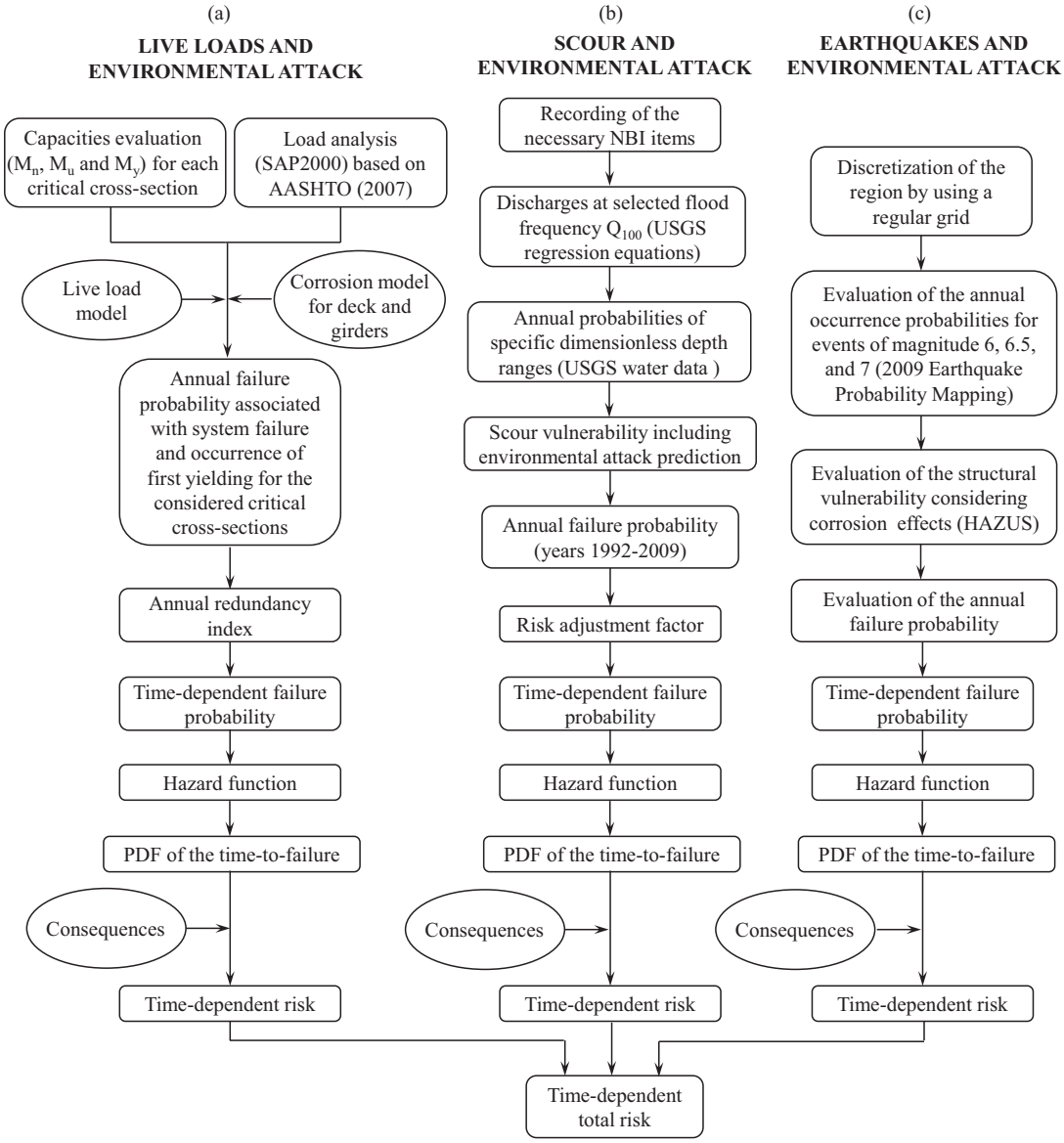

Figure 2.3 General framework for risk assessment of highway bridges subjected to hazard induced by (a) live loads and environmental attack, (b) scour and environmental attack, and (c) earthquakes and environmental attack.

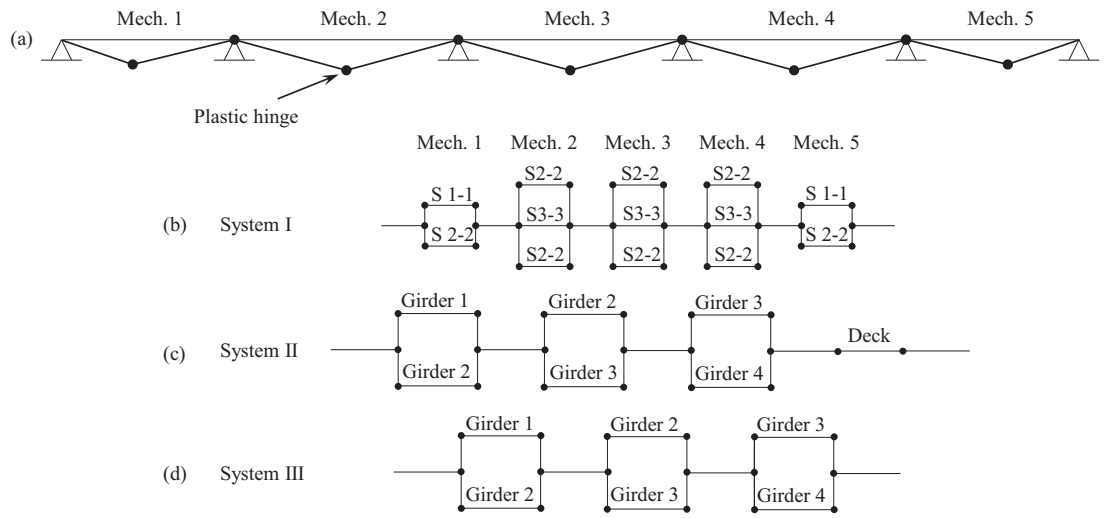

Figure 2.4 (a) Critical failure mechanisms of a single girder, (b) series-parallel system model collapse of a single girder (System I), (c) series-parallel system used for bridge superstructure collapse (System II), and (d) series-parallel system used for the evaluation of bridge redundancy (System III).

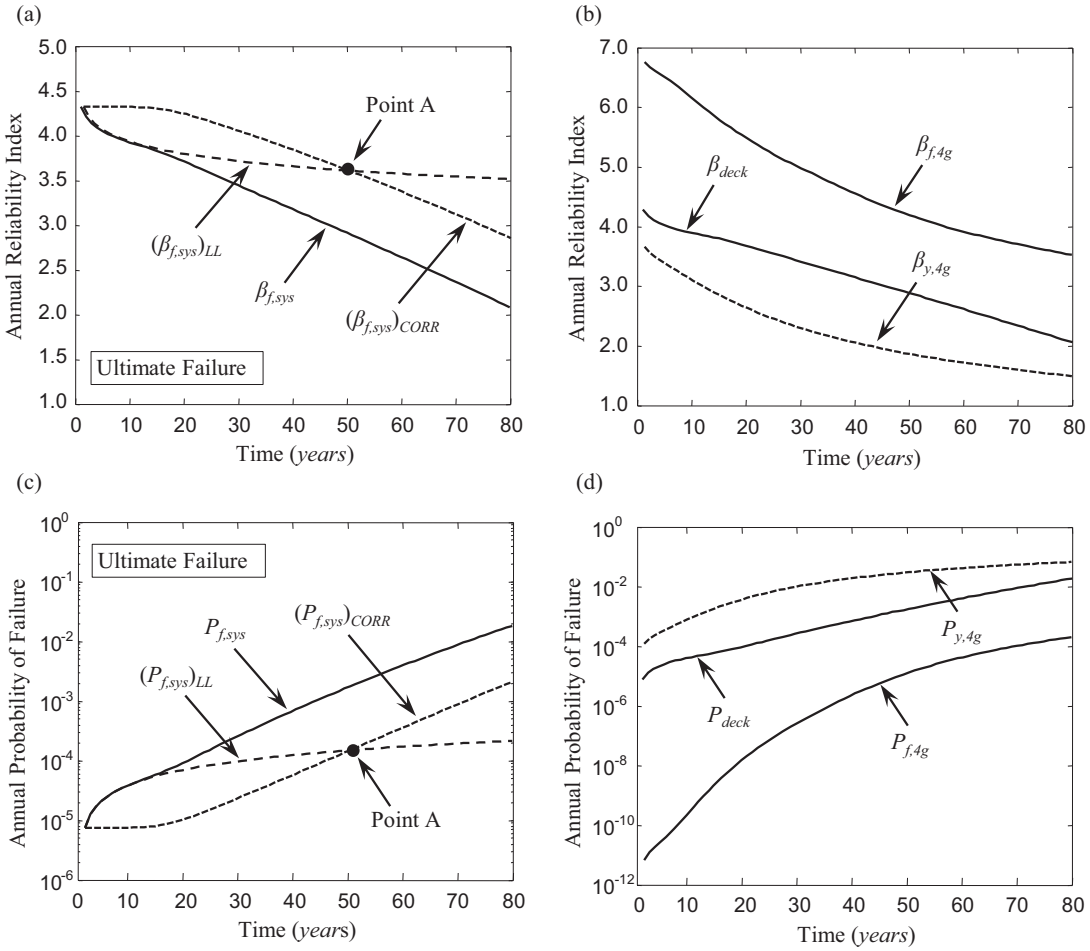

Figure 2.5 Profiles of annual reliability associated with bridge superstructure failure $\beta_{f,sys}$ (a); four-girder system failure $\beta_{f,4g}$, exceedance of the yielding limit state (first yielding) $\beta_{y,4g}$, and deck failure β_{deck} (b); and the profiles of annual failure probability associated with bridge failure $P_{f,sys}$ (c); four-girder system failure $P_{f,4g}$, deck failure P_{deck}, and exceedance of the yielding limit state (first yielding) $P_{y,4g}$ (d). Point A refers to year 50, where the effects on reliability and failure probability profiles induced only by corrosion $(\beta_{f,sys})_{CORR}$, $(P_{f,sys})_{CORR}$ become more severe than the ones due only to the variation of live loads $(\beta_{f,\,sys})_{LL}$, $(P_{f,\,sys})_{LL}$ over time.

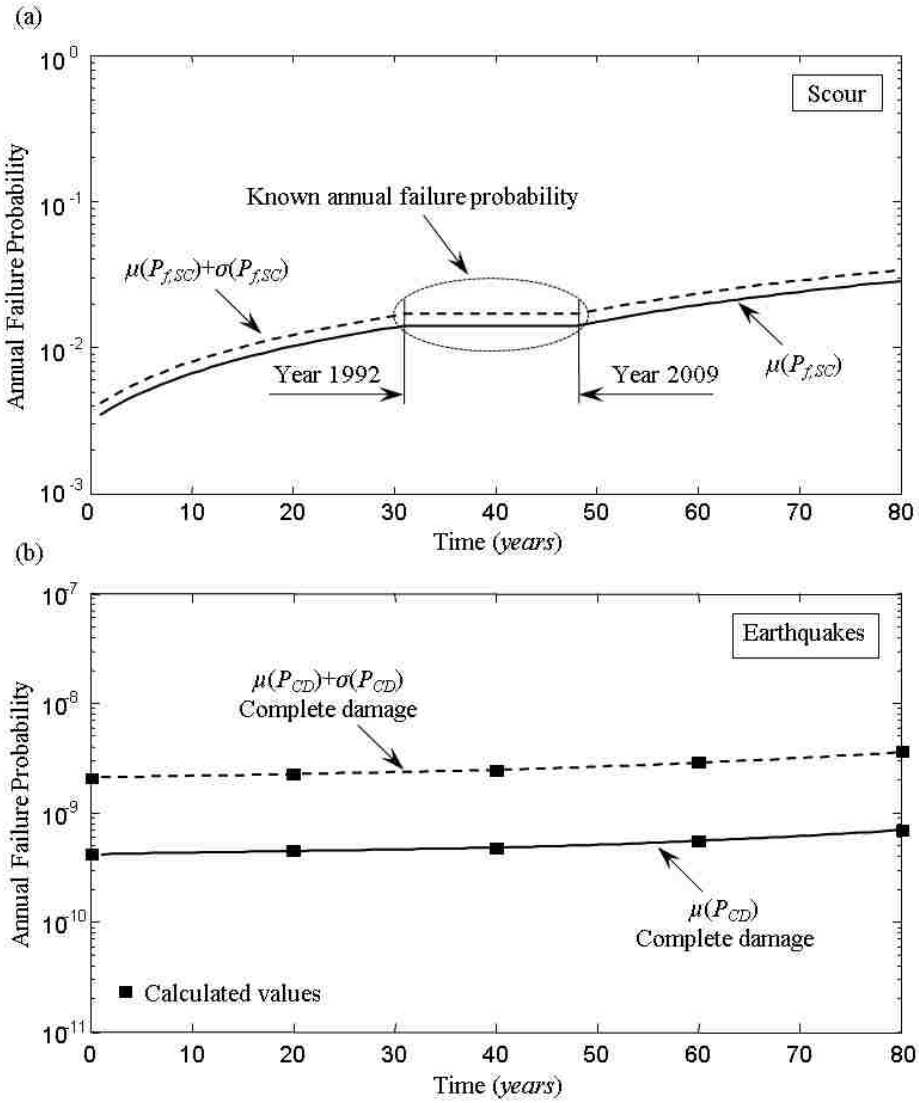

Figure 2.6 Profiles of mean and mean plus one standard deviation of (a) the annual failure probability due to scour, and (b) the annual occurrence probabilities of complete damage due to earthquakes. Scour annual failure probabilities are known for the time interval between 1992 and 2009. The probability profiles associated with complete damage due to earthquakes are evaluated for years 0, 20, 40, 60, and 80. The intermediate values are given by a third-order fitting polynomial equation.

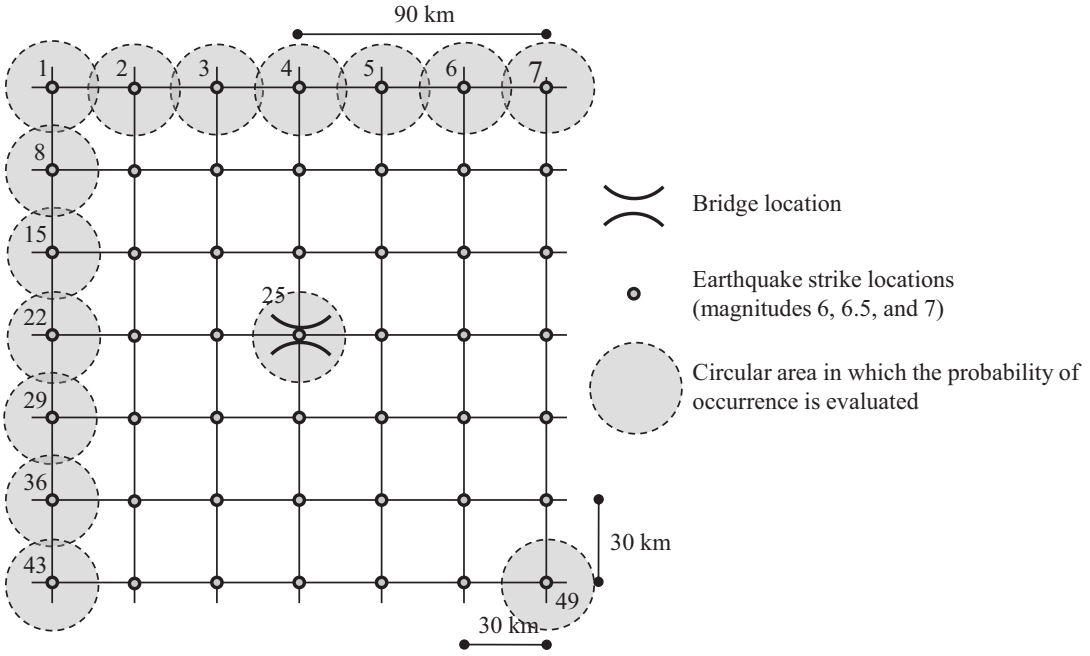

Figure 2.7 Grid for the considered earthquake scenarios (magnitudes 6, 6.5, and 7).

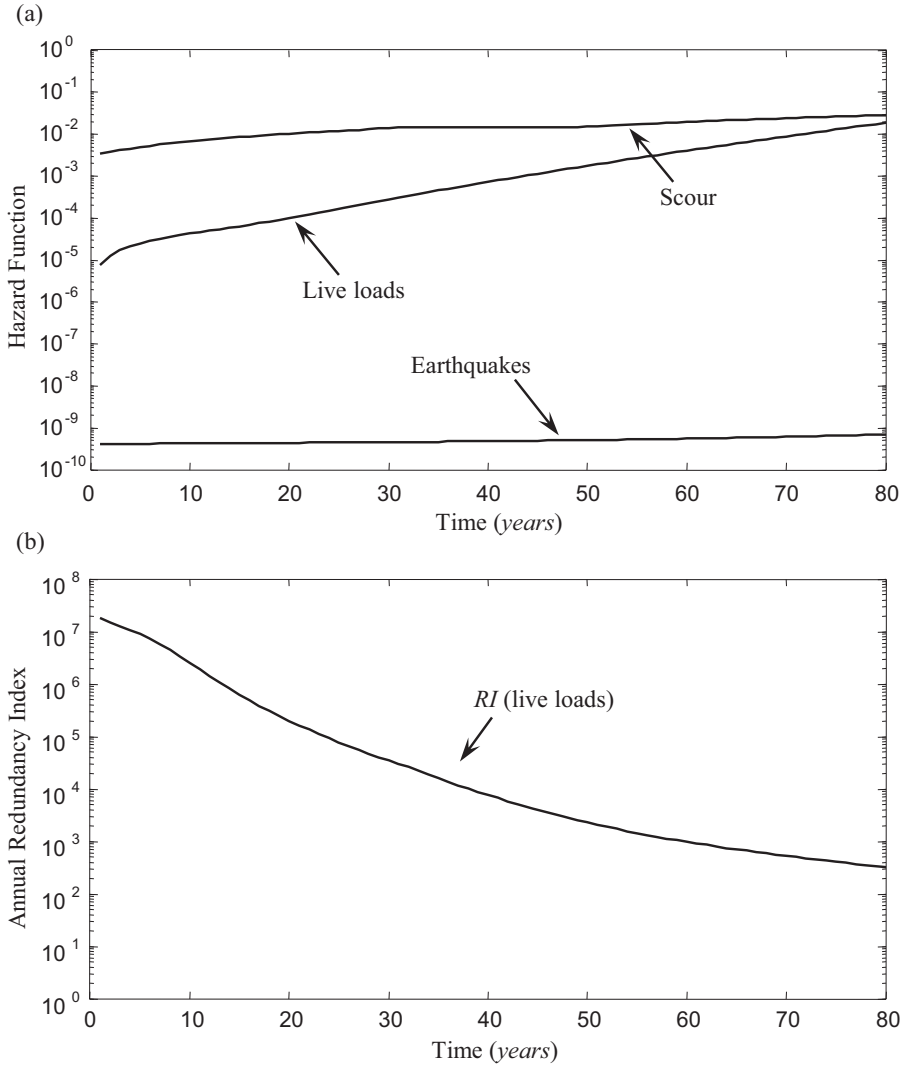

Figure 2.8 (a) Hazard functions associated with the live loads, scour, and earthquakes, and (b) redundancy index profile of the bridge superstructure associated with the effect induced by live loads.

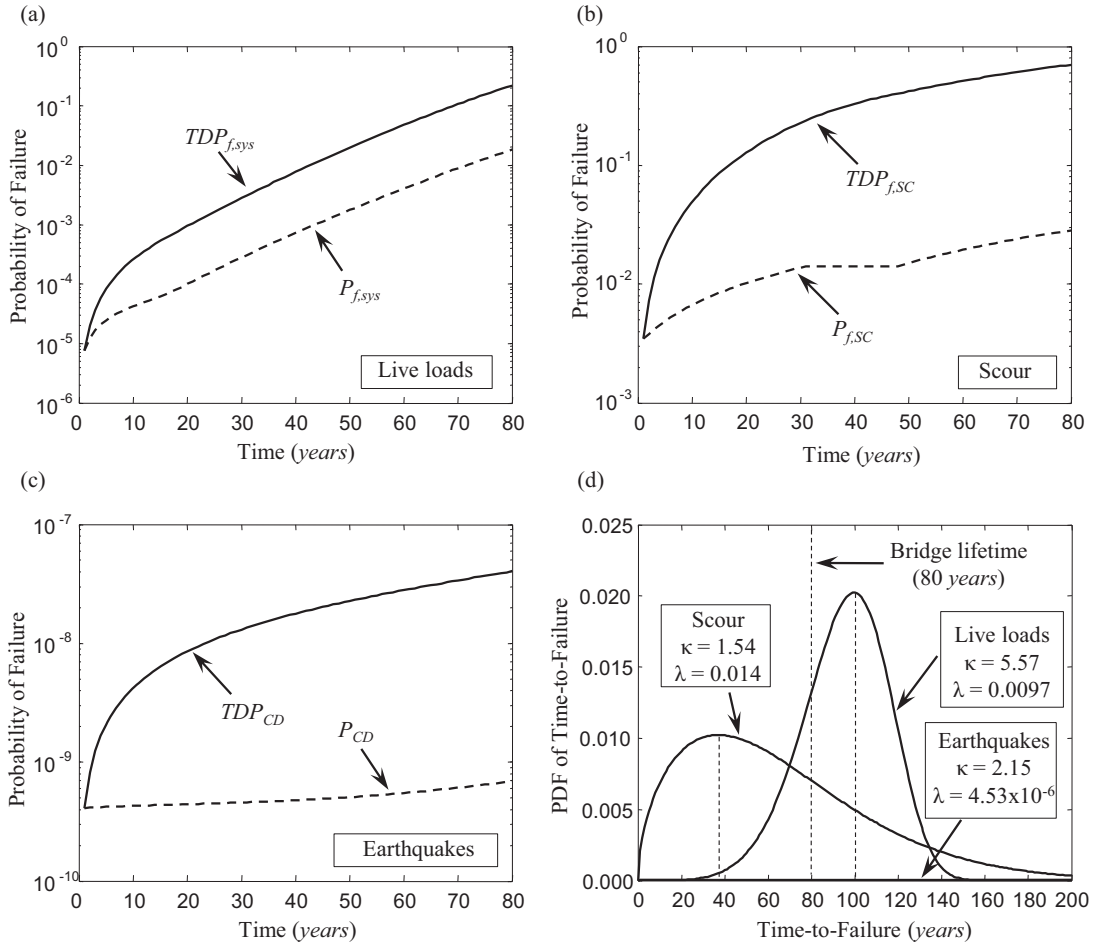

Figure 2.9 Profiles of annual and time-dependent failure probabilities associated with hazards due to (a) live loads $P_{f,sys}$, $TDP_{f,sys}$, (b) scour $P_{f,SC}$, $TDP_{f,SC}$, and (c) earthquakes P_{CD}, TDP_{CD}. (d) PDFs (Weibull functions) of the time-to-failure associated with each hazard.

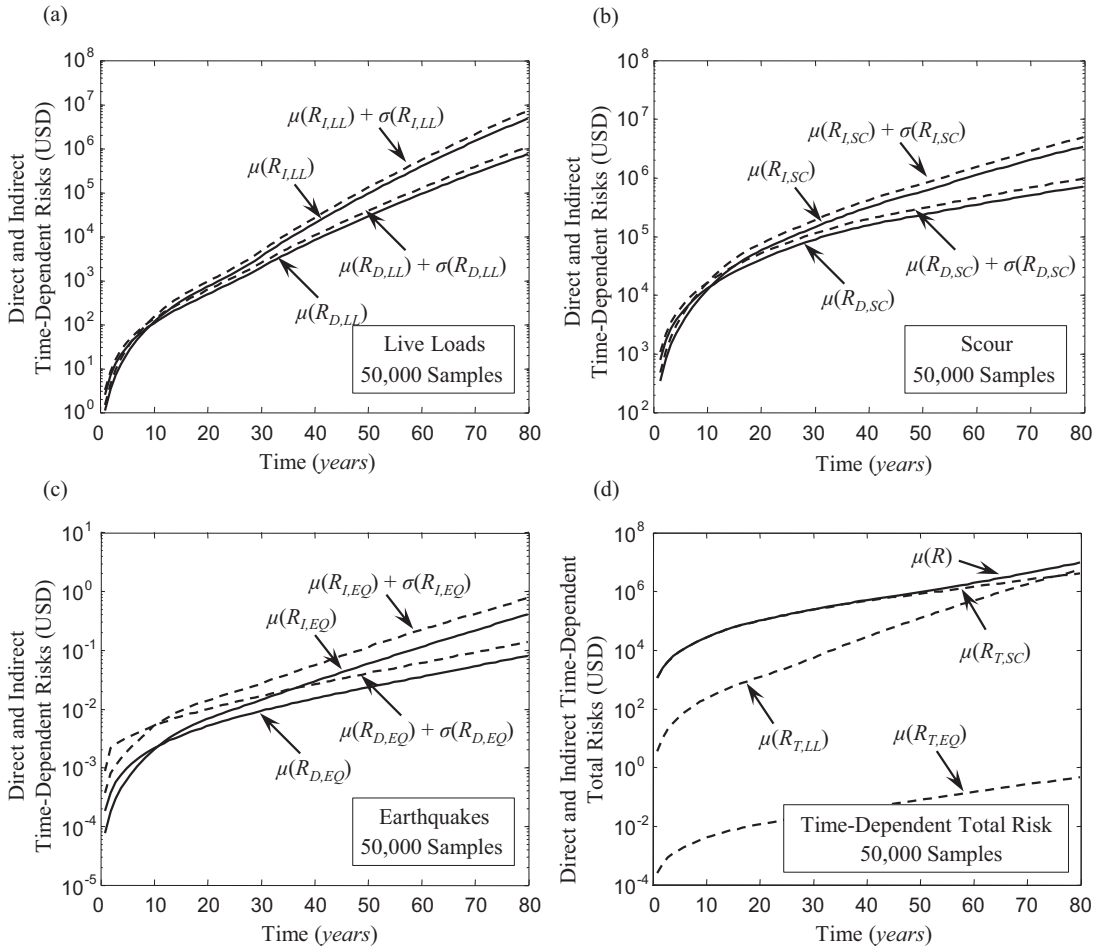

Figure 2.10 Profiles of mean (μ) and mean plus one standard deviation ($\mu + \sigma$) of direct and indirect risks associated with hazards due to (a) live loads $R_{D,LL}$, $R_{I,LL}$, (b) scour $R_{D,SC}$, $R_{I,SC}$, and (c) earthquakes $R_{D,EQ}$, $R_{I,EQ}$, and (d) profiles of mean time-dependent total risk R, and mean total risks for live loads $R_{T,LL}$, scour $R_{T,SC}$, and earthquakes $R_{T,EQ}$.

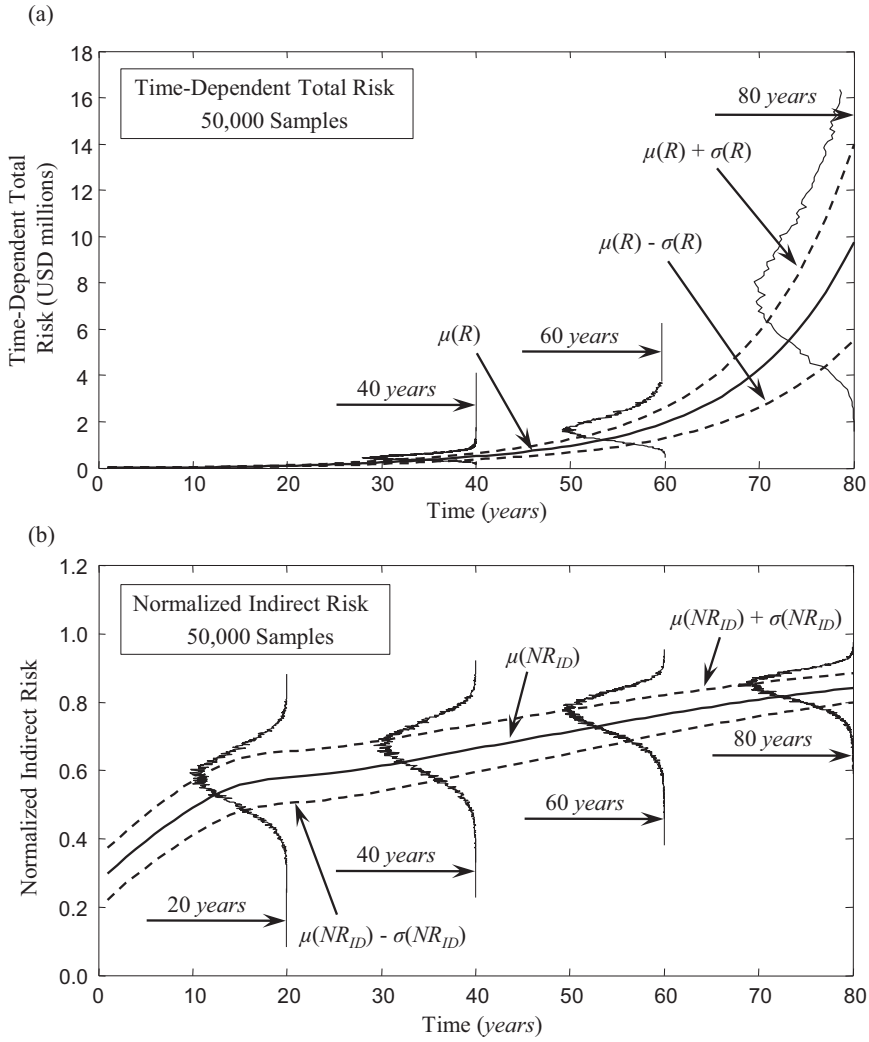

Figure 2.11 Profiles of (a) mean (μ) and mean plus ($\mu + \sigma$) and minus ($\mu - \sigma$) one standard deviation of the total time-dependent risk, and (b) normalized indirect risk index (NR_{ID}).

CHAPTER 3

LIFE-CYCLE RISK ASSESSMENT OF SPATIALLY DISTRIBUTED AGING BRIDGES UNDER SEISMIC AND TRAFFIC HAZARDS

3.1 INTRODUCTION

Life-cycle management of single structures or groups of structures has become an issue of great relevance for many countries, including the United States. Maintenance and retrofit are crucial in preventing excessive deterioration of structural performance over time. Efficient and optimal maintenance strategies must be included in a general framework able to capture the social effects produced by the gained benefit. In this context, life-cycle risk assessment provides a tool that directly relates the effects of potential hazards with the associated consequences. During their designed lifetime, structures and infrastructures are intended to withstand the effects produced by a spectrum of hazards that could generate major safety and serviceability concerns. Transportation networks rely on the serviceability of their single bridges in order to allow users to reach their destinations in a reasonable time.

The aim of this chapter, which is based on Decò and Frangopol (2012) and Decò and Frangopol (2013a), is to provide a probabilistic approach for the assessment of lifecycle risk of a group of aging bridges within a transportation network. Both

structural vulnerability and potential consequences induced by hazards are time-dependent. Bridge vulnerabilities are evaluated with respect to hazards induced by earthquakes and abnormal traffic. Based on the original approach proposed by Cornell (1968) and on the method used by Jones, Middelmann and Corby (2005), the adopted probabilistic seismic hazard analysis is based upon the generation of random earthquakes spatially distributed over a region and having a random magnitude that follows a truncated-exponential relationship. Then, according to Basöz and Mander (1999) and including aging considerations, time-dependent fragility analysis provides the probability of exceeding specific damage states (slight, moderate, extensive, and complete) over time. Time-dependent vulnerability due to traffic, mainly affecting the bridge superstructure, is modeled assuming for each bridge a Weibull distribution of the time-to-failure (Maunsell Ltd.1999). Risk is assessed for different levels of bridge serviceability and, therefore, different consequences are associated with each serviceability level. Direct and indirect consequence analyses include the probabilistic evaluation of the monetary values associated with rebuilding costs, rehabilitation costs, material damage costs, operating costs, time-loss costs, loss of human life costs, and injury costs. Both epistemic and aleatory uncertainties are considered. The profiles of time-dependent direct, indirect, and total risk are developed for each bridge within the network. A simplified method is used to compute the risk associated with a small transportation network.

This chapter develops a rational framework for the quantitative assessment of life-cycle risk of spatially distributed aging bridges under seismic and traffic hazards. Section 3.2 develops the approach for the evaluation of the bridge vulnerability due to

seismic and traffic hazards. Section 3.3 performs the comprehensive consequence analysis. Section 3.4 assesses life-cycle risk of groups of bridges based on the level of serviceability of single bridges within a transportation network. In Section 3.5, a group of existing bridges located north of the San Diego metropolitan area is investigated by applying the proposed approach. Finally, Section 3.6 provides the conclusions of this chapter that is based on a published paper (Decò and Frangopol 2012, Decò and Frangopol 2013a).

3.2 BRIDGE VULNERABILITY UNDER MULTIPLE HAZARDS

The estimation of time-dependent bridge vulnerability is affected by the level of detail required by the type of analysis. When dealing with analyses at the network scale, simplifications must be introduced, and, consequently, the accuracy of the analysis is affected by approximations (Frangopol and Bocchini 2012).

Seismic and traffic hazards affect the whole bridge structure. However, different bridge components are more likely to fail due to different effects that can be caused by specific hazards. For instance, vertical loads (due to traffic hazard) mainly affect the bridge superstructure that mostly involves flexural failure mode (Akgül 2002), while seismic fragility of the bridge is largely dependent on bridge substructure components (columns, abutments, and bearings, according to Padgett and DesRoches (2007) and Ghosh and Padgett (2010)). Therefore, load effects can be analyzed separately for bridge superstructure and substructure, respectively. Moreover, load effects induced by seismic and traffic hazards are considered to be statistically independent since their occurrences are independent.

3.2.1 SEISMIC VULNERABILITY

During the last decade, seismic vulnerability of bridges was a topic extensively studied (Basöz and Mander 1999, Nielson and DesRoches 2007). Fragility analysis of bridges is conducted based on a simulated set of ground motions caused by earthquakes having random magnitudes and random spatial epicenter coordinates over a region (Chang, Shinozuka and Moore 2000, Sánchez-Silva and Rackwitz 2004, Jones, Middelmann and Corby 2005).

3.2.1.1 Probabilistic ground motion

In this study, the assessment of risk relies on simulations of seismic events striking within a considered region. The following steps summarize the adopted procedure to simulate the seismic scenarios:

- *Definition of a set of random seismic events*: a specific number of random earthquake events *EQ*, is generated within the region under investigation.
- *Assignment of a random Richter magnitude M*: according to Cosentino, Ficara and Luzio (1977), depending on the defined seismic region, and during a given time period, the frequency-magnitude relationship can be modeled by adopting a truncated exponential probability density function (PDF) defined as

$$f_{TE}(M) = \begin{cases} \dfrac{\beta \exp\left(-\beta\left(M - M_0\right)\right)}{1 - \exp\left(-\beta\left(M_p - M_0\right)\right)} & \text{for } M_0 \le M \le M_p \\ 0 & \text{for } M < M_0 \quad \text{and} \quad M > M_p \end{cases} \tag{3.1}$$

where M_0 is the threshold magnitude value, M_p is the maximum regional finite magnitude value, and β is a distribution parameter.

- *Assignment of a random location and temporal occurrence for each seismic event*: event coordinates (latitude *Lat* and longitude *Long*) are randomly generated within the considered area. The epicenter coordinates (x and y) of the i-th random earthquake, over the considered square seismic region, are assumed to be random variables triangularly distributed. Moreover, the temporal occurrence of the seismic events is assumed to be uniform distributed over the considered life span.
- *Definition of the characteristics of each generated seismic event*: information regarding earthquake characteristics must be assigned, including rupture geometry parameters (depth, width, and dip angle). Furthermore, earthquake depth is randomly generated following a triangular distribution. The rupture length R_l and width R_w of each seismic event depends on the random magnitude (Wells and Coppersmith 1994)

$$\log(R_l) = a_l + b_l M \tag{3.2}$$

$$\log(R_w) = a_w + b_w M \tag{3.3}$$

where a_l, a_w, b_l, and b_w are coefficients depending on the earthquake characteristics (their values are given in Wells and Coppersmith 1994). Furthermore, the orientation angle of the rupture trace is also considered random for each generated event.

Based on historical data, correlation among epicenter coordinates, depths, and magnitudes is obtained and implemented while generating the random events.

3.2.1.2 Bridge fragility analysis

The distance between the rupture traces of the *i*-th earthquake and the locations of the *j*-th distributed bridge influences the level of expected structural damage. The attenuation relationship proposed by Campbell and Bozorgnia (2007) is implemented while modeling the effect of seismic hazard. The median ground motion model is described by

$$\ln \hat{Y}^j = f_{mag} + f_{dis}^j + f_{flt} + f_{hng} + f_{site}^j + f_{sed}^j \tag{3.4}$$

where $\ln\hat{Y}$ is the natural logarithm of the median value of the peak ground acceleration (*PGA*) or of the response spectra accelerations (*PSA*) for several oscillator periods, f_{mag} is the magnitude term, f_{dis} is the distance term, f_{flt} is the style-of-faulting term, f_{hng} is the hanging-wall term, f_{site} is the shallow site response term, and f_{sed} is the deep site response term. Epistemic uncertainties are accounted for by (Campbell and Bozorgnia 2007)

$$\ln Y_{unc}^j = \ln \hat{Y}^j \pm \Delta \ln \hat{Y} \tag{3.5}$$

where $\ln Y_{unc}$ is the predicted value of $\ln\hat{Y}$ accounting for epistemic uncertainties and $\Delta\ln\hat{Y}$ is the incremental value of the median ground motion due to epistemic uncertainties. All the terms introduced (in Equations (3.4) and (3.5)) and their relevant evaluations are discussed in detail in Campbell and Bozorgnia (2007).

According to Mander (1999), by means of fragility analysis, four curves describing the probability of exceeding specific damage states (slight, moderate, extensive, and

complete) can be developed for each seismic scenario and for each considered bridge. Fragility curves are defined by log-normal cumulative probability functions

$$P\left[DS^j \mid PSA^j\right] = \Phi\left[\frac{1}{\beta_c}\ln\left(\frac{PSA^j}{A_{DS}^j}\right)\right] \tag{3.6}$$

where $P[DS|PSA]$ is the probability of exceedance of a specific damage state DS given a specific PSA (period of 1 sec), β_c is the normalized composite log-normal standard deviation, A_{DS} is the median spectral acceleration associated with the occurrence of the damage state DS, and Φ is the standard normal cumulative distribution function. The approach necessitates bridge data (bridge class, number of spans, skew angle, site class, and year of construction), which can be obtained from the National Bridge Inventory (NBI) (FHWA 2010).

3.2.1.3 Fragility time-dependency

The effect of corrosion on the substructure due to exposure to chloride ions may influence the seismic response of a bridge (Ghosh and Padgett 2010). Life-cycle analysis must account for the potential increase of seismic effects on aged structures. In this context, the bridge fragility depends on the time t at which the simulated earthquake strikes. Thus, Equation (3.6) changes as

$$P\left[DS^j \mid PSA^j\right](t) = \Phi\left[\frac{1}{\beta_c}\ln\left(\frac{PSA^j}{A_{DS}^j(t)}\right)\right] \tag{3.7}$$

where $A_{DS}(t)$ represents the time-dependency of the fragility parameters. General methods accounting for the deterioration process of seismic-sensitive components for

different bridges and deterioration typologies are usually missing in the existing literature. Although this is a formidable task, if further studies are developed and validated (for instance, by means of collecting field data, which are usually unavailable for long-term predictions), the proposed general framework would be able to accommodate such considerations. In the proposed approach, the time-dependent median spectral acceleration $A_{DS}(t)$ associated with the occurrence of a specific damage state of the j-th bridge is assumed to vary in time by following a linear degradation

$$A_{DS}^{j}(t) = A_{DS}^{j}[0] \cdot (1 - t \cdot \gamma) \tag{3.8}$$

where $A_{DS}[0]$ is the original fragility parameter (Basöz and Mander 1999), t is the time, and γ is the aging coefficient. Indications concerning possible values of the aging coefficient can be derived from Ghosh and Padgett (2010), where a reduction of about 30%–40% of the initial fragility parameter was reported in 100 years. The use of a linear degradation law captures the total reduction of the fragility parameters over the bridge's lifetime. However, the adopted degradation law may lead to some approximations that are usually unavoidable for analyses of groups of bridges at the network scale, mainly due to the lack of detail and/or insufficient data (Frangopol and Bocchini 2012).

3.2.2 TRAFFIC-INDUCED VULNERABILITY

In the past, lifetime functions have been developed for bridge life-cycle-related topics (Maunsell Ltd. 1999). For the bridge superstructure, the effects caused by corrosion

processes or general aging phenomena can be accounted for by means of lifetime functions (van Noortwijk and Klatter 2004, Yang, Frangopol and Neves 2004). Accordingly, time-dependent bridge performance with respect to vertical load may be modeled by considering the time-to-failure of the superstructure as a random variable (see Chapter 2). Weibull distribution can be used for the assessment of single bridge superstructures due to the effects of traffic and aging. The PDF and the associated cumulative distribution function (CDF) of the time-to-failure of the superstructure (f_{ttf} and F_{ttf}, respectively) for the j-th bridge are modeled by a Weibull distribution as follows (Leemis 1995)

$$f_{ttf}^{j}(t) = \lambda^{j}\kappa^{j}\left(\lambda^{j}t\right)^{\left(\kappa^{j}-1\right)}e^{-\left(\lambda^{j}t\right)^{\kappa^{j}}} \qquad t \geq 0 \tag{3.9}$$

$$F_{ttf}^{j}(t) = 1 - e^{-\left(\lambda^{j}t\right)^{\kappa^{j}}} \qquad t \geq 0 \tag{3.10}$$

where κ and λ are the shape and scale parameter, respectively, that can be found by statistical inference of observations as shown in previous studies (van Noortwijk and Klatter 2004), or by analyzing bridge failure modes considering the failure of one or more components as described in Yang, Frangopol and Neves (2004).

The annual failure rate of the superstructure due to traffic hazard, which coincides with its annual failure probability $P_{T,f}$, given that the structure has survived until time t and given that the time interval is one year, is obtained by (see Chapter 2)

$$P_{T,f}^{j}(t) = \frac{f_{ttf}^{j}(t)}{1 - F_{ttf}^{j}(t)} \tag{3.11}$$

3.3 CONSEQUENCE ANALYSIS

This section presents the consequence analysis of specific risks that are associated with seismic and traffic hazards. The quantification of risk requires the evaluation of bridge vulnerability for each identified hazard and the assessment of the negative consequences. Moreover, while performing life-cycle analyses, time is a variable of extreme importance to be incorporated. In fact, some types of consequences may vary with time, such as those associated with the average daily traffic (ADT) of a carried route. In this chapter, consequence analysis uses an economic approach in order to associate regional economic impacts with a monetary value expressed in United States dollars (USD).

Direct consequences include rebuilding costs, rehabilitation costs, and material damage costs, whereas indirect consequences include operating costs, time-loss costs, and accident costs (loss of human lives and injuries). Material damage costs and accident costs depend on the number of accidents associated with bridge failure.

When consequences are estimated in terms of monetary values, the prediction of future risk must account for the difference between present and future values of monetary losses. Thus, future consequences in terms of monetary values are given by

$$FV(t) = PV(1+r)^t \tag{3.12}$$

where $FV(t)$ is the future monetary value with respect to year t, PV is the present monetary value, and r represents the annual discount rate of money.

Time-dependent direct $C_D(t)$ and indirect $C_I(t)$ consequences associated with a bridge damage/failure for a specific year t are defined in Table 3.1, where E_{Reb}, E_{Reh},

E_{MD}, E_{Op}, E_{TL}, E_{LHL}, and E_{Inj} are the factors accounting for epistemic uncertainties associated with rebuilding costs, rehabilitation costs, material damaged in a vehicular accident, operating costs, time-loss costs, loss of human lives, and injury costs, respectively, c_{Reb} is the rebuilding cost per square meter (USD/m^2), c_0 are costs that do not depend on the level of damage (USD), $c_{S,car}$ is the car salvage value (USD), $c_{S,truck}$ is the truck salvage value (USD), $c_{S,cargo}$ is the value of the cargo (USD), $c_{Op,car}$ and $c_{Op,truck}$ are the operating costs of cars and trucks per kilometer (USD/km), respectively, c_W is the wage per hour (USD/h), c_{TC} is the total compensation per hour (USD/h), c_{Inv} is the inventory cost (USD/h), c_{VSL} is the value of a statistical life (VSL) (USD), c_{Inj} is the cost associated with injuries (USD), W and L are the bridge width (m) and length (m), respectively, δ is a coefficient accounting for the level of damage depending on bridge residual serviceability, $A(t)$ is the ADT referred to year t, τ represents the average daily truck traffic as percentage of ADT, $S(t)$ is the traveling speed (km/h), D_l is the bypass detour length (km), d is the duration of the detour (days), O_{Car} and O_{Truck} are the vehicle occupancies for cars and trucks, respectively, $T_m(t)$ is the marginal travel time (h) required to cover the traveled route or the detour depending on bridge serviceability and traffic speed, and α_{LHL} and α_{Inj} are the percentages of expected human losses and injuries, respectively.

In summary, rebuilding costs are based on the cost per square meter of deck surface (based on Stein *et al.* 1999), while rehabilitation costs depend on the level of damage affecting the bridge. It has been assumed that rehabilitation costs should not exceed 60% of the construction costs, otherwise the bridge would be replaced (based on Sánchez-Silva and Rackwitz 2004). Material damage costs are associated with

material losses in terms of the residual values of cars and trucks involved in potential accidents when a sudden failure occurs. Operating costs are generated when users travel through a bypass detour that is longer than the original route while time-loss costs are associated with the marginal time loss for users and goods while traveling through a partially serviceable bridge or through the bypass detour (based on Stein *et al.* 1999). Costs due to the loss of human lives and injuries are associated with the number of expected fatalities and injuries due to a potential sudden failure, respectively.

The time needed for the restoration of bridge serviceability is assumed as: 36 months for ADT $\leq$ 100; 24 months for 100 < ADT $\leq$ 500; 18 months for 500 < ADT $\leq$ 1,000; 12 months for 1,000 < ADT $\leq$ 5,000; and 6 months for ADT > 5,000 (Stein *et al.* 1999). Regarding the costs due to the loss of human life, the VSL includes out-of-pocket costs, lost work and housework-related costs, human capital costs, and the expenses people are willing to face to prevent injury, according to Caltrans (2009) and USDOT (2011). Meanwhile, as per Spicer and Miller (2010), costs associated with injuries are a fraction of VSL depending on the injury severity, based on the concept of Quality Adjusted Life Years (QALYs). Most of the parameters included in the evaluation of costs are affected by uncertainties, hence they are treated as random variables.

The estimation of the traffic volume of a route containing a bridge is provided by the ADT information of the bridge, which can be obtained from the National Bridge Inventory (NBI) data file (FHWA 2010). The ADT value varies over time. The magnitude of this variation can be assessed by investigating NBI data files referring to

different years. The proposed model for the prediction of ADT, associated with the *j*-th bridge, is assumed based on a linear estimator function and on a time interval of 10 years as follows

$$A^j(t) = A^j[k] \cdot \left(1 + \frac{\rho^j t}{1000}\right) \tag{3.20}$$

$$\rho^j = \left(\frac{A^j[k+10]}{A^j[k]} - 1\right) \cdot 100 \tag{3.21}$$

where $A[k]$ is the ADT value referred to year k, ρ is the percentage of traffic increment between two available ADTs spaced 10 years apart, and t is the time (years). If ADT is expected to decrease over time, ρ is negative.

The speed $S(t)$ required to cover a certain route distance depends on the route capacity and traffic conditions. According to Martin and McGuskin (1998), for each considered route or detour associated with the *j*-th bridge, such speed is defined as

$$S^j(t) = \frac{S_0^j}{\left[1 + 0.15\left(\frac{F^j(t)}{F_C^j n_l^j}\right)^4\right]} \tag{3.22}$$

where S_0 is the free-flow traffic speed, $F(t)$ is the total traffic flow, F_C is the bridge traffic flow capacity (usually considered to be 2,000 and 1,000 vehicles per hour per lane for highways and minor arterials, respectively), and n_l is the number of lanes carried by the bridge. The total traffic flow can be obtained by the ADT associated with each bridge. Based on TRB (2000) and Caltrans (2009), the relationship between traffic flow and ADT accounting for peak and off-peak hours is defined as

$$F^j(t) = \begin{cases} K_1 D A^j(t) & \text{peak hours} \\ K_2 D A^j(t) & \text{off-peak hours} \end{cases} \tag{3.23}$$

where K_1 and K_2 are the percentages of traffic associated with the portion of ADT during the peak and off-peaks hours, respectively, and D is the directional factor. Accordingly, the consequence analysis is performed for these two time periods considering every single day.

3.4 LIFE-CYCLE RISK ASSESSMENT

The identification of the most dangerous hazards depends on the level of detail that a specific risk assessment requires. The required scale of specific approaches determines the level of the analysis. Moreover, the identification of critical scenarios to be considered depends on the desired accuracy level. In this chapter, the effects of hazards induced by earthquakes and traffic are investigated for a group of bridges belonging to a transportation network. Since structural vulnerabilities and consequences are time-dependent, lifetime considerations are necessary.

3.4.1 SERVICEABILITY

Risk assessment is based on the level of serviceability of the single bridges within a transportation network. Bridge serviceability can be defined as the ability to provide adequate service to users. Although risk is affected when failure occurs, other circumstances may put the bridge at risk. For instance, the closure of one traffic lane causes indirect consequences in terms of traffic delay. The vehicular traffic capacity and the speed required to cover the link associated with the *j*-th bridge are affected by

the level of serviceability of the bridge. Different service levels have already been investigated in previous studies (Adey, Hajdin and Brühwiler 2003, Bocchini and Frangopol 2011a). Accordingly, a bridge may be subjected to interventions in order to improve its performance with respect to the considered hazard-induced effects. Serviceability may vary over time depending on the performance level and damage level experienced by the bridge during its lifetime. In this chapter, the bridge serviceability is classified into four main service states:

1. Fully serviceable ($S1$): the bridge is open and fully available to users.
2. Partially serviceable ($S2$): the bridge is only partially available to users due to minor rehabilitation work. Some of the lanes are closed to traffic and these conditions potentially increase delay for travelers.
3. Closed ($S3$): the bridge is closed due to major rehabilitation work. This restriction causes travelers to drive through a bypass detour, thus generating loss of time and longer travel distance.
4. Collapsed ($S4$): the bridge needs to be rebuilt. The vehicular traffic must follow the bypass detour.

It is assumed that a fully serviceable bridge does not generate any kind of negative consequences, and users traveling on the associated link reach their destination without being affected by any loss of time.

3.4.2 RISK DEFINITION

Depending on the level of performance, the bridge serviceability will be associated with probabilities of being in one of the four service states ($S1$ to $S4$) defined

previously. For both seismic and traffic hazards, the probabilities of being in a specific service state for the *j*-th bridge at time t are summarized in Table 3.2, where $P_{E,S1}(t)$ and $P_{T,S1}(t)$, $P_{E,S2}(t)$ and $P_{T,S2}(t)$, $P_{E,S3}(t)$ and $P_{T,S3}(t)$, and $P_{E,S4}(t)$ and $P_{T,S4}(t)$ are the probabilities of the bridge being in service state *S*1, *S*2, *S*3, and *S*4, respectively, due to seismic (subscript *E*) and traffic (subscript *T*) hazards; $P[ND](t)$, $P[SL](t)$, $P[MOD](t)$, $P[EXT](t)$, and $P[COM](t)$ are the probabilities of having no damage *ND*, slight damage *SD*, moderate *MOD*, extensive damage *EXT*, and complete damage *COM*, respectively, $P[S1|Surv](t)$, $P[S2|Surv](t)$, and $P[S3|Surv](t)$ are the probability of being in service states *S*1, *S*2, and *S*3, respectively, given that the bridge does not fail, $P_{T,f}(t)$ is the probability of failure, and *t* is the time. For a bridge, the events of being in specific service states are mutually exclusive events within the single hazard.

The event tree of Figure 3.1 shows how serviceability states, traffic capacity, bridge vulnerability, and consequences are considered. The values of the conditional probabilities $P[S1|Surv](t)$, $P[S2|Surv](t)$, and $P[S3|Surv](t)$ of Equations (3.28–2.30) in Table 3.2, are based on the percentage of time for which a bridge experiences full service, partial service, or closure, respectively. Such values can be obtained by considering the yearly duration of maintenance works (such as preventive or essential maintenance).

Finally, based on the general definition of risk reviewed in Appendix A and recalling that service state *S*1 does not cause any consequences, the proposed life-cycle risk definitions for seismic and traffic hazards are, respectively, as follows

$$R_E^j(t) = \sum_{Si=S1}^{S4} \left\{ P_{E,Si}^j(t) \cdot \left[C_{D,Si}^j(t) + C_{I,Si}^j(t) \right] \right\} \tag{3.32}$$

$$R_T^j(t) = \sum_{Si=S1}^{S4} \left\{ P_{T,Si}^j(t) \cdot \left[C_{D,Si}^j j(t) + C_{I,Si}^j(t) \right] \right\} \tag{3.33}$$

where $C_{D,Si}(t)$ and $C_{I,Si}(t)$ are the time-dependent direct and indirect consequences, respectively, given a specific serviceable state *Si*.

In a bridge, although a specific service state due to seismic hazard and a specific service state due to traffic hazard are statistically independent events, their potential conjunct occurrence cannot be excluded, even though it is unlikely to happen. If this occurs, the consequences are determined by those associated with the worse service state. Therefore, the life-cycle total risk $R_{Tot}(t)$ for the *j*-th bridge is

$$\begin{aligned} R_{Tot}^j(t) = & \sum_{Si=S1}^{S4} \left\{ \left[P_{E,Si}^j(t) + P_{T,Si}^j(t) \right] \cdot C_{Tot,Si}^j(t) \right\} - \\ & \sum_{Sk=S1}^{S4} \sum_{Sn=S1}^{S4} \left\{ P_{E,Sk}^j(t) \cdot P_{T,Sn}^j(t) \cdot \max \left[C_{Tot,Sk}^j(t), C_{Tot,Sn}^j(t) \right] \right\} \end{aligned} \tag{3.34}$$

where $C_{Tot,Si}(t)$, $C_{Tot,Sk}(t)$, and $C_{Tot,Sn}(t)$ are the time-dependent total consequences for each service state *Si*, *Sk*, and *Sn*, respectively. The introduced formula accounts for the cases in which the bridge is affected by a specific service state due to a single hazard or to the conjunction of both.

3.4.3 BRIDGE NETWORK

The approach for the evaluation of risk of a complex transportation network requires the study of traffic flow distribution within it. For instance, graph theory may be used to assign an origin-destination matrix for each vertex included in the model, and bidirectional links connecting the vertex represent the traffic flow directions (Gibbons

1985). Although such a method is powerful, the assumption that all the travelers remain within the considered network may lead to approximations. Bocchini and Frangopol (2011a) enhanced graph theory applied to transportation networks, including the effect on traffic flows through the quantification of the level of damage of the bridges carrying the links.

For some small networks, a good approximation for the evaluation of network risk consists in considering the actual traffic flow traveling on each bridge, which can be obtained by Equation (3.23). In this way, and according to Cesare *et al.* (1993), life-cycle total risk for the network R_{Net} may be evaluated as the sum of the risks generated by all the single bridges as

$$R_{Net}(t) = \sum_{j=1}^{B} R_{Tot}{}^{j}(t) \tag{3.35}$$

where B is the total number of bridges within the network. Equation (3.35) can provide indications on the risk associated with some small transportation networks, whereas for complex ones, the use of more sophisticated methods is required, including those presented for network reliability assessment (Liu and Frangopol 2005, Liu and Frangopol 2006).

Figure 3.2 shows the developed flowchart for the assessment of the life-cycle network risk.

3.5 CASE STUDY: GROUP OF EXISTING BRIDGES

The proposed approach is applied to a group of existing bridges in order to investigate the life-cycle risk caused by seismic and traffic hazards. Figure 3.3 shows the schematic layout of the considered group of highway and secondary bridges within a specific network. A segment of the northbound of Interstate 15 belonging to the city of Escondido, California (north of the San Diego metropolitan area), and a segment of the northbound of the Centre City Parkway form the considered one-way network. There are two origin points, $A1$ and $A2$, and one destination point, E. The intersection of the two routes is in point C. Five bridges denoted as 1, 2, 3, 4, and 5 are included in this analysis.

A Monte Carlo simulation is the core of the developed program performed by the software MATLAB (The MathWorks 2011). Based on simulated samples generated by the Latin Hypercube technique (McKay, Conover and Beckman 1979) (reviewed in Appendix A), histograms, expected values, and specific percentiles of life-cycle risk are evaluated for a group of bridges. According to McKay, Conover and Beckman (1979) the generation of random numbers by using the Latin Hypercube technique is a valid alternative to crude Monte Carlo simulation, providing a better represented sample space with a limited number of samples.

3.5.1 BRIDGE VULNERABILITIES

Time-dependent structural performances by means of structural vulnerability are evaluated for seismic and traffic-induced hazards. Over time, structural vulnerability

increases due to aging considerations. All the obtained profiles span over 70 years, starting from 1978 (year in which the last bridge of the network has been built according to the collected NBI data (FHWA 2010)).

The effect of seismic hazard is modeled herein by means of fragility analysis (Basöz and Mander 1999). The ground motion at each bridge location is simulated starting from 20,000 earthquakes randomly generated over a square area having a width of 100 km. From a parallel analysis performed by using 10,000 samples it was found that the difference in terms of mean total network risk is about 1%; therefore, it was deduced that 20,000 samples satisfy an acceptable level of convergence. The center of gravity of this region has the following coordinates: *Lat*. = 33.16° and *Long* = −117.10°. As shown in Figure 3.4, the epicenter coordinates (*x* and *y*) of the random seismic events are triangularly distributed between −50 km and 50 km with mode of 50 km, for the *x*-axis, and −50 km and 50 km with mode of 42 km for the *y*-axis, respectively (see Figure 3.4). The magnitude of the random seismic events is provided by a sample obtained from a truncated exponential PDF (β in Equation (3.1) has been set to be equal to 1.1). The depth of the seismic source is triangularly distributed between 1 km and 30 km with mode of 8 km. The parameter β and the parameters of the triangular distributions (*x*-*y* axes and depth) are obtained by using the method of moments (Ang and Tang 2007) based on the analysis of the historic earthquakes database for the region under investigation (USGS 2011). The minimum and maximum magnitudes (Richter scale) considered are set as 4 and 8, respectively. Strike-slip earthquakes are randomly generated causing rupture lengths and widths evaluated according to Equations (3.2) and (3.3), respectively. Considering the

predominant direction (southeast to northwest) of the faults in the area, the orientation of the rupture traces are uniformly distributed with angles between 90° and 180°. For instance, Figure 3.4 shows the graphical representation of rupture traces over the considered region for 50 samples. The rupture traces are represented by solid lines in the plane *x*-*y* (inspired by Jones, Middelmann and Corby 2005). Epicenters and extreme points of the traces are shown as well. The projection of the shortest distance between a bridge and the random rupture trace is evaluated depending on rupture location and orientation.

Each bridge is affected by ground motion depending on many factors accounted in the attenuation functions proposed by Campbell and Bozorgnia (2007). Once a set of *PSA* values is evaluated for the *j*-th bridge and for the *i*-th sample, time-dependent fragility analysis can be performed and exceedance probabilities of various damage states are calculated. The initial values of the fragility parameters are those calibrated by Basöz and Mander (1999). Further needed information and parameters concerning the bridges are found in the NBI database (FHWA 2010). By using Equation (3.8), the dependency of the median spectral acceleration $A_{DS}(t)$ associated with the occurrence of a specific damage state is evaluated by introducing the aging coefficient γ. The value of γ is set in order to obtain an assumed reduction of about 25% of the fragility parameter after 70 years (consistent with the results reported in Ghosh and Padgett 2010). The result of this seismic analysis is a set of time-dependent probabilities of the bridges being in specific damage states: no damage $P[ND](t)$, slight damage $P[SL](t)$, moderate damage $P[MOD](t)$, extensive damage $P[EXT](t)$, and complete damage $P[COM](t)$.

The vulnerability due to traffic hazard is evaluated by assuming that the PDF of the time-to-failure follows a Weibull distribution with parameters κ and λ. For this network analysis, κ and λ are assumed to be equal to 3 and 0.01 for bridges 1 and 2, respectively, and 5 and 0.01 for bridges 3, 4 and 5, respectively. These values are consistent with those reported in previous studies (van Noortwijk and Klatter 2004, Yang, Frangopol and Neves 2004). The time-dependent probability of failure of the superstructure is obtained by applying Equation (3.11).

3.5.2 EVALUATION OF THE CONSEQUENCES

The time-dependent monetary values associated with direct and indirect consequences are evaluated at this stage. Total costs depend on the knowledge of unitary costs (such as cost per square meter, cost per hour, etc.). Direct costs are those associated with structural and material losses (Equations (3.13–3.15) of Table 3.1). Rehabilitation costs are also defined as direct because they correspond to the amount of money that is needed towards the renewal of damaged structures. Indirect costs are associated with the loss of time, the marginal traveled distance, and with the losses due to the number of potential fatalities and injuries (Equations (3.16–3.19) of Table 3.1). The cost, for the years preceding 2011, are provided by Equation (3.12) by setting a negative time interval t, while the cost values for the years following 2011 are obtained by considering the future cost, using a positive time interval t in Equation (3.12).

Some of the costs depend on the ADT of the road carried by the considered bridges. The prediction of the ADT may be provided by Equation (3.20), which considers their increment or decrement percentage within a time interval of 10 years

by means of ρ (Equation (3.21)). The speed of the traffic flow (Equation (3.22)) depends on the practical capacity of the route and on the total traffic flow over time (Equation (3.23)). According to Caltrans (2009), the peak period lasts five hours per day and the percent coefficients K_1 and K_2 of Equation (3.23) are equal to 8.48% and 3.03%, respectively. Upon these considerations, the traveling speed and the marginal travel time within the network are accordingly affected depending also on the route the users are using (normal route or bypass detour).

All the assumed values of the included basic statistical descriptors and their distribution types are summarized in Table 3.3. According to Ang (2010), a practical evaluation of epistemic uncertainty may usually rely on intuitive/engineering judgments, which lead to a specific reasonable range of possibilities, with an associated plausible distribution.

Latin Hypercube (McKay, Conover and Beckman 1979) sampling is used with 20,000 trials for the basic random variables, allowing the probabilistic calculation of the consequences, and for the simulation of the ground motion.

3.5.3 LIFE-CYCLE RISK

Seismic and traffic vulnerabilities determine the service states of each bridge ($S1$ to $S4$). Although losses are generated when a structural failure occurs ($S4$), service states $S2$ and $S3$ may also cause both direct and indirect consequences.

By applying Equations (3.24–3.35), life-cycle risks can be calculated. Given that a bridge survives, conditional probabilities of being in service states $S1$, $S2$, and $S3$ for traffic hazard are assumed to be 0.94, 0.05, and 0.01, respectively. Such values are

based upon considerations on the annual percentage of time for which a bridge is open or subjected to rehabilitation actions requiring its closure or partial closure. Figure 3.5 shows risk referred to the year 2011 induced by seismic (a,b,c,d,e) and traffic hazards (f,g,h,i,j) for each considered bridge of the transportation network in Figure 3.3. It can be noted that risk of bridges 1 and 2 is relatively smaller than risk for the other three bridges carrying the northbound of I-15. The results shown in Figure 3.5 can provide the sensitivity analysis of risk associated with different routes within the network. The predicted histograms of life-cycle risks referred to the year 2048 and, based on the simulated earthquakes and consequences, are shown in Figure 3.6. According to the proposed framework, it can be noticed that the expected predicted risk at year 2048 can be three times higher than the risk associated with the year 2011. Moreover, although ADT is predicted to slightly increase over time and considering the future value of money (Equation (3.12)), seismic risk significantly increases over time for each considered bridge (Figure 3.5 and Figure 3.6). It was found that seismic risk is very sensitive to the decay of the fragility parameters; therefore seismic life-cycle analyses must address these aspects. From a parallel analysis, it is found that, based on a maximum reduction over time of the fragility parameters of about 25%, time-dependent risk is about 44% higher than risk obtained with time-independent fragility parameters. Both Figure 3.5 and Figure 3.6 help analyze different routes for the small network studied in this chapter, but for complex networks, a comprehensive method that includes traffic redistribution must be considered in order to account for the increasing number of alternative routes.

Figure 3.7(a,b) shows the profiles of the mean value of direct and indirect life-cycle risks, respectively, for the five bridges of the network. As shown, direct risks are consistent with bridge dimensions and types, indicating that bridge 1 is the smallest among the others, while indirect risk is found greater for those bridges carrying more traffic (i.e., 3, 4, and 5), causing more disruption in case of closures or failures. Figure 3.7(c,d) reports on the mean and dispersion of risk showing the profiles (mean and 90% and 95% percentiles) associated with direct and indirect risks for bridge 5 of Figure 3.3. Based on the proposed model, it can be concluded that total life-cycle risk is very sensitive to the indirect consequences that are significantly larger than the direct ones. Accordingly, higher dispersion has been found for indirect risk, which involves a great number of random variables adding further uncertainty. The contribution of the single types of consequences to total risk for the entire network is illustrated in Figure 3.8. Mean value profiles of all the types of direct (Figure 3.8(a)) and indirect (Figure 3.8(b)) risks are computed. The most significant loss contributions are found in rehabilitation costs and time-loss costs. Therefore, the parameters involved in the analysis of the costs associated with the loss of time require special attention for their estimation. A relevant outcome to be noticed is that, according to the proposed model, expected rehabilitation costs are greater than expected rebuilding costs depending on bridges and network service states (Figure 3.8(a)).

Finally, the profiles of the life-cycle network risk are obtained. In Figure 3.9(a), the risk contribution of each bridge with respect to the network risk is reported. Figure 3.9(b) shows the profiles of the mean value and 90% and 95% percentiles of the total life-cycle risk associated with the whole bridge network. Percentiles give an indication

of the dispersion of the obtained data and can set the basis for the calibration of life-cycle risk-informed management of bridges within a transportation network.

3.6 CONCLUSIONS

Recently, life-cycle management of structures and infrastructures addressed issues related to risk-informed decision analysis. In this context, decisions may be based on the quantification of monetary values of most of the consequences caused by potential structural failures or malfunctions.

This chapter, which is based on Decò and Frangopol (2012) and Decò and Frangopol (2013a), presented some important issues emerging from the life-cycle risk assessment of spatially distributed aging bridges within a transportation network. A detailed consequence analysis has been performed in order to evaluate the effects associated with different bridge service states (serviceability). Two of the most common hazards are considered in this chapter. The time-dependent effects of traffic hazard, including aging phenomena and seismic hazard, for an earthquake-prone region have been investigated.

The following conclusions are obtained:

1. When life-cycle risk is assessed under multiple hazards, the predominant hazard must be adequately modeled in order to achieve reliable estimates of total risk. The current case study helps to understand that, for the considered region, it is crucial to model the seismic hazard (earthquake scenarios) with a powerful tool such as the probabilistic ground motion and associated fragility analysis. In fact, for the

studied network, it was found that the only inclusion of risk induced by traffic hazard provides an incomplete analysis that may lead to a wrong decision process.

2. As expected, the risk induced by seismic hazard increases over time due to structural aging consideration. However, a maximum reduction over time of the fragility parameters of about 25% leads to a much higher increase in risk (about 44% higher than risk obtained with time-independent fragility parameters). Additional risk increment is due to the predicted increase of ADTs over time.
3. The failure of any of the three bridges belonging to the I-15 (i.e., bridges 3, 4, and 5 in Figure 3.3) generates dramatically high consequences. Within the network, risk for the bridges belonging to Centre City Parkway (i.e., bridges 1 and 2 in Figure 3.3) is almost negligible.
4. It can be noted that the dispersion of seismic risk increases over time depending on the uncertainty affecting the prediction. Histograms and percentiles give an indication of such dispersion in the obtained risk profiles. The inclusion of epistemic uncertainties enhances the probabilistic model but adds further dispersion to the initial sample.
5. According to the proposed framework, it is found that expected rehabilitation costs are greater than expected rebuilding costs. Whilst this is true in this case, this observation may change depending on the extent of damage, on the method of computation, and on the funding model.

The implementation of risk profiles into a life-cycle framework helps the development of risk-informed optimal maintenance planning. The provided approach is useful for the evaluation of risk associated with single bridges within small

networks that may be ranked. Based on this, appropriate maintenance prioritization plans could be adopted. However, for complex networks, methods that include traffic redistribution must be considered.

Table 3.1 Summary of the considered direct and indirect consequences.

	Consequence type		Eq. no.
Direct costs $C_D(t)$	* Rebuilding	$C^j_{Reb}(t) = E_{Reb} c^j_{Reb} W^j L^j (1+r)^t$	(3.13)
	† Rehabilitation	$C^j_{Reh}(t) = E_{Reh} \cdot \min\left[0.6 c^j_{Reb} W^j L^j , c_0 + \frac{c^j_{Reb} W^j L^j}{\delta^j} \right] (1+r)^t$	(3.14)
	* Material damage	$C^j_{MD}(t) = E_{MD} \left[\begin{array}{l} c_{S,car}\left(1 - \frac{\tau^j}{100}\right) + \\ + \left(c_{S,truck} + c_{S,cargo}\right)\frac{\tau^j}{100} \end{array} \right] \frac{A^j(t) L^j}{24000 S^j(t)} (1+r)^t$	(3.15)
Indirect costs $C_I(t)$	* Operating	$C^j_{Op}(t) = E_{Op} \left[\begin{array}{l} c_{Op,car}\left(1 - \frac{\tau^j}{100}\right) + \\ + c_{Op,truck}\frac{\tau^j}{100} \end{array} \right] D^j_l A^j(t) d^j (1+r)^t$	(3.16)
	* Time loss	$C^j_{TL}(t) = E_{TL} \left[\begin{array}{l} c_W O_{Car}\left(1 - \frac{\tau^j}{100}\right) + \\ + \left(c_{TC} O_{Truck} + c_{Inv}\right)\frac{\tau^j}{100} \end{array} \right] T^j_m(t) A^j(t) d^j (1+r)^t$	(3.17)
	* Loss of human lives	$C^j_{LHL}(t) = E_{LHL} \frac{\alpha_{LHL} c_{VSL}}{100} \left\{ \begin{array}{l} O_{Car}\left(1 - \frac{\tau^j}{100}\right) + \\ + O_{Truck}\frac{\tau^j}{100} \end{array} \right\} \frac{A^j(t) L^j}{24000 S^j(t)} (1+r)^t$	(3.18)
	* Injuries	$C^j_{Inj}(t) = E_{Inj} \frac{\alpha_{Inj} c_{Inj}}{100} \left\{ \begin{array}{l} O_{Car}\left(1 - \frac{\tau^j}{100}\right) + \\ + O_{Truck}\frac{\tau^j}{100} \end{array} \right\} \frac{A^j(t) L^j}{24000 S^j(t)} (1+r)^t$	(3.19)

* Based on Stein *et al.* (1999)
† Based on Sánchez-Silva and Rackwitz (2004)

Table 3.2 Probabilities for a bridge of being in specific damage states in case of seismic (subscript *E*) and traffic (subscript *T*) hazards.

Hazard type	Service state	Probability	Eq. no.
Seismic	*S1*	$P^j_{E,S1}(t) = P\left[ND^j\right](t)$	(3.24)
	S2	$P^j_{E,S2}(t) = P\left[SL^j\right](t)$	(3.25)
	S3	$P^j_{E,S3}(t) = P\left[MOD^j\right](t) + P\left[EXT^j\right](t)$	(3.26)
	S4	$P_{E,S4}{}^j(t) = P\left[COM^j\right](t)$	(3.27)
Traffic	*S1*	$P^j_{T,S1}(t) = P\left[S1^j \mid Surv^j\right](t) \cdot \left[1 - P^j_{T,f}(t)\right]$	(3.28)
	S2	$P^j_{T,S2}(t) = P\left[S2^j \mid Surv^j\right](t) \cdot \left[1 - P^j_{T,f}(t)\right]$	(3.29)
	S3	$P^j_{T,S3}(t) = P\left[S3^j \mid Surv^j\right](t) \cdot \left[1 - P^j_{T,f}(t)\right]$	(3.30)
	S4	$P_{T,S4}{}^j(t) = P^j_{T,f}(t)$	(3.31)

Table 3.3 Statistical descriptors and deterministic parameters used for the evaluation of the consequences. The costs refer to their values at year 2011, which corresponds to year 33 of the profiles.

Random variables	Mean	COV	Distribution type	References
ADT	Varies	DNA	DNA	FHWA (2010)
ADTT/ADT ratio	Varies	DNA	DNA	FHWA (2010)
Compensation for truck drivers (USD/*h*)	29.28	0.31	LN	AASHTO (2003)
Detour speed (*km*/*h*)	30	0.15	LN	Assumed
Vehicle occupancies for cars	1.50	0.15	LN	AASHTO (2003)
Vehicle occupancies for trucks	1.05	0.15	LN	AASHTO (2003)
Wage for car drivers (USD/*h*)	23.36	0.28	LN	AASHTO (2003)
Epistemic uncertainty factor for injury costs	1	0.30	LN	Assumed
Epistemic uncertainty factor for loss of human life costs	1	0.30	LN	Assumed
Epistemic uncertainty factor for material damage costs	1	0.20	LN	Assumed
Epistemic uncertainty factor for material damage costs	1	0.20	LN	Assumed
Epistemic uncertainty factor for rebuilding costs	1	0.20	LN	Assumed
Epistemic uncertainty factor for rehabilitation costs	1	0.20	LN	Assumed
Epistemic uncertainty factor for operating costs	1	0.20	LN	Assumed
Epistemic uncertainty factor for time loss costs	1	0.20	LN	Assumed
Fixed rehabilitation costs (USD)	50,000	0.20	LN	Assumed
Length of detour (*km*)	Varies	DNA	DNA	FHWA (2010)
Value of a statistical life (USD)	6,200,000	0.45	LN	USDOT (2011)
Operating costs for cars (USD/*km*)	0.40	0.19	LN	AASHTO (2003)
Operating costs for trucks (USD/*km*)	0.56	0.19	LN	AASHTO (2003)
Inventory costs (USD/*h*)	3.81	0.20	LN	AASHTO (2003)
	Min.	Max.		
Annual discount rate (%)	2	3	Uniform	Assumed
Injury costs (USD)	651,000	6,200,000	Uniform	USDOT (2011)
Rebuilding costs (USD/m^2)	993 - 1,324	1,655 - 2,207	Uniform	DOTCA (2010)

Note: LN = log-normal distribution; COV = coefficient of variation; DNA = does not apply.

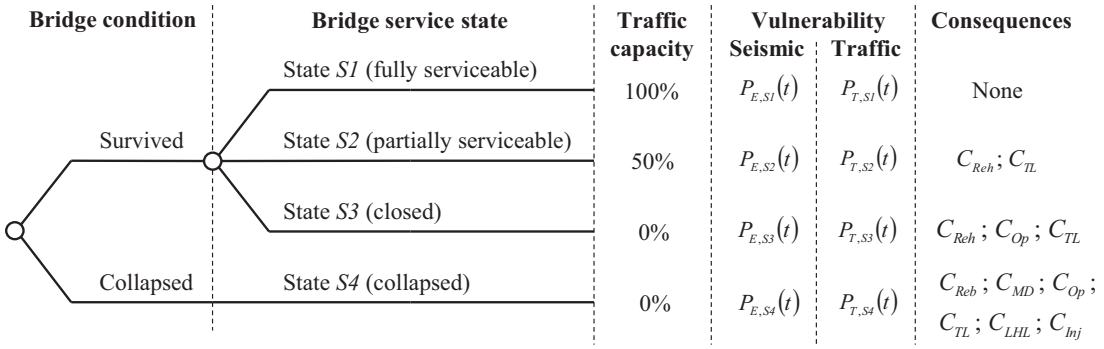

Figure 3.1 Event tree summarizing bridge serviceability under seismic and traffic hazards. Different consequences (Equations (3.13–3.19) of Table 3.1) are associated with the serviceability states (*S*1 to *S*4).

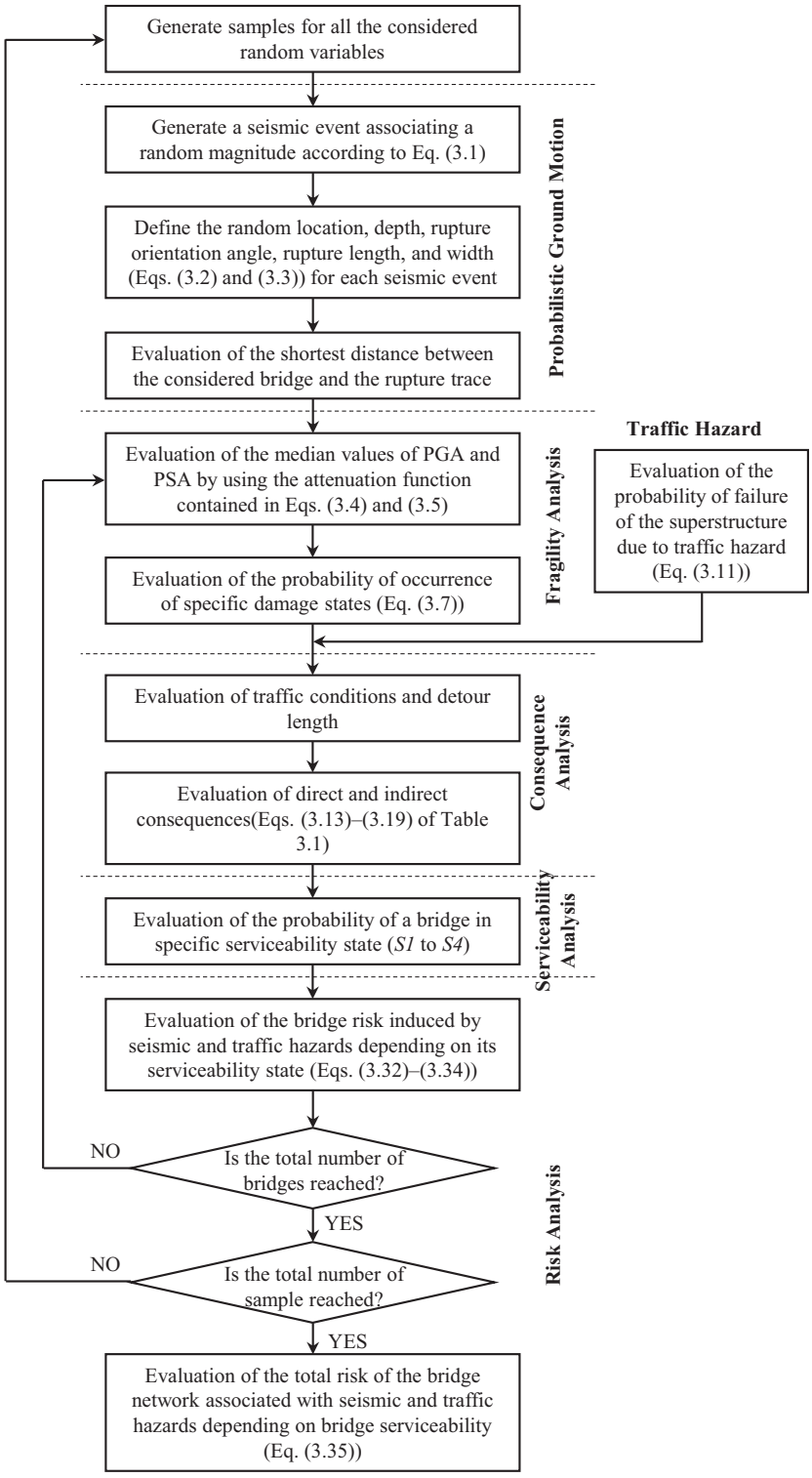

Figure 3.2 Flowchart for the computation of the life-cycle risk for a network under seismic and traffic hazards.

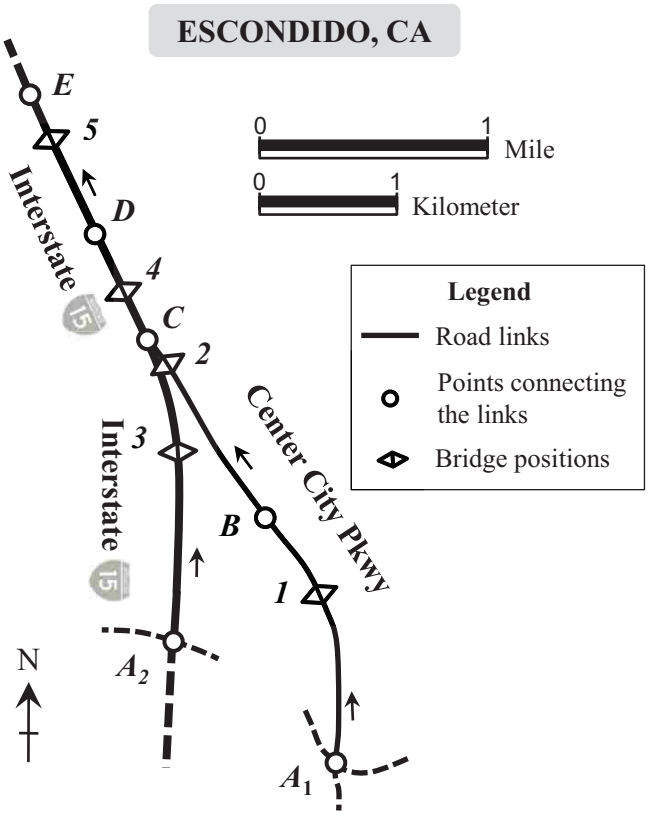

Figure 3.3 Schematic layout of the transportation network.

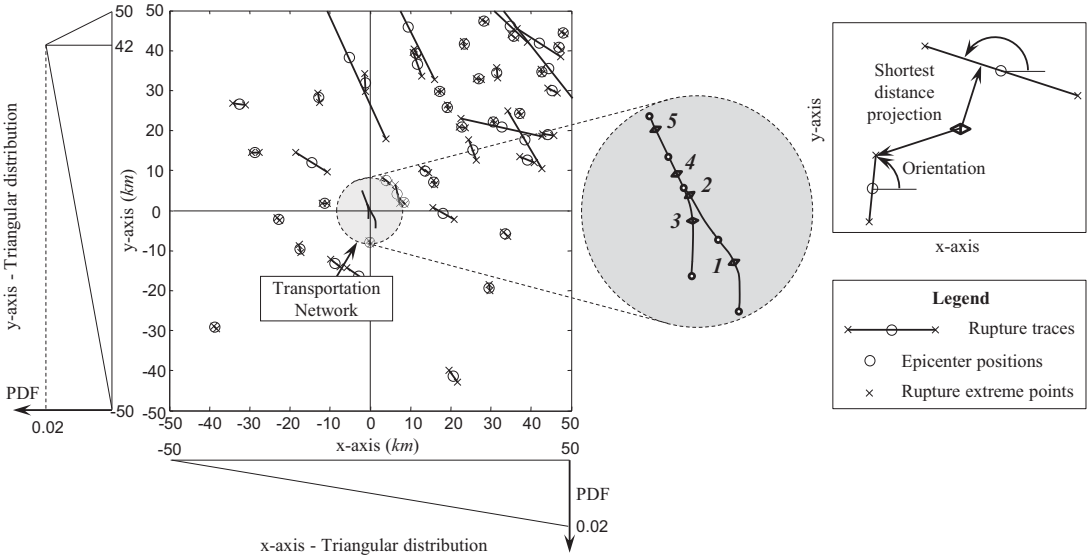

Figure 3.4 Graphical representation of random epicenters, rupture traces, and bridge network over the considered region. The triangular distributions of the *x*-*y* axes and the representation of the projection of the shortest distance between a bridge and the rupture trace for different rupture locations and orientations are also reported.

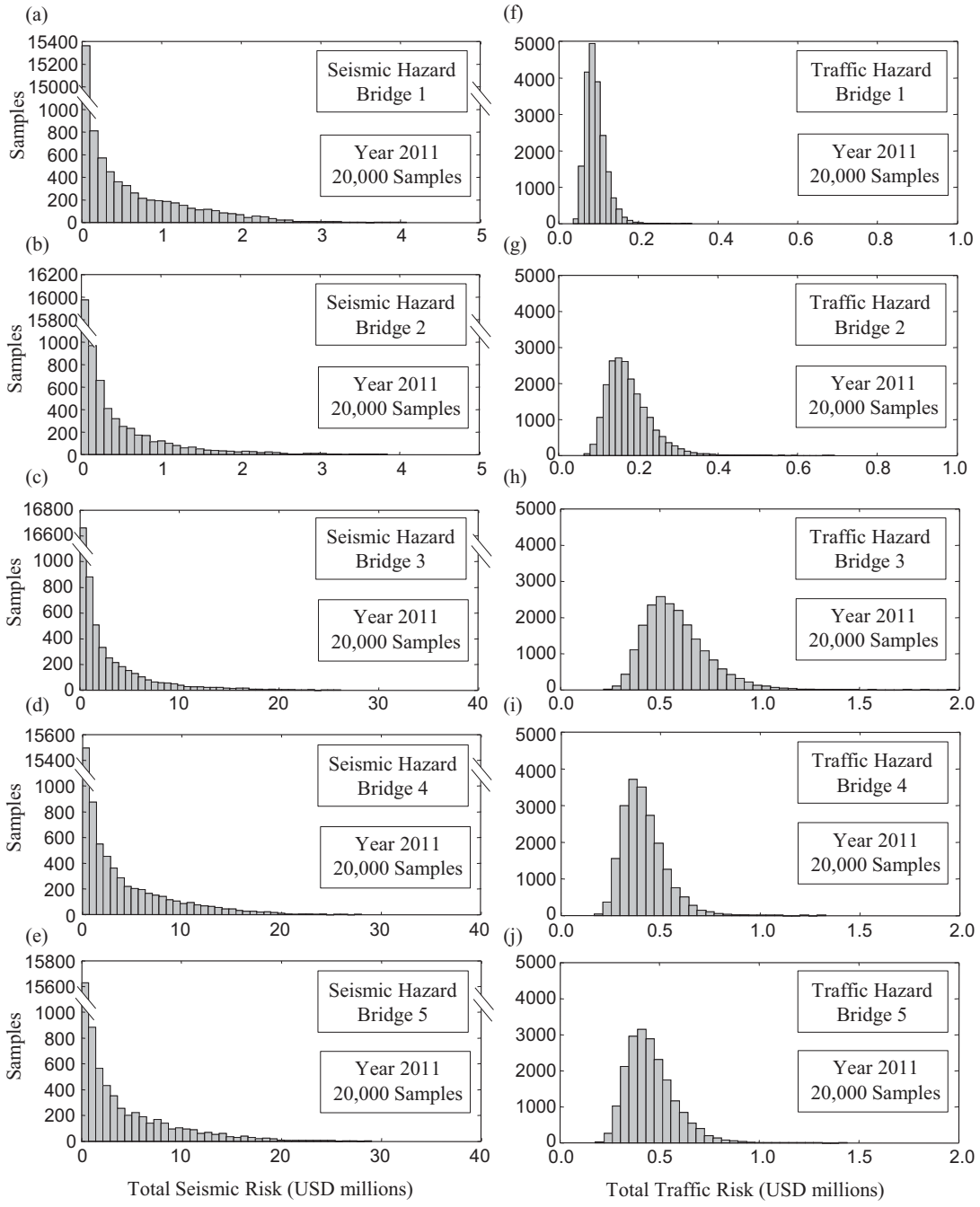

Figure 3.5 Histograms of the current total risk (direct and indirect) due to (a,b,c,d,e) seismic hazard and (f,g,h,i,j) traffic-induced hazard for each bridge within the network at the year 2011.

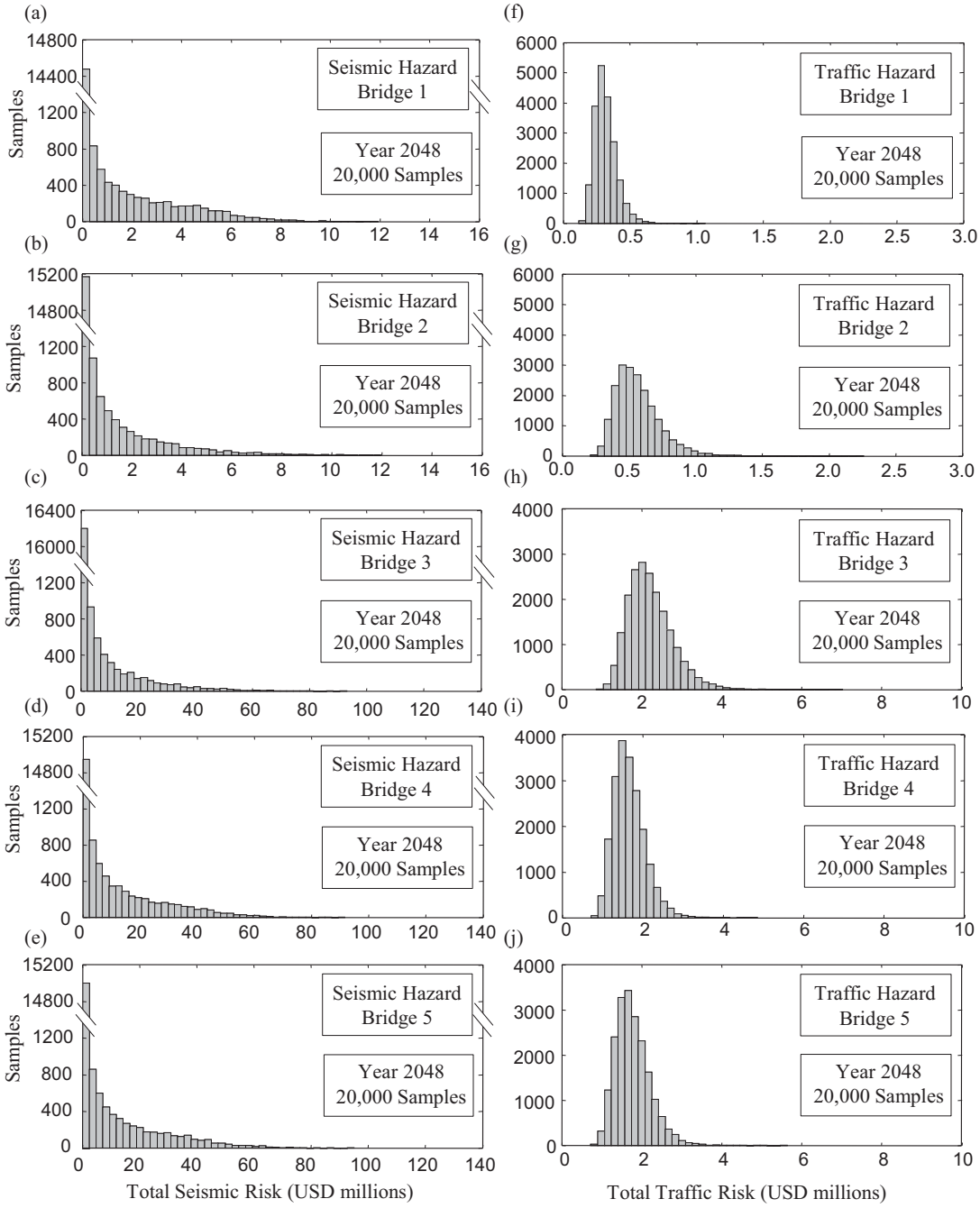

Figure 3.6 Histograms of the predicted total risk (direct and indirect) due to (a,b,c,d,e) seismic hazard and (f,g,h,i,j) traffic-induced hazard for each bridge within the network at the year 2048.

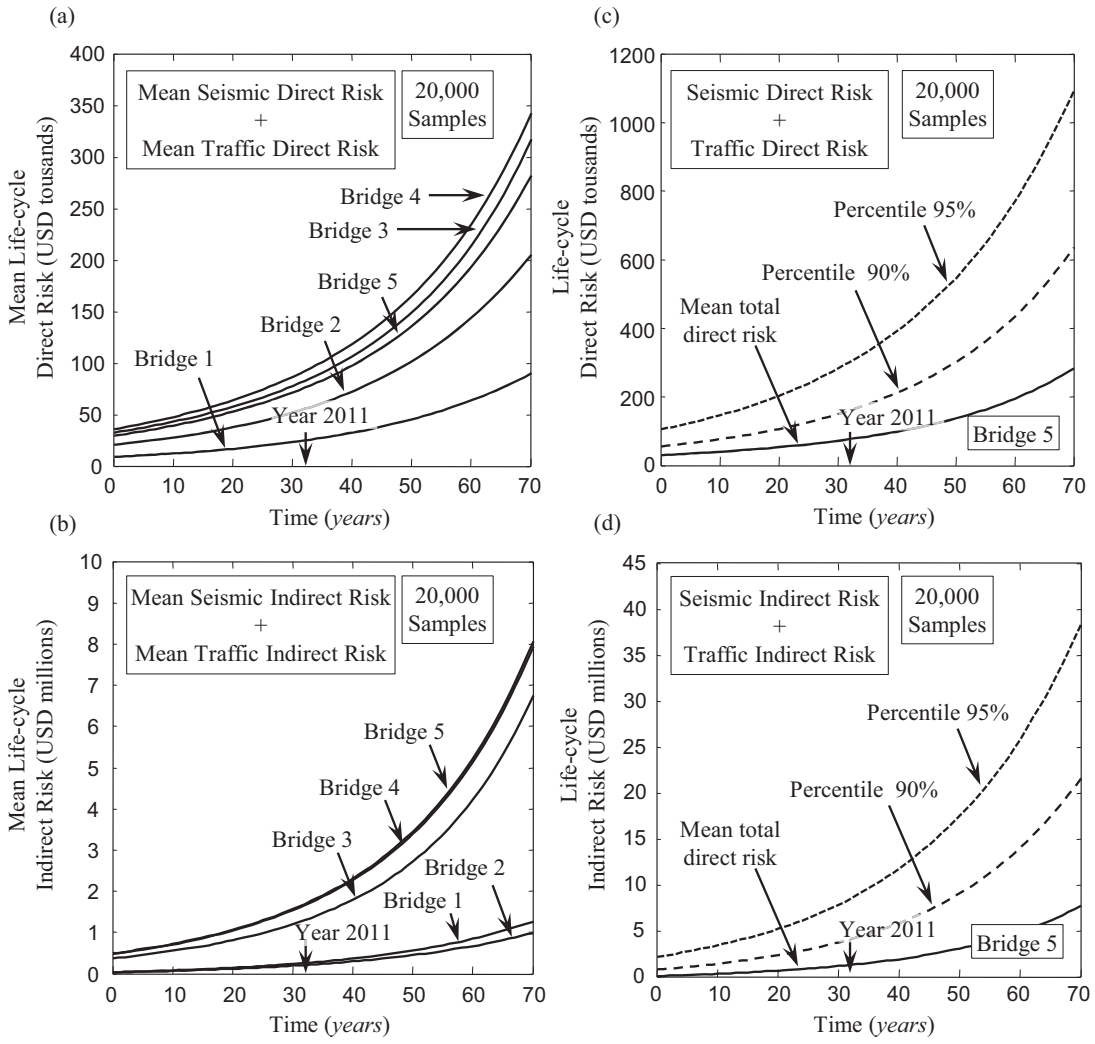

Figure 3.7 Profiles of the mean values of (a) direct and (b) indirect life-cycle risks of each bridge within the transportation network due to seismic and traffic hazards. Profiles of the mean values and 90% and 95% percentiles of (c) direct and (d) indirect life-cycle risks for the selected bridge 5 of Figure 3.3 due to seismic and traffic hazards.

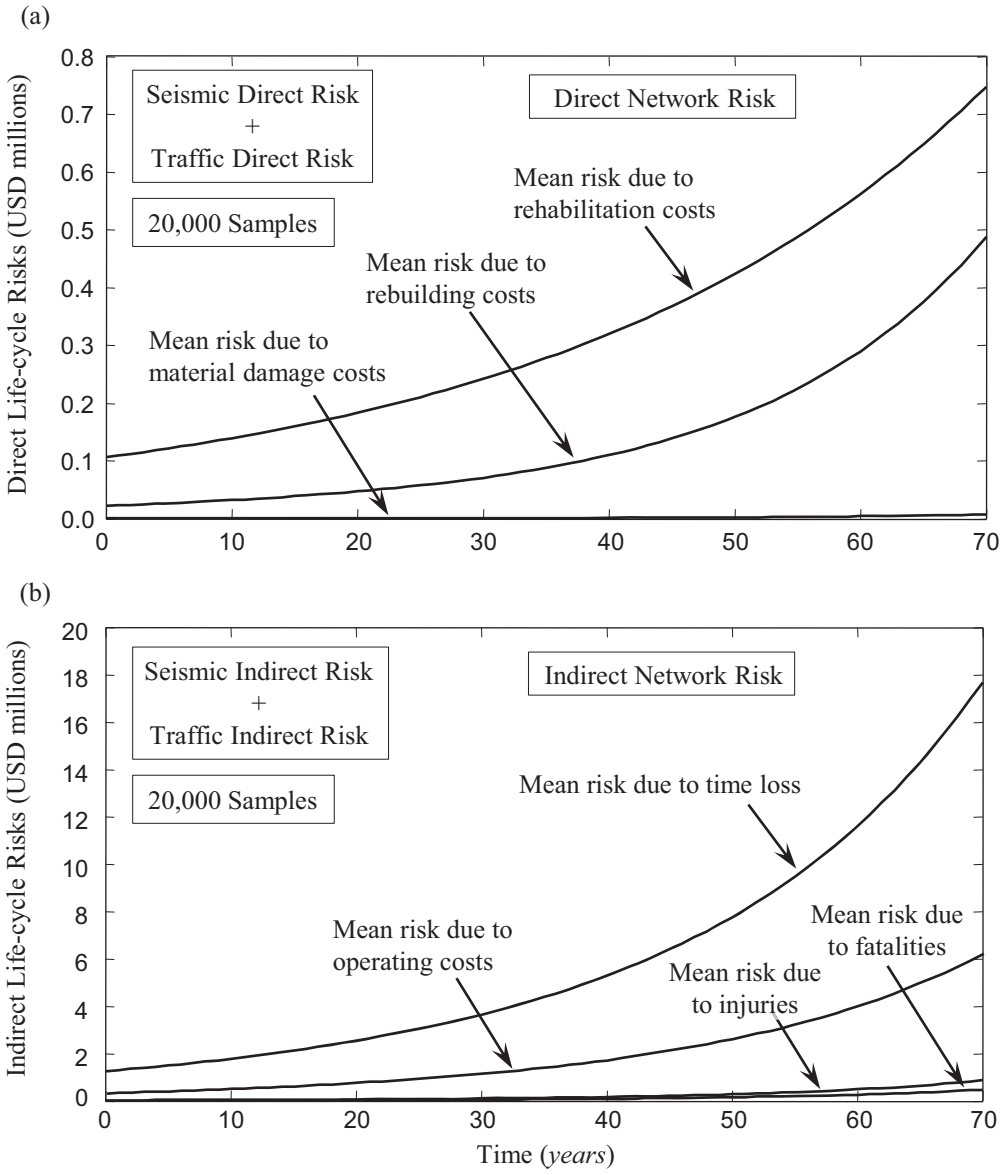

Figure 3.8 Profiles of the mean values of life-cycle network risks associated with (a) direct consequences: rebuilding costs, rehabilitation costs, and material damage costs; and (b) indirect consequences: operating costs, time-loss costs, loss of human life costs, and injury costs.

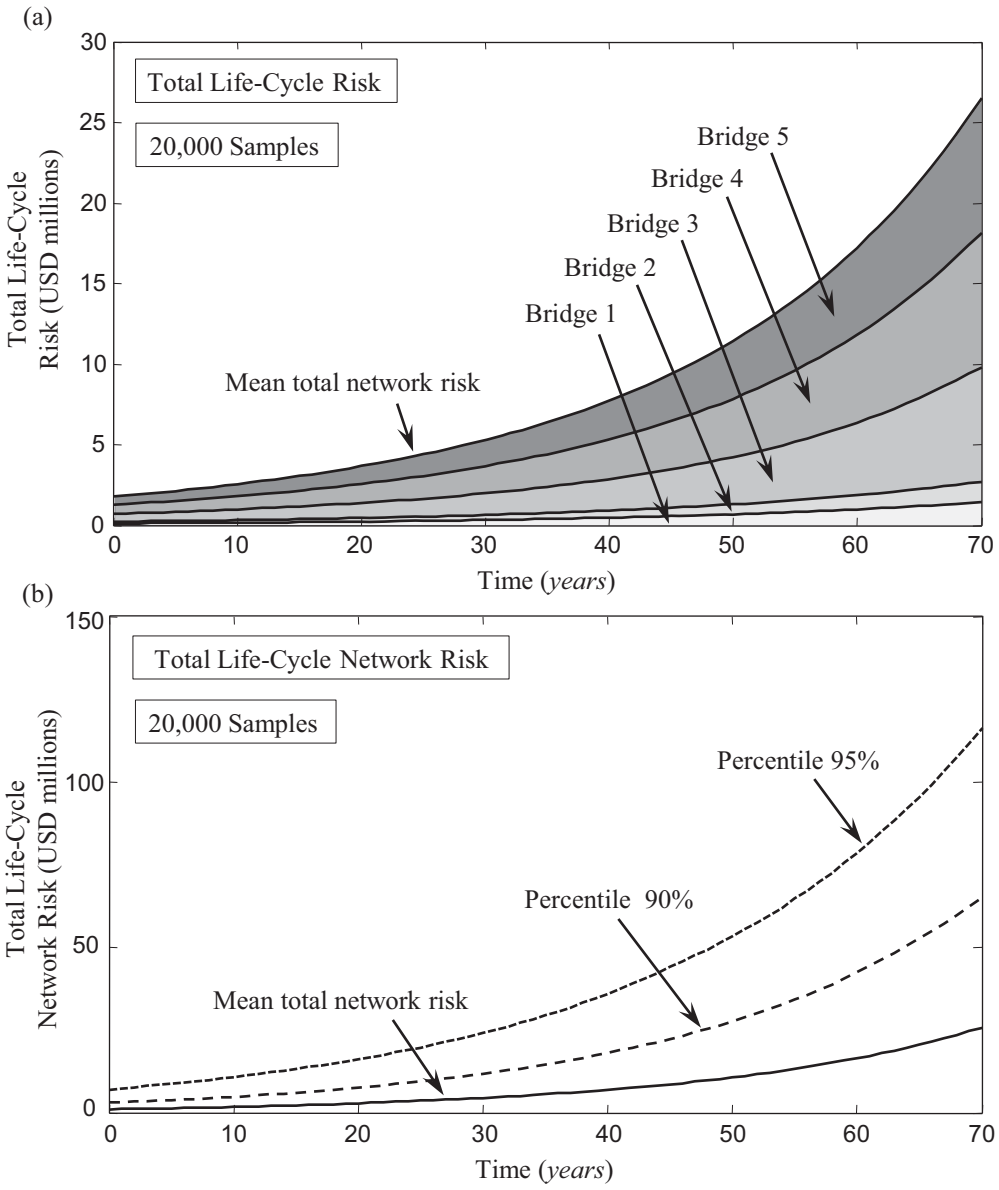

Figure 3.9 (a) Profile of total life-cycle network risk including the risk contribution of each bridge within the network. (b) Profiles of the mean value and 90% and 95% percentiles of total life-cycle network risk.

CHAPTER 4

PROBABILISTIC APPROACH FOR THE EVALUATION OF SEISMIC RESILIENCE OF SINGLE BRIDGES AND BRIDGE HIGHWAY SEGMENTS

4.1 INTRODUCTION

In studies dealing with seismic hazard, resilience can be considered as a performance indicator that quantifies the residual functionality along with the effort of the society in responding to a seismic event. In the last decade, some progress has been achieved by the introduction of analytical deterministic definitions of resilience (Bruneau *et al.* 2003, Frangopol and Bocchini 2011, Bocchini and Frangopol 2011b), many of them focusing on post-event recovery analysis. Further developments (Bruneau and Reinhorn 2007, Xu *et al.* 2007, Cimellaro, Reinhorn and Bruneau 2010, Zobel 2011) opened the path for the probabilistic treatment of resilience, in order to develop models oriented to its prediction (pre-event assessment).

The scope of this chapter, which is based on Decò, Bocchini and Frangopol (2013) and Decò, Frangopol, and Bocchini (2013), is to provide a new methodology to evaluate the probabilistic seismic resilience (PSR) of bridges, assess the impact in terms of direct and indirect costs, and provide indications to decision makers regarding potential restoration strategies. The inclusion of uncertainty extends resilience

quantification towards a fully probabilistic approach that can be embedded in a comprehensive structure/infrastructure management tool, based on expected and characteristic values. The estimation of the residual functionality after an exceptional event (called "robustness", according to Cimellaro, Reinhorn and Bruneau 2010) is a process affected by a large amount of uncertainty, and the subsequent response phase adds further uncertainty to the prediction of resilience. The probabilistic quantification of the seismic-induced damage on bridges is performed by means of fragility analysis. Based on the assessed damage level (probability of the bridge being in a particular damage state), a recovery function is proposed. Bridge functionality is directly influenced by restoration activities. Different damage-functionality relationships are adopted based on the data provided by Shinozuka *et al.* (2005) and the expert opinions collected by ATC-13 (ATC 1985). A six-parameter sinusoidal-based recovery model proposed by Bocchini, Decò and Frangopol (2012) is used in this study.

In this chapter, consequence analysis is performed in a probabilistic context with respect to direct and indirect costs. Direct costs are those associated with rebuilding-rehabilitation expenses and directly correlated to the level of bridge damage. Indirect costs account for the losses caused by marginal travel distance and for marginal travel time when a bridge is partially or fully closed. Traffic flows along the highway segment containing the bridge (called "link") and along the shortest detour route are assessed on the basis of the average daily traffic (ADT) obtained by the NBI database (FHWA 2010).

The final outcome of an exceptional event in terms of consequences is strongly affected also by the different choices of the decision makers. For this reason, multiple

potential strategies adopted by the decision makers are investigated. In order to satisfy potential financial constraints, decision makers need to be informed about available possibilities associated with different bridge damage levels and recovery processes.

The assessment of resilience of a single bridge does not fully exploit the concept of community resilience associated with a regional area. Therefore, a framework that extends the same concepts used for a single bridge to highway segments is also presented in this chapter. The performance of the bridge highway segments can be obtained by considering the performance of each single bridge and accounting for the interconnections among the investigated routes. Network performance indicators such as Total Travel Time (TTT) and Total Travel Distance (TTD) are considered for the assessment of network resilience (Bocchini and Frangopol 2012a, Bocchini and Frangopol 2012b). Only direct costs deriving from rehabilitation/reconstruction of damaged bridges are evaluated for the investigated bridge highway segments. Different types of analyses are performed based upon different scenarios accounting for specific earthquake intensities and recovery strategies.

This chapter develops a probabilistic approach for the prediction of seismic resilience of single highway bridges and bridge highway segments. Section 4.2 introduces the used models for resilience and rapidity. Section 4.3 develops the probabilistic recovery model and the considered restoration strategies used to predict resilience for single highway bridges. Section 4.4 describes probabilistic network recovery model developed for bridge highway segments. In Section 4.5, a comprehensive cost analysis is performed including direct and indirect losses. In Sections 4.6 and 4.7, apply the developed approach to an existing highway bridge

located carrying a segment of the northbound I-15 crossing the Temescal Wash, located between the cities of Corona and Murrieta in California and to four different configurations of unidirectional bridge highway segments. Finally, Section 4.8 provides the conclusions of this chapter that is based on a published paper (Decò, Bocchini and Frangopol 2013) and on two conference papers (Bocchini, Decò Frangopol 2012, Decò, Frangopol, and Bocchini 2013).

4.2 RESILIENCE

Various definitions of resilience can be found in several disciplinary fields (Chang and Shinozuka 2004, Rose 2004, Park, Nojima and Reed 2006, Xu *et al.* 2007). According to Bruneau *et al.* (2003), seismic resilience is "the ability of social units (e.g., organizations, communities) to mitigate hazards, contain the effects of disasters when they occur, and carry out recovery activities in ways that minimize social disruption and mitigate the effects of future earthquakes". This definition is general and can also be extended to different types of hazard and various structural and infrastructural systems.

However, the qualitative definitions of resilience have not converged yet to a single generally accepted definition because resilience covers social and technical aspects too broadly. Therefore, the quantification of resilience R can lead to several slightly different analytical definitions (Bruneau *et al.* 2003, Bocchini and Frangopol 2011b, Cimellaro, Reinhorn and Bruneau 2010). Based on general definition (Cimellaro, Reinhorn and Bruneau 2010), the definition proposed by Frangopol and Bocchini (2011) is adopted

$$R = \frac{\int_{t_0}^{t_h} Q(t)dt}{t_h - t_0} \tag{4.1}$$

where $Q(t)$ is the time-dependent functionality, t is the time, t_0 is the time at which the seismic event occurs, and t_h is the investigated time horizon (see Figure 1 in Bocchini, Decò and Frangopol 2012). The functionality of a structure or infrastructure can generally be defined as its ability to provide adequate service to the users. Functionality is usually expressed as a percentage of the service associated with the intact structure (which is set to be 100%), thus it is dimensionless. Therefore, resilience as defined by Equation (4.1) is dimensionless as well.

The effort of a community to recover from damage and activity disruptions caused by an extreme event can also be evaluated by means of "rapidity" that is defined as (Cimellaro, Reinhorn and Bruneau 2010)

$$r = \arctan\left(\frac{Q[t_f] - Q[t_0]}{t_f - t_0}\right) \qquad t_0 \le t \le t_f = \min(t_r, t_h) \tag{4.2}$$

where t_r is the time at which the recovery process ends.

The main uncertainties affecting resilience are those introduced by Figure 1 in Decò, Bocchini and Frangopol (2013).

4.3 PROBABILISTIC RECOVERY MODEL FOR SINGLE BRIDGES

The assessment of PSR and of the economic loss induced by potential traffic disruption is based upon the knowledge of the relationship between bridge damage level and associated loss of functionality. Although recent studies have tried to provide general approaches for the determination of such relationship (e.g. Padgett and DesRoches 2007), the decision to totally or partially close a bridge is usually made by inspectors and officials who analyze case by case after a seismic event strikes. Therefore, the a-priori determination of bridge functionality, which is most likely to depend on human judgment, can be done only under some assumptions.

Empirical approaches, such as the one proposed by Stein *et al.* (1999), can estimate the recovery of functionality based on the importance of the route carried by the bridge under investigation. Analytical methods have been proposed, such as the one developed by Mackie and Stojadinović (2006), in which the functionality is measured in terms of the traffic load-carrying capacity. Additionally, expert opinions were collected by surveys for the establishment of recovery curves for given specific damage states (ATC 1985, Padgett and DesRoches 2007). In this study a six-parameter sinusoidal-based function proposed by Bocchini, Decò and Frangopol (2012) is used to model the time-dependent functionality.

4.3.1 RECOVERY PATTERN

The functionality recovery is a process fraught with uncertainty. The most representative sources of un-certainty are accounted for by the adopted recovery model for single bridges (Bocchini, Decò and Frangopol 2012). This model is based on the use of a six-parameter curve that describes the evolution of functionality over time (see Figure 4.1(a)). Briefly, the recovery pattern is governed by six selected parameters that include (see Figure 4.1(a)): (a) residual functionality Q_r; (b) idle time δ_i; (c) recovery duration δ_r; (d) target functionality Q_t; (e) parameter s; and (f) parameter A. The relationship between the bridge damage level, obtained by fragility analysis, and the residual functionality level is set according to the ACT-13 project (ATC 1985) and HAZUS (FEMA 2009), whereas the other parameters are based on the study conducted by Shinozuka *et al.* (2005) and engineering judgments. The shape of the recovery pattern is governed by parameters s and A shown in see Figure 4.1(a). For the pre-event assessment of resilience, these introduced parameters are treated as random variables, making the recovery process a random function with a parametric representation. Figure 4.1(b) qualitatively shows the recovery patterns associated with the four damage levels.

4.3.2 RESTORATION STRATEGY

As already mentioned, the final seismic resilience and economic losses will depend also on the recovery strategy adopted by decision makers and the priority given to the restoration of the investigated bridge. These decisions are extremely difficult to

predict, and they are strongly affected by the regional impact of a seismic event (Bocchini and Frangopol 2012b), which is not the focus of this study. Therefore, the proposed technique investigates the resilience associated with different potential recovery strategies. In particular, it is assumed that the rehabilitations-constructions can be performed with three different velocities: fast, average, and slow pace (denoted *F*, *A*, and *S*, respectively). Since these velocities affect duration and costs of the recovery phase, different velocity coefficients for duration V_t and costs V_c are introduced. Hence, the updated recovery duration $\delta_r' = \delta_r(1+V_t)$ depends on the effort in the intervention, where V_t is positive and negative for slow and fast recovery, respectively, whereas the velocity coefficient for costs V_c has opposite signs. These coefficients can be evaluated by analyzing historical records of bridge rehabilitation and reconstruction regarding early completion bonuses or late completion penalties (e.g. Engius 2002 among others). From the review of this document and similar ones, it is found that the V_t is usually about ±20%, while the V_c is about ±15%.

Therefore, considering the above mentioned velocity coefficients and including the option that does not consider any intervention (called "*DN*" in Figure 4.2), the investigated individual recovery patterns are represented by the 20 outcomes (N_{out} = 20), as reported in the decision tree of Figure 4.2. Accordingly, the fragility analysis provides the first five outcomes (chance node A), then depending on the damage level, different decisions regarding the recovery velocity can be made (decision nodes B, C, D, E, F, and G).

A wide spectrum of recovery strategies is investigated depending on the effort of the recovery process (with velocities *F*, *A*, and *S*) and on the bridge damage level.

Restoration strategies are represented by combinations of the possible outcomes of Figure 4.2 considering a selection of one recovery patterns for each damage level. The outcomes included within a single considered strategy are collectively exhaustive and the sum of their associated probabilities leads to one. For instance, in the case study, among all the possible mutually exclusive combinations, 24 restoration strategies (N_{res} = 24) are investigated, as summarized in Table 4.1. Strategy no. 1 provides that all the recovery activities are performed at the maximum velocity (i.e. selecting outcomes 2, 6, 10, 14 of Figure 4.2 for slight, moderate, extensive, and complete damage, respectively), thus disregarding potential budget constraints and achieving full recovery in the shortest time after the event occurrence. On the other hand, decision makers can decide to fit potential budget constraints by selecting strategy no. 18, which provides fast recovery for slight and moderate damage (outcome 2 and 6 of Figure 4.2, respectively), while no action are taken for the cases of extensive and complete damage (outcome 13 and 20 of Figure 4.2, respectively), in order to recover in the shortest time for small earthquakes and do not consider recovery in case of large damage (extensive and complete).

For each considered strategy, the PSR, rapidity, and direct and indirect costs are computed by performing a Monte Carlo simulation based on Latin Hypercube sampling (McKay, Conover and Beckman 1979). This provides a better representation of the sample space, compared to crude Monte Carlo simulation. Figure 4.3 shows the flowchart of the proposed procedure.

4.4 PROBABILISTIC NETWORK RECOVERY MODEL

The functionality of a single bridge is defined as the ability to provide service to users, and is quantified by the ratio of traffic capacity when the bridge is damaged to the traffic capacity when the bridge is intact (set as 100%). On the other hand, segment functionality can depend on many factors, including the layout of the segment, and the vehicular traffic capacities and demands of each route within the segment. Therefore, the evaluation of network resilience is based upon the above mentioned segment characteristics and quantified as (Bocchini and Frangopol 2012a)

$$Q(t) = 100\frac{\Gamma(t) - \Gamma^0}{\Gamma^{100} - \Gamma^0} \tag{4.3}$$

$$\Gamma(t) = \frac{1}{\gamma_T TTT(t) + \gamma_D TTD(t)} \tag{4.4}$$

where $\Gamma(t)$ is the time-dependent segment performance, Γ^0 and Γ^{100} are the segment performances in the cases in which all the bridges are out of service and in service, respectively, $TTT(t)$ and $TTD(t)$ are the time-dependent total travel time and total travel distance of the users within the network, respectively, γ_T and γ_D are the relative weights of importance associated with the travel time and distance, respectively (both assumed 0.5 for the case study 2). Network analysis is conducted according to Decò, Frangopol and Bocchini (2013).

4.4.1 COMPUTATIONAL APPROACH

Monte Carlo simulation based on Latin Hypercube sampling (McKay, Conover and Beckman 1979) is performed for the probabilistic pre-event assessment of resilience and associated direct losses. Latin Hypercube (see Appendix A) provides a better representation of the sample space, compared to the crude Monte Carlo simulation. Samples are generated based on the statistical descriptors of the included random variables. The considered random variables associated with the cost analysis are assumed to be statistically independent, whereas the random variables of the recovery process of each bridge are assumed to be correlated depending on multiple factors, including the construction material of the bridges, their lengths, the relative distance between bridges, and the importance of the carried link within the segment. Due to the lack of statistical information and the unavailability of data regarding the interactions of the recovery process of damaged bridges, in order to perform a fully statistical analysis of damaged highway segments, the correlation coefficients among the residual functionality Q_r and parameters governing the bridge recovery process δ_i and δ_r of two bridges b_1 and b_2 ($b_1 \neq b_2$) are assumed as

$$\rho_{Q_r}\left(Q_{r,b_1}, Q_{r,b_2}\right) = \gamma_{typ} c_{typ}\left(b_1, b_2\right) + \gamma_L c_L\left(b_1, b_2\right) + \gamma_{dis} c_{dis}\left(b_1, b_2\right) \tag{4.5}$$

$$\rho_{\delta_i}\left(\delta_{i,b_1}, \delta_{i,b_2}\right) = \gamma_{typ} c_{typ}\left(b_1, b_2\right) + \gamma_{imp} c_{imp}\left(b_1, b_2\right) \tag{4.6}$$

$$\rho_{\delta_r}\left(\delta_{r,b_1}, \delta_{r,b_2}\right) = \gamma_{typ} c_{typ}\left(b_1, b_2\right) + \gamma_L c_L\left(b_1, b_2\right) + \gamma_{imp} c_{imp}\left(b_1, b_2\right) \tag{4.7}$$

where *typ* is the bridge type (e.g. concrete or steel beams), *L* is the bridge length, *dis* is the relative distance between two bridges, *imp* is the importance of the carried link within the segment (e.g. primary and secondary roads), ρ_{Qr}, $\rho_{\delta i}$, and $\rho_{\delta r}$ are the correlation coefficients of the residual functionality, idle time, and recovery duration, respectively, γ_{typ}, γ_L, γ_{dis}, and γ_{imp} are the relative weights of importance associated with the above listed factors (assumed equal to each other within the same equation), and c_{typ}, c_L, c_{dis}, and c_{imp} are the correlation coefficients assumed according to

$$c_{typ}(b_1,b_2)=\begin{cases}c_c & if\ \ typ(b_1)=typ(b_2)\\ 1-c_c & otherwise\end{cases} \tag{4.8}$$

$$c_L(b_1,b_2)=\begin{cases}c_c & if\ \ 1/1.2\le L(b_1)/L(b_2)\le 1.2\\ 1-c_c & otherwise\end{cases} \tag{4.9}$$

$$c_{dis}(b_1,b_2)=\begin{cases}c_c & if\ \ |dis(b_1,b_2)|\le 5\,miles\\ 1-c_c & otherwise\end{cases} \tag{4.10}$$

$$c_{imp}(b_1,b_2)=\begin{cases}c_c & if\ imp(b_1)=imp(b_2)\\ 1-c_c & otherwise\end{cases} \tag{4.11}$$

where c_c is the assumed correlation coefficient (0.8 for the case study 2).

For the case of segment analysis, when performing the main Monte Carlo simulation, also the bridge damage level is treated as a random variable and its samples are obtained based on a multinomial distribution having probability mass function as

$$f(\mathbf{x}\,|\,\mathbf{p})=\frac{1}{x_1!\cdots x_k!}\,p_1^{x_1}\cdots p_k^{x_k} \tag{4.12}$$

where $\mathbf{x} = (x_1,\ldots,x_k)$ identifies one out of k possible outcomes with fixed probabilities $\mathbf{p} = (p_1,...,p_k)$. In order to identify the outcome, one entry of vector **x** is equal to 1 and the others are 0; $k = 5$, and the probabilities are defined as $\mathbf{p} = (p_{ND}, p_{SD}, p_{MD}, p_{ED}, p_{CD})$, where the subscripts represent no damage, slight, moderate, extensive, and complete damages, respectively. Then, according to Section 4.3, bridge functionality is simulated for each bridge.

4.5 COST ANALYSIS

The losses induced by an earthquake are usually quantified by their associated monetary values. This chapter accounts for direct and indirect costs. Direct costs include all the rehabilitation-reconstruction costs, while operating costs and time loss costs belong to the indirect cost category. For bridge highway segments, only direct costs are considered. In this chapter the discount rate of money is neglected, given that resilience is evaluated over a short period of time (i.e. usually one to two years after the occurrence of an extreme event).

4.5.1 DIRECT COSTS

Direct costs include those associated with the rehabilitation-reconstruction of the bridge, removal of debris, and the construction of a temporary bypass. A simplified method for their estimation is adopted, as customary. Rehabilitation-reconstruction costs are assumed to be proportional to the bridge replacement values. The proportionality factor is called “damage ratio” and it can be related to the bridge damage level (Shinozuka *et al.* 2005, FEMA 2009b). Similarly, the cost of the

construction of a temporary bypass is assumed to be a ratio of the bridge replacement value and the costs of debris removal are proportional to the bridge deck area. Direct costs for single bridges associated with the *i*-th restoration strategy are evaluated as follows (based on Stein *et al.* 1999 and Shinozuka *et al.* 2005)

$$C_{dir,i} = WL\sum_{j=1}^{N_{out}}\left\{P_{ij}\left[\overbrace{\alpha_j c_{reb} d_{r,j}\left(1+V_{c,ij}\right)}^{\text{rehabilitation and reconstruction costs}} + \overbrace{\beta_j c_{rem}}^{\text{debris removal cost}} + \overbrace{\gamma_j c_{reb} b_r\left(1+V_{c,ij}\right)}^{\text{temporary bypass costs}}\right]\right\} \quad (4.13)$$

where W and L are the bridge width (m) and length (m), respectively, index j runs over the outcomes, c_{reb} is the rebuilding cost per square meter (USD/m^2), $d_{r,j}$ is the damage ratio immediately after the occurrence of the earthquake (i.e. the proportionality factor between bridge repair costs and the bridge replacement value), $V_{c,ij}$ is the velocity coefficient for costs, c_{rem} is the debris removal cost per square meter (USD/m^2), b_r is the bypass cost ratio (i.e. the proportionality factor between the cost for the construction of a temporary bypass and the bridge replacement value), and α_j, β_j, and γ_j are coefficients such that $\alpha_j = 1$ if outcome j includes rehabilitation/reconstruction (i.e. outcomes included in set **A**={2,3,4,6,7,8,10,11,12,14,15,16,17,18,19} according to Figure 4.2), $\beta_j = 1$ if outcome j includes debris removal (i.e. outcomes included in set **B**={14,15,16,17,18,19} according to Figure 4.2), $\gamma_j = 1$ if outcome j includes the construction of a temporary bypass (i.e. outcomes included in set **C**={14,15,16} according to Figure 4.2), and $\alpha_j = 0$, $\beta_j = 0$ and $\gamma_j = 0$ otherwise. Each j-th outcome is associated with an initial damage state with probability $P_{DS,j}$ and its inclusion into the i-th strategy is determined by coefficient δ_{ij} leading to $P_{ij} = \delta_{ij}P_{DS,j}$. If outcome j is

included by strategy i, then $\delta_{ij} = 1$, otherwise $\delta_{ij} = 0$. For instance, Figure 4.2 shows that for strategy 1 (i.e. $i = 1$) the coefficients are $\delta_{1\,1} = \delta_{1\,2} = \delta_{1\,6} = \delta_{1\,10} = \delta_{1\,14} = 1$ and $\delta_{1\,3} = \delta_{1\,4} = \delta_{1\,5} = \delta_{1\,7} = \delta_{1\,8} = \delta_{1\,9} = \delta_{1\,11} = \delta_{1\,12} = \delta_{1\,13} = \delta_{1\,15} = \delta_{1\,16} = \delta_{1\,17} = \delta_{1\,18} = \delta_{1\,19} = \delta_{1\,20} = 0$. In this study, according to Figure 4.2, the cases in which no damage occurs and no actions are taken (i.e. outcomes 1, 5, 9, 13, and 20 of Figure 4.2) do not generate any direct costs. Since uncertainty highly affects the estimation of costs, unitary costs c_{reb} and c_{rem}, damage ratio $d_{r,j}$, and bypass cost ratio b_r are treated as random variables in the case study.

For bridge highway segments, the considered economic analysis includes the costs associated with rehabilitation/reconstruction activities, removal of debris, and the potential construction of a temporary bypass (Decò, Frangopol and Bocchini 2013). They are represented by the three addends of Equation (4.14). The estimation of the total cumulative costs C_b for each bridge of the segment is as follows

$$C_b = \int_{t_0}^{t_h} W_b L_b \left[\begin{array}{l} \dfrac{\beta_b c_{rem,b} + \gamma_b c_{reb,b} b_{r,b}\left(1+V_c\right)}{\delta_{i,b}} + \\ \dfrac{\alpha_b c_{reb,b} d_{r,b}\left(1+V_c\right)}{\delta'_{r,b}} \end{array} \right] dt \tag{4.14}$$

where the included variables are the same of those in Equations (4.13) referring to bridge b of the segment. Since costs are affected by uncertainty, unitary costs $c_{reb,b}$ and $c_{rem,b}$, and the bypass cost ratio $b_{r,b}$ are treated as random variables; the damage ratio $d_{r,b}$ is random as well.

For a given network recovery scenario s, the total direct cost for the bridge highway segment $C_{net,s}$ is obtained by summing the costs generated by each single bridge C_b as follows

$$C_{net,s} = \sum_{b=1}^{B} C_b \tag{4.15}$$

where B is the total number of considered bridges.

4.5.2 TRAFFIC FLOW ANALYSIS IN THE CASE OF SINGLE BRIDGES

The bridge functionality is directly related to the number of operable lanes within each traffic direction, and according to the level of induced damage, the bridge can be fully serviceable ($Q(t)$ = 100%), partially serviceable (0% < $Q(t)$ < 100%), or temporary closed ($Q(t)$ = 0%). The traffic flow will accordingly redistribute between the route segment containing the bridge, called "link" in the reminder, and the detour.

The traffic flow carried by a route can be evaluated on the bases of the ADT traveling on the link. In the United States, the ADT for every bridge is provided by the National Bridge Inventory (NBI) database (FHWA 2010). Based on TRB (2000) and accounting for peak and off-peak hours (Caltrans 2009), the total traffic flow F_t (vehicles/h/lane) on a given link direction is given by

$$F_t = \begin{cases} K_1 DA_t & \text{peak hours} \\ K_2 DA_t & \text{off}-\text{peak hours} \end{cases} \tag{4.16}$$

where K_1 and K_2 are the percentages of traffic associated with the portion of ADT during the peak and off-peaks hours, respectively, D is the directional factor, and A_t is the ADT.

Depending on the capacity and traffic, the traffic speed on the link or on the detour is provided by (Bureau of Public Roads 1964)

$$S_t = \frac{S_0}{\left[1 + 0.15\left(\frac{F_t}{F_C n_l}\right)^4\right]} \tag{4.17}$$

where S_0 is the free-flow traffic speed (km/h), F_C is the traffic flow capacity (number of vehicles/h), and n_l is the number of lanes.

Since a comprehensive traffic analysis is out of the scope for the analysis of single bridges, a simplified method for the traffic redistribution between link and detour is adopted herein. The traffic flows carried by the link and the detour are considered in equilibrium before the strike of an earthquake. It is assumed that their ADTs depend only on the respective traffic flow capacities, called $F_{C,l}$ (vehicles/h/lane) and $F_{C,d}$ (vehicles/h/lane) for the link and detour, respectively. Since the ADT of the link and the capacities $F_{C,l}$ and $F_{C,d}$ are known, the total ADT associated with both link and detour can be obtained as

$$A_{tot} = \frac{A_l\left(F_{C,l} n_{l,l} + F_{C,d} n_{l,d}\right)}{F_{C,l} n_{l,l}} \tag{4.18}$$

where A_l and A_{tot} are the link and the total ADTs, respectively, and $n_{l,l}$ and $n_{l,d}$ are the number of lanes of the link and detour, respectively. In a similar way, the ADT of the detour A_d can be obtained

$$A_d = \frac{A_{tot} F_{C,d} n_{l,d}}{F_{C,l} n_{l,l} + F_{C,d} n_{l,d}} \tag{4.19}$$

When an earthquake strikes and the rehabilitation phase begins, the bridge functionality $Q_{ij}(t)$, associated with the *i*-th strategy (see Table 4.1) and the *j*-th outcome (see Figure 4.2), varies over the restoration time, affecting the traffic flow of the link and of the detour. Simplified expressions for the estimation of their associated ADTs are

$$A'_{l,ij}(t) = \frac{A_{tot} F_{C,l} n_{l,l} Q_{ij}(t)}{F_{C,l} n_{l,l} Q_{ij}(t) + F_{C,d} n_{l,d}} \tag{4.20}$$

$$A'_{d,ij}(t) = \frac{A_{tot} F_{C,d} n_{l,d}}{F_{C,l} n_{l,l} Q_{ij}(t) + F_{C,d} n_{l,d}} \tag{4.21}$$

where $A'_{l,ij}(t)$ and $A'_{d,ij}(t)$ are the time-dependent post-event ADTs of link and detour, respectively. Therefore, the time-dependent traffic speed accounting for peak and off-peaks hours (Equation (4.16)) can be assessed for both link and detour (Equation (4.17)).

4.5.3 INDIRECT COSTS

Indirect costs are mainly caused by traffic disruption. Marginal operational costs occur when users travel through detours, which are usually longer than the original route.

The proposed general formulation accounts for cars and trucks, and for traffic at peak and off-peaks hours (based on Stein *et al.* 1999):

$$C_{op,i} = \sum_{j=1}^{N_{out}} \left\{ P_{ij} D_l \left[c_{op,car}(1-\tau) + c_{op,truck}\tau \right] \int_{t_0}^{t_h} \left[A'_{d,ij}(t) - A_d \right] dt \right\} \tag{4.22}$$

where $c_{op,car}$ and $c_{op,truck}$ are the operating costs of cars and trucks per kilometer (USD/km), respectively, τ represents the average daily truck traffic (ADTT) as percentage of ADT, D_l is the additional travel distance (km), $A'_{d,ij}(t)$ is the time-dependent ADT of the detour after the seismic event, A_d is the ADT of the detour before the seismic event, t_0 is the time at which the seismic event occurs, t_h is the investigated time horizon, t is time, and dt is the variable of integration (time).

After the seismic event, if traffic disruption occurs, users are forced to travel through the link and detour at a lower speed than usual, thus marginal travel time generates monetary losses. Time loss costs associated with the i-th strategy are (based on Stein *et al.* 1999):

$$\begin{aligned} C_{tl,i} = {} & \left[c_w O_{car}(1-\tau) + (c_{tc} O_{truck} + c_{inv})\tau \right] \cdot \\ & \sum_{j=1}^{N_{out}} \left\{ P_{ij} \int_{t_0}^{t_h} A'_{b,ij}(t) \left(\frac{L_l}{S'_{b,ij}(t)} - \frac{L_l}{S_b} \right) + A'_{d,ij}(t) \left(\frac{L_l + D_l}{S'_{d,ij}(t)} - \frac{L_l + D_l}{S_d} \right) dt \right\} \end{aligned} \tag{4.23}$$

where c_w is the wage per hour (USD/h), c_{tc} is the total compensation per hour (USD/h), c_{inv} is the inventory cost (USD/h), O_{car} and O_{truck} are the vehicle occupancies for cars and trucks, respectively, L_l is the link length (km), $S'_{l,ij}(t)$ and $S'_{d,ij}(t)$ are the time-dependent traffic traveling speeds (km/h) of link and detour after the seismic

event, respectively, and S_l and S_d are the traffic speeds (km/h) of link and detour before the seismic event, respectively.

In most practical cases, the majority of the involved parameters, $c_{op,car}$, $c_{op,truck}$, c_w, c_{tc}, c_{inv}, S_l, and S_d are affected by uncertainties; therefore, the proposed technique treats them as random variables.

4.6 CASE STUDY 1: SINGLE HIGHWAY BRIDGES

The proposed approach is applied to an existing bridge (structure no. 560680R according to FHWA 2010) carrying a three-lane segment of the northbound I-15 highway crossing the Temescal Wash, located between the cities of Corona and Murrieta in California. The investigated structure is a continuous concrete bridge.

The historical epicenter of the May 15, 1910 earthquake, having latitude 33º 42', longitude -117º 24', and depth of 10 km, is situated at a distance of about 4 km from the bridge. The impact on the highway bridge of an earthquake with this epicenter and magnitude 8 (Richter scale) is assessed. Bridge vulnerability is obtained by means of a fragility analysis performed using the software HAZUS (FEMA 2009a).

By setting 1/10 of a month as computational time interval and considering 14 months as time horizon t_h (with $t_0 = 0$ being the moment when the event strikes), the mean profiles of the bridge functionality over time associated with different restoration strategies (Table 4.1) are obtained by performing Monte Carlo simulation. By using Latin Hypercube, sets of 50,000 samples are generated for each outcome of Figure 4.2, for a total of 1,000,000 samples. Then, the results of each set of samples (50,000) are weighted by the probability of their associated j-th outcomes P_{ij} for each

selected *i*-th strategy. The software MATLAB (The MathWorks 2011) is used to run the simulation based on a parallel processing code which requires about 10 minutes for 1,000,000 samples on a DELL Precision T7400 workstation with two quad core Intel Xeon processors with 8 GB of RAM.

The time-dependent bridge functionality (recovery model) is modeled by using the six-parameter function (Bocchini, Decò and Frangopol 2012). This approach is based on the assessment of the parameters involved in the recovery process. Although this is not an easy task, the types of distribution and their associated statistical descriptors are proposed based on literature surveys and engineering judgment. Table 4.2 summarizes the values of the random variables and parameters assumed for the adopted six-parameter recovery function, and the associated bibliographic references. The involved random variables are assumed to be statistically independent. For slight, moderate, and extensive damage, different triangular distributions for the residual functionality Q_r are provided (see Figure 4.1(a)), while for the case of complete damage, residual functionality is null. The modes of the triangular distributions coincide with the values provided by ATC-13 (1985) and FEMA (2009b). Since conducting estimates on the bridge importance is outside the scope of this chapter, the values of the idle time interval δ_i have been assumed uniformly distributed (see Figure 4.1(a)) between one and two months for all the recovery patterns of Figure 4.1(b). The assumed values for the recovery duration δ_r follow a triangular distribution (see Figure 4.1(a)) and are estimated in accordance with those provided by Shinozuka *et al.* (2005) for each damage state. Although the proposed model can treat the target functionality Q_t as random variable, in this case study, it has been assumed that the recovery

patterns completely restore the bridge functionality (100%). Finally, parameters A and s are functions of the random post-event damage, determined by engineering judgment in order to obtain the recovery pattern of Figure 4.1(b).

Strategy 6 (see Table 4.1) prescribes an average recovery velocity for any initial damage, without the construction of the bypass and is selected as example to illustrate the results. Figure 4.4(a) shows five random sample recovery patterns for each of the random post-event damage levels for the selected strategy 6. As shown in Figure 4.4(a), and in accordance with Figure 4.1(b), five groups of curves associated with the five bridge damage levels may be identified for strategy 6. The complete simulation of these recovery patterns (1,000,000 samples) leads to the mean recovery pattern shown in Figure 4.4(b). Indication on the dispersion of the functionality pattern is also shown in Figure 4.4(b), which provides the frequency of the functionality when the earthquake strikes, and four and eight months after, for strategy 6. Additionally, the frequency of the full recovery time is shown (vertical bars). It can be noticed that, due to the results of the fragility analysis, functionality is quite dispersed. This is caused by the fact that HAZUS considers two distinct failure modes (ground shaking and ground failure) that provide dispersed probabilities of the bridge being in specific damage states. Figure 4.4(c) shows the mean recovery patterns of ten representative strategies (1, 4, 5, 6, 7, 8, 12, 14, 19, and 23 of Table 4.1). The fastest expected full recovery is about eight months (strategies 1 and 14), whereas the slowest expected full recovery is achieved only about 13 months after the earthquake occurrence (strategies 7 and 23). Moreover, during the investigated time frame, it can be noticed that strategy 19 only recovers about 40% of the expected value of functionality, while according to

its definition (Table 4.1), strategy 4 does not account for any rehabilitations, hence the residual functionality does not increase over time. Figure 4.4(c) shows also that in this case the expected residual functionality of the bridge is about 30%.

PSR and rapidity are then assessed based on the simulated functionality profiles by applying Equations (4.1) and (4.2), respectively. Figure 4.5 shows the frequency histogram of (a) resilience and (b) rapidity for strategy 6. The two frequency histograms are clearly subdivided into two parts. One part is represented by the bars located at values 1 and 0 for resilience and rapidity, respectively, which represent no damage, while the remaining bars are associated with the occurrence of any damage level. For the representative strategy 6, the expected resilience and rapidity are μ_R = 0.687 and μ_r = 6.050º, respectively.

Mean values and standard deviations of resilience and rapidity are shown for all the 24 considered strategies in Figure 4.6(a) and Figure 4.6(b), respectively. Bars represent intervals equivalent to ± one standard deviation. It can be noticed that strategy 4 (which according to Table 4.1 considers no actions) provides the lowest level of resilience and rapidity, and together with strategies 18, 19, and 20, is affected by the largest standard deviations depending exclusively on the dispersion obtained by the fragility analysis. Smaller standard deviations are found when functionality is approaching full recovery (100%). Hence, strategies with higher expected resilience and rapidity (such as strategies 1 and 14, which require greater social effort) have relatively small standard deviations (the coefficient of variation is around 15%). The impact of the earthquake in terms of expected direct costs and external consequences (time loss and additional operating costs) is shown in Figure 4.6(c). Costs are

evaluated based on the deterministic and random variables summarized in Table 4.3 and Table 4.4. Figure 4.6(c) shows the importance of large investments in trying to reduce indirect losses. Accordingly, strategies 1 and 14 limit indirect costs, while strategies 4, 18, 19, and 20 do the opposite. Minimum expected indirect costs (about 7 USD millions) are obtained only if about 4 USD millions are invested (strategy 1). Finally, as observed in Figure 4.6(c), the construction of a temporary bypass (e.g. strategies 1, 2, and 3) heavily decreases the impact on indirect costs against an investment that is almost twice with respect to the same strategy without the bypass (e.g. strategies 5, 6, and 7).

Indications regarding the available options for post-event response can be based on the results reported in Figure 4.7, where the expected direct costs are shown along with expected resilience and full recovery time for each strategy. Figure 4.7(a) shows decreasing expected resilience and associated direct costs provided for the 24 strategies, while Figure 4.7(b) shows decreasing direct investments against resilience. Moreover, as illustrated in Figure 4.7(c), the expected full recovery time is also computed for those strategies that imply recovery from each damage state (i.e. strategies 4, 8, 9, 10, 11, 12, 13, 18, 19, and 20 are excluded because they include the outcomes "*DN*" of Figure 4.2). Depending on the priorities of decision makers, such as full and fast restoration disregarding budget limitations versus available options subjected to budget constraints, different restoration strategies can be used for the assessment of expected resilience. For instance, if a fast recovery that reduces external costs is the priority, strategy 1 is likely to be selected (see Figure 4.6(c) and Figure 4.7(a)), while if the available budget is limited for instance, to 2.5 USD millions

(Figure 4.7(b,c)), the available options remain strategies 4, 5, 6, 7, 11, 12, 13, 16, 17, 18, 19, 20, 23, and 24. Strategy 5, being the one with largest mean resilience and shortest mean full recovery time among the remaining available options, is the most likely to be selected. It can be further noticed that resilience does not increase considerably when a much greater investment is provided, while the reduction of indirect costs is more significant. The construction of a temporary bypass determines a large reduction of external costs; instead, only slight resilience is gained by adopting these strategies, as shown in Figure 4.7.

4.6.1 SENSITIVITY ANALYSES

Three sensitivity analyses are also provided. The first sensitivity analysis deals with two different cases. In the first case, it is assumed that the recovery duration δ_r is based on the values provided by Shinozuka *et al.* (2005) (previously analyzed), whereas for the second case, the recovery duration δ_r is based on the values adopted by HAZUS (FEMA 2009b) and summarized in Table 4.5. Figure 4.8(a) shows the functionality over time of the same representative strategies investigated in Figure 4.4(a). It can be observed that the obtained profiles significantly differ from the previous ones (first case). This demonstrates that the choice of appropriate values for the recovery duration δ_r is of critical importance. Additional effort is needed in order to obtain estimators that better fit the real rehabilitation process. Figure 4.8(b) reports on the differences in terms of resilience. It can be observed that the second case provides lower resilience and overall larger standard deviation than the first case.

The second sensitivity analysis is performed considering that the earthquake magnitude varies from 6.0 to 8.4 (with steps of 0.2), maintaining the same epicenter. Figure 4.9(a) shows how the profiles of the expected functionality are affected by events with increasing magnitude. Expected resilience and direct costs evaluated for different earthquake magnitudes are shown in Figure 4.9(b) for strategy 6. When the magnitude increases, the decrease of resilience is relatively low, while the needed investment exponentially raises, approaching a plateau of about 2.2 USD millions for earthquakes greater than magnitude 8.

The third and last sensitivity analysis investigates the computational accuracy in terms of mean resilience associated with the selection of different sampling size for the Monte Carlo simulation of strategy 6 (100, 500, 1,000, 5,000, 10,000, 50,000, 100,000, 500,000, and 1,000,000 samples). 100 independent computations have been performed for each of the considered sample sizes (Figure 4.10). The estimation of the mean resilience in the case of 1,000,000 samples is affected by a negligible error. The 100,000 samples case already shows good agreements to the trend line.

4.7 CASE STUDY 2: BRIDGE HIGHWAY SEGMENTS

Four highway segment layouts are analyzed in this paper (Figure 4.11) in order to investigate how network functionality and resilience are affected by different highway segment configurations. Three different bridges denoted B_1, B_2, and B_3, are shown in the layouts of Figure 4.11, including a series system with identical bridges B_1 (layout 1), and series (layout 2), series/parallel (layout 3), and parallel (layout 4) systems with different bridges B_1, B_2, and B_3.

It is assumed that layouts 1, 2, and 3, containing at least one edge in series, are subjected to 5,000 car-equivalent vehicles per hour traveling from node O to node D, whereas for layout 4, 15,000 car-equivalent vehicles per hour are considered. The reason for this distinction is that the resulting segment traffic volume for all the layouts is approximately kept constant and balanced with each route traffic capacities. The distance O-D equal to 10 miles (16.1 km) is covered in 10 minutes at free flow, whereas the practical capacities of the intact links are 4,000 cars/h.

For the single bridges within the layouts, only three recovery strategies are analyzed, including: a) fast recovery with the construction of a temporary bypass bridge that carries a portion of the original traffic flow in case of complete damage; b) slow recovery without the construction of any bypass bridge; and c) no intervention. Whereas, for each segment layouts, four recovery scenarios s are investigated, depending on the combination between the adopted recovery strategies for each single bridge within the highway segment. Accordingly, the four network recovery scenarios are: 1) B_1, B_2, and B_3 recover at fast pace (strategy a); 2) B_1, B_2, and B_3 recover at slow pace (strategy b); 3) equal to scenario 1 but for B_2 no actions are taken (strategy c); and 4) equal to scenario 2 but for B_2 no actions are taken (strategy c). The used recovery parameters are based on Table 4.2 and Table 4.4. In Table 4.6 the remaining input data are specified. The program MATLAB (The Mathworks 2011) has been used to perform the necessary calculations. By conducting the Monte Carlo simulation (50,000 samples) and considering an investigated time horizon of 12 months, the mean functionality profiles for each bridge are as shown in Figure 4.12. As expected, the largest functionality is obtained when considering the recovery strategy a, whereas

strategy c does not improve the residual bridge functionality. It can be also noted that the three bridges have different residual functionality and that strategy b differently affects the three bridges, especially in the initial part of the recovery process.

Moreover, the correlations between the residual functionality Q_r and the parameters governing the bridge recovery process δ_i and δ_r of different bridges are accounted for according to Equations (4.5)–(4.11).

Figure 4.13 shows the mean functionality profiles for each one of the four investigated layouts, whereas Figure 4.14 shows the frequency histograms of resilience associated with scenarios 1 and 3 for the layouts 2 and 3. It can be noticed that the expected functionality is fully restored for scenarios 1 and 2, which include recovery actions for all the bridges. Therefore, the associated expected resilience is higher for scenarios 1 and 3, if compared to the others (2 and 4) for all the considered layouts. Among the layouts with the same assumed volume of car-equivalent vehicles per hour (layouts 1, 2, and 3), layout 3 performs better than those in series (layouts 1 and 2) when considering scenarios 3 and 4. This is clearly shown in Figure 4.13, in terms of segment functionality, and in Figure 4.14, in terms of resilience. Although a direct comparison between layout 2 (series configuration) and 4 (parallel configuration) is not possible because of the different car-equivalent vehicles per hour, it can be noted that if this input is kept proportional with the sum of the capacities of different layouts, the differences in terms of network functionality are small. Finally, Figure 4.15 shows the mean profiles of the direct costs for B_1, B_2, B_3, and those associated with layouts 2, 3, and 4. Since bridge B_2 is the largest among the others and

it suffered considerable damage (Table 4.6), its direct cost is higher compared with that of the other bridges.

4.8 CONCLUSIONS

From this chapter, which is based on Decò, Bocchini and Frangopol (2013) and Decò, Frangopol, and Bocchini (2013), the following conclusions are obtained:

1. The assessment of seismic resilience can be conducted in a probabilistic way by including uncertainty affecting both bridge vulnerability and recovery phase. The fragility analysis provides very disperse results for the post-event damage state. Therefore, resilience and rapidity are affected by large uncertainty.
2. The combined information given by resilience and direct and indirect costs allows to investigate the benefits of different restoration strategies. It is found that the average functionality recovery heavily depends on the gain obtained by the rehabilitations associated with extensive and complete damages.
3. For both single bridges and highway segments, in the case of complete damage, the construction of a temporary bypass helps mitigating the impact on indirect costs. However the gain of resilience is not as high as expected.
4. The results provided in the sensitivity analysis of the first case study show that the appropriate selection of the parameter distributions is critically important for conducting a reliable assessment.
5. For bridge highway segments, the number of random variables considered for each bridge is large; therefore when the number of bridges increases, different methods other than the adopted Monte Carlo simulation may be considered.

Table 4.1 Definition of the restoration strategies for single bridges indicating the recovery velocity from specific damage levels.

Restoration strategy no.	Recovery velocity from damage level				Restoration strategy no. (cont.)	Recovery velocity from damage level			
	SD	MD	ED	CD		SD	MD	ED	CD
1	F	F	F	F(wb)	13	DN	DN	S	S(w/ob)
2	A	A	A	A(wb)	14	S	S	F	F(wb)
3	S	S	S	S(wb)	15	S	S	A	A(wb)
4	DN	DN	DN	DN	16	S	S	F	F(w/ob)
5	F	F	F	F(w/ob)	17	S	S	A	A(w/ob)
6	A	A	A	A(w/ob)	18	F	F	DN	DN
7	S	S	S	S(w/ob)	19	A	A	DN	DN
8	DN	DN	F	F(wb)	20	S	S	DN	DN
9	DN	DN	A	A(wb)	21	F	F	S	S(wb)
10	DN	DN	S	S(wb)	22	A	A	S	S(wb)
11	DN	DN	F	F(w/ob)	23	F	F	S	S(w/ob)
12	DN	DN	A	A(w/ob)	24	A	A	S	S(w/ob)

Note: SD = slight damage, MD = moderate damage, ED = extensive damage, CD = complete damage, F = fast recovery, A = average recovery, S = slow recovery, DN = do nothing, wb = with bypass, w/ob = without bypass

Table 4.2 Values of the random variables and parameters of the assumed six-parameter recovery model that describes the evolution of functionality over time for each recovery pattern associated with a specific bridge damage state (see Figure 4.1).

Type of recovery	* Residual functionality Q_r			Idle time interval δ_i (months)		†Recovery duration δ_r (months)			Target functionality Q_t			‡ Fixed parameters	
	$Q_{r,min}$	$Q_{r,mode}$	$Q_{r,max}$	$\delta_{i,min}$	$\delta_{i,max}$	$\delta_{r,min}$	$\delta_{r,mode}$	$\delta_{r,max}$	$Q_{t,min}$	$Q_{t,mode}$	$Q_{t,max}$	s	A
No damage	1 (deterministic)			does not apply		does not apply			does not apply			does not apply	
Slight damage	0.5	0.75	1	1	2	0.333	2.667	5	1	1	1	0.1	0.0
Moderate damage	0	0.25	0.5	1	2	0.667	3.667	6.667	1	1	1	0.5	-0.1
Extensive damage	0	0.1	0.2	1	2	2	5.167	8.333	1	1	1	0.9	0.1
Complete damage - Rebuilding with bypass	0 (deterministic)			1	2	2.5	6.25	10	1	1	1	0.5	-0.1
Complete damage - Rebuilding without bypass	0 (deterministic)			1	2	2.5	6.25	10	1	1	1	0.9	0.1

* Data assessed based on the ATC-13 (1985) and FEMA (2009b)
† Data assessed based on Shinozuka *et al.* (2005)
‡ Based on engineering judgment

Table 4.3 Values of the statistical descriptors of the triangularly distributed damage ratio d_r (based on FEMA 2009b).

Type of recovery	Damage ratio d_r		
	$d_{r,min}$	$d_{r,mode}$	$d_{r,max}$
No damage	0 (deterministic)		
Slight damage	0.01	0.03	0.03
Moderate damage	0.02	0.08	0.15
Extensive damage	0.10	0.25	0.40
Complete damage - Rebuilding with bypass	0.30	1.00	1.00
Complete damage - Rebuilding without bypass	0.30	1.00	1.00

Table 4.4 Statistical descriptors and deterministic parameters used for the cost analysis. Costs refer to their values at year 2011.

Deterministic parameter	Value	Reference
ADT	39,500	FHWA (2010)
ADTT/ADT ratio	13%	FHWA (2010)
Bridge length (m)	115.5	FHWA (2010)
Bridge width (m)	21	FHWA (2010)
Detour additional travel distance (km)	2	FHWA (2010)
Detour number of lanes	1	Google Inc. (2011)
Detour traffic flow capacity (vehicle/hour/lane)	1,000	Assumed
Directional factor	0.5	Assumed
Length of the link (km)	5.95	Google Inc. (2011)
Link traffic flow capacity (vehicle/hour/lane)	2,000	Assumed
Link number of lanes	3	Google Inc. (2011)
Parameter K_1	0.085	Caltrans (2009)
Parameter K_2	0.030	Caltrans (2009)
Vehicle occupancies for cars	1.50	AASHTO (2003)
Vehicle occupancies for trucks	1.05	AASHTO (2003)

Random variable	Mean	COV	Distribution type	Reference
Compensation for truck drivers (USD/hour)	29.87	0.31	* LN	AASHTO (2003)
Detour speed (km/hour)	50	0.20	* LN	Assumed
Inventory costs (USD/hour)	3.81	0.20	* LN	AASHTO (2003)
Operating costs for cars (USD/km)	0.40	0.19	* LN	AASHTO (2003)
Operating costs for trucks (USD/km)	0.57	0.19	* LN	AASHTO (2003)
Wage for car drivers (USD/hour)	11.91	0.28	* LN	AASHTO (2003)

Random variable	Min.	Max.	Distribution type	Reference
Link speed (km/hour)	90	120	* Uniform	Assumed
Debris removal cost (USD/m^2)	224	560	Uniform	DOT-FL (2009)
Rebuilding costs (USD/m^2)	1,318	3,294	Uniform	Caltrans (2010)

Random variable	Min.	Mode	Max.	Distribution type
Bypass cost ratio	0.3	0.5	0.7	* Triangular

* Assumed
Note: LN = log-normal distribution, COV = coefficient of variation

Table 4.5 Values of the statistical descriptors of the triangularly distributed recovery duration δ_r (based on FEMA 2009b).

Type of recovery	Recovery duration δ_r (months)		
	$\delta_{r,min}$	$\delta_{r,mode}$	$\delta_{r,max}$
No damage	does not apply		
Slight damage	0.033	0.067	0.100
Moderate damage	0.167	0.250	0.333
Extensive damage	3	4	5
Complete damage - Rebuilding with bypass	8	12	14
Complete damage - Rebuilding without bypass	8	12	14

Table 4.6 Statistical descriptors and additional parameters used for the case study 2.

Random Variable	Values									DT	Reference
	Bridge B_1			Bridge B_2			Bridge B_3				
	Min.		Max.	Min.		Max.	Min.		Max.		
c_{reb}	1,318		3,294	1,976		3,294	1,318		1,647	U	Caltrans (2010)
c_{rem}	224		560	224		560	224		560	U	FL-DOT (2009)
	Min.	Mode	Max.	Min.	Mode	Max.	Min.	Mode	Max.		
b_r	0.3	0.5	0.7	0.3	0.5	0.7	0.3	0.5	0.7	T	Assumed

Parameter	Values			Reference
	Bridge B_1	Bridge B_2	Bridge B_3	
L	85	395	66	FHWA (2010)
W	19.8	19.4	26.8	FHWA (2010)
P_{ND}	0.093	0.233	0.093	Assumed
P_{SD}	0.041	0.000	0.142	Assumed
P_{MD}	0.085	0.000	0.114	Assumed
P_{ED}	0.179	0.231	0.202	Assumed
P_{CD}	0.602	0.536	0.449	Assumed

Note: DT = Distribution type, U = Uniform, T = Triangular

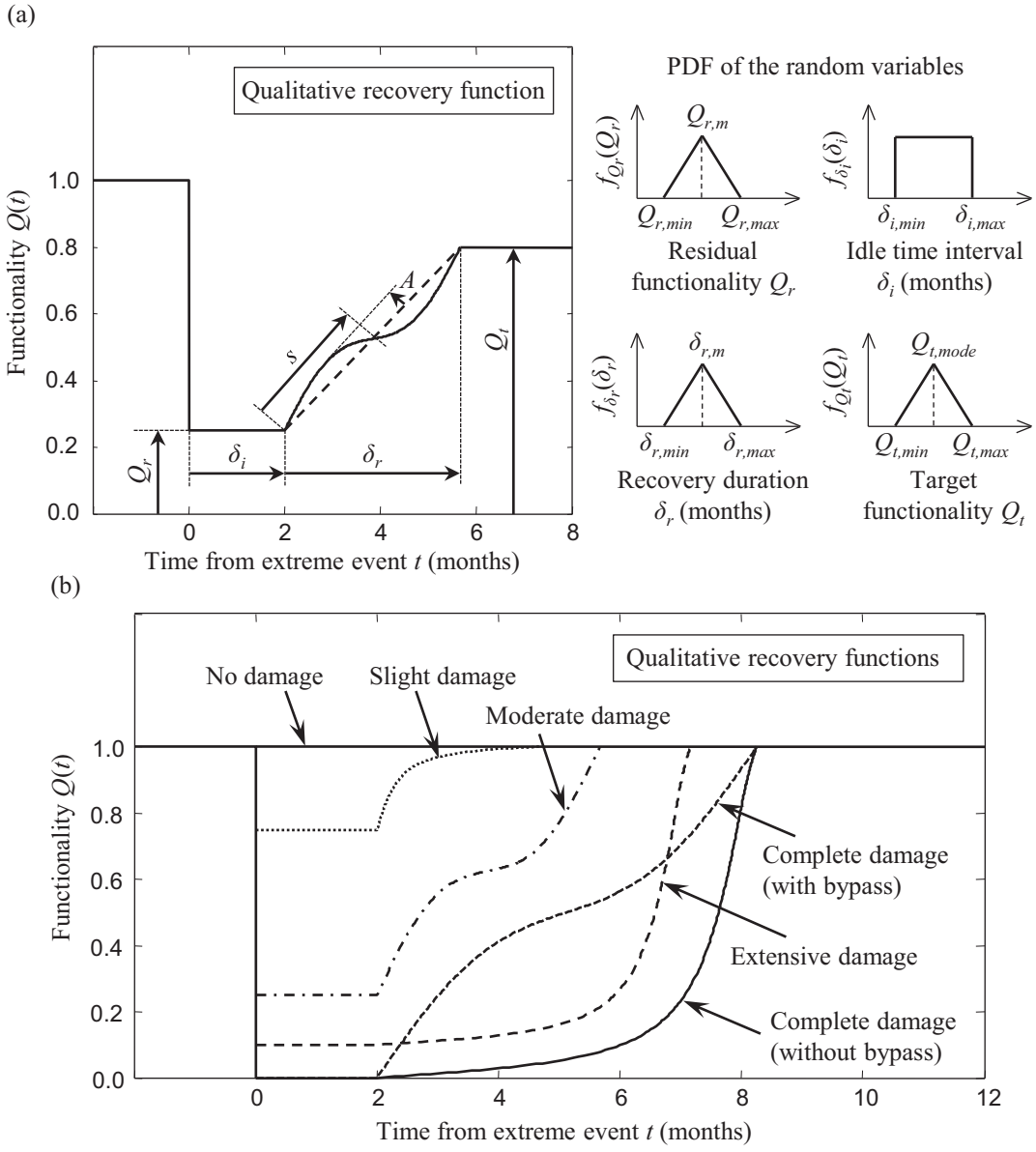

Figure 4.1 Qualitative representation of (a) the adopted six-parameter bridge recovery function including the distribution types of specific random variables, and of (b) the recovery patterns associated with different types of damage and recovery options.

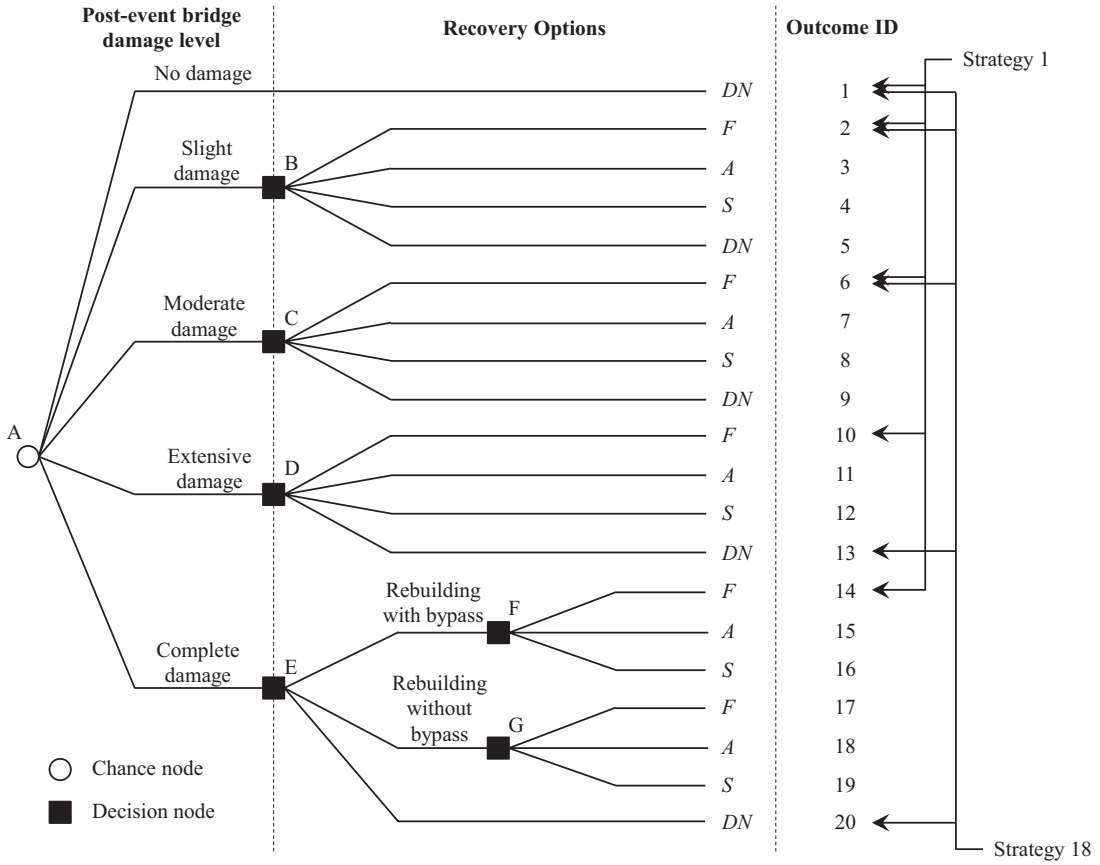

Figure 4.2 Decision tree indicating the 20 considered outcomes that include the velocity of the recovery actions and the options without repair. Note: *DN* = do nothing, *F* = fast recovery, *A* = average recovery, *S* = slow recovery.

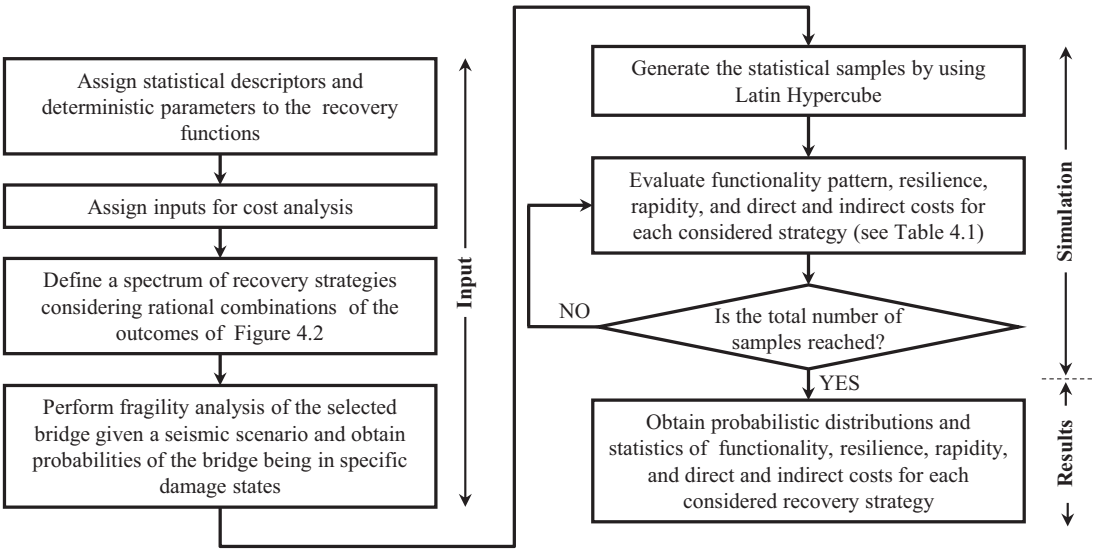

Figure 4.3 Flowchart of the proposed procedure for the evaluation of probabilistic seismic resilience (PSR), rapidity, and socio-economic impact.

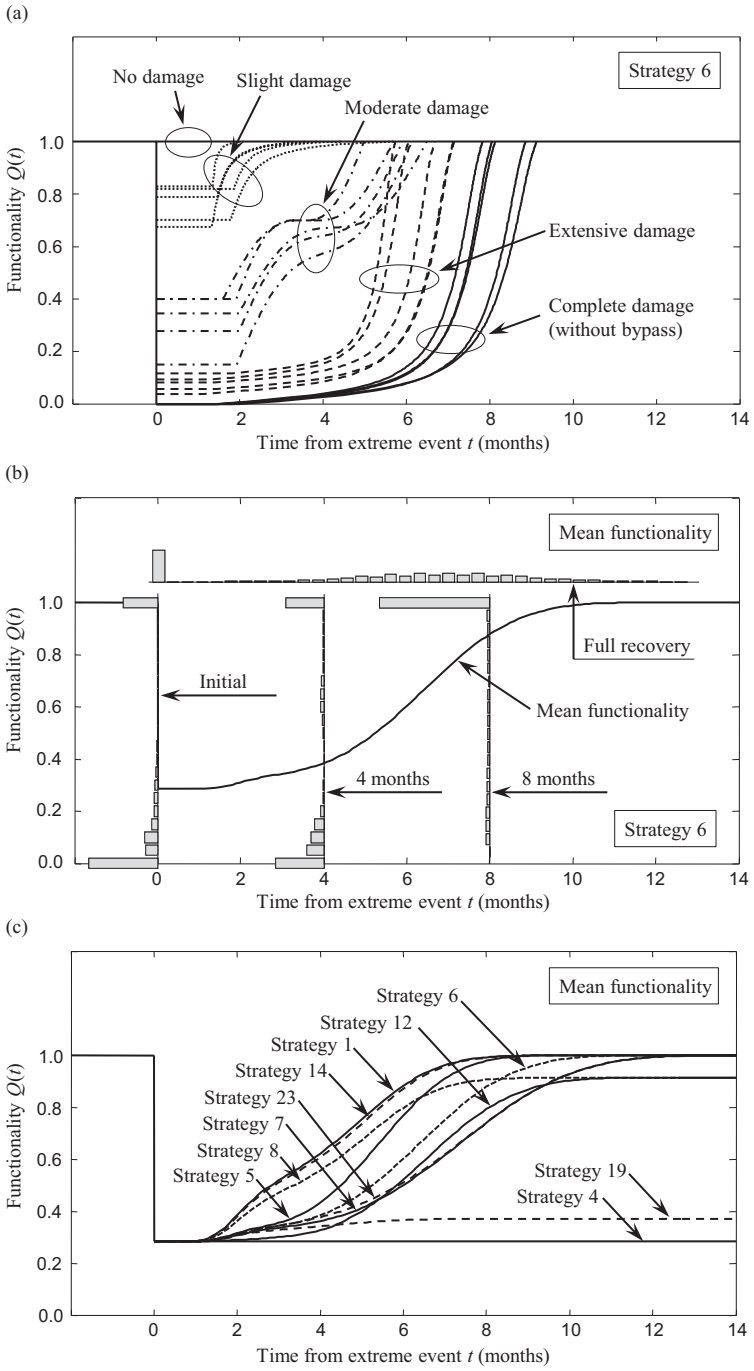

Figure 4.4 (a) Random sample recovery patterns for strategy 6. (b) Expected functionality of strategy 6 and graphical representation of the frequency histogram of functionality when the earthquake strikes, 4 and 8 months after, and frequency histogram of the full recovery time. (c) Expected functionality profiles associated with the representative strategies 1, 4, 5, 6, 7, 8, 12, 14, 19, and 23 of Table 4.1.

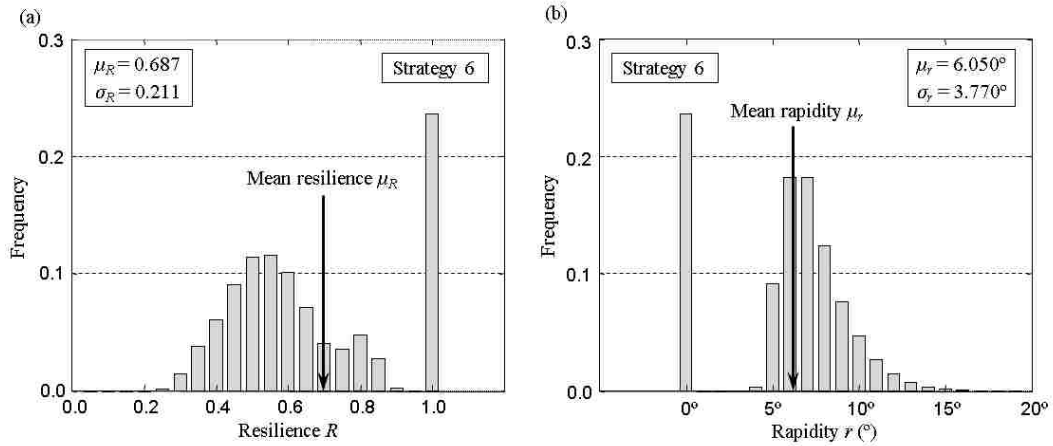

Figure 4.5 Frequency histograms of the obtained (a) resilience and (b) rapidity for strategy 6. μ and σ are the mean and standard deviation, respectively.

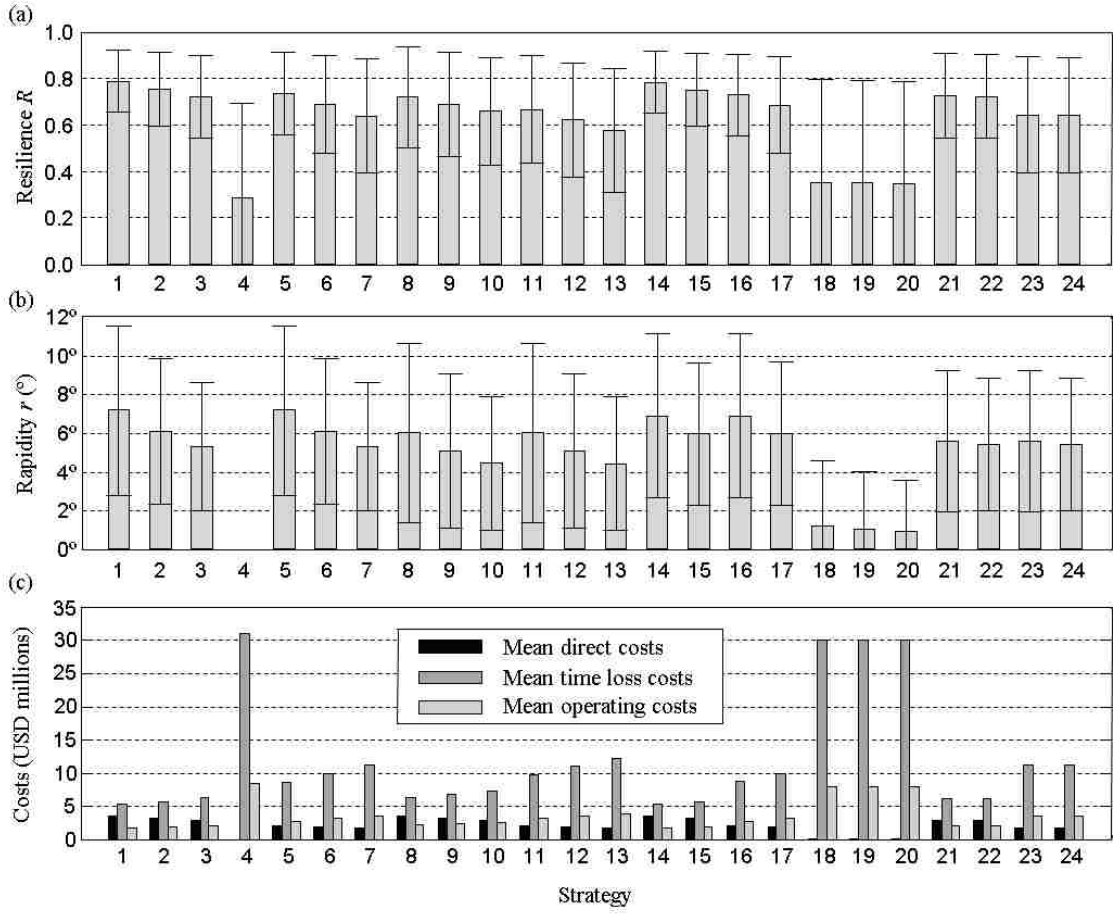

Figure 4.6 Bars reporting on the mean and standard deviation of (a) resilience and (b) rapidity for all the 24 considered strategies. The intervals refer to ± one standard deviation. (c) Histogram of the expected direct and indirect costs for each strategy.

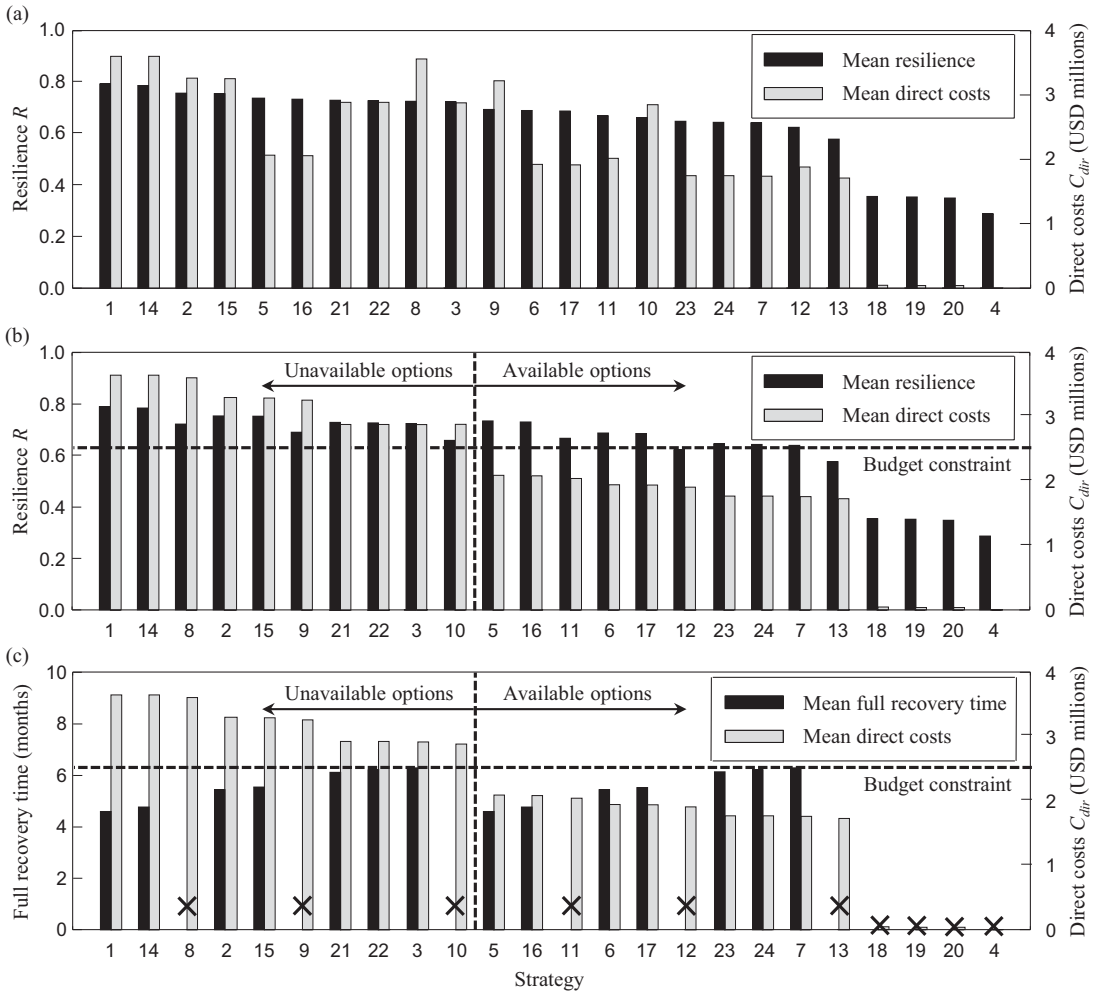

Figure 4.7 Histograms of expected resilience versus expected direct costs in the cases where strategies are sorted by (a) decreasing resilience and (b) decreasing direct costs, and (c) expected full recovery time versus decreasing expected direct costs. Note: symbol × is used for those strategies where the expected full recovery time cannot be evaluated.

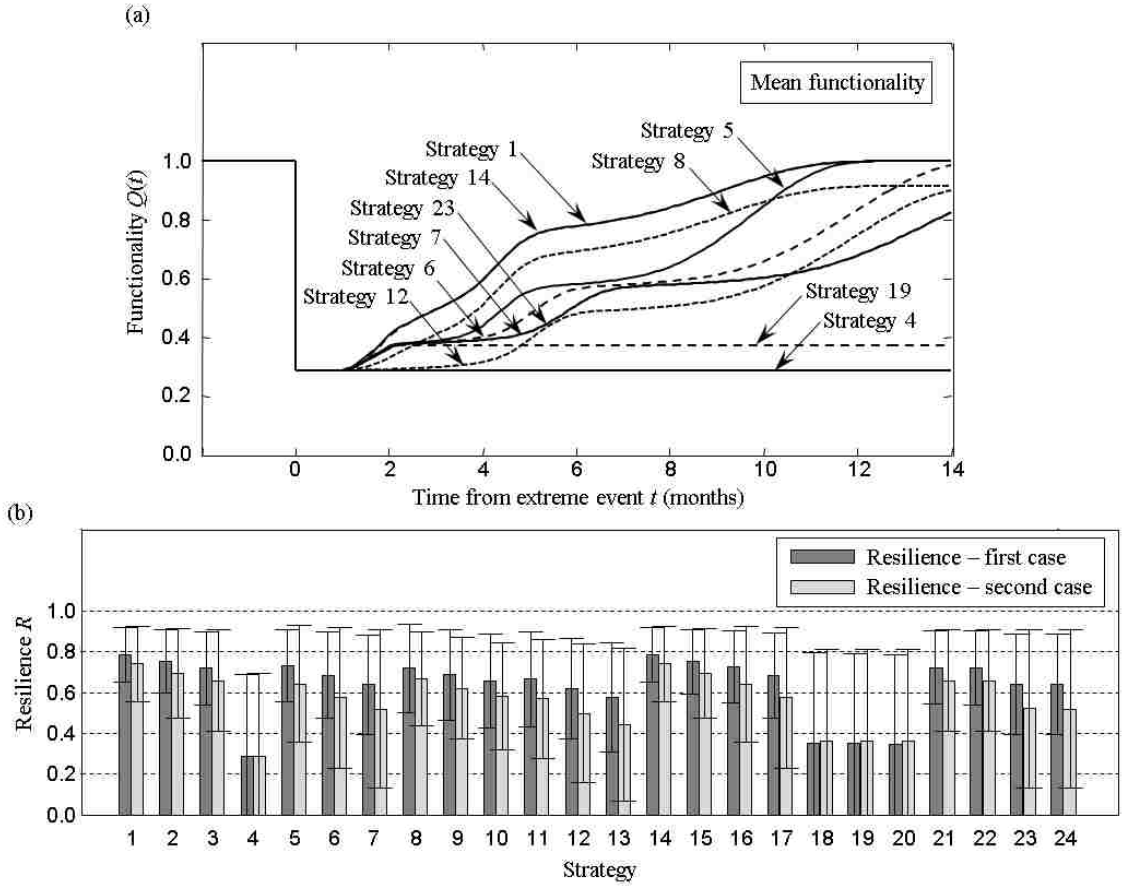

Figure 4.8 (a) Expected functionality profiles associated with the representative strategies 1, 4, 5, 6, 7, 8, 12, 14, 19, and 23 of Table 4.1. (b) Comparison between resilience obtained for case 1 (data from Table 4.3) and case 2 (data from Table 4.5).

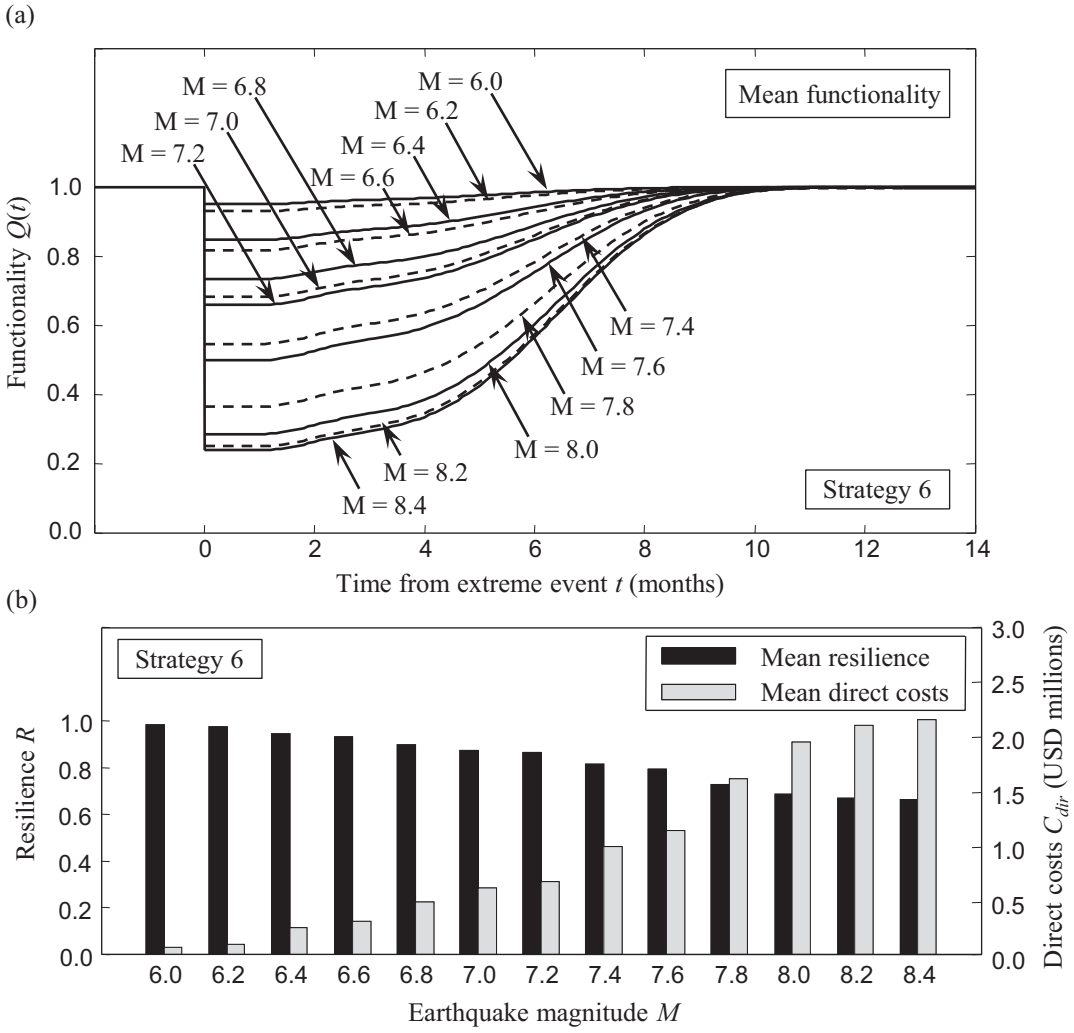

Figure 4.9 (a) Expected functionality profiles associated with strategy 6 varying the seismic event magnitude. (b) Trend of expected resilience and direct costs when the earthquake magnitude varies between 6.0 and 8.4.

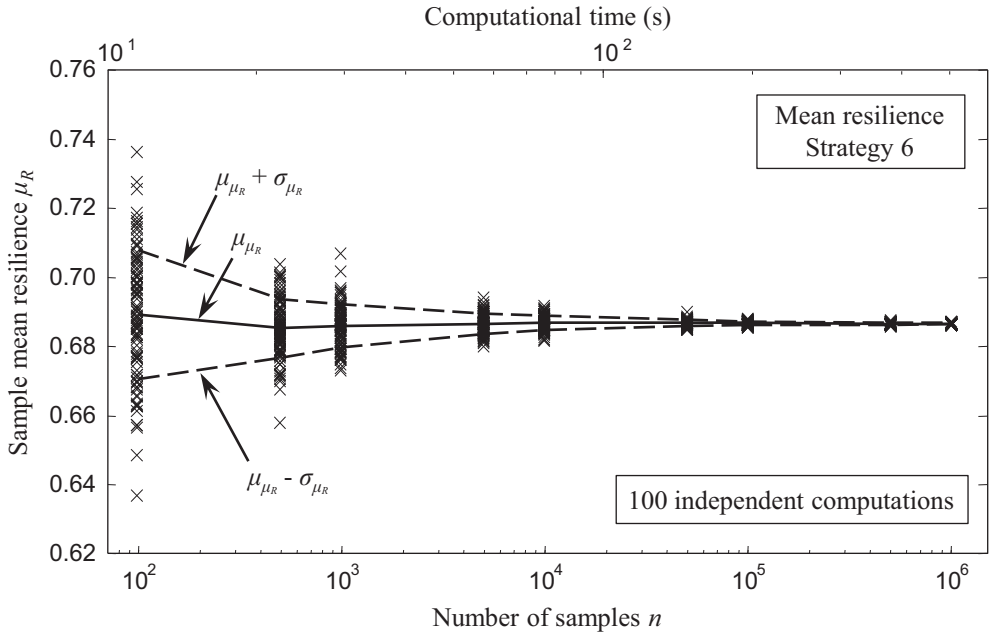

Figure 4.10 Mean value of resilience for each of the 100 independent computations in the case of varying the sample size between 100 and 1,000,000 samples. Trend of the mean and mean plus and minus one standard deviation are obtained. The computation time refers to a single independent computation with different number of samples.

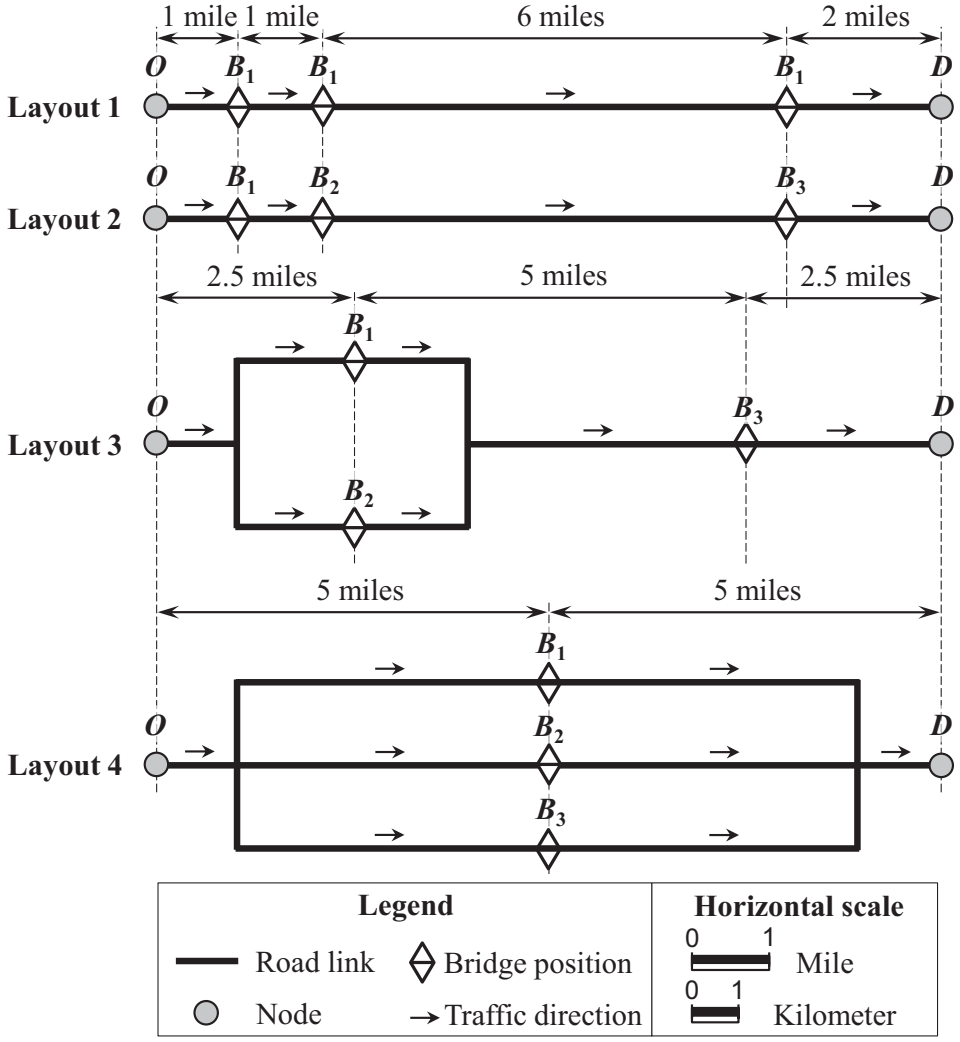

Figure 4.11 Highway segment layouts considered in the numerical example, including series system with identical bridges (layout 1), and series (layout 2), series/parallel (layout 3), and parallel (layout 4) systems with different bridges.

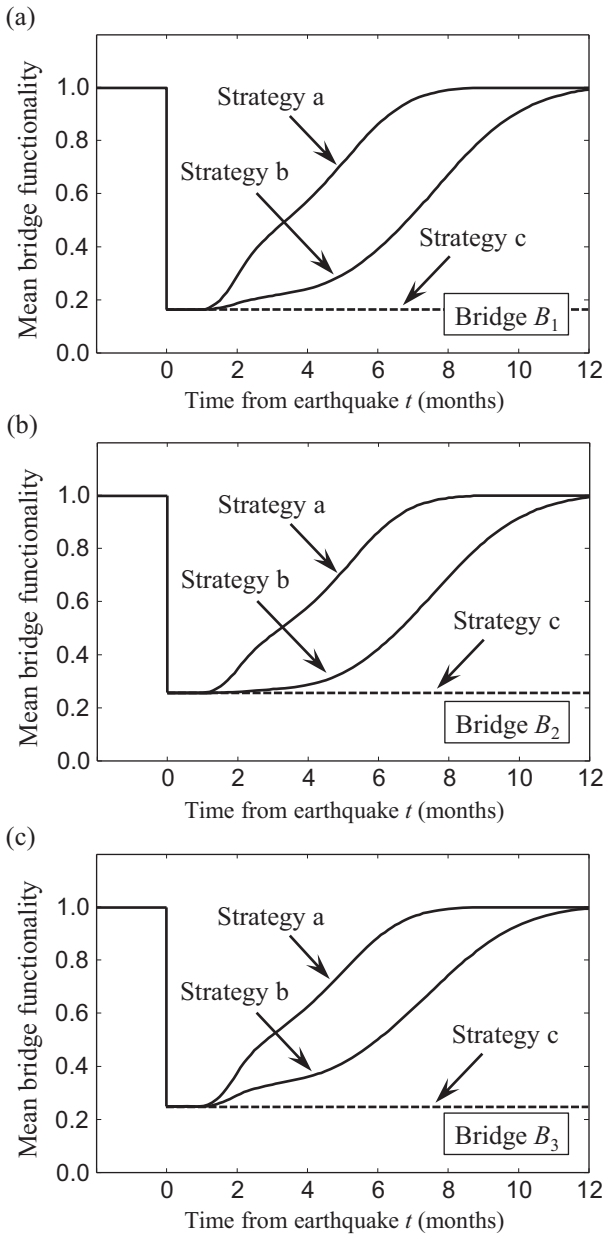

Figure 4.12 Mean functionality associated with the three considered recovery strategies for each bridge (B_1, B_2, and B_3) within the four assumed layouts in Figure 4.11.

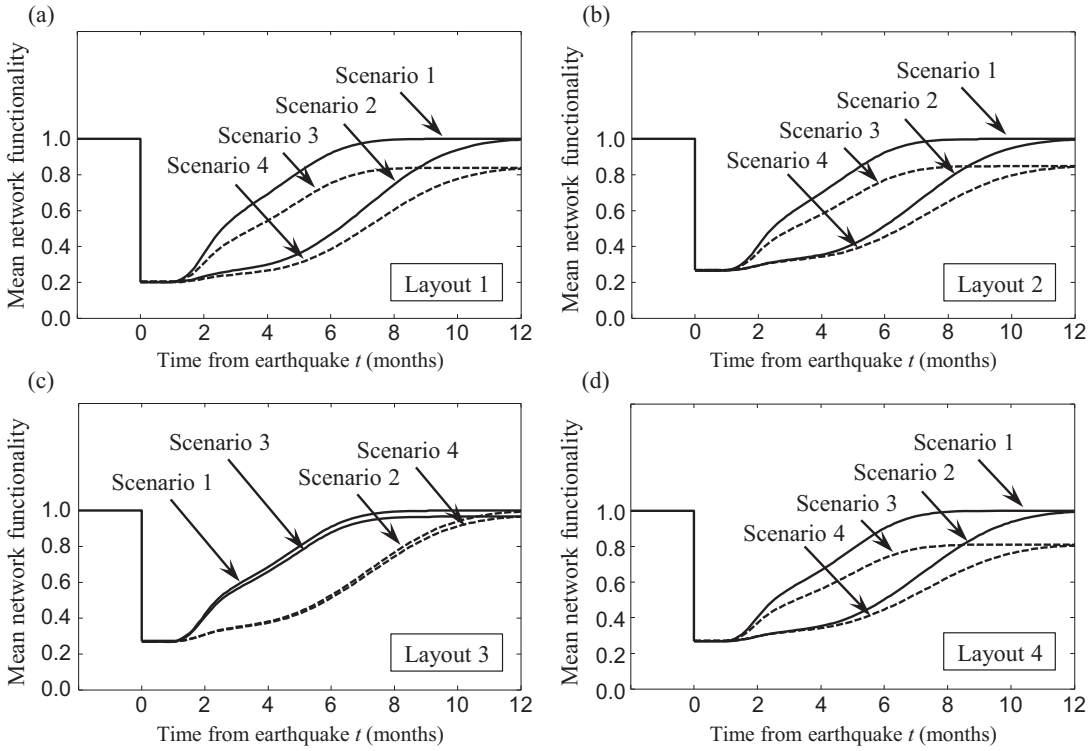

Figure 4.13 Mean segment functionality profiles associated with (a) layout 1, (b) layout 2, (c) layout 3, and (d) layout 4 in Figure 4.11, showing each considered four network recovery scenarios.

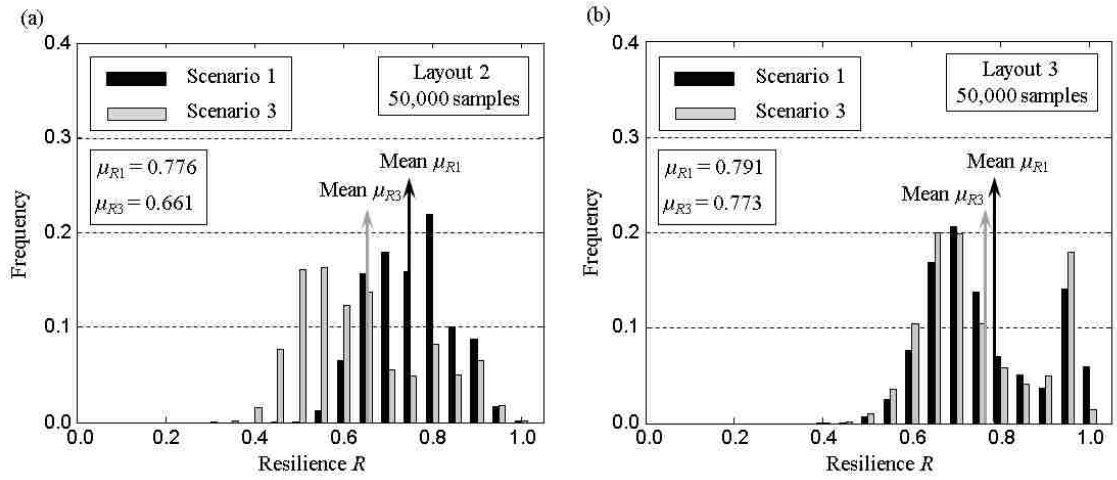

Figure 4.14 Frequency histograms of resilience associated with scenarios 1 and 3 for (a) layout 2 and (b) layout 3 in Figure 4.11.

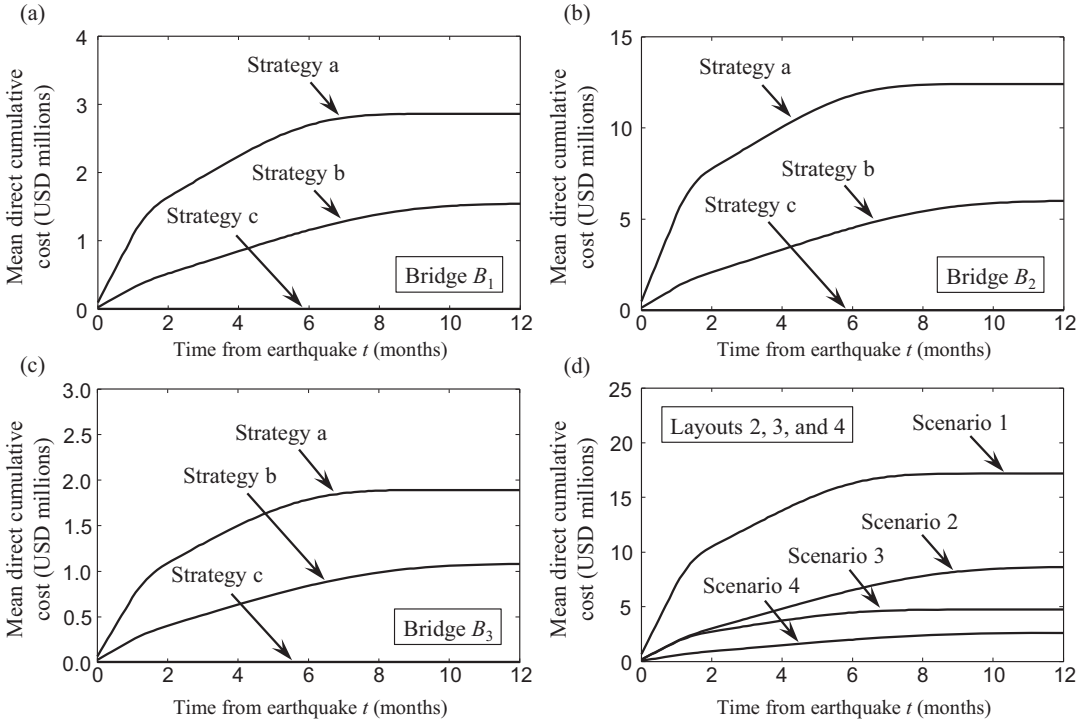

Figure 4.15 Profiles of the mean direct costs associated with each considered recovery strategy (single bridges) and recovery scenarios (network) for single (a) bridge B_1, (b) bridge B_2, and (c) bridge B_3, and (d) layouts 2, 3 and 4 in Figure 4.11.

PART II

OPTIMALITY-BASED APPROACH FOR THE MANAGEMENT OF AGING SHIP STRUCTURES CONSIDERING RELIABILITY, REDUNDANCY, AND RISK OF SHIPS UNDER DIFFERENT OPERATIONAL CONDITIONS AND INTEGRATING STRUCTURAL HEALTH MONITORING

CHAPTER 5

RELIABILITY AND REDUNDANCY ASSESSMENT OF SHIPS UNDER DIFFERENT OPERATIONAL CONDITIONS

5.1 INTRODUCTION

The proper knowledge of ship structural vulnerability under specific operational conditions is the key to maintain an adequate safety level. Due to time and distance constraints, sometimes vessels are forced to plan routes that put their structure at risk, possibly experiencing dramatic drops of their operational safety. In fact, ship structures are subjected to the effects of the environment in which they operate. Depending on the encountered sea conditions, the load effects on the hull may vary over a journey potentially inducing extreme danger.

Several studies focused on the assessment of ship reliability associated with ultimate flexural capacity (Mansour and Hovem 1994, Mansour 1997, Ayyub, Assakkaf and Atua 2000, Luís, Teixeira and Guedes Soares 2009) and fatigue failure mode (Kim and Frangopol 2011 and Kwon, Frangopol and Kim 2011). Furthermore, the variation over time of reliability, also associated with ultimate flexural capacity, has been extensively investigated (Paik, Kim and Lee 1998, Guedes Soares and Garbatov 1999, Paik and Frieze 2001, Akpan *et al.* 2002). Ship reliability has been

investigated also with respect to flexural capacity associated with the failure of the first element (stiffened plate) within a ship cross-section (Lua and Hess 2003, Lua and Hess 2006). Although the maximum vertical bending moments (sagging and hogging) generally occur amidship, in order to properly assess the overall ship safety, a system composed by multiple cross-sections is investigated herein.

Even if few comprehensive studies have been conducted for the evaluation of structural performance and mostly focusing on performance-based design other than safety estimates (Glen, Paterson and Luznik 1999, Dinovitzer 2003), literature lacks in studies that assess structural reliability and redundancy of ships under different operational conditions, including aging consideration. This chapter, which is based on Decò, Frangopol and Okasha (2011), Decò, Frangopol and Okasha (2012), Decò, Frangopol and Zhu (2012), provides a comprehensive study reporting on ship reliability and redundancy for a wide spectrum of operational options. Accounting for corrosion effects and depending on different sea states, vessel speeds and headings (i.e., angle between the ship direction and wave moving direction), polar plots indicating ship reliability and redundancy are obtained in order to quantify safety for each encountered operational and environmental condition.

Due to the presence of uncertainties, dimensions, material properties, corrosion effects, applied loads, and model-related parameters are treated as random variables. According to Ayyub *et al.* (1998), common practice is the use of strip theory that provides ship structural responses due to waves by superposing the effects of different waves (Korvin-Kroukowski and Jacobs 1957). FREE!ship (2006), an open source surface-modeling program based on subdivision surfaces, is used to model the ship

body and estimate the hydrostatic parameters. Load statistical descriptors due to wave effects are evaluated upon the inclusion of an assumed sea spectrum by using a developed MATLAB (The MathWorks 2011) code linked with PDSTRIP (2006), which is a program performing strip analysis. Ship reliability is computed using a hybrid Latin Hypercube (McKay, Conover and Beckman 1979) scheme based on SORM technique.

This chapter develops an approach for the evaluation of time-dependent reliability and redundancy of ship structures under different operational conditions. Section 5.2 describes the adopted model for the probabilistic evaluation of the load effects induced by still water and waves. Section 5.3 develops the model for the evaluation of the time-dependent flexural capacity that includes the effects of corrosion. Section 5.4 quantitative evaluates the time-dependent reliability and redundancy under different ship operational conditions. In Section 5.5, the proposed approach is applied to the Joint High Speed Sealift (JHSS) reported by Devine (2009). Finally, Section 5.6 provides the conclusions of this chapter that is based on several published papers (Decò, Frangopol and Okasha 2011, Decò, Frangopol and Okasha 2012, Decò, Frangopol and Zhu 2012).

5.2 LOADING MODEL

The effects induced by the sea on the hull are due to still water and induced by waves. Safety evaluation of ship structures operating in different sea and cargo conditions requires a probabilistic estimation of the load effects due to still water and waves (Guedes Soares 1992). Since design considerations are not the goal of this chapter,

"long-term" statistics are not accounted for. This study provides indications on the assessment of structural safety of ships undergoing different operational conditions without making any assumption on the possible ship routes, therefore "short-term" (i.e., mission oriented) loads are quantities of interest. The estimation of the load effects is summarized in the Module (1) of Appendix B.

As recognized by previous studies (Guedes Soares and Teixeira 2000), the primary load effects within the hull are sagging and hogging vertical bending moments (VBM), that induce compression in the stiffened panels composing the deck and the keel, respectively. The main contributions to the overall VBMs are due to still water and encountered waves. In order to assess the reliability of a whole ship structure (that can be seen as a stiffened box girder), load effects at different locations along the ship length (e.g. amidship and quarter points) should be examined. Hence, system reliability analysis is based on those analyzed cross-sections.

5.2.1 STILL WATER BENDING MOMENT

The adopted probabilistic model for the evaluation of the VBM due to still water relies on the method proposed by Hussein and Guedes Soares (2009). Since detailed information regarding the location and magnitude of the loads within the vessel is generally not available or seldom recorded, the methodology is based on conservative rule values, such as those provided in IACS (2008). Accordingly, the VBMs $M_{sw,sag,CS}$ and $M_{sw,hog,CS}$ (sagging and hogging, respectively) for a specific ship cross-section *CS* are (IACS 2008)

$$M_{sw,sag,CS} = 0.05185 f_{sw,CS} C_{wv} l^2 b(C_b + 0.7) \qquad \text{for sagging} \qquad (5.1)$$

$$M_{sw,hog,CS} = 0.01 f_{sw,CS} C_{wv} l^2 b(11.97 - 1.9 C_b) \qquad \text{for hogging} \qquad (5.2)$$

where $f_{sw,CS}$ is the factor accounting for the variation of VBMs along the vessel length (with 1.0 at midship), C_b is the ship block coefficient, l is the ship length (m), b is the ship breadth (m), and C_{wv} is a wave coefficient calculated as follows (IACS 2008)

$$C_{wv} = \begin{cases} 10.75 - \left(\dfrac{300 - l}{100}\right)^{\frac{3}{2}} & \text{for } 150 \le l \le 300 \\ 10.75 & \text{for } 300 < l \le 350 \\ 10.75 - \left(\dfrac{l - 350}{150}\right)^{\frac{3}{2}} & \text{for } 350 < l \le 500 \end{cases} \qquad (5.3)$$

When information regarding the configuration of the cargo is not sufficient to develop an accurate analysis, according to Hussein and Guedes Soares (2009), the maximum still water bending moments can be taken as 90% of those obtained by common rules (e.g. IACS 2008). Hussein and Guedes Soares (2009) proposed the use of a normal distribution with mean and standard deviation to be taken as 70% and 20% of the maximum still water bending moment, respectively.

5.2.2 WAVE-INDUCED BENDING MOMENT

The interaction between sea waves and ship structures is summarized in this section. The system composed by ship and waves generates responses in terms of ship motion, pressure distribution, body forces and moments. The structural response can be evaluated by means of linear response theory, which is commonly recognized as an

efficient usual practice (Ayyub *et al.* 1998). The main idea is the linear superposition of single waves (given a frequency and a unitary amplitude) in order to obtain a wave spectrum that conveniently covers a large number of wave configurations. The main advantage in using linear theory is that the response to natural sea conditions is evaluated by superimposing the responses obtained by the generated regular waves. However, linear theory becomes inaccurate when dealing with wave heights that are greater than wave lengths (Hughes 1983).

Since, in general, the vertical flexural failure mode is the most critical structural concern (Guedes Soares and Teixeira 2000), this chapter focuses on the evaluation of VBM of ships subjected to different operational conditions by applying the linear method. Estimates of VBM must be provided for each investigated ship operational condition, represented by a group of input parameters such as sea states, ship speeds and headings. Figure 5.1 shows the flowchart describing the general approach that can be followed in order to obtain a comprehensive set of structural responses by using linear theory.

5.2.2.1 Regular wave response

The structural responses for regular waves become crucial when assessing the ship response due to natural sea given by linear superposition. Responses for single waves are based on hydrodynamic analyses of the ship in case of having steady conditions (steady harmonic variation of the loads on the structure), disregarding the transient effects (Faltinsen 1990). Forces and moments on ships induced by waves mostly rely on hydrodynamic rather than structural analysis. Generally, hydrodynamic analyses

are complex tasks that involve the use of computer-based tools, and abundantly lay outside the common role of ship structural engineers (Hughes 1983). A relatively simple technique to perform hydrodynamic analysis of operating vessels is based on strip theory or strip method (Korvin-Kroukowski and Jacobs 1957). With respect to other techniques, simplifications are introduced by the strip theory, in which the ship hull is divided into prismatic segments (strips). Hydrodynamic forces induced by harmonic waves are evaluated within the individual segments, disregarding any interaction between adjacent ones. Then, shear and bending moment within the entire hull are evaluated by integrating the obtained hydrodynamic forces along the segments (Hughes 1983). This method relies on a two-dimensional flow theory, therefore interaction between segments is neglected.

According to Faltinsen (1990), when the structure is excited by regular waves, hydrodynamic forces vary harmonically with the same frequency of the wave loads. Hydrodynamic forces and moments can be subdivided into two types:

1. Forces and moments acting when the ship structure is restraint against oscillating (Froude-Kriloff and diffraction forces and moments).
2. Forces and moments acting when the ship structure is forced to oscillate according to the excitation frequency (hydrodynamic loads include added mass, damping, and restoration).

Generally, Froude-Kriloff forces are those induced by the undisturbed pressure distribution of the waves, reduced by the hydrostatic pressure acting over the wetted surface. Froude-Kriloff forces $F_{FK,i}$ are evaluated by integrating the obtained pressure p over the section contour (Faltinsen 1990)

$$F_{FK,i} = -\iint_S p n_i \mathrm{d}s \tag{5.4}$$

where n_i are the unit vectors normal to the body surface according to the assumed coordinate system (n_1, n_2, and n_3, respectively), S is the wetted surface, and s is the variable of integration. Actually, the presence of the ship body generates changes in the pressure field (disturbed waves). Such pressure changes are accounted for by the diffraction forces $F_{D,i}$ defined as (Faltinsen 1990)

$$F_{D,i} = A_{i1}a_1 + A_{i2}a_2 + A_{i3}a_3 \tag{5.5}$$

in which A_{i1}, A_{i2}, and A_{i3} are the added mass coefficients (inertia added due to an accelerating body that moves part of the volume of the surrounding fluid) with respect to the assumed coordinate axis, respectively; and a_1, a_2, and a_3 are the acceleration components of the undisturbed wave field with respect to the assumed coordinate axis, respectively.

Beyond Froude-Kriloff and diffraction forces (based on a non-moving body), other forces directly related to the motion of the vessel (considered as a rigid body) have to be evaluated. Added mass, damping, restoration forces and moments can be obtained upon evaluating the motions by solving the equations of rigid body motions (Faltinsen 1990)

$$\sum_{k=1}^{6}\left[\left(M_{jk} + A_{jk}\right)\ddot{\eta}_k + B_{jk}\dot{\eta}_k + C_{jk}\eta_k\right] = F_j \exp\left(-\mathrm{i}\omega_e t\right) \qquad \left(j = 1,...,6\right) \tag{5.6}$$

where M_{jk} are the components of the mass matrix, A_{jk}, B_{jk}, and C_{jk} are the added mass, damping, and restoring coefficients, respectively; $\ddot{\eta}_k$, $\dot{\eta}_k$, and η_k are the acceleration,

velocity, and displacement of the rigid body, respectively; F_j are the complex amplitudes of the exciting forces and moments, i is the complex unit, ω_e is the circular encounter frequency that depends on the circular frequency ω, and on the ship speed U, and heading angle H, as discussed in the following section, t is the time, and j and k are the degrees of freedom. The first term (accounting for the acceleration of the body) in the sum of Equation (5.6) is responsible for the added mass forces and moments, while the second term (referring to the velocity of the body) represents the damping forces and moments, finally the third term (associated with the displacement of the body) is related to the restoration forces and moments. In the context of the strip method, the above introduced forces are evaluated by modified equations accommodating for the two-dimensional flow theory (PDSTRIP 2006).

Although several commercial software performing linear analysis are available, freeware software developed by field specialists or academic institutions is also accessible. For instance, the freeware program PDSTRIP (2006) developed in FORTRAN language has been proved to be a useful tool computing the seakeeping of ships and other floating bodies according to the strip method (Bertram, Söding and Graf 2006, Palladino *et al.* 2006).

5.2.2.2 Vertical bending moment response amplitude operator

One of the key points while using linear theory for the determination of hull loads is obtaining the Response Amplitude Operator (RAO) from ship hydrodynamic analysis. In this chapter, VBM RAOs are of interest. While dealing with time-varying processes, their representation in terms of spectral density function can be a great

advantage, especially for the response analysis of linear systems. In this case, if both the input $X(t)$ and output $Y(t)$ of the system are expressed by spectral density functions, their relation is associated with the transfer function $\Phi(\omega)$ as follows (Hughes 1983)

$$S_Y(\omega) = |\Phi(\omega)|^2 S_X(\omega) \tag{5.7}$$

where $S_Y(\omega)$ and $S_X(\omega)$ are the spectral density functions of the output and input, respectively; and ω is the circular frequency (rad/s).

In marine engineering, RAOs are represented by curves describing the structural response in the frequency-domain. Within the linear methods (e.g. strip method), RAOs are defined as the ratio between the amplitude of the harmonic function of the response and the amplitude of the wave elevation (Drummen, Wu and Moan 2009). This means that RAOs are the ship responses obtained by imposing unitary amplitude to the exciting regular waves (ABS 2010). A practical way to find the RAOs is the analysis of structural responses due to different waves (with unitary amplitude) by varying their lengths.

The assessment of the loads for operational conditions requires the evaluation of the encountered frequency in order to account for different ship speeds and headings. Accordingly, RAOs have to be evaluated for the same operational conditions and for each considered ship cross-section *CS*. Consequently, the encountered wave frequency $\omega_{e,U,H}$ is defined as follows (ABS 2010)

$$\omega_{e,U,H} = \left| \omega - U\frac{\omega^2}{g}\cos H \right| \tag{5.8}$$

in which g is the gravitational acceleration (m/s^2), U is the forward ship speed (m/s), and H is the heading angle considering 0º, 90º, 180º for following, beam, and head seas, respectively.

5.2.2.3 Natural sea conditions

The ocean surface is extremely irregular and the prediction of wave configurations is a complex issue. In this context, statistical tools can provide the basis for a probabilistic study of the structural response for ships in natural sea (irregular sea). The mathematical representation of the sea surface becomes feasible and relatively simple when the problem is solved linearly. Practically, this allows to evaluate the ship structural response for each individual regular wave, and thus to obtain statistical estimates by superposing the results of a large number of waves. Since the instantaneous value of the ocean elevation follows a Gaussian distribution, and in accordance with Faltinsen (1990), the probability density function (PDF) of the peak values of the wave elevation A_w is assumed to be described by the Rayleigh distribution, defined as

$$f\left(A_w\right) = \frac{A_w}{m_0} \exp\left(- \frac{{A_w}^2}{2m_0} \right) \tag{5.9}$$

where m_0 is the zero-*th* moment of the wave spectrum S_W (i.e., the area under the spectrum), expressed as (Hughes 1983)

$$m_0 = \int_0^\infty \omega^0 S_W\left(\omega\right) \mathrm{d}\omega \tag{5.10}$$

The use of the Rayleigh distribution may introduce bias results that are too high in case of severe sea state (Bai 2003).

Various sea spectra are adopted in numerous studies, depending on ocean/sea characteristics (Michel 1999). The spectrum for fully developed sea, suggested by the International Ship and Offshore Structures Congress (ISSC) and representing a modified version of the Pierson-Moskowitz sea spectrum, is selected (Faltinsen 1990)

$$S_{W,SS}(\omega) = \frac{0.11 H_{1/3}^2 T_1}{2\pi} \left(\frac{\omega T_1}{2\pi} \right)^{-5} \exp\left[-0.44 \left(\frac{\omega T_1}{2\pi} \right)^{-4} \right] \tag{5.11}$$

where $S_{W,SS}(\omega)$ is the sea spectrum for a given sea state *SS*, T_1 is the wave mean period (s), and $H_{1/3}$ is the significant wave height corresponding to the mean of the one third highest waves (m). The sea state scale for wind sea plays a fundamental role for the evaluation of the load magnitude. The values of the wave mean period and significant height depend upon the intensity of the sea states.

For long crested sea and for low frequency waves, the correlation coefficients between two loads components denoted *i* and *j* are given by (Mansour and Thayamballi 1994)

$$\rho_{ij} = \frac{1}{\sigma_i \sigma_j} \int_0^\infty \mathrm{Re}\left[\Phi_i(\omega) \Phi_j^*(\omega) \right] S_W(\omega) d\omega \tag{5.12}$$

where $\Phi_i(\omega)$ is the transfer function of load component *i*, $\Phi_j^*(\omega)$ is the complex conjugate of the transfer function of load component *j*, $S_W(\omega)$ is the sea spectrum, σ_i and σ_j are the individual standard deviations, and Re denotes the real part of the complex quantity within parenthesis.

Once RAO curves for wave-induced VBM $M_{w,CS,SS,U,H}$ are obtained for each considered operational condition and each section, the response spectrum $S_{M,CS,SS,U,H}(\omega_e)$ can be obtained as (Hughes 1983)

$$S_{M,CS,SS,U,H}\left(\omega_{e,U,H}\right)=\left|\Phi\left(\omega_{e,U,H}\right)\right|^2 S_{W,SS}\left(\omega_{e,U,H}\right) \tag{5.13}$$

For a linear system, once the response spectra for the VBMs are evaluated, the associated PDF of the Rayleigh distributions of the investigated structural response considering several operational conditions is provided (Hughes 1983)

$$f\left(M_{w,CS,SS,U,H}\right)=\frac{M_{w,CS,SS,U,H}}{m_{0,CS,SS,U,H}}\exp\left(-\frac{\left(M_{w,CS,SS,U,H}\right)^2}{2m_{0,CS,SS,U,H}}\right) \tag{5.14}$$

Thus, the relevant descriptor of the probability distribution of the VBM (mode α) is

$$\alpha\left(M_{w,CS,SS,U,H}\right)=\sqrt{m_{0,CS,SS,U,H}} \tag{5.15}$$

The mean μ_r and standard deviation σ_r are (Papoulis 1984)

$$\mu_r\left(M_{w,CS,SS,U,H}\right)=\sqrt{\frac{\pi}{2}}\alpha\left(M_{w,CS,SS,U,H}\right) \tag{5.16}$$

$$\sigma_r\left(M_{w,CS,SS,U,H}\right)=\sqrt{\frac{4-\pi}{2}}\alpha\left(M_{w,CS,SS,U,H}\right) \tag{5.17}$$

5.3 RESISTANCE MODEL

The evaluation of the probabilistic hull strength, in terms of flexural capacity associated with the occurrence of first failure within a given ship cross-section and ultimate flexural capacity, can be performed by a classical incremental curvature

method such as that provided by IACS (2008), or by the simple progressive collapse method provided by Hughes (1983). These techniques are computationally demanding, especially when a great number of samples is simulated.

The first failure is represented by the occurrence of failure of a stiffened panel within a selected cross-section, induced by the combination of in-plane compression and bending moment. According to Hughes (1983), the failure of a stiffened panel is due to the buckling or yielding of the plating and/or the attached stiffener. This approach based on Decò, Frangopol and Okasha. (2011) is extensively used in order to efficiently evaluate the strength associated with the first failure of a stiffened panel within a selected cross-section (flexural capacity herein called first failure moment). In summary, the first failure moment is calculated by using a simplified progressive collapse method (Hughes 1983). Although this approach is designed for the evaluation of the ultimate capacity, it can also be used for the analysis of the failures preceding the ultimate failure. The proposed procedure stops when the first failure is encountered within the analyzed ship cross-section.

The ultimate flexural capacity is defined as the peak value of the moment-curvature curve for a given ship cross-section. In order to significantly reduce the computational time, Okasha and Frangopol (2010b) developed a new optimization-based method providing as accurate results as those of the incremental curvature. Briefly, Okasha and Frangopol (2010b) discovered that, by optimizing the moment-curvature, treated as a non-linear implicit function, it is possible to find the value of the curvature κ associated with the maximum corresponding flexural capacity $M_c(\kappa)$. By the use of an optimization algorithm, the searching process is performed in a few

steps leading to obtain the ultimate failure moment for a given ship cross-section. In this method, since only few values of the curvature are processed, the computational time is dramatically reduced.

The two above mentioned techniques rely on the assumption that the structure is composed by hard corners (plating areas adjacent to intersecting plates) and stiffened plates (structural systems that include portions of the plating and stiffener) in accordance with IACS (2008). Furthermore, buckling effects of stiffened plates (such as panel/stiffener buckling and tripping) are accounted for, and the effects of initial imperfections and residual stresses are considered by introducing reduction factors applied to the effective width of the plating (Özgüc, Das and Barltrop 2006). Due to the presence of uncertainties associated with geometrical and material properties (such as plating thickness, elastic modulus, plating yielding stress, and stiffener yielding stress), a probabilistic analysis must be conducted. These two procedures can be accommodated in a simulation technique based on Latin Hypercube sampling (McKay, Conover and Beckman 1979) (reviewed in Appendix A) in a time-effective way. The obtained moment capacities associated with first and ultimate failures are fitted by lognormal distributions, from which their statistical descriptors are derived. The assessment of the flexural capacity of the hull is included in the Module (2) of Appendix B.

5.3.1 CORROSION EFFECTS

Over time, the loss of thickness of plates and stiffeners due to corrosion effects leads to reduction of both first and ultimate failure moments. The thickness loss within a

cross-section is assumed to follow the law proposed by Paik, Kim and Lee (1998) and recalled by Akpan *et al.* (2002)

$$r(t) = C_1 (t - t_0)^{C_2} \tag{5.18}$$

where $r(t)$ is the thickness loss (mm), t is the time (year), t_0 is the corrosion initiation time depending on coating life (year), C_1 is the annual corrosion rate (mm/year), and C_2 is a constant set to unity. Both the annual corrosion rate and the corrosion initiation time are considered as random variables.

The general methodology adopted in this study for the probabilistic estimation of the resistance of a hull (first and ultimate bending moments) is summarized in the flowchart of Figure 5.2.

5.4 RELIABILITY AND REDUNDANCY INDICES

The quantitative evaluation of the safety of the hull is based on reliability and redundancy indicators. The level of safety depends on both the strength of the hull and ship operational conditions. Although ship reliability is generally assessed only amidship (Guedes Soares and Teixeira 2000), several cross-sections are investigated in order to enhance the assessment of hull safety by using a system-oriented procedure. The procedure for the assessment of reliability and redundancy is summarized in the Module (3) of Appendix B.

Ship reliability analysis can be performed based upon the knowledge of the probability distributions of loads and resistances for each cross-section (following the methods previously explained) and including model (i.e., epistemic) uncertainties. The

failure probabilities and the corresponding reliability indices, with respect to flexural capacities associated with a specific cross-section *CS*, are based on the following limit state equations (Paik and Frieze 2001)

$$G_{UF,sag,CS,SS,U,H}(t) = x_R UFM_{sag,CS}(t) - x_{sw} M_{sw,sag,CS} - x_w M_{w,CS,SS,U,H} = 0 \quad (5.19)$$

$$G_{UF,hog,CS,SS,U,H}(t) = x_R UFM_{hog,CS}(t) - x_{sw} M_{sw,hog,CS} - x_w M_{w,CS,SS,U,H} = 0 \quad (5.20)$$

$$G_{FF,sag,CS,SS,U,H}(t) = x_R FFM_{sag,CS}(t) - x_{sw} M_{sw,sag,CS} - x_w M_{w,CS,SS,U,H} = 0 \quad (5.21)$$

$$G_{FF,hog,CS,SS,U,H}(t) = x_R FFM_{hog,CS}(t) - x_{sw} M_{sw,hog,CS} - x_w M_{w,CS,SS,U,H} = 0 \quad (5.22)$$

where the subscripts *UF*, *FF*, *sag*, *hog*, *CS*, *SS*, *U*, and *H* refer to ultimate failure, first failure, sagging, hogging, ship cross-section, sea state condition, ship speed, and ship heading, respectively; $G_{UF,sag,CS,SS,U,H}(t)$, $G_{UF,hog,CS,SS,U,H}(t)$, $G_{FF,sag,CS,SS,U,H}(t)$, and $G_{FF,hog,CS,SS,U,H}(t)$ are the time-dependent performance functions; $UFM_{sag,CS}(t)$ and $UFM_{hog,CS}(t)$ are time-dependent ultimate failure bending moments, $FFM_{sag,CS}(t)$ and $FFM_{hog,CS}(t)$ are time-dependent first failure bending moments; $M_{sw,sag,CS}$ and $M_{sw,hog,CS}$ are the still water bending moments, $M_{w,CS,SS,U,H}$ is the wave-induced bending moment given by linear theory; x_R, x_{sw}, and x_w are the model uncertainties associated with the resistance determination, still water bending moment prediction, and wave-induced bending moment prediction, respectively. Moreover, the reliability of the series system composed by the investigated cross-sections is performed.

The assessment of the time-variant redundancy index is necessary in order to study the behavior of structures prone to sudden failure. A redundant system is a system able to redistribute the loads throughout multiple components even though one or more

components fail (Frangopol 2011). The redundancy of ship structures can be based on the following reliability-based time-variant redundancy definitions

$$RI_1(t) = \frac{P_{f,FF}(t) - P_{f,UF}(t)}{P_{f,UF}(t)} \tag{5.23}$$

$$RI_2(t) = \beta_{UF}(t) - \beta_{FF}(t) \tag{5.24}$$

where $P_{f,UF}(t)$ and $P_{f,FF}(t)$ are the failure probabilities associated with the ultimate failure of a cross-section and the failure of the first stiffened plate within a cross-section, respectively; and $\beta_{UF}(t)$ and $\beta_{FF}(t)$ are the corresponding reliability indices. The relationship between the reliability index β and the failure probability P_f is

$$\beta = \Phi^{-1}(1 - P_f) \tag{5.25}$$

where Φ^{-1} is the inverse standard normal distribution function.

5.5 CASE STUDY

Reliability and redundancy indicators under different operational conditions are assessed for the Joint High-Speed Sealift (JHSS) discussed in Devine (2009). The following geometrical properties are considered for the JHSS: length l = 290 m, breadth b = 32 m, height h = 22.3 m, and block coefficient C_b = 0.4835. Figure 5.3(a) shows the 3-D geometrical model obtained by using the software FREE!ship (2006). Three representative transversal ship cross-sections, denoted *CS*1 (fore quarter point 72.5 m aft FP), *CS*2 (midship 145 m aft FP), and *CS*3 (aft quarter point 217.5 m aft FP) have been investigated (see Figure 3(b,c,d)). The dimensions of the components

are provided by Devine (2009). Due to speed requirements, the design of the JHSS was focused on minimizing structural weight, leading to very thin plates (Devine 2009).

Polar representations enable to directly visualize the effects on ship structural performance by varying the heading angle of the ship with respect to the wave direction given specific sea state and ship speed. Figure 5.4 qualitatively shows the layout of the adopted polar representation. Any load and performance profile obtained for angles between 0º (following sea) and 180º (head sea) is symmetric with respect to those with angles between 180º and 360º. 90º and 270º indicate beam sea. Thus, the figure showing the structural performance is divided into two parts; the right and left parts show the performance for sagging and hogging, respectively. Further profiles can be drawn in the polar plots reporting the cases in which some operational conditions are changed (i.e., sea state or ship speed) or when different ship cross-sections, limit states, or even ship aging effects are investigated. Given that for linear theory wave-induced loads effects are the same for sagging and hogging, their polar representation spans between 0º and 180º. Polar plots including the load effects in terms of VBM, reliability and redundancy indices of the ship for each of three representative transversal ship cross-sections in Figure 5.3(a) are obtained and discussed.

5.5.1 LOAD EFFECTS

Since the loading manual of the JHSS is not available, and given that the loads can vary between missions, the load effects induced by still water in terms of VBM are evaluated based on the conservative rule values provided in IACS (2008) and given by

applying Equations (5.1) and (5.22) for sagging and hogging, respectively. According to the method proposed by Hussein and Guedes Soares (2009), the VBMs for each investigated cross-section are assumed to be normally distributed with statistical descriptors reported in Table 5.1. Being the scope of this chapter the development of a general procedure for the assessment of ship reliability and redundancy with respect to VBM, among other methods, strip theory is adopted for this case study.

RAO curves and load descriptors (based on Rayleigh distribution) are evaluated with respect to the VBM for each of the three ship cross-sections (in Figure 5.3) and for each operational condition. Since the JHSS is a fast naval vessel, and assuming that the maximum forward speed can reach up to 20 m/s (38.9 knots), the following five speeds are considered: 0 m/s (0 knots), 5 m/s (9.7 knots), 10 m/s (19.4 knots), 15 m/s (29.2 knots), and 20 m/s (38.9 knots). Ship structural performances are evaluated for different ship headings. Angles between 0º (following sea) and 180º (head sea) by multiples of 20º are accounted for.

Wind sea accounting for sea states 4, 5, 6, and 7, described by statistical properties according to Table 5.2, is included in the analysis. The used wave spectrum is calculated according to Equation (5.11) and its representation is provided in Figure 5.5. Based on considerations on operational profiles (Ayyub *et al.* 1998), few ship speed/sea state combinations believed to be very unlikely are disregarded. Hence, when the ship encounters sea state 7 (which is a very low probability event), its maximum allowed speed is assumed to be 10 m/s. For all the other cases, any combination between speed and sea state is allowed.

As shown in Figure 5.3(a), the body of the JHSS has been modeled by the freeware software FREE!ship (2006). Based on this model, hydrostatic properties are assessed. The evaluated ship displacement of 30,350 Mton is a value compatible with that provided by Devine (2009) for normal operational conditions, proving that the accuracy of the model is acceptable. Offset points describing 19 cross-sections spaced 14.5m are obtained by using the exporting tool of FREE!ship. Hull wetted areas associated with these cross-sections were also evaluated.

Cross-section geometries are managed by a developed MATLAB (The MathWorks 2011) code that converts the exported file to a suitable format for the software PDSTRIP (2006) in order to perform linear response analysis under regular waves (strip theory). VBMs for the three ship cross-sections are obtained with respect to different waves having unitary amplitude and length between 24 m and 1300 m (95 values irregularly spaced). A large number of wave lengths is necessary in order to achieve enough values to build the RAO curves with sufficient accuracy. Moreover, the input file of PDSTRIP allows accounting for different ship speeds and headings.

After handling the output file with another developed MATLAB code, the results obtained are expressed in terms of VBM RAOs considering variations of ship speed and heading. For instance, Figure 5.6(a) shows the VBM RAOs associated with ship speed 0 m/s and by varying the heading angles from 0º to 80º for the midship cross-section. It can be noted that the variation of ship heading induces a kind of translation of the structural response, primarily shifted on higher frequencies due to the changed wave encountered frequency (Equation (5.8)). In Figure 5.6(b), the heading angle H is assumed constant (i.e., H = 180º), while the ship speed varies between 0 and 20 m/s

for the midship cross-section. Again, it can be noticed that RAOs shift to higher frequencies when the speed increases in head sea.

Once RAOs have been obtained, by selecting a sea spectrum (given by Equation (5.11) after inputting specific significant wave height and average wave period) and by applying Equation (5.13), the response spectra can be assessed. Figure 5.6(c) shows the response spectra for VBM when the JHSS is subjected to the same conditions as those associated with Figure 5.6(a) and sea state 5 is selected. It can be seen that the responses are greater when the ship is traveling with heading equal to 60º. This can be explained analyzing the relevant wave spectrum and noting that responses associated with encountered frequencies lower than 0.7 (rad/s) are not significantly affected. Similarly, Figure 5.6(d) depicts the responses by varying the ship speed according to Figure 5.6(b). Responses associated with higher speeds are heavily affected by sea state 5.

According to Rayleigh distribution, for each considered operational condition it is possible to evaluate the mode, mean, and standard deviation of the response distribution given by Equations (5.15), (5.16), and (5.17), respectively. According to Equation (5.10), the values of the loads are proportional to the areas subtended by the response spectrum curves. Figure 5.7(a) shows the polar representation of the vertical bending moment (VBM) for the three ship cross-sections (*CS*1, *CS*2, and *CS*3) in the case of sea state 6 and speed of 5 m/s. Obviously, the highest load effects are found for the cross-section amidship (*CS*2) and lower load values for the other two cross-sections at quarter points. Figure 5.7(b) gives indications about the dispersion of the VBM for the cross-section amidship by showing the profiles of the mean μ and mean

plus and minus one standard deviation σ, ($\mu+\sigma$ and $\mu-\sigma$, respectively) in case of sea state 6 and no speed (U = 0 m/s). VBM responses associated with beam sea (90º and 270º) become insignificant.

Figure 5.7(c) shows the effects on the mean VBM for *CS*2 due to the variation of speed under sea state 5. As the speed increases, VBM mostly increase for head sea, while they are irrelevant during following sea conditions (i.e., RAOs are mostly concentrated in frequency regions far from the wave spectrum for sea state 5). Some of the points within Figure 5.7(c) are directly obtained from Figure 5.6(c,d) and are proportional to the areas subtended by the relevant response spectrum curves; the remaining points are evaluated in the same way. In particular, it can be noted that the sharp curve associated with heading angles of 60º and 300º (i.e., the load is the same on the two sides of the ship) with null ship speed (point A) and sea state 5 is associated with the greater response obtained by the relevant curve of Figure 5.6(c). Further VBM values for null ship speed, sea state 5, and corresponding to heading angles of 0º, 20º, 40º, and 80º can be directly associated with the curves presented in Figure 5.6(c).

Moreover, points B, C, and D in Figure 5.6(d) are derived from the areas subtended by the curves associated with ship speeds 0, 10, and 20 m/s, respectively; and for sea state 5 of *CS*2. The increasing of the subtended area determines greater mean VBMs. Figure 5.7(d) reports on the variation of the mean VBM for three sea states (*SS* 5, *SS* 6, and *SS* 7). Setting a speed U of 5m/s, the mean VBM for *CS*2 increases with the severity of the sea state. Moreover, sea state 7 provides relatively high mean VBMs in case of following sea because the propagation of the wave profile

(wave speed) is faster than the travelling vessel (high wave speed due to long waves). Hence, the waves overtake the ship and generate load effects on the hull based on the encountered frequency. In order to better represent some small values shown in the polar plots of Figure 5.7(a,d), Cartesian plots are shown in Figure 5.7(e,f).

Although the use of a linear approach provides conservative approximated results (Ayyub *et al.* 1998), improved results can be obtained by applying methods that accounts for non-linearity in the wave-induced loading as well as vibration effects such as springing and whipping loads, usually associated with high frequency excitations. These effects are here neglected, being their evaluation outside the scope of this case study. Due to linear theory, the resulting bending moments are the same for both sagging and hogging (Hughes 1983, Lua and Hess 2006) and the results shown in the polar plots can be affected by inaccuracy, especially when the responses are concentrated in very low or very high encountered frequencies. Profiles are also affected by the error made while discretizing the input data, sometimes leading to sharp angles.

5.5.2 ASSESSMENT OF FLEXURAL CAPACITY

The assessment of flexural capacity probability distributions is based upon the knowledge of material properties: mean value of the steel elastic modulus E = 210,000 MPa and mean value of the plating and stiffener yielding stresses of high strength steel $\sigma_{Yp} = \sigma_{Ys}$ = 351.6 MPa (Devine 2009). The included random variables E, σ_{Yp}, σ_{Ys}, and the plating thickness t_p are assumed to be log-normally distributed with coefficients of variation taken as 0.03, 0.1, 0.1, and 0.05, respectively (Paik and Frieze 2001). The

mean values of t_p can be obtained from Figure 5.3(b,c,d). Residual stress value has been assumed to be equal to 5% of the plating yielding stress. According to Akpan *et al.* (2002), the annual corrosion rate C_1 is treated as a log-normally distributed random variable. It was found by Okasha, Frangopol and Decò (2010) that the use of very high values of corrosion penetration (as suggested by Akpan *et al.* 2002) together with the very thin plate used in the cross-section of this JHSS, leads to very conservative estimates, and the obtained corrosion loss after only few years becomes greater than some of the generated plate thickness samples. Therefore, according to Okasha, Frangopol and Decò (2010), Table 3 presents proportional fractions of those values in Akpan *et al.* (2002). However, for this type of fast and light weight vessels, more accurate corrosion models are needed for time-variant reliability assessment.

The simulation of the hull flexural strength, with respect to first and ultimate failure for each considered ship cross-section and based on 5,000 generated Latin-Hypercube samples, is performed over time. The generated frequencies of flexural capacities (for both sagging and hogging) are fitted by a log-normal distribution in order to obtain the relevant statistical descriptors (mean and standard deviation) for each simulated year (two year increments). The targeted ship service life is assumed to be 30 years.

Figure 5.8 illustrates the time-variant flexural capacities for ship (a,b) cross-section 1, (c,d) cross-section 2, and (e,f) cross-section 3, respectively. Profiles of mean μ and mean plus and minus one standard deviation ($\mu+\sigma$ and $\mu-\sigma$, respectively) of the first and ultimate failure moments for sagging (a,c,e), and for hogging (b,d,f) are shown. Flexural capacities decrease over time according to the applied corrosion rate.

5.5.3 SHIP RELIABILITY AND REDUNDANCY

Once statistical descriptors of load effects and capacities are obtained, reliability can be performed based on flexural failure mode described by Equations (5.19) to (5.22). The reliability index is obtained for both sagging and hogging and for each investigated ship cross-section, sea state, ship speed, and heading. Moreover, accounting for the decay of flexural capacities over time, reliability at different years can be obtained. The reliability of the series system composed by the three cross-sections shown in Figure 5.3 is also investigated. The time-variant reliability is performed by the program RELSYS (Estes and Frangopol 1998), that computes reliability according to First-Order Reliability Method (FORM). Once the simulation phase is complete, the correlation among the capacities of different cross-sections is directly evaluated from the obtained samples, whereas the correlation among the load effects along the ship is calculated by using Equation (5.12). These correlations are accounted for while performing reliability analysis of the series system.

Similarly to the obtained results for the VBMs, Figure 5.9 shows the polar representation of the reliability index associated with the load effects due to still water and waves with respect to ultimate failure for sagging (right part) and hogging (left part). Figure 5.9(a) reports on the reliability index of the three ship cross-sections in the case of having sea state 6 and speed 5 m/s for the intact structure (year 0). The shape of the obtained profiles is based on the resulting wave-induced loads. Accordingly, higher reliability values are found for following sea and beam sea. Consequently, the reliability associated with the series system (accounting for cross-

sections *CS*1, *CS*2, and *CS*3) is below but quite close to the minimum reliability among the three cross-sections. The system reliability is mostly affected by the reliability of *CS*1 for following sea and by *CS*2 for head sea.

Figure 5.9(b) compares the reliability of an intact structure (year 0) with the one of an aged structure (year 30) for *CS*2 under sea state 6 and no speed. It is found that the profile for the aged case is a scaled offset of the profile for the intact case. It can be noticed that the aged state further limits the ship operability options. Figure 5.9(c) shows the variation of reliability for *CS*2 under sea state 5 by varying the speeds and with respect to the intact structure. As the speed increases, the reliability for head sea decreases. Figure 5.9(d) reports on the variation of reliability due to different encountered sea states. Sea state 7 provides very low reliability indicating very poor operability conditions for each considered heading (probability of failure is approximately 50%). Furthermore, it can be noticed that for the same operational conditions, reliability for sagging is greater than reliability with respect to hogging conditions. In order to better represent some results reported in Figure 5.9(a,d), Cartesian plots are provided in Figure 5.9(e,f).

The time-variant redundancy indices are calculated according to Equations (5.23) and (5.24), and based upon the assessment of the failure probabilities associated with first and ultimate flexural failures. By investigating the same operational conditions as those used in the reliability case, a similar polar representation for redundancy (sagging and hogging) is shown in Figure 5.10. These plots follow the other two developed polar representations (Figure 5.7 and Figure 5.9) considering the same operational conditions as those used in Figure 5.7 and Figure 5.9. It can be noticed

from Figure 5.10(a) that redundancy in sagging for *CS*3 is much higher than the one in hogging, due to the geometry of this cross-section. In fact, the upper part of the cross-section is interrupted and most of the inertia is concentrated at the bottom part of the cross-section leading to worse performance in hogging. Generally, redundancy of *CS*2 is greater than that of *CS*1 for both sagging and hogging as reported in Figure 5.10(a). According to Figure 5.10(b), the redundancy profile of an aged structure (year 30) is a scaled offset of the profile for the intact case (year 0). Furthermore, it is found that redundancy decreases to critical values when the ship speed increases from 0 to 20 m/s, especially for head sea (see Figure 5.10(c)). Redundancy dramatically decreases also when the sea state becomes more severe (from sea state 5 to 7) as shown in Figure 5.10(d). According to Figure 5.11, very similar results are obtained by adopting the definition of redundancy provided in Equation (5.24).

During ship lifetime and depending on specific operational conditions, structural safety may drop dramatically. The inclusion of constant thresholds (i.e., circular in polar coordinates) for the reliability index helps maintain adequate safety. When the performance decreases below a set warning level, the operational condition is poor and decisions on varying speed and direction must be made in order to restore the ship performance to an acceptable level.

5.6 CONCLUSIONS

Ship lifetime safety can be estimated upon assessing ship structural performance for a large spectrum of operational conditions. Maintaining a specific speed and heading angle for different sea states may lead to dangerous structural performance, putting at

risk the integrity of the whole ship and crew lives. This chapter presents an efficient approach for the evaluation of ship reliability and redundancy including the effects of corrosion. This approach allows to investigate aging vessels accounting for the deterioration of their performance over time due to corrosion effects. The strip method is used for the assessment of the VBM RAOs for three ship cross-sections. Linear theory provides conservative results especially for severe sea states, however, other methods can be accommodate in the proposed approach. The probabilistic analysis of structural responses for natural sea is conducted by investigating specific sea states. Moreover, reliability and redundancy indices are assessed for similar operational conditions.

The following conclusions are obtained:

1. The proposed polar representation for reliability and redundancy improves the interpretation of the structural safety level under specific operational conditions, helping the ship operator make appropriate decisions.
2. Aging considerations are included into reliability and redundancy analyses showing how performance is affected by corrosion. The same operation could lead to greater consequences if conducted with an aged ship. However, it has been found that the impact of corrosion effects (ship aging) on reliability and redundancy is in general limited compared with the effects of specific critical operations.
3. In the case of hogging, it has been found that the cross-sections CS1 and CS2 have lower redundancy than that of amidship (i.e., cross-section CS2). However,

reliability indices of the three ship cross-sections are quite similar, indicating that the design is adequate for the hull cross-sections.

4. It can be noted that some operational conditions lead to significant drop of redundancy. When the structural performance reaches a set threshold (warning situation), operational conditions must be modified according to the residual structural safety by reducing the forward speed, or by changing the heading angle in order to improve the structural performance.
5. Generally, when speed increases, sea state becomes more severe, and when under head sea (heading 180^{o}), the structural performance reduces significantly. An extreme combination of these three factors may lead to catastrophic consequences. For instance, it has been found that if the JHSS travels in sea state 7 at a relatively low speed (5 m/s) the associated probability of failure can be very high, with redundancy critically approaching zero.
6. The proposed framework could be enhanced by including structural health monitoring (SHM) technologies able to provide further information regarding "real time" stresses in the hull. The proposed study can accommodate SHM by means of updating the prior information with new obtained datasets.

Polar plot representations open new research scenarios. This potential can also be fully exploited while dealing with planning the optimum ship route within a trip. Although time and distance are of primary importance, the level of structural safety is also crucial, especially when a vessel is facing critical operational conditions. The optimization of reliability and redundancy combined with route direction and ship speed leads to a new challenge for structural and marine engineers.

Table 5.1 Statistical descriptors of the distributions of still water bending moments for the three cross-sections in Figure 5.3.

Load type	Mean (Nm)	Standard deviation (Nm)
Sagging still water bending moment (cross-sections 1 and 3)	7.246×10^{8}	2.070×10^{8}
Sagging still water bending moment (cross-section 2)	1.115×10^{9}	3.185×10^{8}
Hogging still water bending moment (cross-sections 1 and 3)	1.305×10^{9}	3.729×10^{8}
Hogging still water bending moment (cross-section 2)	2.008×10^{9}	5.736×10^{8}

Table 5.2 Statistical descriptors of the Pierson-Moskowitz sea spectrum (obtained from Resolute Weather 2011).

Sea state	Significant wave height (m)	Average wave period (s)	Average wave length (m)
4	1.83	5.0	24.08
5	2.44	5.5	32.00
6	4.27	7.5	56.09
7	7.62	10.0	100.13

Table 5.3 Statistical descriptors of the annual corrosion rate C_1 for different locations within the hull.

Location	Mean (mm/year)	Standard deviation (mm/year)
Deck plating	0.008125	0.000406
Deck stiffener web	0.008125	0.000406
Side shell plating	0.003750	0.000188
Side stiffener web	0.003750	0.000188
Bottom shell plating	0.021250	0.001063
Bottom stiffener web	0.008125	0.000406

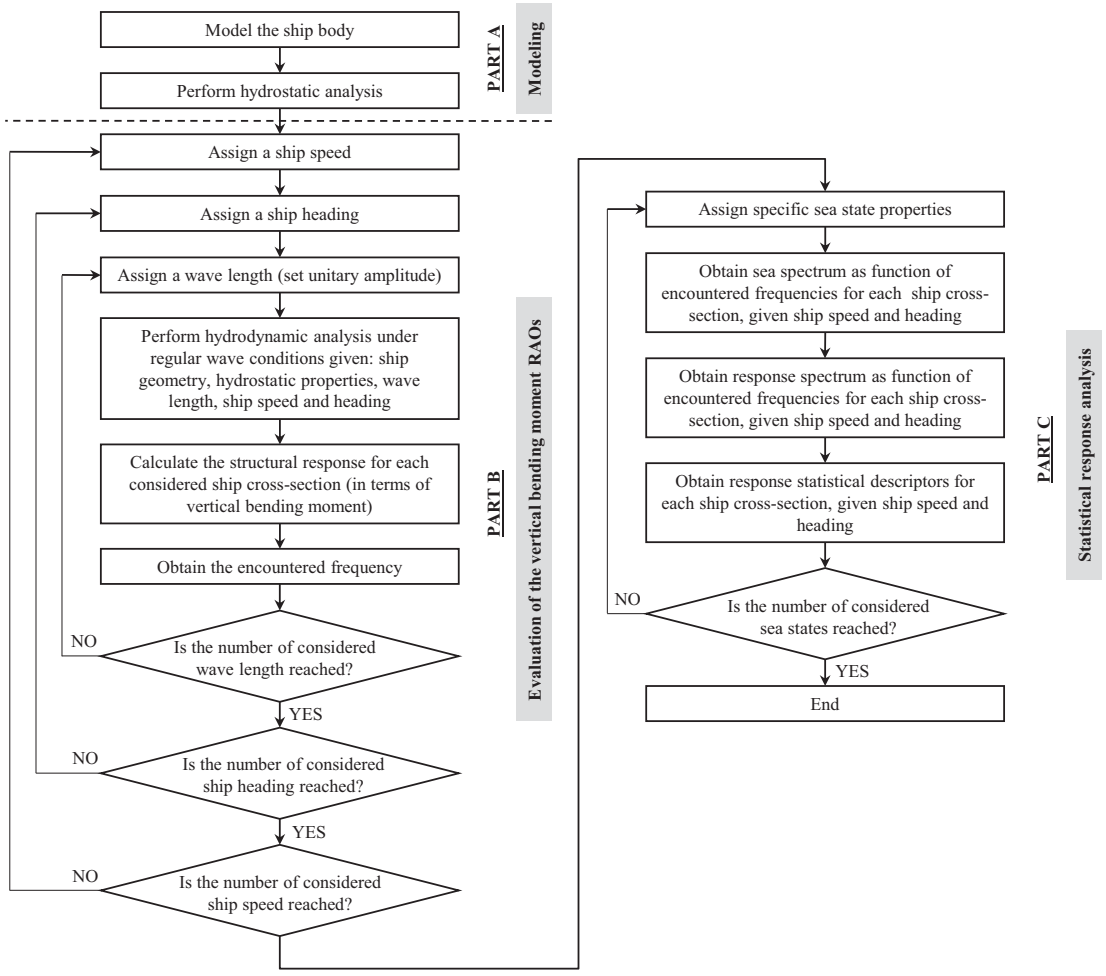

Figure 5.1 Flowchart of the procedure for the probabilistic evaluation of the ship load due to waves for generic operational conditions.

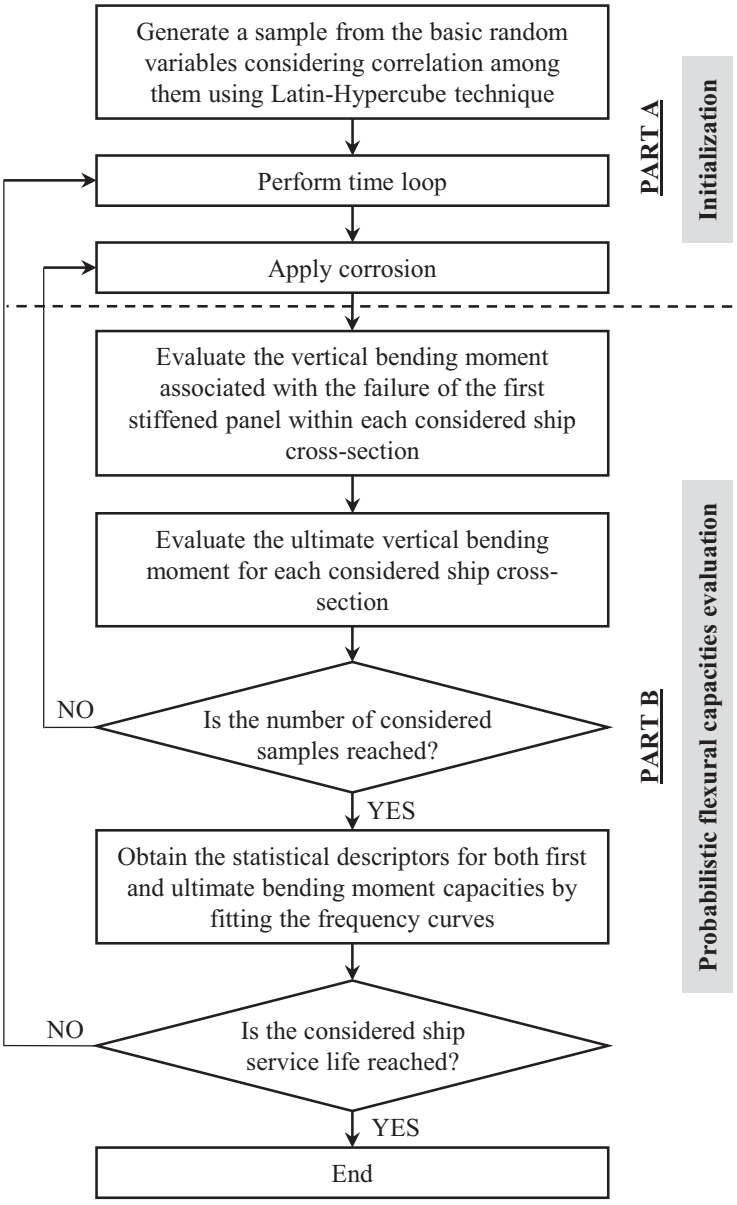

Figure 5.2 Flowchart of the procedure for the probabilistic evaluation of the ship flexural capacities associated with first and ultimate failures.

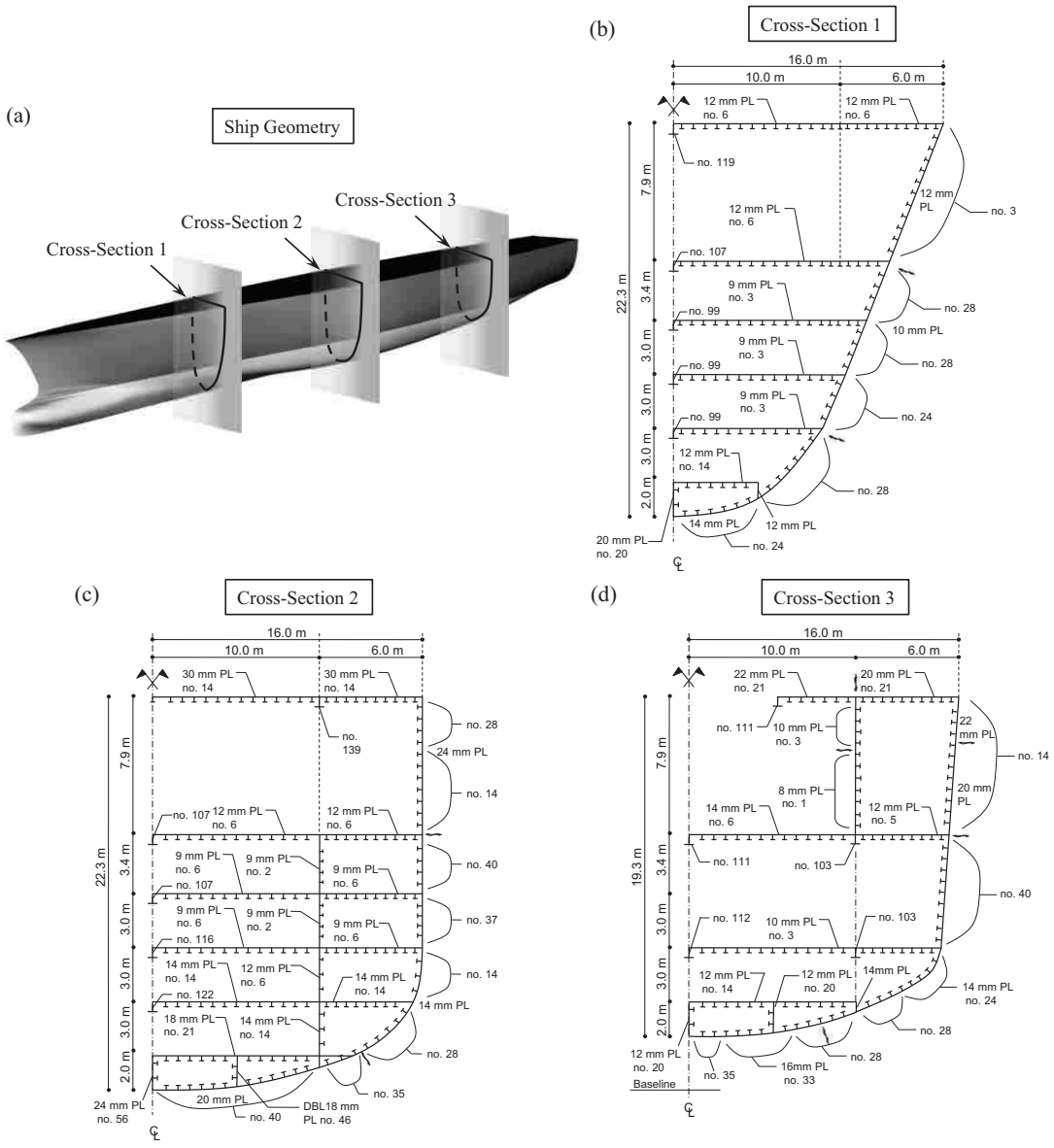

Figure 5.3 (a) Geometrical model of the analyzed JHSS developed by the software FREE!ship (2006). Geometry of (b) cross-section 1 (*CS*1), (c) cross-section 2 (*CS*2), and (d) cross-section 3 (*CS*3).

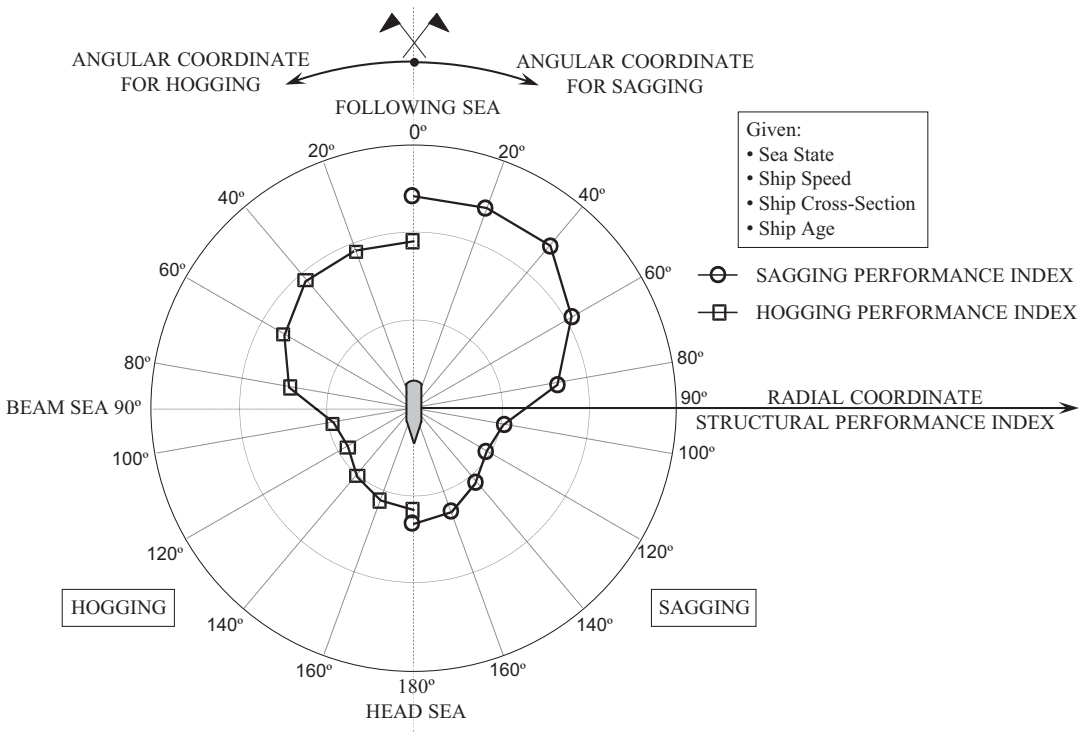

Figure 5.4 Qualitative polar representation of ship structural performance for sagging and hogging conditions given specific sea state, ship speed, ship cross-section, and ship age.

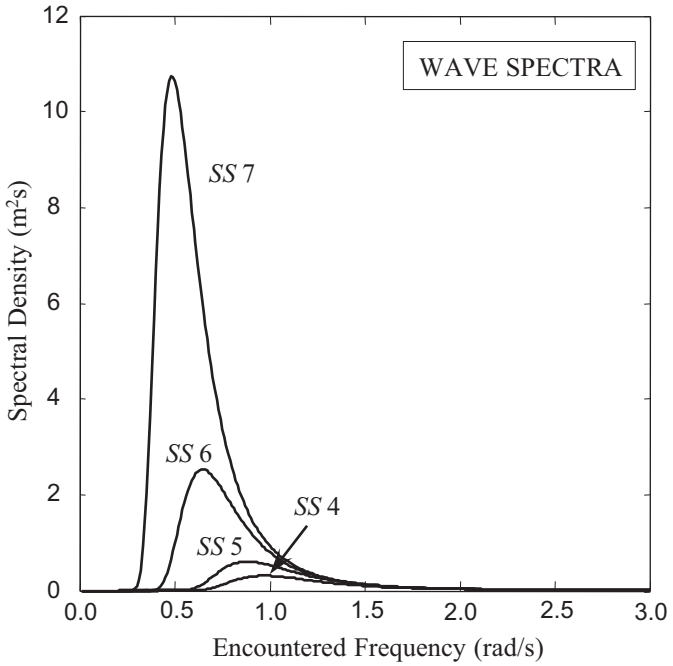

Figure 5.5 Wave spectra for sea states 4, 5, 6, and 7 according to Equation (5.11) and Table 5.2.

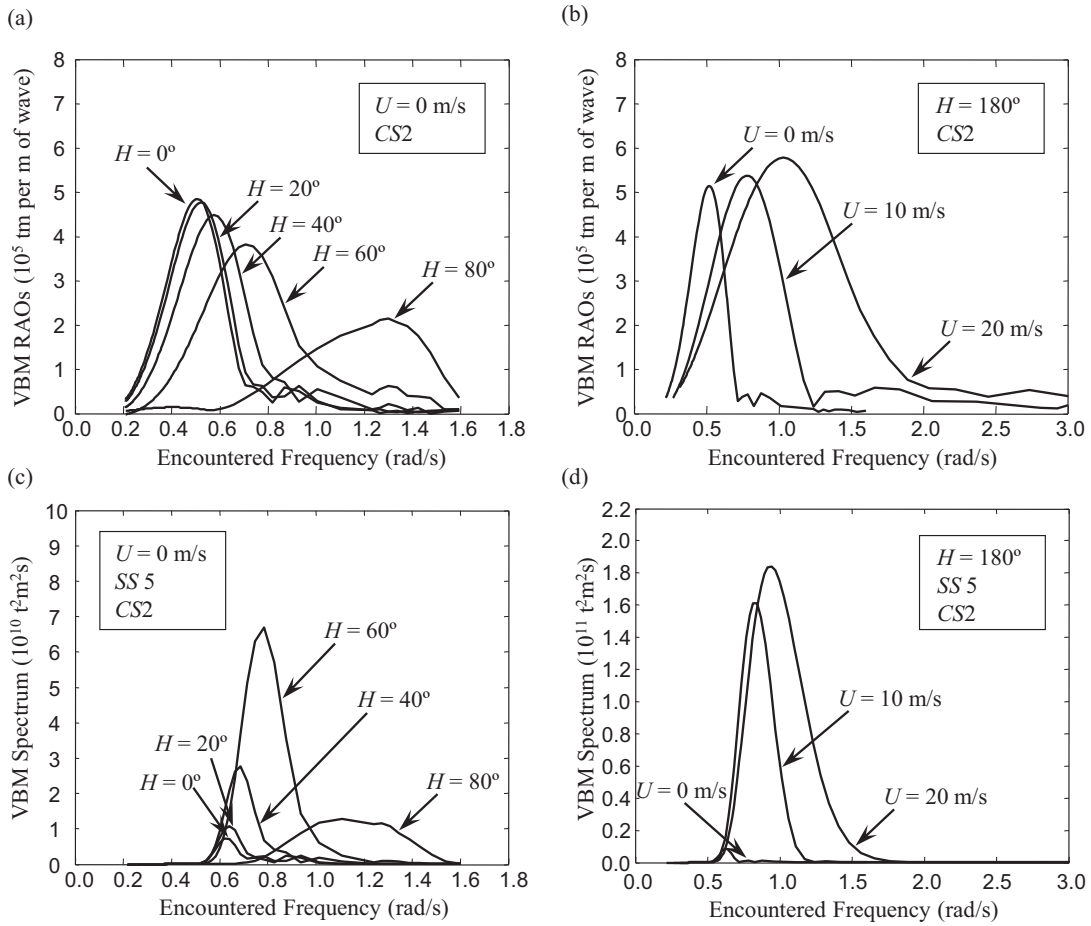

Figure 5.6 VBM RAOs of *CS*2 (a) for different heading angles *H* (0º, 20º, 40º, and 80º) when the ship speed *U* is 0 m/s, and (b) different ship speeds (0, 10, and 20m/s) when the heading angle is 180º. Response spectra at *CS*2 obtained by selecting sea state 5 and by varying (c) ship heading angle and (d) ship speed.

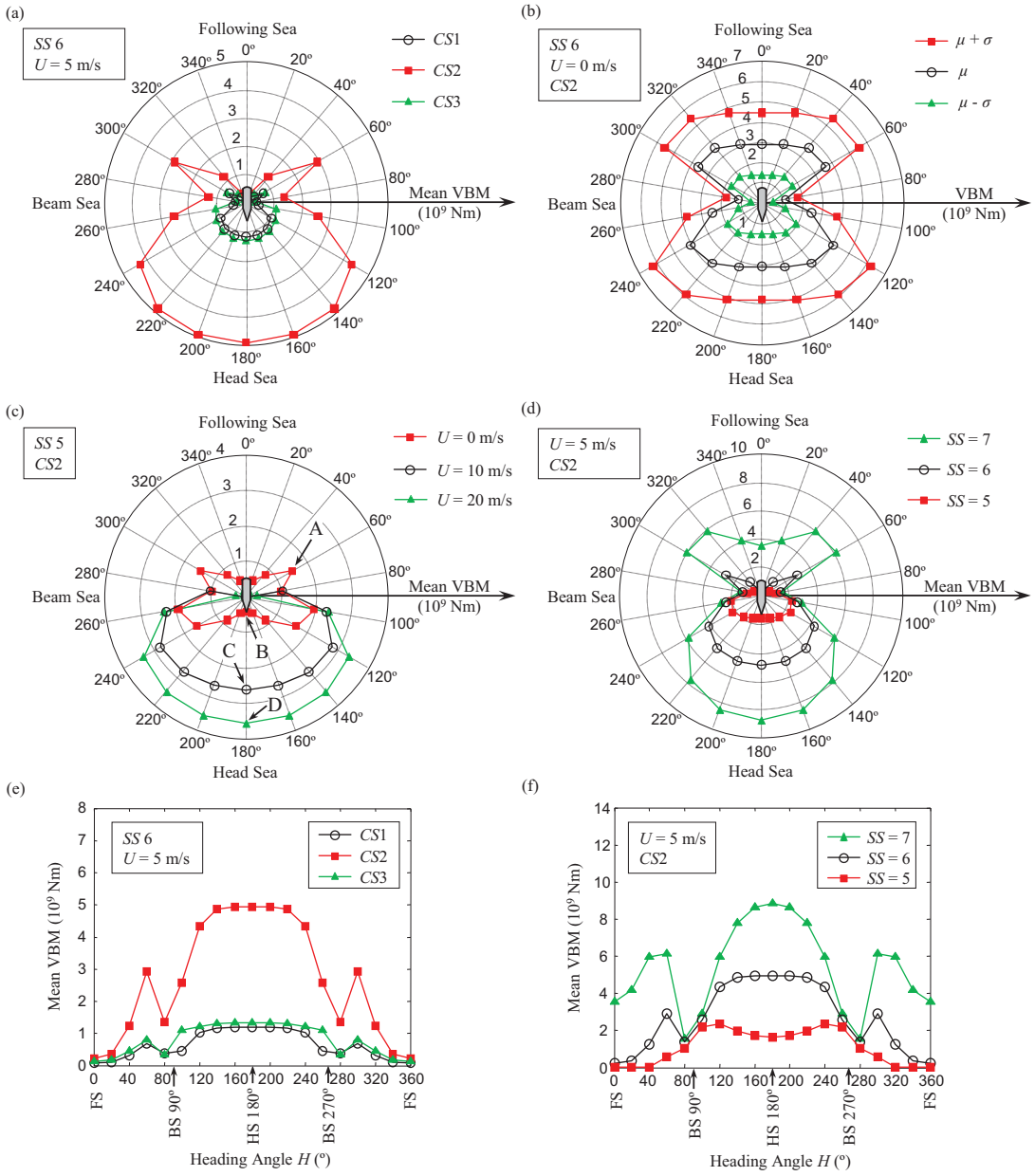

Figure 5.7 Polar representation of the VBM. (a) Profiles of mean VBM for different cross-sections, (b) profiles of mean and mean plus and minus one standard deviation of the VBM, (c) profiles of mean VBM for *CS*2 and sea state 5 by varying ship speed, and (d) profiles of mean VBM for *CS*2 and ship speed of 5 m/s by varying sea state. Plots of mean VBM (e) for different cross-sections and (f) for *CS*2 by varying sea state.

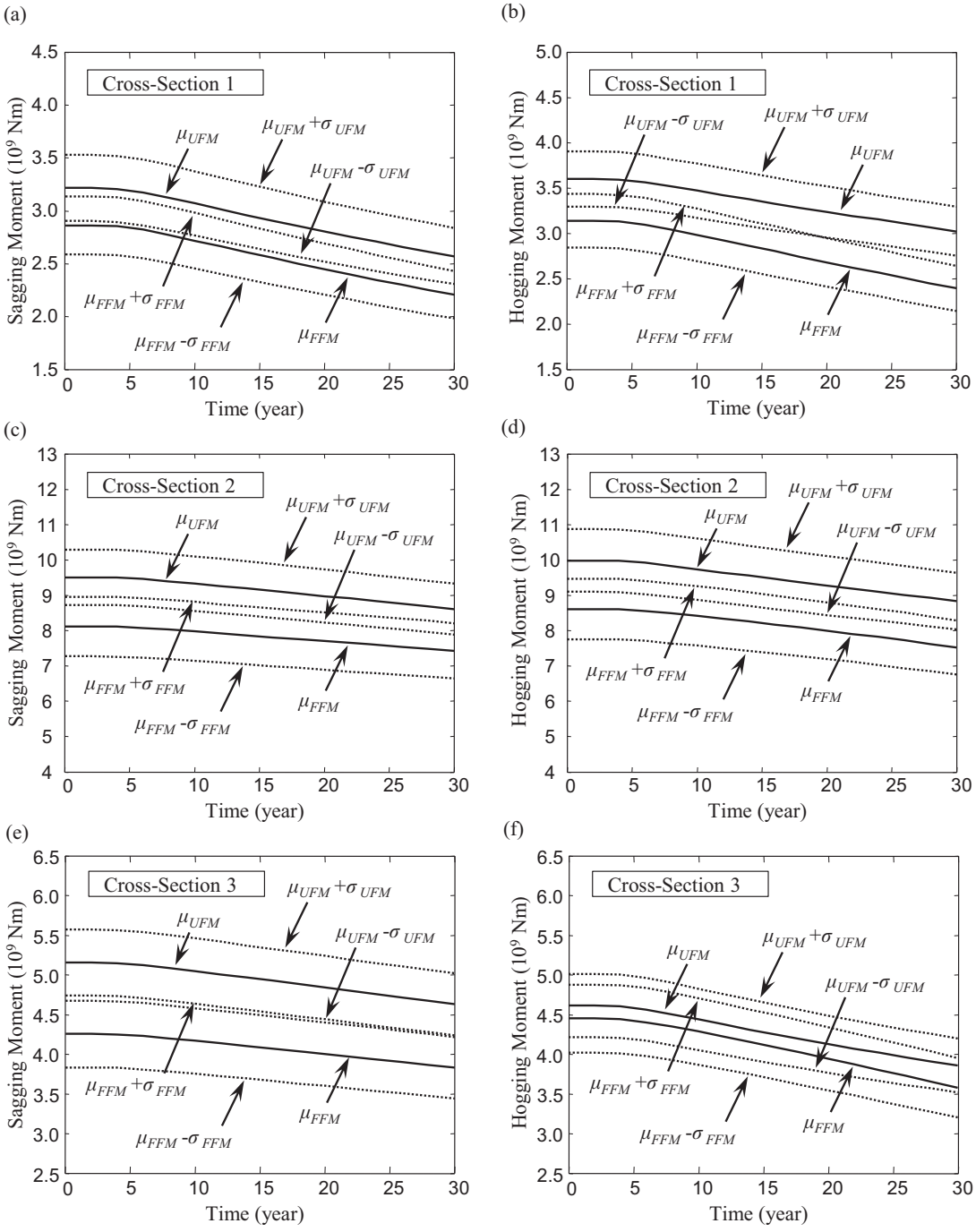

Figure 5.8 Profiles of first (FFM) and ultimate (UFM) failure moments for (a,c,e) sagging, and (b,d,f) hogging. Profile of mean μ and mean plus and minus one standard deviation, ($\mu+\sigma$ and $\mu-\sigma$, respectively) for (a,b) *CS*1, (c,d) *CS*2, and (e,f) *CS*3.

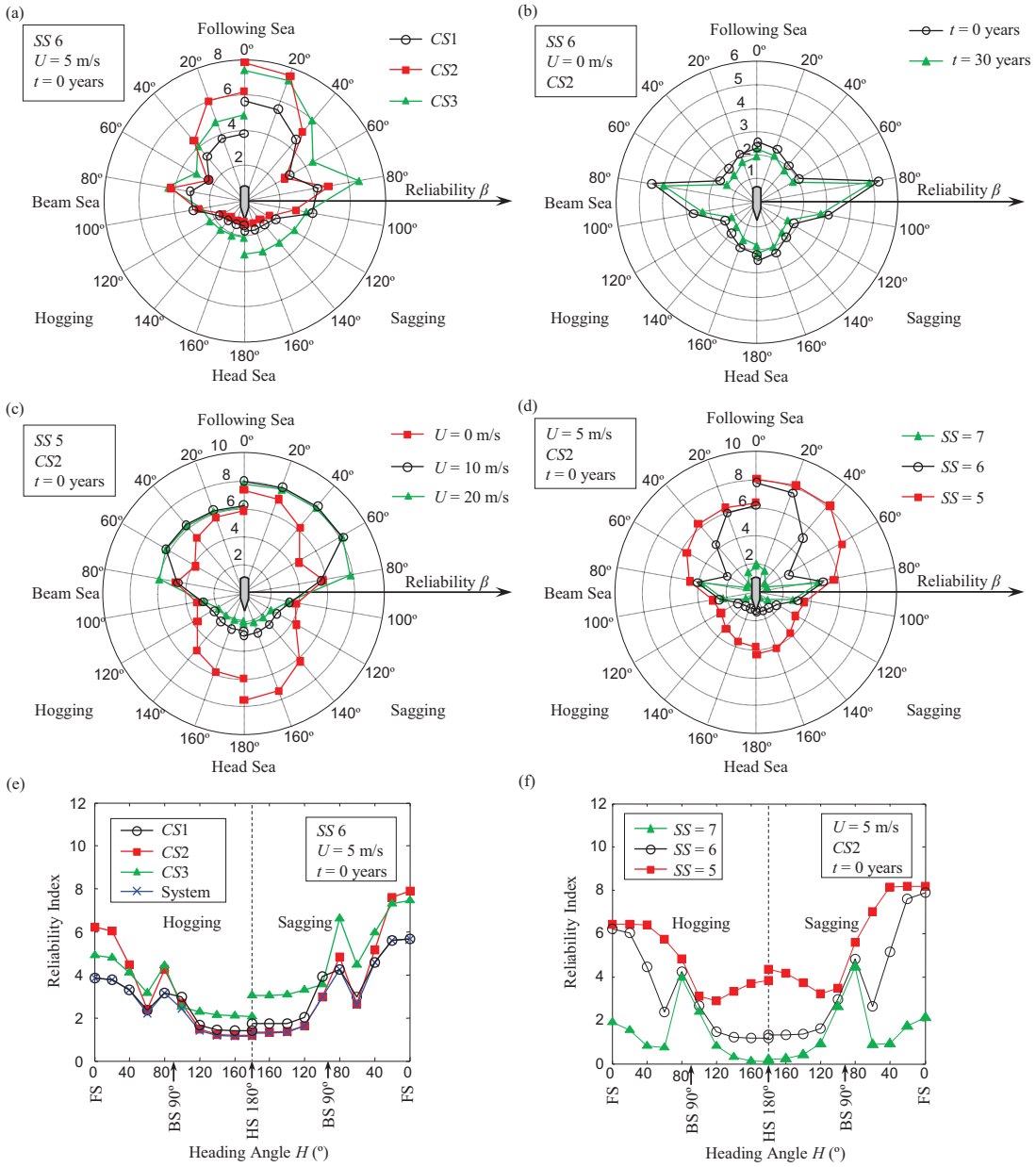

Figure 5.9 Polar representation of reliability associated with the ultimate failure for sagging and hogging. (a) Profiles of reliability for different cross-sections, (b) profiles of reliability for the intact structure (year 0) and aged structure (year 30), (c) profiles of reliability for *CS*2 and sea state 5 by varying ship speed, and (d) profiles of reliability for *CS*2 and ship speed of 5 m/s by varying sea state. Plots of reliability index (e) for different cross-sections and overall system and (f) for *CS*2 varying sea state.

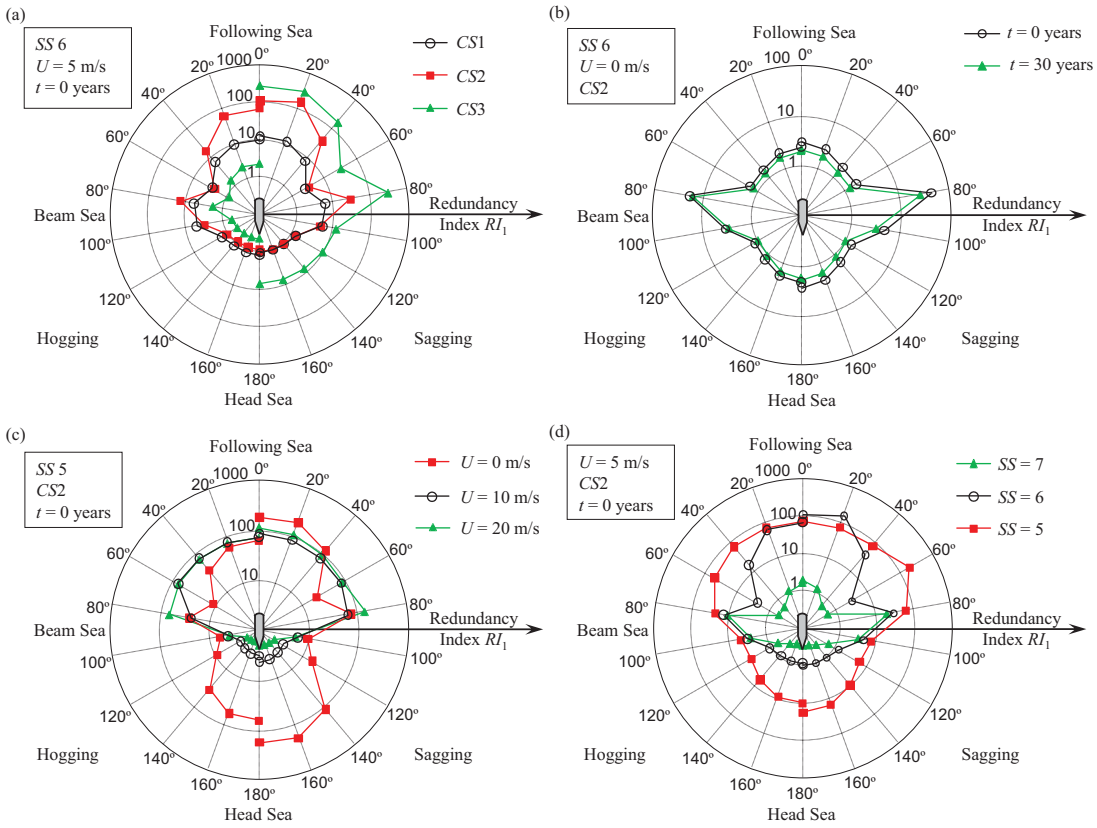

Figure 5.10 Polar representation of the redundancy index RI_1 given by Equation (5.23) associated with ultimate failure for sagging and hogging. (a) Profiles of the redundancy index for different cross-sections, (b) profiles of the redundancy index for the intact structure (year 0) and aged structure (year 30), (c) profiles of the redundancy index for *CS*2 and sea state 5 by varying ship speed, (d) and profiles of the redundancy index for *CS*2 and ship speed of 5 m/s by varying sea state.

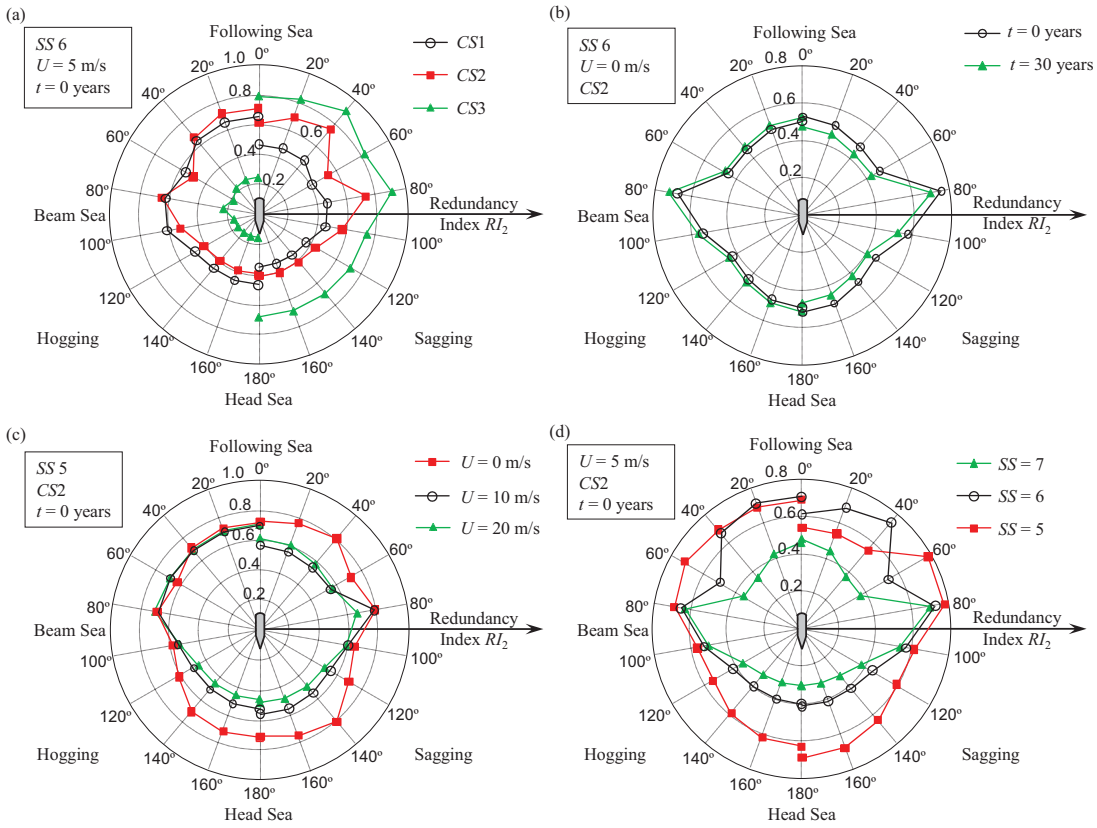

Figure 5.11 Polar representation of the redundancy index RI_2 given by Equation (5.24) associated with ultimate failure for sagging and hogging. (a) Profiles of the redundancy index for different cross-sections, (b) profiles of the redundancy index for the intact structure (year 0) and aged structure (year 30), (c) profiles of the redundancy index for *CS*2 and sea state 5 by varying ship speed, (d) and profiles of the redundancy index for *CS*2 and ship speed of 5 m/s by varying sea state.

CHAPTER 6

RISK-INFORMED OPTIMAL ROUTING OF SHIPS CONSIDERING DIFFERENT DAMAGE SCENARIOS AND OPERATIONAL CONDITIONS

6.1 INTRODUCTION

The worldwide maritime transportation of goods and services rely on the proper ship routing. Decisions regarding the ship route are made according to the encountered sea conditions and ship strength capability, and are usually subjected to time constraint. The proper ship route planning relies on decision making tools that estimate the optimum ship direction and speed based on cost minimization and best estimated time of arrival (ETA). Sometimes, ships are forced to travel along routes that put their structure at risk, potentially facing drastic drops of their operational safety. Therefore, it is crucial to include in the optimal routing the analysis of structural performance indicators such as reliability and risk, which account for the consequences of potential failures or malfunctions. It is also important to provide decision tools that prevent ship structures from down-crossing safety thresholds (Frangopol *et al.* 2012), which may cause important economic losses and loss of lives among the crew and/or passengers.

In this chapter, which is mostly based on Decò and Frangopol (2013b), a finite element simulation is performed in order to estimate the interaction between the

combined actions of vertical and horizontal bending moments of the hull midship section. A technique based on response surfaces (Bucher and Bourgund 1990) using the design of experiments concept is adopted for the probabilistic evaluation of ships flexural strength. The probabilistic load effects are obtained for different ship operational conditions by using linear strip theory; then, reliability analysis is conducted for each considered limit state. On the basis of "fragility analysis", usually used for the evaluation of damage of building and bridges subjected to seismic hazard (Shinozuka *et al.* 2000), intermediate states considering different damage limits, including yield limit state and specific hull plastification thresholds, are investigated in addition than considering only the ultimate limit state. Therefore, reliability analyses are performed when the first yielding occurs and when different limit states are reached as plastification propagates throughout the hull midship section and different ship operational conditions are considered.

This chapter focuses on the risk assessment of hull girders with respect to flexural failure modes induced by different sea conditions. Within the proposed approach, risk assessment is enhanced by analyzing intermediate states, thus providing the opportunity of assessing risk considering the appropriate direct consequences induced by potential structural failures or malfunctions. Polar plots are used to represent load effects, reliability, and risk profiles accounting for different ship reliability levels and operational conditions.

The aim of this chapter is to develop a framework for the risk-informed ship routing minimizing ETA and the expected direct risk, which is associated with the probability of occurrence of different levels of damage within the hull. The optimal

solutions are represented in the form of a Pareto-optimal set that minimizes the two conflicting objectives. An analysis considering the intact and corroded aged ships is also performed when optimizing the ship route.

Uncertainties associated with plate thicknesses, material properties and load effects are modeled and included in the proposed framework. JHSS flexural strength is evaluated using finite element method (FEM), modeling a portion of the hull that includes the midship section by using the software ABAQUS (Dassault Systèmes Simulia 2011). The seakeeping analysis of this ship is performed by using the software PDSTRIP (2006) that is based on strip theory (Korvin-Kroukowski and Jacobs 1957). Other computer programs used include FREE!ship (2006) for the evaluation of hydrodynamic parameters, RELSYS (Estes and Frangopol 1998) for reliability analysis, and MATLAB (The MathWorks 2011) for the optimization using the Genetic Algorithm (GA) and the handling and organization of the input and output files.

This chapter develops an approach for the risk-informed optimal routing of ships considering different damage scenarios and operational conditions. Section 6.2 describes the developed approach for the assessment of risk. Section 6.3 develops the model for the probabilistic evaluation of the vertical and horizontal flexural capacities, including the effects of corrosion. Section 6.4 summarizes the adopted model for the probabilistic evaluation of the load effects induced by still water and waves. Section 6.5 introduces the approach developed for risk-informed optimal routing of ships. As reported in Section 6.6, the implementation of the proposed risk-informed approach is applied to the Joint High Speed Sealift (JHSS), traveling between two points for an

assumed sea weather map. Finally, Section 6.7 provides the conclusions of this chapter that is based on a published paper (Decò, Frangopol and Zhu 2012) and on a paper submitted for possible publication (Decò and Frangopol 2013b).

6.2 RISK FRAMEWORK

The evaluation of the consequences due to potential failures or malfunctions plays a fundamental role in decision analysis. The use of reliability leads to decisions that do not account for any type of consequences. Therefore, every decision should actually be based on risk, which associates the probability of occurrence of specific events with the generated consequences, usually expressed as expected losses. The inclusion of risk, seen as a further performance indicator, can enhance structural safety analysis in order to provide the decision makers with a wide spectrum of options, also accounting for the economic aspect. Risk of marine structures has been qualitatively assessed with respect to manifold failure modes (Akpan *et al.* 2002, Ayyub *et al.* 2002), whereas other studies have quantified risk due to different hazards (Skjong 2002, Skjong and Bitner-Gregersen 2002).

Among different types of hazards, such as fire, collision, grounding (Skjong and Bitner-Gregersen 2002), in this chapter, the vulnerability of ship hulls is evaluated with respect to the flexural failure mode under normal as well as under extreme sea conditions and considering different ship operational conditions. The general procedure for the assessment of reliability and risk is summarized in the Module (3) of Appendix B. Due to the fact that yielding or slight damage may be present within the structures of operating ships, different limit states *LSi* accounting for the occurrence of

yielding and propagation of plastification throughout the hull are investigated. The following states *Si* are emphasized:

- *State S*1: the ship hull is within the elastic range and buckling has not occurred in the plates or in the stiffened panels.
- *State S*2: the ship hull is right over the elastic behavior, experiencing local buckling of the extreme stiffeners with respect to the neutral axis, which induces local plastification. In order to allow small regions of the hull extremities to plastify, it is assumed that the plastified area is located within the extreme plates and up to 20% of the largest distance to the neutral axis. Buckling of the compressed extreme stiffeners occurs.
- *State S*3: the plastification propagates throughout the section reaching values between 20% and 50% of the largest distance to the neutral axis. Buckling effects are extended through a large portion of the stiffened panels. The hull deforms significantly and ship service is at risk.
- *State S*4: the plastification propagates throughout the section (greater than 50% of the largest distance to the neutral axis) until the ultimate flexural capacity is reached. Ship serviceability is compromised and the collapse is imminent due to large deformations.
- *State S*5: ship collapse occurs.

The above mentioned five states (*S*1 to *S*5) are evaluated by investigating four different limit states: yielding (*LS*1), plastification propagation up to 20% (*LS*2) and 50% (*LS*3) of the largest distance to the neutral axis, respectively, and ultimate

capacity (*LS*4). The reaching of a specific limit state is in general due to the combined effects of vertical and horizontal bending moments. Therefore, based on the studies of Paik, Thayamballi and Che (1996), Gordo and Guedes Soares (1996), and Gordo and Guedes Soares (1997), for each limit state the associated hull strength is given by the following equation providing limit state contours

$$\left(\frac{M_v}{M_{v,LSi}}\right)^{c_{1,LSi}} + \left(\frac{M_h}{M_{h,LSi}}\right)^{c_{2,LSi}} = \delta \tag{6.1}$$

where δ is a parameter, M_v and M_h are the vertical and horizontal bending moments, respectively, due to sea load effects, $M_{v,LSi}$ and $M_{h,LSi}$ are the vertical and horizontal flexural capacities associated with a specific limit state *LSi*, respectively, and $c_{1,LSi}$ and $c_{2,LSi}$ are parameters. M_v and $M_{v,LSi}$ can be taken as either sagging or hogging, depending on the load combination under analysis.

Time processes may decrease the mechanical properties of the hull, and corrosion effects may generate loss of thickness throughout the hull section. This causes the deterioration of the section modulus, thus reducing the section flexural capacity. Therefore, considering the effects of corrosion on ship structures, Equation (6.1) can be rewritten as

$$\left(\frac{M_v}{M_{v,LSi}(t)}\right)^{c_{1,LSi}} + \left(\frac{M_h}{M_{h,LSi}(t)}\right)^{c_{2,LSi}} = \delta \tag{6.2}$$

where t is time.

6.2.1 RELIABILITY ANALYSIS

Other than considering different ship operational conditions, reliability analysis is also conducted with respect to different limit states *LSi* previously introduced. Ship reliability analysis can be performed based upon the knowledge of the probability distributions of the flexural strengths and the statistical descriptors of the load effects, later discussed. Based on Equation (6.2), the time-dependent failure probabilities and the corresponding reliability indices are based on the time-dependent performance function $G_{LSi,SE,U,H}(t)$, associated with a *LSi* and for different operational conditions. This function is (Guedes Soares and Teixeira 2000, Paik and Frieze 2001)

$$G_{LSi,Hs,U,H}(t) = \delta - \overbrace{\left(\frac{x_{sw}M_{sw} + x_w k_W\left(M_{wv,Hs,U,H} + k_D M_{WH}\right)}{x_R M_{v,LSi}(t)}\right)^{c_{1,LSi}}}^{VBM} - \overbrace{\left(\frac{x_w M_{wh,Hs,U,H}}{x_R M_{h,LSi}(t)}\right)^{c_{2,LSi}}}^{HBM} \tag{6.3}$$

where the subscripts *Hs*, *U*, and *H* refer to significant wave height, ship speed, and ship heading angle, respectively, δ is a parameter theoretically set to one, x_R, x_{sw}, and x_w are parameters accounting for the model uncertainties associated with the resistance determination, still water bending moment prediction, and wave-induced bending moment prediction, respectively, k_W is the correlation factor for the wave-induced bending moment set to one (Mansour *et al.* 1984), k_D is the correlation factor between wave-induced and dynamic bending moments (Mansour *et al.* 1984), M_{sw} is the still water bending moment, $M_{wv,Hs,U,H}$ and $M_{wh,Hs,U,H}$ are the vertical and horizontal wave-

induced bending moments given by linear theory, respectively, M_{WH} is the whipping bending moment, $M_{v,LSi}$ and $M_{h,LSi}$ are the vertical and horizontal flexural capacities, and $c_{1,LSi}$ and $c_{2,LSi}$ are parameters referring to the selected *LSi*. Depending on the load effects under analysis, the terms M_{sw}, $M_{wv,Hs,U,H}$, $M_{v,LSi}$, $c_{1,LSi}$, and $c_{2,LSi}$ assume different values for sagging and hogging.

The evaluation of the probability of failure associated with the ultimate capacity (*LS*4) and the probabilities of exceedance of three different limit states (*LS*1, *LS*2, and *LS*3) are necessary in order to relate the right level of consequences. These time-dependent probabilities $P_{LSi,Hs,U,H}(t)$ are generally calculated as follows

$$P_{LSi,Hs,U,H}(t) = P\left[G_{LSi,Hs,U,H}(t,\mathbf{X}) < 0\right] = \int_{G_{LSi,Hs,U,H}(t,\mathbf{X})<0} f(t,\mathbf{X})dx \tag{6.4}$$

where $f(t,\mathbf{X})$ is the joint PDF of the considered random variables $\mathbf{X} = x_1, x_2,\ldots,x_k$ at a given time t. Given that usually this integral cannot be solved analytically, these probabilities can be evaluated using approximate methods such as the first-order reliability method (FORM), among others. The relationship between the time-dependent reliability index $\beta_{LSi,Se,U,H}(t)$ and probability $P_{LSi,Hs,U,H}(t)$ for a given *LSi* and for different ship operational conditions is

$$\beta_{LSi,Hs,U,H}(t) = \Phi^{-1}\left(1 - P_{LSi,Hs,U,H}(t)\right) \tag{6.5}$$

where Φ^{-1} is the inverse standard normal distribution function.

In order to find the time-dependent probabilities $P_{Si,Hs,U,H}(t)$ of the hull being in the previously defined states *S*1 to *S*5, which are based on the exceedance probabilities $P_{LSi,Hs,U,H}(t)$ for the limit states *LS*1 to *LS4*, a procedure similar to the fragility analysis

(Shinozuka *et al.* 2000), is used herein. The difference is that variables such as sea elevation and ship speed and heading angle are those that affect the loads on the hull. Since the five introduced states consider progressive plastification of the hull ($S1$ to $S5$), the probabilities of the hull being in specific states $P[Si|Hs,U,H](t)$ are

$$P[Si \mid Hs,U,H](t) = \begin{cases} P_{S1,Hs,U,H}(t) = 1 - P_{LS1,Hs,U,H}(t) & i = 1 \\ P_{Si,Hs,U,H}(t) = P_{LS(i-1),Hs,U,H}(t) - P_{LSi,Hs,U,H}(t) & 2 \le i \le 4 \\ P_{S5,Hs,U,H}(t) = P_{LS4,Hs,U,H}(t) & i = 5 \end{cases} \quad (6.6)$$

In other words, these probabilities are conditioned by the occurrence of specific sets of Hs, U, and H that are statistically independent from each other, leading to the evaluation of the conditional probabilities

$$P_{Si,Hs,U,H}(t) = P[Si \mid Hs,U,H](t) \quad (6.7)$$

Moreover, the occurrences of the ship being in the above defined five states are mutually exclusive and collectively exhaustive events.

6.2.2 CONSEQUENCE ANALYSIS

This section presents the consequence analysis including specific costs associated with the potential failure of a ship hull or the exceedance of specific limit states such as those associated with the propagation of plastification. Direct consequences are the losses due to the damage or the failure itself, whereas indirect consequences are those related to system failure or malfunctions that induce external monetary losses. The main indirect losses/costs for marine structures can be summarized as those due to (IMO 1997, Ayyub *et al.* 2002, Skjong 2002): injuries and fatalities to passengers and

crew, damage to ship equipment, transported goods, and port facilities, and commercial and environmental impacts, among others.

The focus of this chapter is risk-informed routing of ships based on the quantification of the hull structural safety (i.e. in terms of risk); therefore direct consequences, including construction and rehabilitation costs, are emphasized among other types of potential consequences and operational costs. This chapter provides a direct link between the structural performance in terms of hull flexural strength and the economic direct impact, however indirect consequences can be accommodated in the proposed framework. Consequence analysis uses an economic approach and a monetary value expressed in United States Dollar (USD). The considered direct costs are:

- *Construction costs* C_{Con}: weight-based costs of construction. These costs are evaluated by using the equations proposed by Miroyannis (2006) based on empirical Cost Estimation Relationships (CERs). This method is in agreement with the NAVY standards, being the NAVY's cost estimates mostly based on weights only. Accordingly, considering the Ship Work Breakdown System (SWBS), ship costs are subdivided in categories, such as structure, propulsion, and electrical, among others. The estimated costs (USD) are obtained considering ship preliminary design and the structural SWBS category denominated "100". These costs are given by (Miroyannis 2006)

$$C_{Con} = \overbrace{CF \times 177 \times WGT_{100}{}^{0.862}}^{\text{Labor Manhours}} + \overbrace{800 \times WGT_{100}}^{\text{Material Dollars}} \tag{6.8}$$

where

$$CF = STF \times SF \tag{6.9}$$

$$SF = 32.47 \times DISPL^{-0.3792} \tag{6.10}$$

in which CF is the complexity factor, WGT_{100} is the weight of the SWBS 100 (long tons), STF is the ship type factor, SF is the size factor, and $DISPL$ is the ship full load displacement (long tons).

- *Rehabilitation costs* $C_{Reh,Si}$: considered as fractions of the ship construction costs based on the estimated level of damage. These costs are evaluated as

$$C_{Reh,Si} = d_{r,Si} C_{Con} \tag{6.11}$$

where $d_{r,Si}$ is the damage ratio (i.e. the proportionality factor between ship repair costs and the ship construction costs). The criterion adopted for the quantification of the damage is based on the percentage of plastification within the considered hull section. Therefore, the damage ratios associated with each specific state Si are evaluated in accordance with each of the specified hull states, discussed in Section 6.2. Accordingly, state $S1$ does not generate any consequences, since by definition the hull section is within the elastic range and buckling has not occurred, whereas the other states cause direct consequences proportional to the damaged area. In the cases of the ship being in states $S2$ to $S4$, C_{Con} is assumed to refer to the portion of the hull surrounding the damaged midship section damage, while for the state $S5$, C_{Con} is assumed to account for the structure of the entire ship hull.

According to Ayyub *et al.* (2002), these economic quantities must be quantified numerically for the purpose of risk assessment; however, the assigned numerical values do not have to be exact, and may be calculated by using a combination of expert opinion, engineering judgment, classification society requirements, and historical data.

6.2.3 RISK ASSESSMENT

Risk is defined as the combination of occurrences and consequences of events generated by specific hazards. According to the definition reviewed in Appendix A, risk $R(t)$ referred to a specific time t can be expressed as (CIB 2001)

$$R(t) = \int\int ... \int \delta(t, \mathbf{X}) f(t, \mathbf{X}) dx \tag{6.12}$$

where $\delta(t,\mathbf{X})$ represents the consequences and $f(t,\mathbf{X})$ is the joint PDF of the considered random variables $\mathbf{X} = x_1, x_2,\ldots,x_l$. The solution of Equation (6.12) is not obvious; therefore, risk is evaluated by considering an approach that accounts for the discrete states associated with the different hull damages described previously. Since the five states are mutually exclusive and collectively exhaustive, and based on the probabilities of Equation (6.6), time-dependent total risk $R_{,Hs,U,H}(t)$ for a given set of *Hs*, *U*, and *H* can be obtained as

$$R_{Hs,U,H}(t) = \sum_{s=S1}^{S5} C_{Si} P_{Si,Hs,U,H}(t) \tag{6.13}$$

where C_{Si} are the total consequences associated with specific states *Si*. Specifically, based on the direct costs evaluated by Equations (6.8) and (6.11), the time-dependent direct risk $R_{D,Hs,H}(t)$ can be obtained as

$$R_{D,Hs,U,H}(t) = \left[\sum_{s=S2}^{S4} C_{Reh,Si} P_{Si,Hs,U,H}(t)\right] + C_{Con} P_{S5,Hs,U,H}(t) \tag{6.14}$$

6.3 PROBABILISTIC HULL STRENGTH

The flexural strength of hulls may be evaluated by using different approaches, incremental methods (e.g. Smith 1977, IACS 2008), or the optimization-based method proposed by Okasha and Frangopol (2010b). Although these methods have provided good estimates, a FEM-simulation is performed instead in order to investigate in detail the propagation of plastification throughout a given ship section. The framework for the evaluation of the hull flexural capacity is presented in the Module (2) of Appendix B.

6.3.1 FINITE ELEMENT MODELING

The recent development of computer technology and commercial FEM-software has allowed researchers to make use of FEM-modeling for the purpose of performing reliability analysis of civil and marine structures (Zheng and Das 2000, Ghosn, Moses and Frangopol 2010). On the other hand, ship designers can also take advantage of this technique allowing them to enhance design to detail levels that were never reached in the past. The proper ship FEM-modeling guidelines can be found in relevant recommendations (Basu, Kirkhope and Srinivasan 1996, CCS 2005). Moreover,

according to Wang and Wiernicki (2004), the key aspects of FEM-modeling are: structural idealization, inclusion of geometric and material non-linearity, consideration of specific loads and boundary conditions, and analysis of different failure or acceptance criteria.

The most general case, in which the hull is subjected to both vertical and horizontal bending moments, is investigated. FEM-modeling is used to obtain vertical and horizontal moment-curvature relationships in order to investigate structural performance, and provide indications about ship reliability, as later discussed in the case study. In order to achieve this goal, a detailed non-linear response analysis of the hull, accounting for both geometric and material non-linearity, is performed. The FEM-simulations provide the vertical and horizontal flexural capacities associated with the limit states defined in Section 6.2. The parameters $c_{1,LSi}$ and $c_{2,LSi}$ of Equation (6.3) can be evaluated by using the method of the least squares, i.e. fitting the output obtained by incremental analyses (FEM-simulations), which includes different ratios between vertical and horizontal bending moments.

6.3.2 RESPONSE SURFACE METHOD

While the use of conventional non-linear FEM is possible for deterministic analysis, this technique is computationally demanding, especially for stochastic analyses of the ship's strength, involving a potentially high number of simulations (e.g. for reliability analysis). Therefore, in order to account for uncertainties and significantly reduce the computational costs to an acceptable level, FEM is used in combination with the Response Surface Method (RSM) (Bucher and Bourgund 1990, Zheng and Das 2000,

Ghosn, Moses and Frangopol 2010). The RSM consists in the execution of deterministic FEM-analyses at specific values of the considered random variables. The obtained results, representing the responses, are collected and summarized into a RSM-equation originated by regression analysis. For instance, if a second-order interpolating polynomial is selected, the fitting RSM-equation leads to

$$RS = \alpha_0 + \sum_{i=1}^{l} \alpha_i x_i + \sum_{i<j}^{l} \alpha_{ij} x_i x_j + \sum_{i=1}^{l} \alpha_{ii} x_i^2 \tag{6.15}$$

where RS is the response, α_0, α_i, α_{ij}, and α_{ii} are the polynomial coefficients to be determined, i and j are indices referring to the selected random variables x_i and x_j, respectively, and l is the total number of random variables. Once all the responses are collected from the FEM-simulations, the coefficients α in Equation (6.15) can be estimated by the method of the least squares. Since the RSM is part of the proposed probabilistic approach, the capacities $M_{v,LSi}$ and $M_{h,LSi}$, which are the evaluated responses, are obtained in the form of Equation (6.15). Therefore, the considered basic random variables associated with the hull strength model (e.g. geometrical and material properties) can be included in Equation (6.15). The statistical descriptors of the responses can be obtained by simulations.

Each FEM-simulation includes a set of perturbed values for each considered random variable, according to a predefined scheme. Among others, the Circumscribed Central Composite (CCC) design is a popular template that satisfies the minimum required values for a full quadratic model (Myers and Montgomery 2002); therefore, CCC is used in this chapter.

6.3.3 EFFECT INDUCED BY CORROSION

The main effect induced by corrosion over time is the loss of thickness of plates and stiffeners. The thickness loss is evaluated in according to Akpan *et al.* (2002), as described in Section 5.3.1.

6.4 STOCHASTIC LOAD EFFECTS

The assessment of the safety of ship structures requires the stochastic evaluation of the effects induced by the loads acting on the hull, that are mainly generated by still water and waves. As indicated in previous studies (Gordo and Guedes Soares 1997, Guedes Soares and Teixeira 2000), the primary load effects on the hull are sagging and hogging vertical bending moments (VBMs) and horizontal bending moment (HBM), which induce compression and/or tension in the stiffened panels composing the whole hull. Since mission-oriented reliability and risk analyses are performed, and design considerations are not included, only short-term statistics of loads are of interest. The procedure for the estimation of the load effects is summarized in the Module (1) of Appendix B.

The stillwater VBM is induced based on the difference between the weight and the buoyancy distributions along the hull. Depending on the distribution and magnitude of the cargo within the ship, the VBM varies for different journeys. The probabilistic approach proposed by Hussein and Guedes Soares (2009) for the evaluation of this load may be adopted. This approach provides a simplified probabilistic estimation of

the stillwater VBM, which is useful when information regarding the cargo is lacking. This method has been described in Section 5.2.1.

The load effects generated by the interaction between the waves and the hull are measured in terms of ship motion, pressure distribution, and body forces and moments. The magnitude of these effects depends on many factors, including ship geometry, encountered sea state, and ship speed and heading. In order to evaluate the ship structural response with respect to generic environmental and operational conditions, linear response theory, which is recognized to be common practice (Ayyub *et al.* 1998). In particular, VBM and HBM are the quantities of interest. A useful tool that makes use of linear theory for the evaluation of these responses is the strip method (Korvin-Kroukowski and Jacobs 1957). Strip theory integrates the hydrodynamic forces (Froude-Krilov part and diffraction part) induced by harmonic waves over the ship wetted surface, that is discretized into prismatic segments (strips). Therefore, the shear and bending moment can be evaluated at each considered location along the overall length. However, linear theory can provide approximate results when dealing with wave heights that are greater than wave lengths (Hughes 1983). Although more sophisticated methods exist, such as non-linear analysis and complete three-dimensional theories, among others, given that performing a very accurate seakeeping analysis is out of the scope of this chapter, the approximations introduced by strip theory are deemed acceptable. The load effects are evaluated following the method used in Section 5.2.2.

VBM and HBM for a given hull section are correlated quantities. For low frequency waves this correlation coefficient is provided by Mansour and Thayamballi (1994)

$$\rho_{VBM,HBM} = \frac{1}{\sigma_{VBM}\sigma_{HBM}} \int_0^\infty \mathrm{Re}\left[\Phi_{VBM}(\omega)\Phi^*_{HBM}(\omega)\right] S_W(\omega) d\omega \tag{6.16}$$

where $\Phi_{VBM}(\omega)$ is the transfer function of VBM, $\Phi^*_{HBM}(\omega)$ is the complex conjugate of the transfer function of HBM, $S_W(\omega)$ is the sea spectrum, σ_{VBM} and σ_{HBM} are the individual standard deviations of VBM and HBM, respectively, and Re denotes the real part of the complex quantity within parentheses.

For short-term statistics and assuming that the instantaneous value of the ocean elevation follows a Gaussian distribution (Faltinsen 1990), the probability density function (PDF) of the peak responses considering several operational conditions (significant wave height *Hs* and ship speed *U* and heading *H*) follows the Rayleigh distribution (Hughes 1983)

$$f\left(M_{w,Hs,U,H}\right) = \frac{M_{w,Hs,U,H}}{m_{0,Hs,U,H}} \exp\left(-\frac{\left(M_{w,Hs,U,H}\right)^2}{2m_{0,Hs,U,H}}\right) \tag{6.17}$$

where $M_{w,Hs,U,H}$ is the wave-induced bending moment response (VBM or HBM) and $m_{0,Hs,U,H}$ is the zero-*th* moment of the associated response spectrum. The relevant statistical descriptors are obtained accordingly. Additional explanations on the used procedure for the evaluation of the statistics of ship flexural responses (in accordance with Hughes 1983, Faltinsen 1990) is discussed in Chapter 5.

6.4.1 DYNAMIC LOAD EFFECTS

The dynamic bending moment on fine bow ships induced by whipping can be evaluated by using the equation proposed by Sikora and Brady (1989)

$$M_{WH} = \begin{cases} 0.0022 LBP^2 b & \text{for } LBP^2 b < 5\times 10^6 \\ 5.4 LBP\sqrt{b} & \text{for } LBP^2 b \geq 5\times 10^6 \end{cases} \tag{6.18}$$

where M_{WH} is the peak-to-peak whipping bending moment (ft-ton), LBP is the length between the perpendiculars of the ship (ft), and b is the ship breadth (ft). These load effects can therefore be accommodated in the adopted framework for the evaluation of ship responses.

6.5 RISK-INFORMED ROUTE OPTIMIZATION

In order to fully exploit the introduced framework to assess risk due to expected losses, among other potential applications, the risk-informed route optimization based on mission-oriented reliability (i.e. accounting for short period load effects) is introduced in this section. The framework for the risk-informed route optimization is presented in the Module (4) of Appendix B.

Although criteria, such as minimization of ship movements, minimization of fuel consumption, and other operating costs, cover a wide set of different optimization problems (Journée and Meijers 1980, Brown, Graves and Ronen 1987, Hinnenthal 2008, Dolinskaya *et al.* 2009, Fagerholt, Laporte and Norstad 2010, Papatzanakis, Papanikolaou and Liu 2012), ship safety criterion has been touched only partially. The aim of this chapter is to cover an analysis that explicitly includes ship structural

reliability and expected risk associated with potential structural failure or deficiencies. The inclusion of costs elevates this problem to an upper level allowing conscious decision making to be risk-informed, thus accounting for the negative consequences.

Once risk has been evaluated for a given set of operational conditions, the optimal route of a ship under various weather conditions can be obtained. Assuming that a weather forecast is given for a specific sea region (described by an *x*-*y* Cartesian coordinate system) and that a ship has to travel between the points O (origin) and D (destination) within this region, the above mentioned optimization problem can be solved by discretizing the travel in *N* segments, that are described by initial and end points in the *x* and *y* coordinates. For each initial point of each *N*-th segment, a ship speed *U* has to be provided. Assuming that the *x*-axis is discretized in a fixed number *N* of intervals, the optimal route is determined by the evaluation of the *N*-1 *y* coordinates required to describe the *N* route segments. Based on the general formulation of a multi-objective optimization problem (reviewed in Appendix A), the optimization problem for optimal ship routing can be formally stated as follows:

Given: sea weather map that includes sea elevation in terms of significant wave height, wave direction, and allowable risk with respect to different operational conditions at a specific ship age *t*

find: a set of ship speeds U_i and coordinates y_i

$$U_i \qquad \forall i = 1, 2, ..., N \tag{6.19}$$

$$y_i \qquad \forall i = 1, 2, ..., N-1 \tag{6.20}$$

to minimize: the estimated time of arrival *ETA* and the risk *R*

$$\min\{ETA, R\} \tag{6.21}$$

subjected to the constraints:

$$U_{\min} \le U_i \le U_{\max} \qquad \forall i = 1,2,...,N \tag{6.22}$$

$$y_{\min} \le y_i \le y_{\max} \qquad \forall i = 1,2,...,N-1 \tag{6.23}$$

where N is the number of the travel discretization based on the map dimensions with respect to the x-axis, U_{min} and U_{max} are the minimum and maximum allowable ship speed, respectively, and y_{min} and y_{max} are the bounds of the map in the y-axis direction. A potential sea weather map, describing the routing optimization is reported in the figures describing the optimization process of the case study later introduced. This risk-based biobjective optimization approach can be extended to a higher order objective optimization, including additional objectives and constraints (Frangopol 2011) that are relevant for the selection of the optimal routes.

Since this optimization problem is not described by a closed form solution, the use of a heuristic optimization tool such as the GA (Goldberg 1989) is preferable with respect to classical gradient-based methods. Therefore, the optimization process is carried out by multiobjective GA provided by the software MATLAB (The MathWorks 2011), which uses a modified version of the NSGA-II algorithm (Deb 2001). The Pareto-optimal set represents the optimal routes guaranteeing that the obtained solutions lead to an optimal result for both objective functions. Therefore, any point belonging to this set can be chosen by the decision makers depending on the acceptable level of risk and on the allowable time to complete the travel.

Another important aspect, addressed in the case study, is to investigate the optimal routing of aged ships, i.e. accounting for the loss of strength of the hull due to corrosion effects. This analysis can be performed by repeating the same optimization problem in order to show how decisions may vary when a ship with greater structural vulnerability is considered.

6.6 CASE STUDY

The proposed framework is applied to the Joint High-Speed Sealift (JHSS) discussed in Devine (2009) having the following properties: length between the perpendiculars LBP = 290 m, breadth b = 32 m, height h = 22.3 m, block coefficient C_b = 0.4835, and full load displacement $DISPL$ = 34,779.1 Mtons. Figure 6.1(a) shows the drawing developed with the software FREE!ship (2006). The strength of the midship section (145 m aft FP) reported in Figure 6.1(b) is investigated in this chapter. Figure 6.1(c) shows the three-dimensional FEM-model of a part of the ship that includes the midship section built in ABAQUS (Dassault Systèmes Simulia 2011). The focus of this chapter is the risk-informed routing of ships based on the quantification of the hull structural safety in terms of risk, and since the JHSS is at the preliminary stage of design and testing and detailed data regarding fuel consumption and wave resistance are not available, only direct losses are considered among other types of potential consequences and operational costs. Table 6.1 summarizes all the statistical descriptors of the random variables and the deterministic parameters necessary for the analysis.

6.6.1 ASSESSMENT OF FLEXURAL STRENGTH

The objective is to build a model that is representative of the flexural behavior of the midship section of the JHSS hull. Special attention is given to modeling in order to implement the response surface method and performing all the required FEM-simulations. The hull is modeled in order to ensure that the area of interest is not affected by any stress concentration or in general by effects that do not represent the actual structural behavior. For this reason, the area of interest is inserted within two regions modeled with a fictitious stiff material in order to eliminate these unwanted effects (Figure 6.1(c)). Moreover, the boundary conditions are moved away from the central area of interest and are applied to the two stiffed regions. Boundary conditions are applied at point A preventing x, y, and z translations and the rotation around the z-axis at one end of the truncated hull, and at point B preventing x and y translations (Figure 6.1(c)). The nodes at which the boundary conditions are applied are rigidly connected to the nodes belonging to the fictitious xy planes in order to obtain plane section movements at the extremities. The elements of this FEM-model are 4-node doubly curved thick shell with reduced integration, S4R (Dassault Systèmes Simulia 2011). A total of 18,216 shell elements and 19,528 nodes are generated for the model. Both material and geometric non-linearities are considered. The behavior of the steel is assumed elastic-perfectly plastic. Material and geometric properties are treated as random variables. The statistical descriptors of the steel elastic modulus E_s, steel yielding stress σ_{Ys}, and thickness multiplier c_{th} are summarized in Table 6.1. The randomness of the thicknesses within the section is assured by multiplying the

deterministic values provided by Devine (2009) with a single random thickness multiplier c_{th}. Different sets of FEM- incremental analyses by using a DELL Precision T7400 workstation are performed. Each FEM-simulation uses the parallel processing capabilities of the workstation and ABAQUS requiring less than 30 minutes to achieve convergence and reaching the section ultimate capacity. Two types of analysis are conducted.

The first type of analysis is represented by a set of FEM-simulations performed by inputting the mean values of the random variables in order to obtain mean moment-curvature relationships for vertical (hogging and sagging) and horizontal bending (Figure 6.2). Based on the obtained results, specific horizontal and vertical capacities are associated with each of the four limit states *LSi* previously introduced. For the hogging case, these capacities are represented by points A, B, C, and D of Figure 6.2, which discretize the moment-curvature relationships into the five states *Si*, previously introduced. Figure 6.3 shows the printouts of the results obtained with ABAQUS in terms of Von Mises mean stress contours in the case of hogging curvature. The images show the midship section stresses for limit states *LS*1 (Figure 6.3(a)), *LS*2 (Figure 6.3(b)), *LS*3 (Figure 6.3(c)), and *LS*4 (Figure 6.3(d)) which are associated to the flexural capacities corresponding to points A, B, C, and D of Figure 6.2. Figure 6.3 does not show the two stiff parts surrounding the midship portion because they only transfer stresses to the included flexible part and rigidly rotate around the active rotation axes. Moreover, as shown in Figure 6.4, incremental analyses considering different ratios between vertical and horizontal bending moments have been performed in order to obtain the contours associated with the four considered limit

states, which account for combined flexure effects. Each obtained pair of capacities is reported by circles in Figure 6.4. The flexural capacities indicated by points A, B, C, and D correspond to those of Figure 6.3. Finally, the parameters $c_{1,LSi}$ and $c_{2,LSi}$ of Equation (6.1) can be determined by regression analysis and using 0.973 as mean value of the parameter δ (Paik, Thayamballi and Che 1996).

The second type of analysis performed with the developed FEM-model includes the implementation of the RSM. The input and the output files of ABAQUS are managed by a developed MATLAB code in order to compute automatically all the required FEM-simulations. The randomness of the flexural capacity is given by the implementation of the three mentioned random variables (i.e. E_s, σ_{Ys}, and c_{th}). CCC design is used to generate 15 design points, being 15 the minimum number of point needed to fit a second order response surface. The points belonging to the cube of the CCC design are obtained by perturbing the random variables by one standard deviation around their means, one at a time (Ghosn, Moses and Frangopol 2010). According to CCC, the remaining design points belonging to the circumscribed sphere are perturbed proportionally to a value greater than one standard deviation, depending on the number of considered random variables. FEM-simulations are performed for each design point. The accuracy of the used approach has been verified by performing additional FE simulations, selecting the cube design points with perturbations of 0.5 (case 1), 1 (case 2), and 2 (case 3) standard deviations, and design points belonging to the circumscribed sphere with perturbations in accordance with CCC method for the ultimate VBM associated with hogging. An additional analysis (case 4) includes all the previous points of cases 1, 2, and 3. By performing a Monte Carlo simulation

(10,000 samples) the PDFs reported in Figure 6.5 are obtained. It can be noticed that only case 1 provides slightly different results with respect to the other cases, and the approximation in terms of mean value is lower than 1%, whereas in terms of standard deviation it is about 9%. This justifies the assumption of perturbation of one standard deviation for those design points belonging to the cube.

Then, by performing regression analysis, the polynomial coefficients α_0, α_i, α_{ij}, and α_{ii} of Equation (6.15) can be estimated. Sets of different polynomial coefficients α_0, α_i, α_{ij}, and α_{ii} of Equation (6.15) are evaluated for each analysis case by combining the following: vertical (sagging and hogging) and horizontal flexures, each limit state *LSi*, and different ship ages (i.e. accounting for the effects induced by corrosion at time t in years), such as t = 0 years, t = 10 years, t = 20 years, and t = 30 years. In order to account for the effects induced by corrosion, RSM-FE analyses are repeated at 10 year increments until the assumed ship service life of 30 years is reached by changing the ABAQUS inputs associated with the thicknesses of plates and stiffeners. are those specified in Table 6.1, depending on the position of the stiffened plates within the hull.

6.6.2 LOAD EFFECTS

Since data regarding the loading of this ship are not available, the load effects induced by still water for both hogging and sagging are evaluated in accordance with Hussein and Guedes Soares (2009). The calculated statistical descriptors of the VBMs for hogging are reported in Table 6.1.

On the other hand, the wave-induced load effects are evaluated based on with linear strip theory (Korvin-Kroukowski and Jacobs 1957). Although the use of a linear

approach could lead to overestimating the actual loads, its use is common practice (Ayyub, Assakkaf and Atua 2000). However, load effects calculated with more accurate non-linear methods can be accommodated in the proposed framework. By using the freeware program PDSTRIP (2006) developed in FORTRAN language, and by managing its input and output files by using the software MATLAB (The MathWorks 2011), RAO curves are determined for the hull midship section, for both VBM and HBM, with respect to all the considered combinations of ship speeds and heading angles. It is assumed that the ship speeds range from 0 m/s to 20 m/s (about 40 knots) by intervals of 2 m/s, whereas the heading angles range from 0º to 360º by intervals of 2º. This dense discretization is necessary in order to later perform optimization of ship routing. The structural responses in term of VBM and HBM for natural sea are evaluated based on the obtained RAOs and by selecting different sea spectra associated with specific significant wave heights *Hs* (representing different sea states). Several responses due to different sea states are investigated in this chapter. Table 6.2 summarizes all the parameters of the Pierson-Moskowitz Sea Spectrum (Resolute Weather 2011) used in this analysis. Based on the Rayleigh distribution of Equation (6.17), the statistical descriptors of all the obtained responses can be evaluated. Due to the use of linear theory, the responses are the same for both sagging and hogging (Hughes 1983). Since polar representations enable to directly visualize the effects on ship structural performance by varying operational condition parameters, the load effects in terms of mode of VMB and HBM are visualized by varying the heading *H* and for different fixed ship speeds *U* and significant wave heights *Hs*. The load profiles refer to angles ranging between 0º (following sea FS)

and 180º (head sea HS). Since the load profiles are symmetric with respect to these angles and between 180º and 360º, the polar plots are divided into two sides reporting on both VBM (right side) and HBM (left side). 90º indicate beam sea BS. Figure 6.6(a) shows the polar representation of the modes of VBM and HBM for sea state 5 (*Hs* = 2.74 m) and considering different ship speeds (0 m/s, 10 m/s, and 20 m/s). As the ship speed increases, VBM and HBM are in general increasing for head sea, whereas for following sea, higher responses are found for lower speeds. Both VBM and HBM are low for beam sea. It can be noticed that the maximum values of the HBM is about one third of the VBMs, and occur at different angles (180º for VBM and about 110º for HBM). Figure 6.6(b) reports on the variation of the modes of VBM and HBM at a fixed ship speed of 10 m/s and for sea states 4, 5, and 6 (*SE* = 1.83 m, *SE* = 2.74 m, and *Hs* = 4.88 m). The modes of both VBM and HBM increase when the sea state becomes more severe for every heading angle. Again, the responses are low for beam sea and generally for following sea. In order to better represent some small values shown in the polar plots of Figure 6.6(a,b), the associated Cartesian plots are shown in Figure 6.6(c,d). A detailed explanation on the assessment of these load effects by using this approach can be found in Chapter 5. The dynamic load effects are also included in this analysis by means of whipping bending moment evaluated in accordance with Equation (6.18).

6.6.3 RISK ASSESSMENT

In order to perform risk assessment, the probabilities associated with reaching the defined four limit states (*LS*1 to *LS*4) of Equation (6.3) are evaluated. The used

parameters are listed in Table 6.1. The software RELSYS (Estes and Frangopol 1998) is used to perform reliability analysis. Using polar representation, Figure 6.7(a) shows the reliability indices associated with the four limit states for intact ship (t = 0 years) and for aged ship (t = 30 years), which are represented at the right and left sides, respectively, for sea state 5 (Hs = 2.74 m) and ship speed of 10 m/s. Obviously, the reliability associated with the first yielding ($LS1$) is lower than the reliability with respect to the ship ultimate capacity ($LS4$) for all the considered operational conditions. Figure 6.7(b) reports on the reliability associated with $LS4$ for intact (right side, t = 0) and aged (left side, t = 0) ship at a fixed speed of 10 m/s and for sea states 4, 5, and 6. Since it is found that the effects induced by hogging are more severe than those induced by sagging, only hogging is considered. The Cartesian plots associated with the polar representations of Figure 6.7(a,b) are shown in Figure 6.7(c,d), respectively.

Once the probabilities defined in Equation (6.4) are evaluated, the probabilities of intact ship being in states $S1$ to $S5$ are obtained by using Equation (6.6). These sets of probabilities are represented in Figure 6.8 which shows their variation with respect to ship speed given Hs = 2.74 m and H = 180º (Figure 6.8(a)), and fixing ship speed to 10 m/s and H = 180º (Figure 6.8(b)). Figure 6.8 reports on the so-called "fragility analysis", usually developed for seismic loss analysis performed on buildings and bridges. The increment of P_{LSi} is much more sensitive to the increase of sea elevation than to the increase of ship speed.

The direct costs are evaluated according to Equations (6.8)–(6.11) using the following ship parameters: WGT_{100} is based on the normalized weights (SWBS 100)

of 463.20 kN/m, 256.03 kN/m, and 290.07 kN/m for hull normalized portions of 0.4 (around midship), 0.3 (fore quarter point), and 0.3 (aft quarter point), respectively (Devine 2009) and assuming ship type factor and damage ratios associated with the states $S1$, $S2$, $S3$, $S4$, and $S5$ in accordance with Table 6.1. Rehabilitation costs $C_{Reh,Si}$ (see Equation (6.11)), used for the evaluation of direct risk associated with the states $S1$ to $S4$, are evaluated based on construction costs C_{Con} referring to an assumed plastification propagation of 40% of the length of the hull around its midship section, whereas C_{Con} associated with the states $S5$ (failure) refers to the entire ship.

Finally, risk is assessed for each state Si and for all the considered operational conditions. Figure 6.9(a) shows the direct risk profiles given ship speed of 10 m/s and Hs = 2.74 m. It can be noticed that the obtained risk profiles cross each other depending on both the probabilities P_{Si} and the evaluated magnitude of direct costs. Direct risk for $S1$ is null, given that the relevant damage ratio is assumed equal to 0 and, therefore it is not reported in Figure 6.9(a). The profile of the total direct risk provided by Equation (6.14) is shown in Figure 6.9(b).

6.6.4 ROUTE OPTIMIZATION

In order to provide an application on risk-informed optimal routing of ships, assumptions have to be made, such as the origin and destination of the route, and the sea weather map for the studied area. Figure 6.10 shows the assumed sea weather map, including a qualitative path, where the x- and y-axis ranges are assumed to be 1000 km, and O ≡ (1000 km, 200 km) and D ≡ (0 km, 400 km) indicate the points of origin and destination, respectively. In the map, the shadings show the intensity of the sea

expressed in terms of significant wave height, and ranging from 1.07 and 6.10, equivalent to lower sea state 3 and upper sea state 6, respectively, and the arrows report on the direction of propagation of the waves, given the weather system. Two areas of disturbance represented by two potential storms are included in the graphical representation. The map covers a short distance, therefore the weather forecast is assumed to be accurate and not affected by uncertainty. According to the optimization problem previously formulated (see Equations (6.19)–(6.23)), the x-axis has been divided in 15 segments ($N = 15$), representing the discretization of a potential journey. Based on this discretization, optimal sets composed by 15 ship speeds U_i and 14 coordinates y_i are evaluated (see Equations (6.19) and (6.20)). These design variables are subjected to the constraints of Equations (6.22) and (6.23), assuming that the relevant ranges are 4 m/s $\leq U_i \leq$ 20 m/s and 0 km $\leq y_i \leq$ 1000 km.

Based on these assumptions, for each step of the optimization, direct risk and reliability can be obtained for each discretization point, given specific sea elevation, ship speed, and heading angle. Multidimensional matrices with a dense discretization containing the above mentioned information have been prepared before starting the optimization process, in order to quickly achieve the Pareto front. Intermediate values required by the optimization algorithm are found by linear interpolation. The developed code works with integer design variables. The population size used is 500 and the number of generations is 100. Since the solution connecting the points O and D with the ship traveling at the maximum speed (20 m/s) is known to be optimal (based on geometry), a proper set of U_i and y_i is forced inside the initial population, in order to achieve a faster convergence to the Pareto front. To solve this optimization

problem, 80% of new generation individuals are obtained by the "two point" crossover function, and for the residual 20% the "Gaussian" mutation function is applied. In this way, the optimization process takes about 30 minutes. Further details on this GA algorithm can be found in the MATLAB user manual (The MathWorks 2011).

Figure 6.11 shows the Pareto-optimal set for the case of intact ship (t = 0 years). The two objectives are the estimated time of arrival *ETA* (h) and the normalized direct risk R_D (USD/km) over the length of the shortest followed path. These are conflicting objectives, because depending on the given weather map, the fastest and shortest solution (point A of the Pareto front) is associated with a high level of risk. Decision makers can adjust path and speed depending on the allowable risk. Three Pareto solutions are selected among the others and are denominated A, B, and C. (Figure 6.11). Figure 6.12(a) shows the paths associated with the three selected solutions. It is noticed that all the three paths share some common segments, especially while traveling in the central part of the journey. These solutions are associated with the values of the objectives as provided in Figure 6.11. Path C covers the longest distance, avoiding the represented storm 1 heading south, whereas path B heads north. The shortest path A directly crosses the storm. Figure 6.12(b,c,d) show the ship speed (first group of design variables as for Equation (6.19)), the reliability index associated with ultimate failure, and the normalized direct risk (second objective in Equation (6.21)), respectively, for each of the 15 segments dividing the map. The paths A and B are covered at the maximum speed of 20 m/s along the entire trip, leading to an important reduction of ETA to the detriment of mission reliability (Figure 6.12(c)), which reduces significantly whenever severe sea state is encountered. The ETA of path C is

larger due to the overall reduced traveling speed (Figure 6.12(b)) and to the longer traveled distance. Although only three solutions are shown for sake of clarity, other Pareto solutions are available to decision makers.

Figure 6.13 shows the comparison for the intact ship case and the aged ship case (t = 30 years). In Figure 6.13(a), two Pareto fronts are shown. By setting the same *ETA*, the aged ship experiences higher risk than the intact ship. Besides, at a fixed level of risk, the *ETA* is lower in the case of intact ship. Figure 6.13(b,c) shows on the mission reliability associated with the ultimate failure and the normalized direct risk, respectively, for the two selected solutions A and A' highlighted in Figure 6.13(a). It is clear that for the case of the aged ship, reliability is lower (approaching critical values for stormy conditions) and mission risk is almost 50% higher than that of the intact case.

6.7 CONCLUSIONS

This chapter, which is mostly based on Decò and Frangopol (2013b), uses risk as a performance indicator accounting for the consequences induced by different limit states, with the purpose of evaluating the optimal routing of ships. Direct risk assessment of ships can be performed with respect to discrete hull damage states and for a large spectrum of operational conditions. Mission parameters such as ship speed and heading angle, structural safety, ETA, and traveled distance are properly assessed for the case of the Joint High-Speed Sealift, hypothetically traveling between two points for an assumed sea weather map. Optimization has been conducted for both the

case in which the ship is intact and when the effects due to corrosion induce deterioration of the structural performance leading to higher direct risk.

The following conclusions are obtained:

1. It has been shown that the Response Surface Method can be efficiently applied for the estimation of the probabilistic flexural strength of ship structures in association with Finite Element modeling.
2. Direct risk of ships can be assessed considering different ship limit states and with respect to several operational conditions. It is found that direct risk profiles associated with specific states can cross each other depending on the magnitudes of the probabilities of the hull being in specific states and direct costs. Overall, greater direct risk is associated with head sea.
3. The inclusion of negative consequences in decision analysis is of paramount importance. Different travel paths can be followed by ships, thus minimizing the effects of such consequences. A future challenge is represented by the development of rules and specifications that address this aspect in order to adequately warn decision makers on ship reliability.
4. The results obtained from the optimization show that several solutions can be adopted depending on the acceptable risk and on the allowable ETA. All the solutions, except for the shortest and fastest one, provide directions that avoid the assumed storm in order to reduce direct risk.
5. Ship aging considerations are included into reliability analysis, risk analysis, and routing optimization, proving that decisions made in the case of managing aged ships lead to higher risk and can be different than those made for intact ships.

Different Pareto-optimal sets are obtained for two cases, highlighting the importance of this aspect in the decision making process.

Although it is known that other factors, such as traveling comfort and fuel consumption may play a role within this optimization problem, the importance of risk-informed decision making is highlighted in this chapter. The inclusion of other factors may be a future development of the proposed approach discussed herein.

Table 6.1 Statistical descriptors of the random variables and deterministic parameters used for the analysis.

Random variable	Mean	COV	Distribution type	Reference
Parameter x_R	1.0	0.10	Normal	Paik and Frieze (2001)
Parameter x_{sw}	1.0	0.05	Normal	Paik and Frieze (2001)
Parameter x_w	0.9	0.15	Normal	Paik and Frieze (2001)
Parameter δ	0.973	0.10	Normal	Paik, Thayamballi and Che (1996)
Steel elastic modulus E_s (MPa)	210,000	0.03	Log-normal	Paik and Frieze (2001)
Steel yielding stress σ_{Ys} (MPa)	351.6	0.10	Normal	Paik and Frieze (2001)
Stillwater VBM for hogging (Nm)	2.008×10^9	0.29	Normal	Evaluated
Thickness multiplier c_{th}	1.0	0.05	Normal	Paik and Frieze (2001)
Wave-induced HBM $M_{wh,Hs,U,H}$ (Nm)	Varies	Varies	Rayleigh	Evaluated
Wave-induced VBM $M_{wv,Hs,U,H}$ (Nm)	Varies	Varies	Rayleigh	Evaluated
Deterministic parameter	**Value**			**Reference**
Annual corrosion rate C_1 for bottom shell plating (mm/year)	0.30			Akpan *et al.* (2002)
Annual corrosion rate C_1 for bottom stiffener web (mm/year)	0.10			Akpan *et al.* (2002)
Annual corrosion rate C_1 for deck plating (mm/year)	0.10			Akpan *et al.* (2002)
Annual corrosion rate C_1 for deck stiffener web (mm/year)	0.10			Akpan *et al.* (2002)
Annual corrosion rate C_1 for side shell plating (mm/year)	0.03			Akpan *et al.* (2002)
Annual corrosion rate C_1 for side stiffener web (mm/year)	0.03			Akpan *et al.* (2002)
Coefficients [$c_{1,LS1}$, $c_{2,LS1}$] for hogging	[1.00, 1.00]			Evaluated
Coefficients [$c_{1,LS2}$, $c_{2,LS2}$] for hogging	[175, 1.31]			Evaluated
Coefficients [$c_{1,LS3}$, $c_{2,LS3}$] for hogging	[1.63, 1.23]			Evaluated
Coefficients [$c_{1,LS4}$, $c_{2,LS4}$] for hogging	[2.14, 1.02]			Evaluated
Constant C_2	1			Akpan *et al.* (2002)
Correlation factor k_D for hogging	0.685			Mansour *et al.* (1984)
Correlation factor k_W	1			Mansour *et al.* (1984)
Corrosion initiation time t_0 (years)	5			Akpan *et al.* (2002)
Damage ratios $d_{r,Si}$ for [$S1$, $S2$, $S3$, $S4$, $S5$]	[0, 0.10, 0.35, 0.75, 1]			Assumed
Ship type factor *STF*	7			Miroyannis (2006)
Whipping bending moment M_{WH} (Nm)	1.573×10^8			Evaluated

Table 6.2 Considered probabilistic descriptors of the Pierson-Moskowitz sea spectrum (Resolute Weather 2011).

Sea state	Significant wave height (m)	Average wave period (s)
1	0.30	2.0
2	0.46	2.5
2.5	0.76	3.0
3	1.07	3.5
3.5	1.37	4.0
4	1.83	5.0
4	2.29	5.5
5	2.74	6.0
5	3.66	7.0
6	4.88	8.0
6	6.10	9.0
7	9.14	11.0
7	12.19	12.5
8	15.24	14.0
8	18.29	15.0
9	24.38	17.5

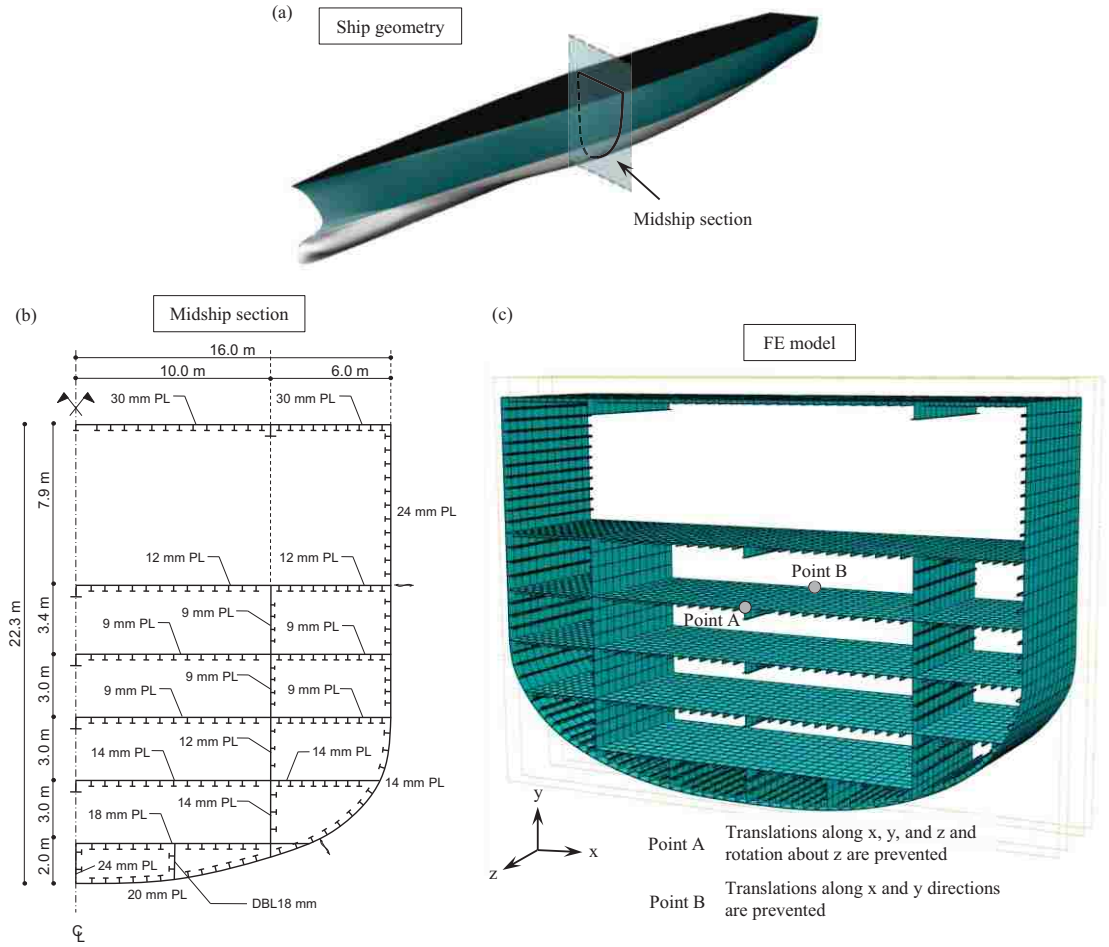

Figure 6.1 (a) Model of the analyzed JHSS built by the software FREE!ship (2006), (b) geometry of the midship section (145 m aft FP), and (c) FEM-model of the part of the hull that includes the midship section built with ABAQUS (Dassault Systèmes Simulia 2011).

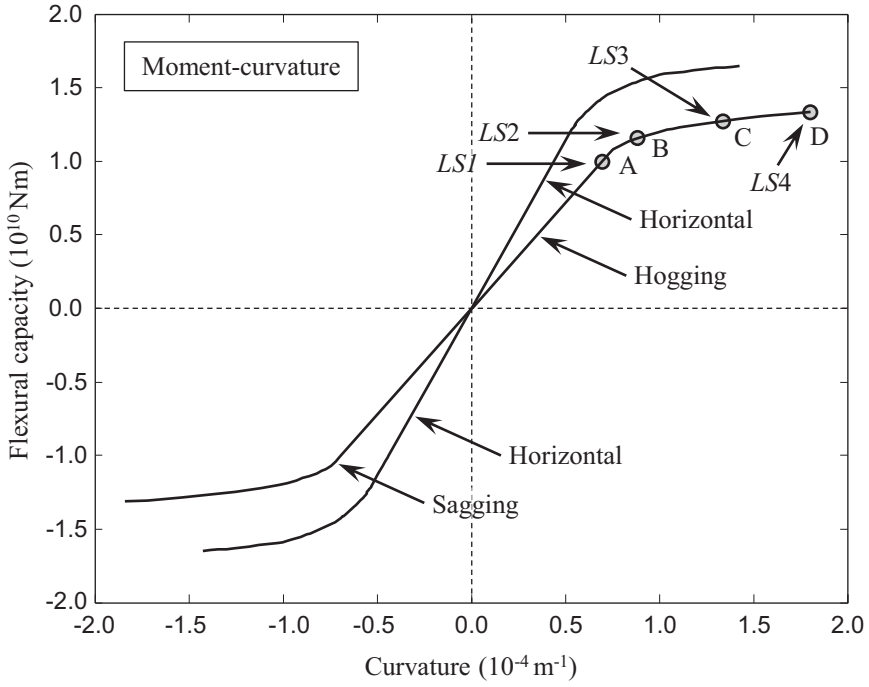

Figure 6.2 Mean moment-curvature relationships for vertical (hogging and sagging) and horizontal flexures. Points A, B, C, and D indicate the capacities associated with the discretization of the limit states *LSi*.

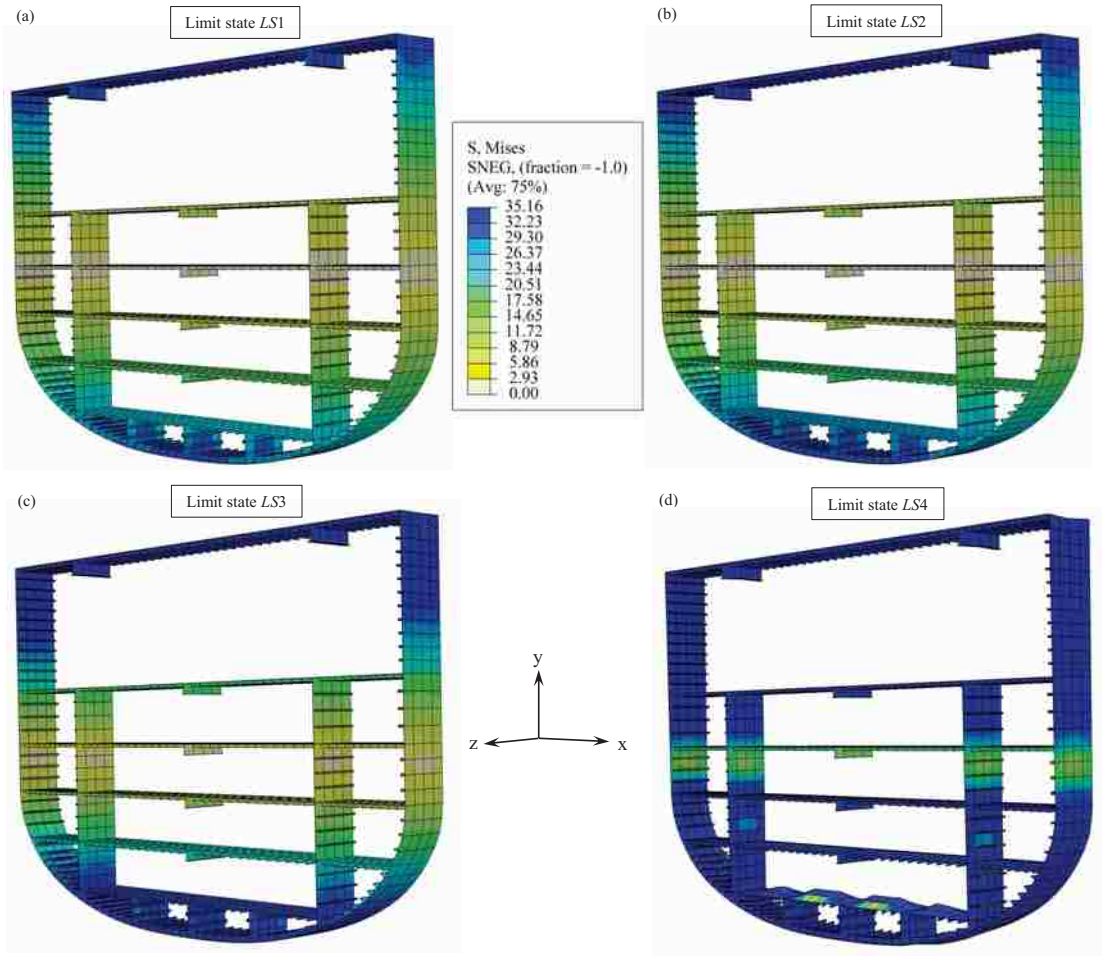

Figure 6.3 Von Mises mean stress contours of the hull midship section for the four considered limit states *LSi*.

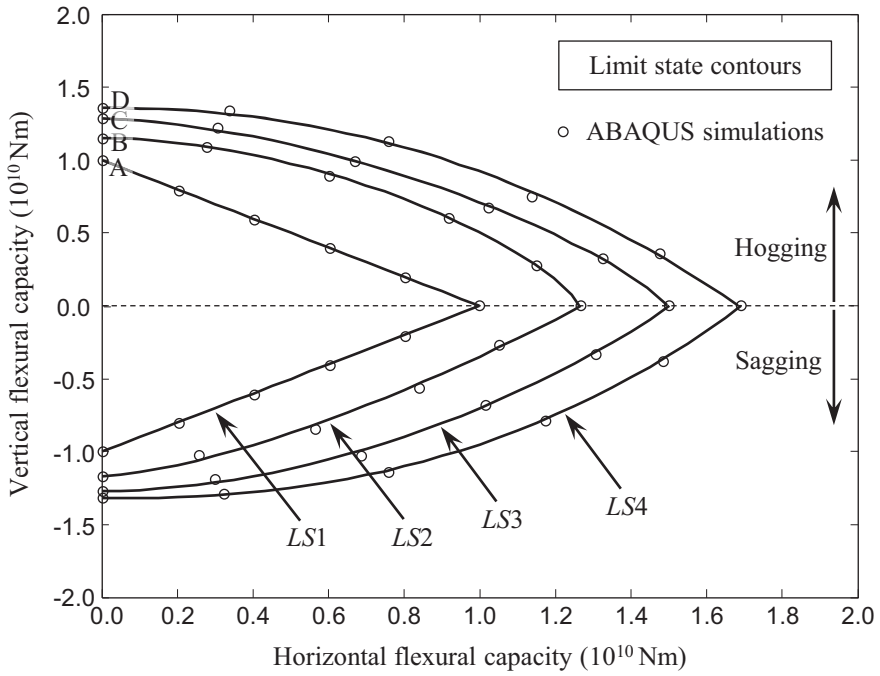

Figure 6.4 Mean contours accounting for the combined effects of vertical (hogging and sagging) and horizontal bending moments, and associated to different limit states *LSi*.

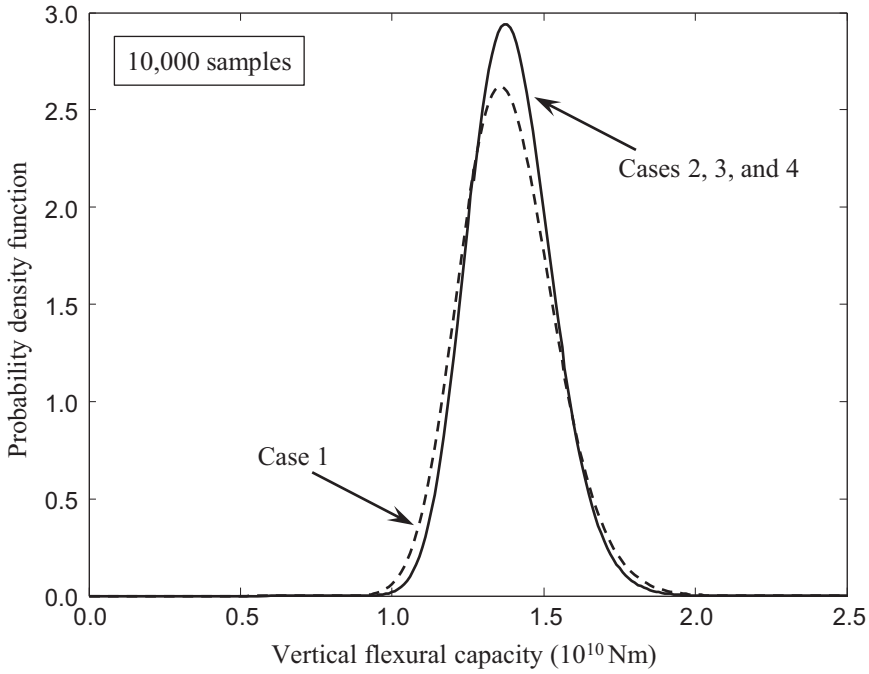

Figure 6.5 PDFs of the ultimate flexural capacity associated with hogging for the analysis cases 1, 2, 3, and 4.

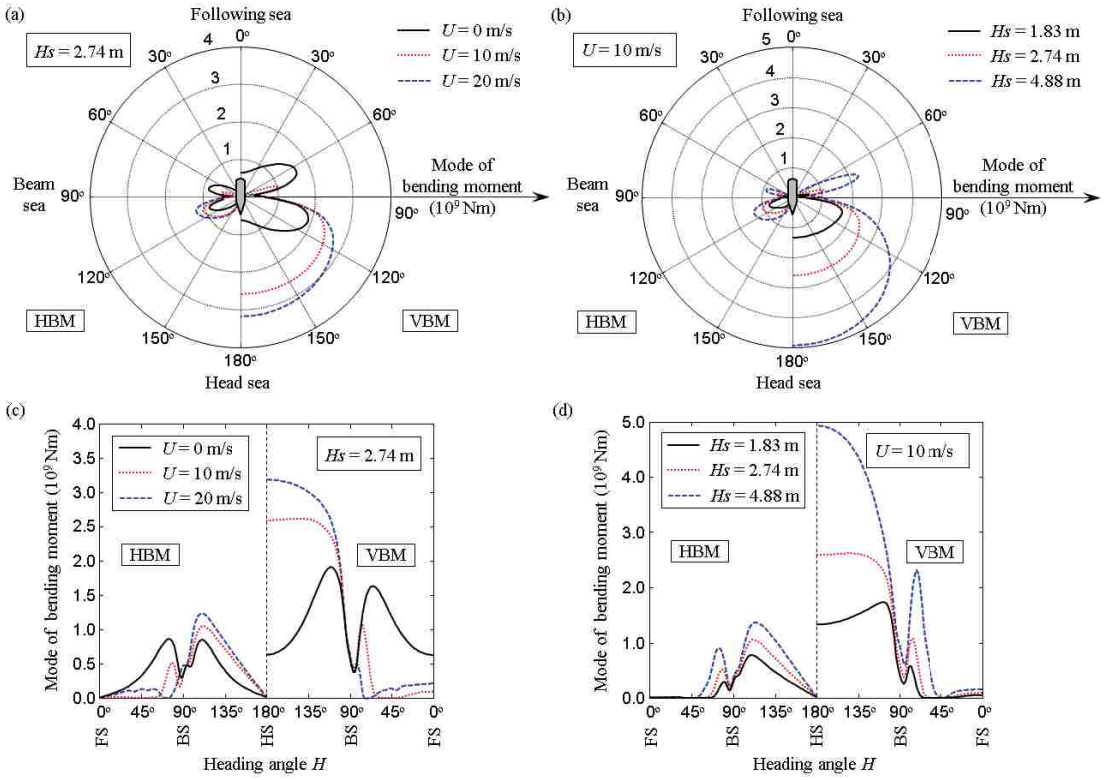

Figure 6.6 (a) Polar profiles of the modes of VBM (right side) and HBM (left side) for *Hs* = 2.74 m by varying ship speed, and (b) polar profiles of the modes of VBM (right side) and HBM (left side) for ship speed of 10 m/s by varying significant wave height. Associated Cartesian plots of the modes of VBM and HBM (c) varying ship speed and (d) sea elevation.

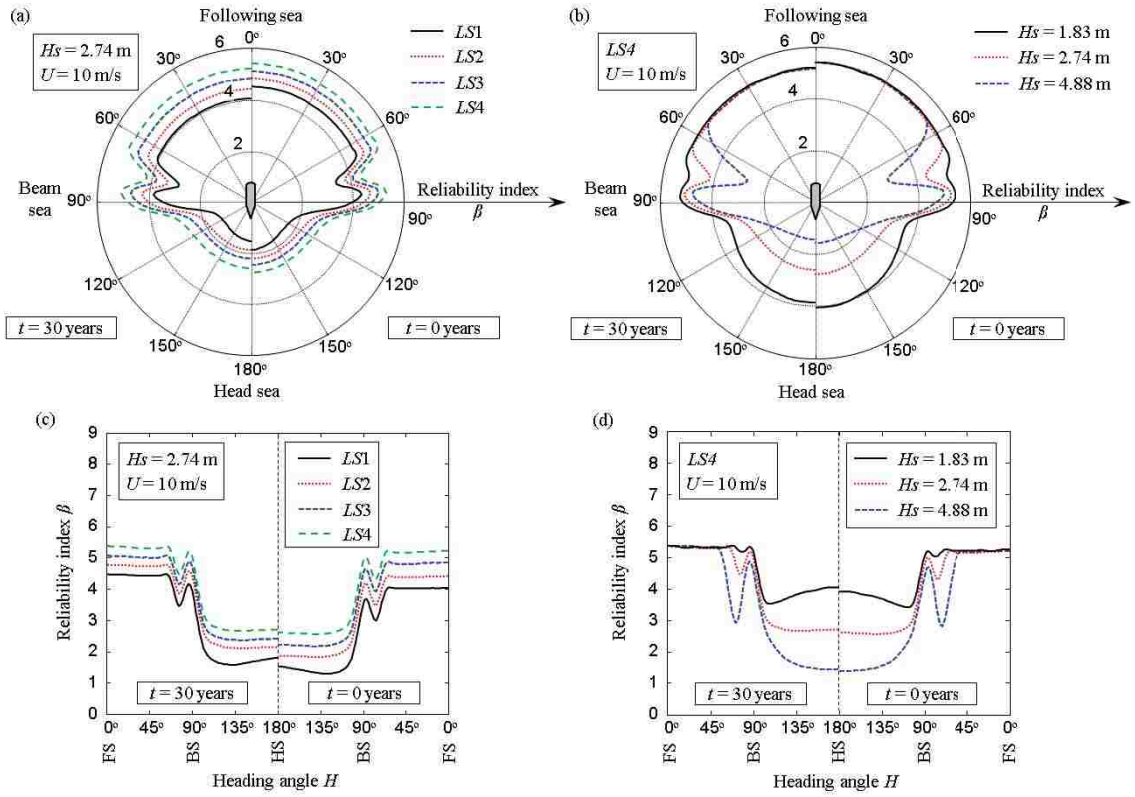

Figure 6.7 Polar profiles of the reliability indices for intact (right side, t = 0 years) and aged (left side, t = 30 years) ship with respect to (a) four limit states given Hs = 2.74 m and ship speed of 10 m/s, and (b) ultimate capacity ($LS4$) for ship speed of 10 m/s by varying significant wave height. Associated Cartesian plots of the reliability indices for intact and aged ship with respect to (c) four limit states and (d) ultimate capacity varying sea elevation.

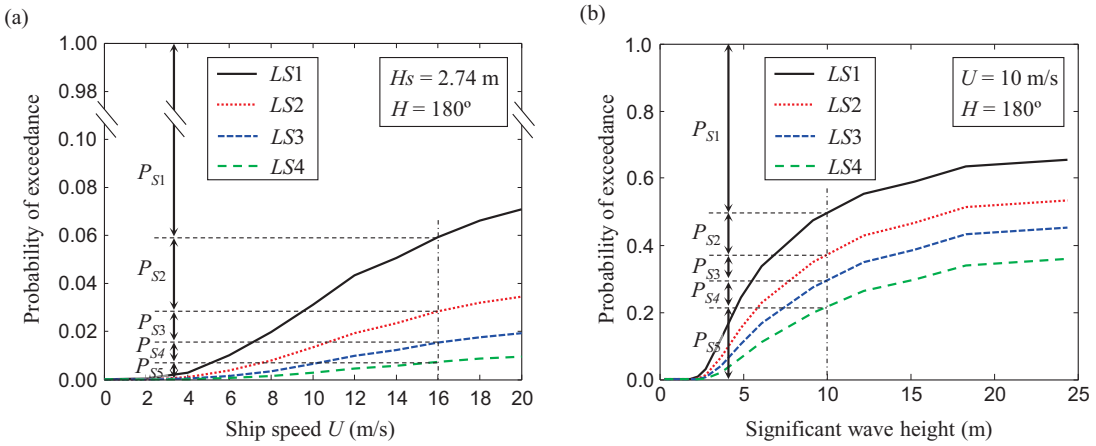

Figure 6.8 Profiles of the probabilities of exceeding the limit states *LSi* for intact ship when (a) ship speed is varying given *Hs* = 2.74 m and *H* = 180º, and (b) significant wave height is varying given ship speed of 10 m/s and *H* = 180º.

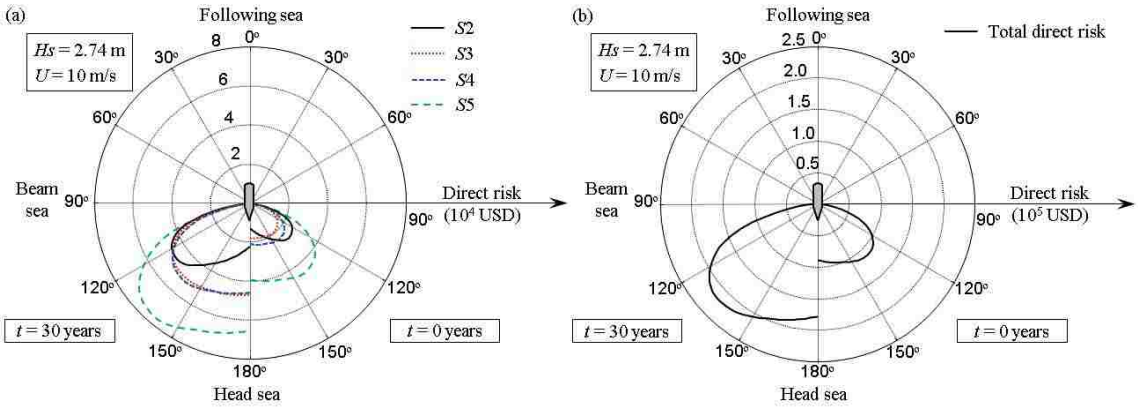

Figure 6.9 Polar profiles of the direct risk for intact (right side, t = 0 years) and aged (left side, t = 30 years) ship with respect to (a) four states given Hs = 2.74 m and ship speed of 10 m/s and (b) ultimate capacity ($LS4$) for ship speed of 10 m/s by varying significant wave height.

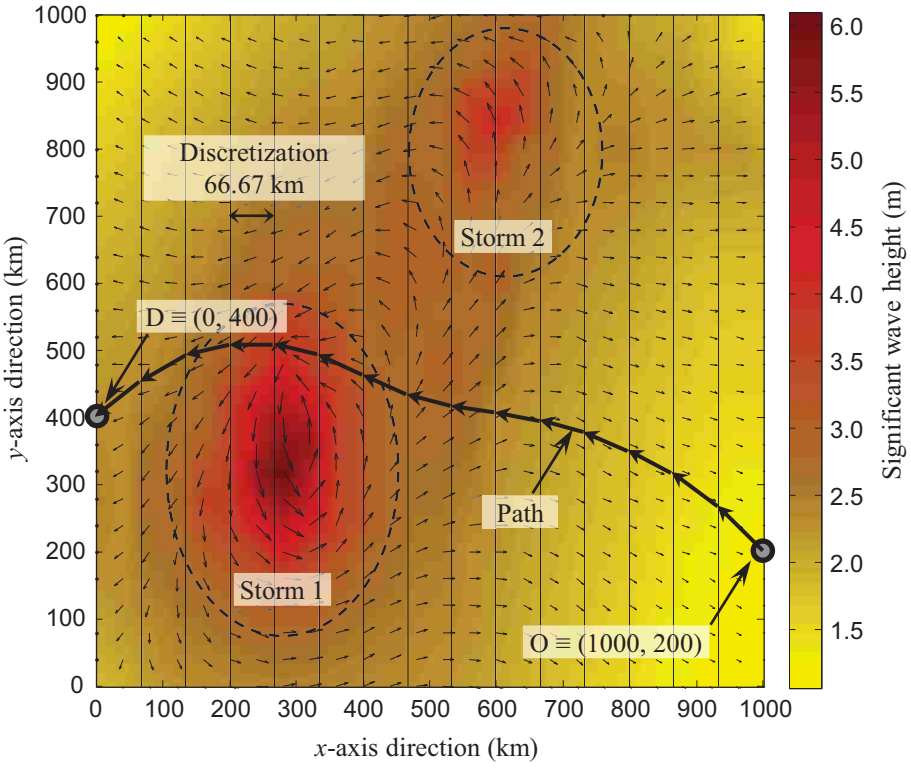

Figure 6.10 Assumed discretized sea weather map of the considered squared area with edges of 1000 km, in which the colors report on the significant wave height, and the thin arrows show the direction of propagation of the waves. The thick arrows represent a potential path connecting the origin point O and the destination point D.

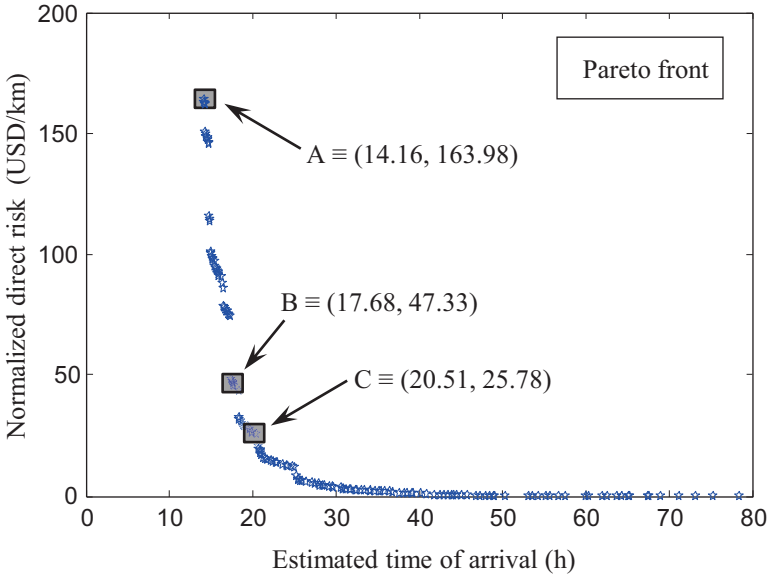

Figure 6.11 Pareto front of the optimization problem obtained by minimizing both estimated time of arrival and normalized direct risk. Three representative solutions denominated A, B, and C are selected in order to evaluate the relevant mission parameters.

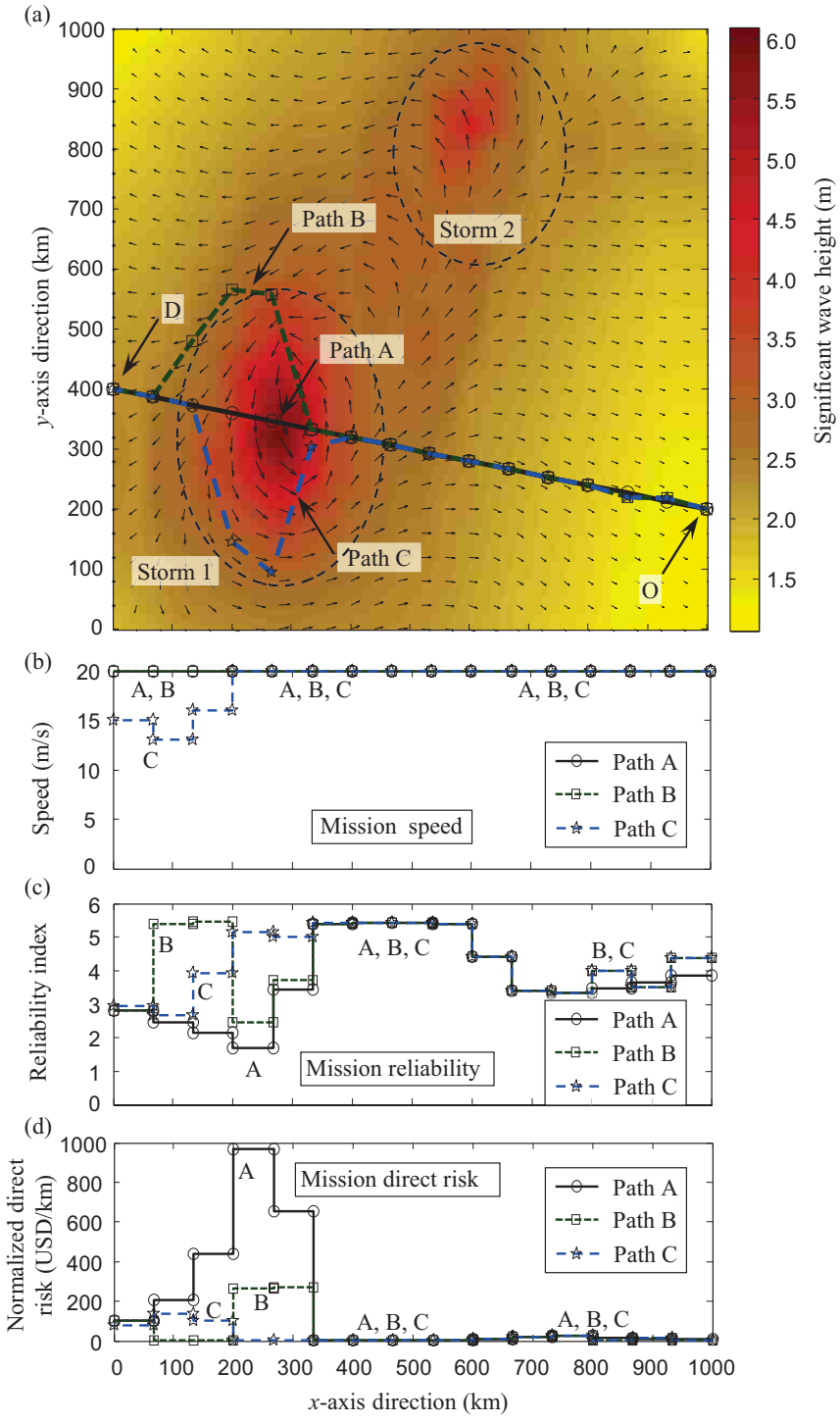

Figure 6.12 (a) Paths of the three selected solutions A, B, and C represented in the assumed sea weather map (Figure 6.10). Profiles of (a) ship speed, (b) mission reliability index associated with ultimate failure, and (c) normalized direct risk for each of the three solutions.

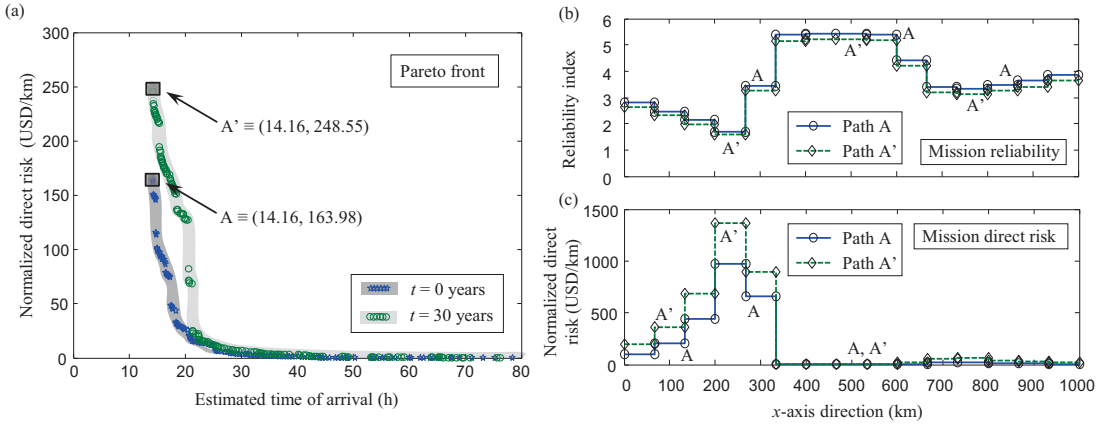

Figure 6.13 Comparison between the case with intact ship (t = 0 years) and the case with aged ship (t = 30 years) in terms of (a) Pareto front, (b) mission reliability associated with ultimate failure, and (c) normalized direct risk for the two selected solutions A and A'.

CHAPTER 7

NEAR REAL-TIME MULTI-CRITERIA OPTIMAL SHIP ROUTING INTEGRATING RISK AND STRUCTURAL HEALTH MONITORING

7.1 INTRODUCTION

The optimal planning of ship routes is a topic that is always current within the research activity, especially nowadays, due to the continuous increase in fuel price. Although operational costs are rising, special attention is also given to the ship structural safety, therefore accounting for the safety of the passengers, crew members, and transported goods, and for the reliability of the provided services. Moreover, both commercial vessels and naval ships must reach their destinations within their allotted time frames. Hence, decision makers are mainly required to reduce fuel cost, maximize ship safety, and minimize the mission/delivery time schedule. In order to achieve these goals, trade-offs among these conflicting objectives must be taken. In this context, besides the initial planned route and initial ship structural performance assessment, the availability of further information during the ship trip becomes a key aspect to consider. For instance, information form structural health monitoring (SHM) systems can improve the evaluation of the structural performance while the ship is traveling. Besides, the continuous weather prediction would make the adjustment of the planned

route possible. This further collected information brings the initial planning process to near real-time decision process, necessary in order to better achieve all the above mentioned objectives.

The explicit novelty of this chapter, which is mostly based on Decò and Frangopol (2013c), is the development of a near real-time approach for decision making, in which the initial prediction obtained in Chapter 6 is updated based on the available new information. Bayesian statistics has been used for this purpose. Both a closed-form solution and a simulation-based technique are used in this chapter based on the assumption that the peak responses follow the Rayleigh distribution (Faltinsen 1990). SHM is considered a very powerful tool to be used for the collection of accurate information about the actual loads that the ships are encountering during their operations. The SHM data used in this chapter are obtained from a scaled model of the JHSS tested in the summer of 2007 in the Naval Surface Warfare Center, Carderock Division - Maneuvering and Sea Keeping (NSWC CD - MASK) basin. The observations in terms of vertical and horizontal bending moments (VBM and HBM, respectively) are then scaled up to the ship full dimensions by using the Froude-scaling factor of 47.2533 (Devine 2009).

Lastly, the risk-informed optimal routing is considered. Another novelty introduced in this chapter is the integration of the information obtained by SHM and weather prediction into the optimization problem with objectives being the minimization of the estimated time of arrival (ETA), minimization of mean total risk, and minimization of the fuel cost. The cases, in which the use of the original and updated (by using SHM data) performance prediction are considered, are investigated

in order to provide insights in whether to use SHM under specific ship operational conditions. The optimal solutions are grouped into Pareto-optimal sets that balance the conflicting objectives.

This chapter develops an approach for the near real-time multi-criteria optimal ship routing integrating risk and structural health monitoring. Section 7.2 describes the developed approach for the quantification of reliability, cost, and risk. Section 7.3 discusses the concepts developed for integrating SHM data and weather prediction into the near real-time performance assessment. Section 7.4 introduces the developed approach for the multi-criteria optimal routing of ships based on time, risk, and fuel cost. As reported in Section 7.5, the implementation of the proposed risk-informed approach is applied to the Joint High Speed Sealift (JHSS), traveling between two points for an assumed sea weather map. Finally, Section 7.6 provides the conclusions of this chapter that is based on a published paper (Decò, Frangopol and Zhu 2012) and on a paper submitted for possible publication (Decò and Frangopol 2013b, Decò and Frangopol 2013c).

7.2 RELIABILITY, COST, AND RISK

Risk can be seen as a performance indicator that includes both the assessment of structural vulnerability and the quantification of consequences induced by potential structural malfunction/failure. Management tools and decision making processes are risk-informed when the quantification of the consequences is part of the developed decision framework. Ships are subjected to numerous types of hazard that may directly or indirectly affect their safety and serviceability. For instance, these hazards could be

(Ayyub *et al.* 2002, Skjong & Bitner-Gregersen 2002) fire, explosion, environmental attack, collision, iceberg impact, grounding, loss of hull integrity, propulsion and steering failures, extreme wave loads, flooding, and capsizing. The above mentioned hazards cause events that can be categorized as "normal" and "extreme" situations, depending on their intensity and frequency of occurrence.

In this chapter, ship vulnerability is assessed with respect to wave-induced loads under normal ship operational conditions and severe encountered sea, in accordance with the method proposed in Chapter 6. The main effects induced on the ship hull are vertical and horizontal bending moments (VBM and HBM, respectively) (Paik, Thayamballi and Che 1996, Gordo and Guedes Soares 1997). In order to perform risk assessment, it is worth investigating different effects on the ship hull by considering multiple and progressive levels of danger (as developed in Chapter 6). Accordingly, the hull strength is discretized into five states ($S1$ to $S5$), accounting for different levels of section plastification characterized by four limit states LSi as follows:

- *Limit state* $LS1$: some stiffened plates at the hull extremities reach the yielding stress, therefore they are likely to plastify.
- *Limit state* $LS2$: it is assumed that the plastification propagates to nearby components up to 20% of the largest distance between the neutral axis and the extreme plates that may experience local buckling.
- *Limit state* $LS3$: it is assumed that the plastification propagates through the hull section, reaching 50% of the largest distance to the neutral.

- *Limit state LS*4: the plastification propagates throughout the whole section, and the hull ultimate flexural capacity is reached.

In this chapter, FE method is integrated with response surface analysis in order to reduce the computational time to feasible levels while still being able to account for uncertainties (Bucher and Bourgund 1990). According to Gordo and Guedes Soares (1997), the interaction domains associated with the plastification propagation, accounting for the combined effects of VBM and HBM, are obtained by FE simulations. The effects of corrosion, which is a time process, are included in the methodology according to the approach proposed by (Akpan *et al.* 2002). The framework for the evaluation of the hull flexural capacity is presented in the Module (2) of Appendix B.

The load effects are evaluated in accordance to the method used in Chapter 5. Therefore, for the evaluation of the load effects associated with stillwater VBM, the approach proposed by Hussein and Guedes Soares (2009) is used. For the evaluation of the wave-induced VBM and HBM, short term statistics are considered. Based on linear theory, the hull responses induced by waves are evaluated by the strip method (Korvin-Kroukowski and Jacobs 1957). Therefore, according to Hughes (1983), the probability density function (PDF) of the peak responses associated with different operational conditions follows the Rayleigh as expressed in Equation (6.17) of Chapter 6. Moreover, the further contribution due to the dynamic bending moment M_{WH} is evaluated according to Sikora and Brady (1989) (Equation (6.18) of Chapter 6). The procedure for the estimation of the load effects is summarized in the Module (1) of Appendix B.

Once the hull strength and the acting load effects are carried out, the probability of a ship hull to exceed the limit states *LSi* are evaluated based on a performance function $G_{LSi,SE,U,H}(t)$ that accounts for damage/failure domains, as proposed in Equation (6.3) of Chapter 6.

There are many types of costs/losses that are involved in ship management. Two types of costs are considered herein, i.e. monetary consequences in terms of losses and operational costs. Both types of costs are included in the proposed approach for ship optimal routing. Monetary consequences induced by potential structural failure or malfunction of marine structures include direct and indirect losses. Direct consequences are directly related to the extension of structural damage, while indirect consequences may include (IMO 1997, Ayyub *et al.* 2002, Skjong 2002) damage to equipment, goods, and port facilities, commercial and environmental impacts, marginal operational costs, fatalities and injuries of crew and passengers, among others.

Direct costs include construction costs C_{Con} (Miroyannis 2006), based on empirical cost estimation relationships, and rehabilitation costs $C_{Reh,Si}$. These costs, that include material and labor, are computed as follows

$$C_{Con} = 5747.19 \times STF \times DISP^{-0.3792} \times WGT_{100}{}^{0.862} + 800 \times WGT_{100} \tag{7.1}$$

$$C_{Reh,Si} = d_{r,Si} C_{Con} \tag{7.2}$$

where WGT_{100} is the weight of the "Ship Work Breakdown System (SWBS) - category 100" (long tons), *STF* is the ship type factor, *DISP* is the ship full load displacement (long tons), and $d_{r,Si}$ is the damage ratio.

Among indirect ones, the costs associated with loss of human lives and injuries are accounted for within the proposed approach. F-N curves are a common tool for the evaluation of the frequency of fatal accidents and the number of involved fatalities. Skjong (2002) developed F-N curves for different types of ships including several kinds of accidents, but without investigating the cause of the fatalities. The only considered cause for fatalities and injuries is the structural damage/failure of the ship hull. Therefore, due to the unavailability of data accounting for different structural performance levels (different levels of risk) and necessary to build ad hoc F-N curves, the losses due to fatalities $C_{fat,Si}$ and injuries $C_{inj,Si}$ associated with each state Si are simply assumed as

$$C_{fat,Si} = f_{Si} c_{VSL} O \tag{7.3}$$

$$C_{inj,Si} = r_{inj} C_{fat,Si} \tag{7.4}$$

where f_{Si} is the percentage of fatalities, c_{VSL} is the value of a statistical life (VSL) (USD), O is the ship occupancy (number of people on board), and r_{inj} is the ratio of costs due to injuries and fatalities.

Operational costs are those strictly related to ship management, including (Journée and Meijers 1980, Deschamps and Greenwell 2009) fuel costs, crew costs, port and handling costs, insurance, maintenance and repairs, among others.

Among other costs, for the purpose of optimal ship routing, fuel costs are considered in this chapter. Fuel costs depend upon the fuel consumption associated with the different ship operations. The evaluation of the wave resistance and hull friction is necessary for the rigorous assessment of the power of the engine/propulsion

system, and consequently of the ship fuel consumption. However, since the evaluation of the wave resistances and hull frictions is outside the scope of this study, a simpler method can be used for the evaluation of the fuel cost rate $C_{fuel,Hs,U}$ (\$/h), based upon the following empirical function (e. g. Rudko 2003)

$$C_{fuel,Hs,U} = c_{fuel}\left(k_1 + k_2 D + k_3 U^3 + k_4 Hs\right) \tag{7.5}$$

where c_{fuel} is the fuel cost per liter (\$/l), and k_1, k_2, k_3, and k_4 are coefficients that may be obtained by interpolating test results. On the other hand, based on the estimation of the fuel consumption rate for a given sea state, a simple approach may be used assuming that ship displacement is constant during a trip. Given the actual ship speed U, the design speed U', the design fuel consumption rate $r'_{fuel,Hs}$ (Mt/h) for a specific sea state (expressed by Hs), and c_{fuel} (\$/Mt), the updated fuel cost rate $C_{fuel,hs,U}$ (\$/h) can be approximately evaluated as follows (Wijnolst and Wergeland 1996)

$$C_{fuel,Hs,U} = c_{fuel} r'_{fuel,Hs}\left(\frac{U}{U'}\right)^3 \tag{7.6}$$

Rigorous quantitative risk assessment requires the estimation of the specific ship operational profiles that indicate the occurrence probability of encountering determinate sea states across a geographic region under different operational parameters, such as speed and heading angle $P[Hs,U,H]$ (Glen, Paterson and Luznik 1999). Therefore, a general definition for the total time-dependent risk $R_{,Hs,U,H}(t)$ may be given by

$$R_{Hs,U,H}(t) = \sum_{Si=S1}^{S5}\left(C_{D,Si} + C_{ID,Si}\right) \times P[Si \mid Hs,U,H](t) \times P[Hs,U,H] \tag{7.7}$$

where $C_{D,si}$ and $C_{ID,si}$ are the total direct and indirect costs, respectively, and $P[Si|Hs,U,H](t)$ is the time-dependent probability for the ship hull of being in state Si ($S1$ to $S5$), given specific encountered significant wave height Hs, ship speed U, and heading angle H, is provided in Equation (6.6) of Chapter 6. Although Equation (7.7) formally addresses risk assessment, route optimization is conditioned to the actual and forecasted weather that the ship will encounter during its journey, therefore leading to

$$R_{Hs,U,H}(t) = \sum_{s=S1}^{S5} \left(C_{D,s} + C_{ID,s}\right) \times P[Si \mid Hs,U,H](t) \tag{7.8}$$

The general procedure for the assessment of reliability and risk is summarized in the Module (3) of Appendix B.

7.3 NEAR REAL-TIME PERFORMANCE AND WEATHER FORECAST

The main scope of this chapter is to provide a flexible approach for the progressive updating of ship performance, depending on the availability of new collected information (in terms of SHM data) and weather forecast. Ship routing prediction will be based on the near real-time information that becomes available while the ship is traveling. Two main topics are presented in this section. The first topic regards the use of monitoring data for the assessment of structural performance, whereas the second topic treats the integration of different weather forecasts into the optimal routing approach.

7.3.1 STRUCTURAL HEALTH MONITORING

The first aspect to be considered in order to make near real-time decision is the availability of further data, additional to those used for the initial assessment, which allows the decision to be more accurate within tight time steps. The principal quantity of interest to be updated is represented by the VBM induced by waves $M_{wv,Hs,U,H}$, which is treated as a random variable with the PDF given in Equation (6.17) of Chapter 6.

The SHM data used in this chapter were obtained by Dr. Devine and his co-workers during different testing sessions of a Froude-scaled test model of a NAVY's Joint High-Speed Sealift (JHSS) at the Naval Surface Warfare Center, Carderock Division - Maneuvering and Sea Keeping (NSWCCD - MSK) basin, and provided us (Devine 2009). Thus, the collected SHM data in terms of VBM are scaled up by using the proper Froude-scaling factor in order to account for the load effects associated with the full-scale ship. The recorded raw signal, obtained by merging different test runs includes the effects of both low- and high-frequency responses, that are associated with the most regular part of the wave excitation and the effects of hull vibrations in terms of slam-induced hull whipping, respectively (Devine 2009). Depending on the availability of SHM data for different ship operational conditions, reliability analysis will include those available runs associated with a specific combination of *Hs*, *U*, and *H*, therefore the updated limit state equation is

$$G'_{LSi,Hs,U,H}(t) = \delta - \left(\frac{x_w M_{wh,Hs,U,H}}{x_R M_{h,LSi}(t)} \right)^{c_{2,LSi}} + \\ - \left(\frac{x_{sw} M_{sw} + x_w k_W \left(\overbrace{M_{low,Hs,U,H}}^{\text{Updated}} + k_D \overbrace{M_{high,Hs,U,H}}^{\text{Directly from SHM}} \right)}{x_R M_{v,LSi}(t)} \right)^{c_{1,LSi}} = 0 \tag{7.9}$$

where $M_{low,Hs,U,H}$ and $M_{high,Hs,U,H}$ are the updated low-frequency and the obtained high-frequency VBM, respectively. Similarly, also the HBM can be updated based upon the availability of SHM data.

In order to separately investigate the effects of low- and high-frequency VBM, the raw signal needs to be filtered and analyzed independently. Butterworth filter is used for this purpose. The right cutoff frequency is properly chosen by analyzing the raw signal within the frequency-domain obtained with the Fourier transform of the raw signal. Accordingly, the Fourier transform $P(\omega)$ of the excitation function $p(t)$, which is represented in this study by the collected raw signal, is given by (Chopra 2006)

$$P(\omega) = \int_{-\infty}^{\infty} p(t) e^{-i\omega t} dt \tag{7.10}$$

where ω is the frequency, i is the complex unit, and t is the time. The chosen cutoff frequency subdivides the frequency-domain into two disjointed parts containing the two frequency peaks related to low- and high-frequency. Additionally, the noise associated with very high frequency is removed from the raw signal.

The filtered signal oscillates from negative to positive values, representing sagging and hogging VBM, respectively (Devine 2009). At this stage, according to Kay (1993), the signal must be mathematically characterized by developing a mathematical estimation of the data (i.e. PDF), and by assessing the relevant statistical descriptors. In order to do so, the peaks of the signal are extracted, and their values are stored. An algorithm has been used for this purpose, implemented with the software MATLAB (The MathWorks 2011). It is found that the best fit for the filtered low-frequency VBM is provided by using the Rayleigh distribution (i.e. Equation (6.17) of Chapter 6). This is in accordance with the theory behind short statistics prediction (Faltinsen 1990). Whereas, for high frequency peaks, the exponential distribution provides better goodness of fit. Therefore, these high-frequency peaks are distributed as follows

$$f\left(M_{high,Hs,U,H}\right)=\frac{e^{\frac{-M_{high,Hs,U,H}}{\lambda_{Hs,U,H}}}}{\lambda_{Hs,U,H}} \qquad \lambda_{Hs,U,H}, M_{high,Hs,U,H} \geq 0 \tag{7.11}$$

where $\lambda_{Hs,U,H}$ is the mean of a specific monitored combination of *Hs*, *U*, and *H*.

7.3.2 BAYESIAN UPDATING

The performance assessment based only on the SHM data, and disregarding the original information, can be restrictive, and may provide bias results. In this context, the Bayesian approach makes it possible to use the additional monitoring information in conjunction with the already available initial information (Kay 1993). The basic theory behind Bayesian updating procedure is reviewed in Section A.2.3 of Appendix

A, in according to Ang and Tang (2007). Both closed-form solution and simulation-based method are used herein.

7.3.2.1 Closed-Form Solution

In this chapter an analytical solution to the updating problem is developed. It is always easier to provide closed-form solution to the Bayes' problem when prior and posterior distributions are conjugated, i.e. belong to the same family (Anscombe 1961). In this analysis, short term statistics has been used, thus the distribution of the prior information follows the Rayleigh distribution of Equation (6.17) of Chapter 6, with mode α given by

$$\alpha = \sqrt{m_{0,Hs,U,H}} \tag{7.12}$$

Since the wave peaks follow the Rayleigh distribution (Faltinsen 1990), it is reasonable to assume that the mode α is a random variable itself, following the Rayleigh distribution. This new distribution represents the prior distribution $f'(\theta)$ of the parameter θ, defined as follows

$$f'(\theta) = \frac{\theta}{\alpha^2} e^{-\frac{\theta^2}{2\alpha^2}} \qquad \alpha, \theta \geq 0 \tag{7.13}$$

It can be noticed that the mode α is the hyperparameter of the prior distribution $f'(\theta)$. According to Equation (A.40) of Appendix A and recalling that the wave peaks follow the Rayleigh distribution, the likelihood function of the observations x_1, x_2,…x_j,…, x_n given the parameter θ is

$$L(\theta) = \frac{e^{-\frac{1}{2\theta^2}\sum_{j=1}^{n} x_j^2} \prod_{j=1}^{n} x_j}{\theta^{2n}} \qquad \theta \geq 0 \tag{7.14}$$

Hence, the posterior distribution $f''(\theta)$ of the parameter θ, evaluated according to Equation (A.41) of Appendix A is given by

$$f''(\theta) = \frac{k_n e^{-\frac{\theta^2}{2\alpha^2}-\frac{1}{2\theta^2}\sum_{j=1}^{n} x_j^2} \prod_{j=1}^{n} x_j}{\alpha^2 \theta^{2n-1}} \qquad \theta \geq 0 \tag{7.15}$$

where the normalizing constant k_n is obtained by solving Equation (A.42) of Appendix A, but integrated within the interval [0, +∞], because both $f'(\theta)$ and $L(\theta)$ are defined for $\theta \in [0, +\infty]$. Thus, k_n, handled with the software Mathematica (Wolfram Research 2010), becomes

$$k_n = \frac{\alpha^{n+1}\left(\sum_{j=1}^{n} x_j^2\right)^{\frac{n-1}{2}}}{\text{besselk}\left[n-1, \sqrt{\frac{1}{\alpha^2}\sum_{j=1}^{n} x_j^2}\right]\prod_{j=1}^{n} x_j} \tag{7.16}$$

where besselk[•] is the modified Bessel function of the second kind. After some math passages, developed with Mathematica (Wolfram Research 2010) and not reported here, the expected value of parameter θ is obtained by Equation (A.43) of Appendix A and provided as follows

$$\hat{\theta}'' = k_n e^{-\sqrt{\frac{1}{\alpha^2}\sum_{j=1}^{n} x_j^2}} \sqrt{\frac{\pi}{2}}\left(\prod_{j=1}^{n} x_j\right)\sum_{j=0}^{n-2} \frac{(2n-4-j)!}{2^{n-2-j}\, j!(n-2-j)!\alpha^{j+2}\left(\sum_{j=1}^{n} x_j^2\right)^{\frac{2n-3-j}{2}}} \tag{7.17}$$

Finally, by substituting this value into Equation (6.17) of Chapter 6, the updated VBM, which represent the underlying random variable X, is given by

$$f\left(M_{w,Hs,U,H}\right)=\frac{M_{w,Hs,U,H}}{\left(\hat{\theta}''\right)^2}e^{-\frac{\left(M_{w,Hs,U,H}\right)^2}{2\left(\hat{\theta}''\right)^2}} \qquad \hat{\theta}'', M_{w,Hs,U,H}\geq 0 \tag{7.18}$$

For large sets of observation, in order to avoid numerical problems (e.g. the likelihood function $L(\theta)$), it is convenient to use an appropriate set of units and consider to use a logarithmic form. Also, it may be recommended to use simulation-based algorithms.

7.3.2.2 Simulation-Based Techniques

Usually, the main computational challenge is the evaluation of the constant k_n (Equation (A.42) of Appendix A). Therefore, especially when prior and posterior are not conjugated, it is convenient to proceed by using numerical techniques, such as those based on simulations. In in order to validate the developed closed-form solution previously discussed, a simulation-based approach is used. The slicer sampling (Neal 2003) is used in this study; its clear advantage is that the constant k_n is not required to build the posterior PDF. The slice sampling algorithm is reviewed in Section A.2.2 of Appendix A.

When the collected SHM data become very large, numerical problems can derive from the evaluation of $L(\theta)$, which requires multiplying all the $f_X(x_j|\theta)$ (PDF of the random variable X evaluated with the SHM data value x_j) functions for all the SHM observation (Equation (A.40) of Appendix A). Therefore, when hundreds of measurements are collected, it is unfeasible to accomplish Bayesian analysis at once.

However, a key aspect of Bayesian updating is that it can be performed by sequential analyses (Gelman *et al.* 2003). Thus, by arranging the collected data into different groups of observations, the obtained posterior of each group becomes the prior of the subsequent analysis. The consecutive collection of SHM data brings the updating process towards real-time performance assessment. Hence, a permanent monitoring system installed on a ship may potentially provide updated structural performance by integrating the new information from SHM through Bayesian sequential analyses.

7.3.3 WEATHER FORECAST

There are many services/agencies that provide weather forecast for traveling ships worldwide. The usual manner of providing weather-related information is in forms of weather sea maps indicating the expected significant wave height, wind and wave direction, obtained and predicted from buoys and satellite readings (Bidlot, Janssen and Abdalla 2006, NOAA 2013, ECMWF 2013). This information is processed over specific regions. The accuracy of weather predictions depends on the forecast interval. Usually, forecasts are provided with time intervals as follows: 0 h (i.e. actual weather), 1 h, 3 h, 6 h, 12 h, 24 h, 48h, and 72 h. The ways to provide weather forecasts are mainly two, deterministic and probabilistic (Bidlot, Janssen and Abdalla 2006). Deterministic forecast represents the development of a specific sea that is the most likely to occur, but without giving any information about its probability of occurrence. Whereas, probabilistic forecast provides ensembles of sea maps obtained by superposition of small perturbations to the operational analysis before launching the forecast calculation (Hinnenthal 2008). Therefore, based on the latter, the probability

of encountering a specific significant wave height is provided. Since the ship routing is based on hypothetical sea maps that cover a short distance, being outside the scope of this study, the probabilistic aspect of the forecasts is not considered; therefore, in the proposed application, the weather forecast is assumed to be sufficiently accurate and deterministic.

7.4 MULTI-CRITERIA OPTIMAL ROUTING BASED ON TIME, RISK, AND FUEL COST

Risk-based optimization of ship routes is worth exploring in order to quantify the level of potential losses (based on structural performance) that are associated with different ship routes depending on the encountered sea conditions. Ship routing may include as objectives: ship movements, operational costs (e.g. fuel consumption), estimated time of arrival (ETA), reliability, probability of failure/serviceability, and risk, among others. These single optimality criteria can also be combined, leading to multi-objective optimization. For instance, ETA and ship movements, or fuel consumption and ship movements may be minimized. In such way the optimal solutions would belong to a Pareto-optimal set. Any point within this set can be chosen by decision makers, depending on fixed thresholds, such as available budget, acceptable level of reliability, probability of failure, risk, and allowable time to complete a trip, among others.

In the past, the quantification of safety within optimal routing has not been often addressed. In this chapter, the minimization of ETA, risk, and fuel cost is explicitly investigated, considering ship safety and including SHM monitoring in terms of

updated reliability and risk profiles. Based on this optimization problem, a wide spectrum of optimal routes is provided to decision makers in the form of Pareto-optimal set. For the optimal routing, it is assumed that the ship starts the trip from a point O (origin) and arrives at a point D (destination), within a given sea region. Based on the approach proposed in Chapter 6, the travel is discretized into N segments with extremities having coordinates x and y. A uniform discretization of the x-axis in N segments is assumed, leaving design values between the map limits for the y-axis. Therefore, the first group of design variables is represented by the N-1 y coordinates required to describe the N route segments. Moreover, time is a further variable of the optimization problem; hence the N ship speeds U represent the second group of design variables. As explained previously, different sea forecasts through different sea maps are provided and accounted for within the proposed optimal approach. Therefore, depending on the time elapsed from the origin of the trip, the proper forecast map is selected. Linear interpolation is used in order to account for intermediate time between different weather maps.

In this chapter, four separate optimization problems, denoted OP-A, OP-B, OP-C and OP-D, are solved in order to exploit the proposed risk-informed method for ship routing. The framework for the risk-informed route optimization is presented in the Module (4) of Appendix B. OP-A and OP-B are bi-objective optimization problems, whereas OP-C and OP-D are three-objective optimization problems. Based on the general formulation of a multi-objective optimization problem (reviewed in Appendix A), optimization problems OP-A, OP-B, OP-C and OP-D are defined as

- OP-A is formulated as follows:

Given: sea weather maps that include the actual state and prediction of significant wave height and wave direction, and total risk $R_{Hs,U,H}(t)$ with respect to different combinations of *Hs*, *U*, and *H* at a specific ship age *t*

find: a set of y_k and U_k

$$y_k \qquad \forall k = 1, 2, ..., N-1 \tag{7.19a}$$

$$U_k \qquad \forall k = 1, 2, ..., N \tag{7.19b}$$

to minimize: the estimated time of arrival ETA and the mean total risk $R_{mean}(t)$

$$\min\left\{\text{ETA}, R_{mean}(t)\right\} \tag{7.20}$$

subjected to the constraints:

$$y_{\min} \le y_k \le y_{\max} \qquad \forall k = 1, 2, ..., N-1 \tag{7.21a}$$

$$U_{\min} \le U_k \le U_{\max} \qquad \forall k = 1, 2, ..., N \tag{7.21b}$$

where y_{min} and y_{max} are the bounds of y coordinate within the map, U_{min} and U_{max} are the minimum and maximum allowable ship speed, respectively, and the objective mean total risk $R_{mean}(t)$ is given by

$$R_{mean}(t) = \frac{\sum_{k=1}^{N} R_{k,Hs,U,H}(t)}{N} \tag{7.22}$$

in which $R_{k,Hs,U,H}(t)$ is the total risk associated with the *k*-th route segment.

- OP-B is described as follows:

Given: sea weather maps and $R_{Hs,U,H}(t)$

find: a set of y_k and U_k

$$y_k \qquad \forall k = 1,2,...,N-1 \tag{7.23a}$$

$$U_k \qquad \forall k = 1,2,...,N \tag{7.23b}$$

to minimize: ETA and $R_{mean}(t)$

$$\min\left\{\text{ETA}, R_{mean}(t)\right\} \tag{7.24}$$

subjected to the constraints:

$$y_{\min} \le y_k \le y_{\max} \qquad \forall k = 1,2,...,N-1 \tag{7.25a}$$

$$U_{\min} \le U_k \le U_{\max} \qquad \forall k = 1,2,...,N \tag{7.25b}$$

$$\beta_{k,LS4,Hs,U,H}(t) \ge \beta_{\text{threshold}} \qquad \forall k = 1,2,...,N \text{ and } \forall(Hs,U,H) \tag{7.25c}$$

$$R_{k,Hs,U,H}(t) \le R_{\text{threshold}} \qquad \forall k = 1,2,...,N \text{ and } \forall(Hs,U,H) \tag{7.25d}$$

where $\beta_{k,LS4,Hs,U,H}(t)$ is the reliability index of *LS*4 associated with the *k*-th route segment, and $\beta_{threshold}$ and $R_{threshold}$ are the assumed minimum and maximum thresholds of the reliability index and total risk, respectively.

- OP-C is formulated as follows:

  Given: sea weather maps, $R_{Hs,U,H}(t)$, and the fuel cost rate $C_{fuel,Hs,U}$

  find: a set of y_k and U_k

$$y_k \qquad \forall k = 1,2,...,N-1 \tag{7.26a}$$

$$U_k \qquad \forall k = 1,2,...,N \tag{7.26b}$$

to minimize: ETA, $R_{mean}(t)$, and total fuel costs $C_{tot,fuel}$

$$\min\left\{\text{ETA}, R_{mean}(t), C_{tot,fuel}\right\} \tag{7.27}$$

subjected to the constraints:

$$y_{\min} \le y_k \le y_{\max} \qquad \forall k = 1,2,...,N-1 \tag{7.28a}$$

$$U_{\min} \le U_k \le U_{\max} \qquad \forall k = 1,2,...,N \tag{7.28b}$$

where the objective total fuel costs $C_{tot,fuel}$ is given by

$$C_{tot,fuel} = \sum_{k=1}^{N} T_k C_{fuel,Hs,U} \tag{7.29}$$

in which T_k is the time necessary for the ship to cover the k-th route segment.

- Finally, OP-D is formulated as follows:

  Given: sea weather maps, $R_{Hs,U,H}(t)$, and $C_{fuel,Hs,U}$

  find: a set of y_k and U_k

  $$y_k \qquad \forall k = 1,2,...,N-1 \tag{7.30a}$$

  $$U_k \qquad \forall k = 1,2,...,N \tag{7.30b}$$

  to minimize: ETA, $R_{mean}(t)$, and $C_{tot,fuel}$

  $$\min\left\{\text{ETA}, R_{mean}(t), C_{tot,fuel}\right\} \tag{7.31}$$

  subjected to the constraints:

  $$y_{\min} \le y_k \le y_{\max} \qquad \forall k = 1,2,...,N-1 \tag{7.32a}$$

  $$U_{\min} \le U_k \le U_{\max} \qquad \forall k = 1,2,...,N \tag{7.32b}$$

$$\beta_{k,LS4,Hs,U,H}(t) \geq \beta_{\text{threshold}} \qquad \forall k = 1,2,...,N \text{ and } \forall(Hs,U,H) \qquad (7.32c)$$

$$R_{k,Hs,U,H}(t) \leq R_{\text{threshold}} \qquad \forall k = 1,2,...,N \text{ and } \forall(Hs,U,H) \qquad (7.32d)$$

The four optimization problems are solved by using Genetic algorithm (GA) (Goldberg 1989, Deb 2001), which is a heuristic optimization tool that is useful when closed form solutions are not available.

7.5 CASE STUDY

Based on the data provided by Devine (2009), the developed framework is applied to the Joint High-Speed Sealift (JHSS). Figure 6.1 of Chapter 6 shows the models of the JHSS. As explained in Chapter 6, through the response surfaces method, the considered random variables are implemented into the strength model in order to evaluate the statistical descriptors of vertical and horizontal flexural capacities of the midship section. Also the load effects are evaluated in accordance to Chapter 6.

7.5.1 RELIABILITY, COST, AND RISK

Reliability analysis is performed for each considered combination of *Hs*, *U*, and *H* and for each defined limit state (*LS*1 to *LS*4), according to Equation (6.3) of Chapter 6. The software RELSYS (Estes and Frangopol 1998) is used for this purpose. The descriptors of the parameters x_R, x_{sw}, and x_w are considered normally distributed with mean values of 1.0, 1.0, and 0.9, and COVs equal to 0.10, 0.05, and 0.15, respectively (Paik and Frieze 2001), whereas k_W is set to unity, k_D is equal to 0.69 for hogging (Mansour *et al.* 1984), and δ is taken as a normally distributed random variable with

mean of 9.73 and COV of 10% (Paik, Thayamballi and Che 1996). Then, the probabilities of the hull being in states $S1$ to $S5$ are obtained by using Equation (6.6) of Chapter 6. These probabilities are necessary to compute the total risk through Equation (7.8). State $S1$ does not generate any consequences. Direct consequences caused by states $S2$ to $S4$ are evaluated by considering the portion of hull surrounding the midship section as 40% of the length of the hull, whereas for state $S5$ the loss of the whole ship hull is considered. Table 7.1 summarizes all the parameters involved in the costs, evaluated according to Equations (7.1)–(7.4) and (7.6). It is assumed that fuel consumption varies depending on the encountered sea state *SS*, with a variation of ±10% for each *SS* greater (+) or lower (-) than the reference *SS*4, at which, a fuel consumption r'_{fuel} of 10 t/h has been assumed for a speed of 20 m/s. The costs due to fatalities rely on the estimation of the number of casualties among the crew. An accurate estimation of the percentage of fatalities f_{Si} is out of the scope of this study and is usually carried out by the Health, Safety, and Environment HSE department in phase of design/assessment, therefore this number is assumed herein. The occupancy of the ship may vary depending on the ship mission. An estimation of the exact number of the crew members is difficult to provide, therefore it is assumed. Moreover, an annual discount rate of money of 3% has been considered in order to obtain the present value of the used unitary costs. Finally, risk is assessed for each considered combination of operational conditions (*Hs*, *U*, and *H*).

7.5.2 SHM AND UPDATING

A segmented seakeeping model of the JHSS was built and tested in the Naval Surface Warfare Center basin in the summer of 2007 in order to obtain the main ship responses (Devine 2009), including VBM and HBM. The model was Froude-scaled down with a scale factor γ of 47.2533. Accordingly, the associated full-scale VBM and HBM, which are the quantities of interest in this chapter to perform reliability analysis, are obtained by multiplying the recorded model-scale VBM and HBM by $1.025\times\gamma^{4}$ (accounting for sea water and scale factor) (Devine 2009). Based on the available data, VBM and HBM data at midship are used for the updating process. The available signals include 21 runs at speed 35 Knots and heading 0° for sea state 7 (*SS*7) (denoted signal 1), and 12 runs at speed 15 Knots and heading 0° for sea state 8 (*SS*8) (denoted signal 2). Data were recorded by using a sampling rate of 200 Hz (for primary hull response), collecting a total of 73,800 observations for signal 1 and 117,000 observations for signal 2. Since the JHSS is at a preliminary stage of design and testing, only these SHM data are available for their implementation within the proposed approach.

Since the raw signals include both low- and high-frequency responses, they are filtered by using the Butterworth filter with cutoff frequency of 0.5 Hz for the VBM and 0.4 Hz for the HBM. These cutoff frequencies were estimated by analyzing the Fourier transform of the raw signals (Equation (7.10)). Figure 7.1 shows (a) signal 1 and (b) signal 2 represented in the frequency-domain. It can be noticed that the signals can be split into two regions containing the low and high peak frequencies. Similar

results are obtained for the HBM. Moreover, a cleaner signal has been obtained by cutting off the noise for frequencies greater than 5 Hz, that are insignificant for the analysis. An example of the filtering process is reported in Figure 7.2 where the raw signals and the filtered low- and high-frequency responses for (a) signal 1 and (b) signal 2 are shown in terms of VBM associated with model- and full-scale ships. The oscillation of the signal around the 0 value subdivides the plot into two parts, sagging (negative) and hogging (positive) VBMs. Hogging peaks are extracted from both low- and high-frequency signals and separately stored. Figure 7.3 shows the histograms of the peaks of signal 1 (Figure 7.3(a,b,c,d)) and signal 2 (Figure 7.3(e,f,g,h)). VBM (hogging) and HBM are both shown in Figure 7.3(a,c,e,g) and Figure 7.3(b,d,f,h), respectively, whereas low- and high-frequency moments are reported in Figure 7.3(a,b,e,f) and Figure 7.3(c,d,g,h), respectively. These histograms are then fitted by using the Rayleigh and exponential distributions for low- and high-frequency moments, respectively, which, among other types of distributions, resulted to be the most appropriate one, in accordance with the theoretical approach. The obtained relevant statistical descriptors are also reported in Figure 7.3 (mode α for Rayleigh and mean λ for exponential).

Next, the low-frequency VBM, obtained by signals 1 and 2, is updated. Figure 7.4 shows the integration of collected observations of VBM through Bayesian updating. Figure 7.4(a,b) show partial updating considering 1 and 30 observations, respectively. It can be noticed that the weight of the SHM data (extracted peaks) with respect to the prior distribution (Rayleigh) becomes more significant when the set of these data gets larger. The posterior distributions (Rayleigh), governed by the expected value of

parameter θ, are evaluated using both close-form solution (Equation (7.17)) and simulation-based techniques by using the slice sampling algorithm. The two methods indicate complete agreement; then, by incorporating all extracted peaks, the final updated posterior distributions are obtained, as shown in Figure 7.4(c,d) for VBM of signals 1 (number of peaks n_{SHM} = 402) and signal 2 (number of peaks n_{SHM} = 449), respectively. Figure 7.4(c,d) report also on partial updating, indicating partial updated posteriors in dashed light gray curves. Besides, the high-frequency VBM is used without being updated, because its prior information is insufficient and not specific for any combination of *Hs*, *U*, and *H*.

Once VBM is initially predicted, and after filtering the SHM data, some of the VBMs belonging to the proper operational condition *Hs*, *U*, and *H* of signals 1 and 2 are updated accordingly. Although the collected SHM data enhance the initial prediction, due to the scarcity of available data, it is assumed that signal 1 can be used to update the VBM associated with 7.62 m $\leq Hs \leq$ 12.19 m, 16 m/s $\leq U \leq$ 20 m/s, and -20° $\leq H \leq$ 20°, and signal 2 used for 13.72 m $\leq Hs \leq$ 18.29 m, 6 m/s $\leq U \leq$ 10 m/s, and -20° $\leq H \leq$ 20°. This approach is generally valid, also for other combinations of *Hs*, *U*, and *H*, if further data become available. Although HBMs are collected for both signals 1 and 2 as well, HBM is not updated because the obtained values for H = 0° are too small to be extended to other angles that become more significant in terms of HBM. Once the updated load effects are evaluated, reliability analysis and risk assessment can be performed. Figure 7.5 shows the profiles of the assessed performances (VBM, reliability index, probability of exceedance, and risk), including both initial prediction and updated information (indicated with a light gray shaded

region). In detail, Figure 7.5(a) shows the polar representation of the VBM (two different scales are shown), given Hs = 9.14 m and U = 18 m/s. Figure 7.5(b) shows the polar profiles of the reliability index associated with the four limit states $LS1$ to $LS4$ for the intact ship (t = 0 years) and for an aged ship (t = 30 years), given Hs = 9.14 m and U = 18 m/s. Figure 7.5(c) shows the profiles of the probability of exceedance associated with the limit states LSi, fixing U = 18 m/s and H = 0º, and reports on the probabilities for the intact ship of being in states $S1$ to $S5$. Figure 7.5(d) shows the profiles of direct and indirect risks associated with states $S2$ to $S5$ of the intact ship ($S1$ does not generate any consequences). According to the cost analysis, indirect risk is much greater that direct risk. The updated risk is almost negligible when the ship is traveling under this specific Hs = 9.14 m, U = 18 m/s, and $20° \leq H \leq 20°$ combination compared to risk with H = 180°.

7.5.3 NEAR REAL-TIME ROUTE MULTI-CRITERIA OPTIMIZATION USING SHM INFORMATION

Weather prediction is provided in the form of sea maps reporting on the significant wave height Hs and wave direction. It is assumed that the sea map has each edge of 1000 km, and the trip starts from point O ≡ (1000 km, 200 km) and ends at point D ≡ (0 km, 400 km), which are the origin and destination, respectively. However, different maps associated with the current sea weather (0 h) and prediction for time frames of 1 h, 3 h, 6 h, 12 h, 24 h, 48 h, and 72 h, are considered as shown in Figure 7.6. The significant wave height is assumed to range between about 3 m and 8 m, representing sea states between 5 and 7, respectively. Two storms are reported in the maps where

sea prediction is within 24 h (i.e. maps 0 h to 24 h). Then they merge forming storm 3 for prediction later than 24 h (i.e. maps 48 h and 72 h). The disturbance areas are moving north-west to south-est. The ship is supposed to travel in the opposite direction, and a decision regarding whether it is convenient to avoid the two encountered storms must be taken. According to the above explained optimization problems (denoted OP-A, OP-B, OP-C, and OP-D), 15 segments (N = 15) represent the discretization of the x-axis. Therefore a total of 29 design variables are considered, including 14 coordinates y_k and 15 ship speeds U_k. Moreover, the following bounds for y_k and U_k are assumed 0 km $\leq y_k \leq$ 1000 km (Equations (7.21a), (7.25a), (7.28a), and (7.32a)) and 4 m/s $\leq U_k \leq$ 20 m/s (Equations (7.21b), (7.25b), (7.28b) and (7.32b)), respectively. In order to solve the optimization problems, multidimensional matrices with a dense discretization of the parameters *Hs*, *U*, and *H* have been obtained for total risk, reliability index, and fuel cost. The significant wave height and the wave direction within the assumed sea maps are discretized into regular meshes. The updated information from SHM, whenever available, is in accordance to the updating process explained above. The optimization problems have been solved numerically by using GA, setting population size of 500 and maximum number of generations of 500.

The considered Pareto fronts are categorized according to Table 7.2 and are obtained by solving the optimization problems formulated based on combining the following:

- *Column* 1: identification number (Roman)
- *Column* 2: type of optimization problems (denoted OP-A, OP-B, OP-C, or OP-D).

- *Column* 3: number of objective (two-objective or three-objective).
- *Column* 4: number of constraints (two or four).
- *Column* 5: ship age (intact case t = 0 years or aged case t = 30 years).
- *Column* 6: (a) weather prediction (WP), accounting for different maps 0 h to 72 h, is accounted for; and (b) WP not considered, therefore, only the current weather associate with map 0 h is accounted for.
- *Column* 7: (c) SHM is not considered; (d) SHM is considered assuming that the updated load effects (VBM) are proportional to the ratio between the modes of the posterior and prior distributions (equal to 1.15) found for signal 1, extended to each combination of *Hs*, *U*, and *H*; and (e) actual updated load effects (VBM) for the specific combinations of *Hs*, *U*, and *H* of signals 1 and 2.

Figure 7.7(a) shows the Pareto fronts (I) and (II) associated without and with SHM data, respectively. Although the available SHM data are limited to signals 1 and 2, performing optimization analysis assuming that the outcomes of one of these signals are extended to all the possible combinations of *Hs*, *U*, and *H* can provide interesting insights concerning optimal routing. Pareto fronts are represented in terms of optimal ETA (h) and mean total risk R_{mean} (USD). It can be noticed that in order to select any solution but the extreme points of the Pareto, a trade-off must be taken into consideration. Since the mode of the updated VBM is larger than the posterior one, by including the new information into risk assessment, the Pareto front (II) shifts to higher values of risk considering a fixed ETA. Therefore, for instance, points A and B, representing the fastest routes within the Pareto fronts (I) and (II) with ETA equal to

14.16 h, respectively, account for different risk levels. These results are very important in order to highlight the potential contribution of a permanent SHM system that records the ship responses under generic conditions. Risk can therefore be more accurate and potential underestimations may be avoided. Figure 7.7(b) shows the Pareto fronts (I) and (III) considering two and four constraints, respectively (see Table 7.2), obtained without considering SHM. The allowable values of minimum and maximum thresholds of the reliability index (Equation (7.25c)) and total risk (Equation (7.25d)) are assumed to be equal to 2.5 and 8×10^6 USD, respectively. It can be noticed that, in order to satisfy the two introduced constraints, the fastest route of Pareto front (III) has ETA equal to 26.13 h (point C). In Figure 7.7(c), the Pareto fronts (II) and (IV), considering two and four constraints, respectively (see Table 7.2), are obtained considering SHM. In this case, being the updated VBM larger than the predicted, Pareto front (IV) shifts to higher ETA when the constraints of Equations (7.25c,d) are considered. Therefore, larger ETAs are found for Pareto (IV) than for Pareto (III), in fact the fastest route of Pareto front (IV) has ETA equal to 33.47 h (point D).

The Pareto fronts (V), (VI), and (VII) (see Table 7.2), obtained by solving the OP-A are shown in Figure 7.8(a). The fact of having different sea maps available allows the decision maker to select routes that potentially reduce risk; in fact the Pareto fronts associated with WP have lower risk than those based on the current sea map only. Four optimal solutions are selected, called routes A, B, C, and D. Figure 7.8(b) reports on the routes A and B within the actual sea map (0 h). Route A is associated with the higher level of risk and linearly crosses the region between O and D, whereas, route B

avoids storm 2 by deviating from the shortest pattern. Figure 7.8(c,d,e,f) show the route profiles associated with total risk (USD), reliability index associated with hull collapse (*LS*4), ship speed (m/s), and cumulative time from departure (h). Total risk and reliability are in accordance to the encountered sea and depend also on the *U* and *H*. Among the selected solutions, route A is the fastest, whereas the other routes seem to allow greater reliability index. The paths of routes C and D are shown in Figure 7.9, where 6 maps are reported, since the ETA of the selected trip is lower than 24 h. These two routes are prone to avoid the storm at different locations and accordingly encounter different sea and travel conditions as reported in Figure 7.8(c,d,e,f). The two-ship shaped symbols indicatively show the location of the ship with respect to the *x*-axis for the two considered routes.

Figure 7.10 shows the Pareto fronts (VIII) of Table 7.2, obtained by solving OP-C and considering SHM. Three objectives are simultaneously minimized. The solution to the problem is a 3D Pareto front as reported in Figure 7.10(a). Solutions that are trade-offs of the three objectives are reported. It can be noticed that higher fuel cost is generally associated with low risk levels because fuel consumption is related to the ship speed and the encountered sea conditions, therefore when longer patterns are chosen, risk decreases, whereas fuel cost increases. Although the latter seems always true, the opposite does not occur. In fact, low fuel cost may be associated with high or low risk levels, depending on the followed route. Moreover, solutions with high ETA are generally associated with low risk, due to longer routes in order to avoid dangerous situations. Four solutions are extrapolated from the Pareto set, called Route E, F, G, and H. Figure 7.10(b,c,d,e,f,g) show the route profiles with respect to total risk (USD),

fuel cost (USD), reliability index, the value of the *y*-axis (km), ship speed (m/s), and cumulative time from departure (h). Instead of presenting the route pattern through sea maps, *y*-axis coordinates are provided (Figure 7.10(e)) in this case. Accordingly, risk is high and reliability index down crosses critical levels when route E is selected, since it is the shortest and fastest path. Although the speed profile of route H is relatively low, and route H has the lowest fuel cost among the selected routes, its risk profile is not as low, because its path goes through the storm. Figure 7.11(a) shows the Pareto front (IX) of Table 2, obtained by solving OP-D, and by keeping the same remaining problem properties included in Figure 7.10, but introducing the additional constraints of Equations (7.32c,d) ($\beta_{threshold}$ and $R_{threshold}$ are equal to 2.5 and 8×10^6 USD, respectively). This Pareto front does not include any more solutions with high risk and generally provides a high ETA. Similarly, four solutions are extrapolated from the Pareto set, called Route I, J, K, and L, for which Figure 7.11(b,c,d,e,f,g) show their profiles with respect to total risk (USD), fuel cost (USD), reliability index, the value of the *y*-axis (km), ship speed (m/s), and cumulative time from departure (h). In this case, the fastest route has ETA equal to 31.74 h, with relatively low risk and fuel consumption. It can be noticed that the additional constraints are active for routes I, J, and L ($\beta_{threshold}$ = 2.5) (Figure 7.11(d)), whereas, as shown in Figure 7.11(b), the risk constraint is almost active for route J.

7.6 CONCLUSIONS

In this chapter, which is mostly based on Decò and Frangopol (2013c), a risk-based approach for near real-time optimal routing of ships integrating structural health

monitoring data has been presented. Two-objective and three-objective optimization problems are solved by minimizing ETA, total risk, and fuel costs. The results are shown in the form of Pareto-optimal sets. Mission profiles including total risk, reliability index, fuel cost, ship path, ship speed, and cumulative time from departure are obtained for a NAVY's JHSS. The information obtained from SHM and different sea weather maps are integrated within the developed optimization framework. Bayesian statistics have been used to update prior information by using both a closed-form solution and a simulation-based technique.

The following conclusions are drawn:

1. SHM provides useful information that is used to update the structural performance. A closed-form solution, based on the accepted assumption that the peak responses follow the Rayleigh distribution, is developed herein. The obtained results have been compared with those provided by numerical simulation using the slicer sampling, obtaining perfect match. The profiles of load effects in terms of VBM and HBM, reliability index, and risk have been updated by using the available information provided by testing a scaled ship model in terms of VBM.
2. It is found that near real-time decision making can be achieved by integrating SHM data with the prior performance information. If a permanent SHM system is installed, the proposed updating process would yield to real-time decision making. The crew members can be advised before down crossing critical performance thresholds, thus adequately avoiding a potential dangerous situation by modifying the ship trajectory and/or reducing the traveling speeds.

3. It is found that optimizing three objectives, including the minimization of ETA, total risk, and fuel cost provides a comprehensive set of optimal solutions. Although some solutions are trivial (e.g. the shortest path), some others need to be further analyzed by decision makers to understand their values. It is found that a higher fuel cost is generally associated with low risk, whereas the opposite is not always true. Moreover, solutions with high ETA are generally associated with low risk, due to longer routes necessary to avoid dangerous situations. Overall, it is also found that having different sea maps available allows the decision maker to select routes that potentially reduce risk; in fact the associated Pareto fronts, when WP is considered, have lower risk than those based on the current sea map only.
4. SHM and sea weather predictions play a fundamental role for optimal ship routing. Integrating this information into the developed framework provides decision makers with more comprehensive sets of optimal solutions that may reduce risk, ETA and fuel cost.
5. The importance of considering constraints within the investigated optimization problems is demonstrated. These constraints limit ship operations so that they remain within specific boundaries, allowing slowest paths and reduced traveling speeds.
6. The developed approach is flexible, and can update the optimal solutions by including additional data about specific fuel consumption and further SHM data accounting for different combinations of *Hs*, *U*, and *H*.

Table 7.1 Parameters involved in the cost analysis.

Parameter	Value	Reference
Damage ratios $d_{r,Si}$ for [$S1$, $S2$, $S3$, $S4$, $S5$]	[0, 0.10, 0.35, 0.75, 1]	Assumed
Fuel consumption r'_{fuel} (t/h) for [$SS1$, $SS2$, $SS3$, $SS4$, $SS5$, $SS6$, $SS7$, $SS8$] at speed U' = 20 m/s	[7, 8, 9, 10, 11, 12, 13, 14]	Assumed
Fuel cost c_{fuel} ($/t)	640	WSC (2008)
Percentage of fatalities f_{Si} for [$S1$, $S2$, $S3$, $S4$, $S5$]	[0%, 0%, 0%, 1%, 2%]	Assumed
Ratio r_{inj}	6.14	Skjong (2002)
Ship occupancy O	200	Assumed
Ship type factor STF	7	Miroyannis (2006)
Value of a statistical life (USD)	6,200,000	USDOT (2011)
Weight of WGT_{100} for $S1$, $S2$, $S3$, and $S4$ (long tons)	5,466	Devine (2009)
Weight of WGT_{100} for $S5$ (long tons)	10,300	Devine (2009)

Table 7.2 Summary of the formulations of all the solved optimization problems leading to the Pareto fronts discussed in Section 7.5.4.

(1) Pareto front	(2) Type of optimization problem	(3) Number of objectives	(4) Number of constraints	(5) Ship age t (years)	(6) Weather prediction (WP)	(7) Extended SHM based on signal 1 (assumed)
(I)	OP-A	2	2	0	(a)	(c)
(II)	OP-A	2	2	0	(a)	(d)
(III)	OP-B	2	4	0	(a)	(c)
(IV)	OP-B	2	4	0	(a)	(d)
(V)	OP-A	2	2	0	(a)	(e)
(VI)	OP-A	2	2	0	(b)	(e)
(VII)	OP-A	2	2	30	(a)	(e)
(VIII)	OP-C	3	2	0	(a)	(e)
(IX)	OP-D	3	4	0	(a)	(e)

Note: (a) denotes that the weather prediction (WP) is accounted for
(b) denotes that only the current weather associate with map 0 h is accounted for
(c) denotes that the SHM is not considered
(d) denotes that the assumed extended SHM based on signal 1 is considered
(e) denotes that the actual SHM based on signals 1 and 2 is considered

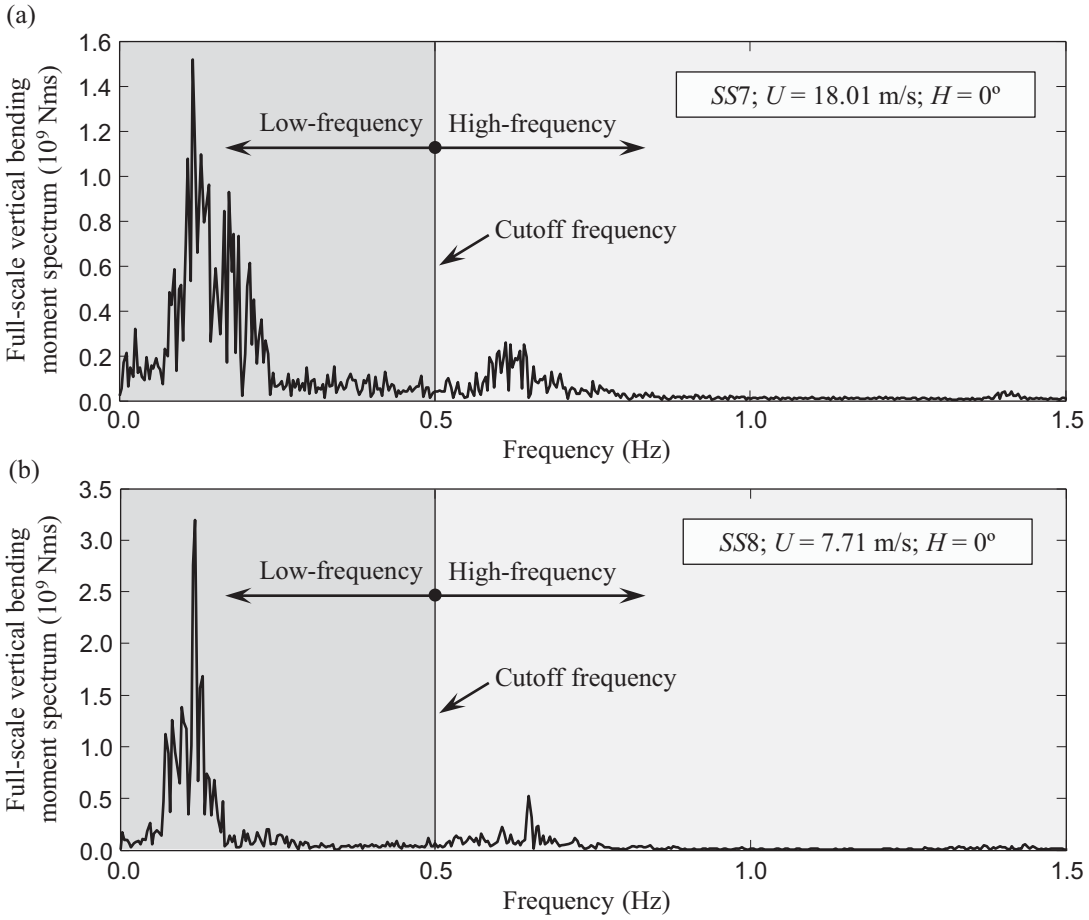

Figure 7.1 (a) signal 1 and (b) signal 2 represented in the frequency-domain, where *SS* indicates the sea state, *S* is the ship speed and *H* is the heading angle.

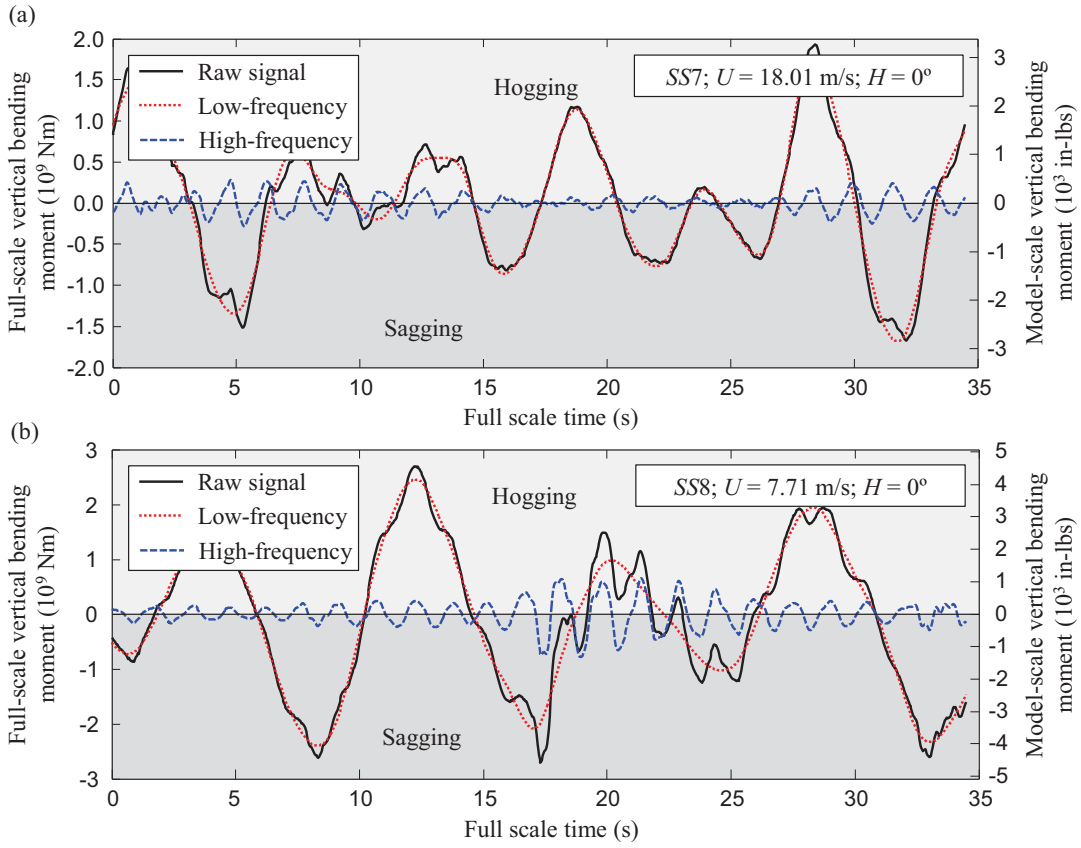

Figure 7.2 Raw signals and filtered low- and high-frequency responses for the VBMs of (a) signal 1 and (b) signal 2, where *SS* indicates the sea state, *S* is the ship speed and *H* is the heading angle.

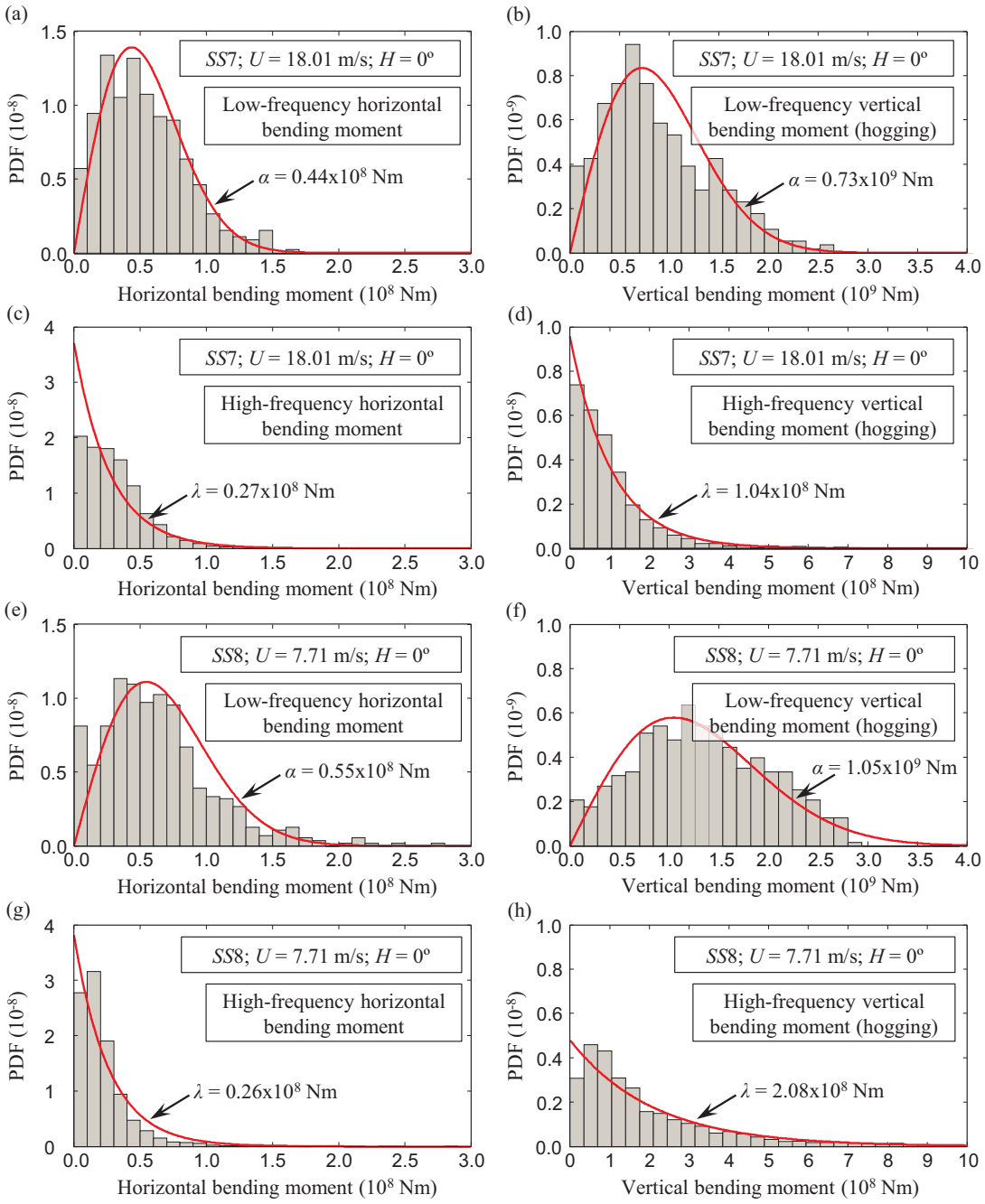

Figure 7.3 Histograms of the peaks of signal 1 (a,b,c,d) and signal 2 (e,f,g,h) associated with (a,c,e,g) HBM and (b,d,f,h) VBM, and with respect to (a,b,e,f) low- and (c,d,g,h) high-frequency moments. Low- and high-frequency histograms are fitted with Rayleigh and exponential distributions, respectively, of which statistical descriptors are also reported (mode α for Rayleigh and mean λ for exponential). *SS* indicates the sea state, *S* is the ship speed and *H* is the heading angle.

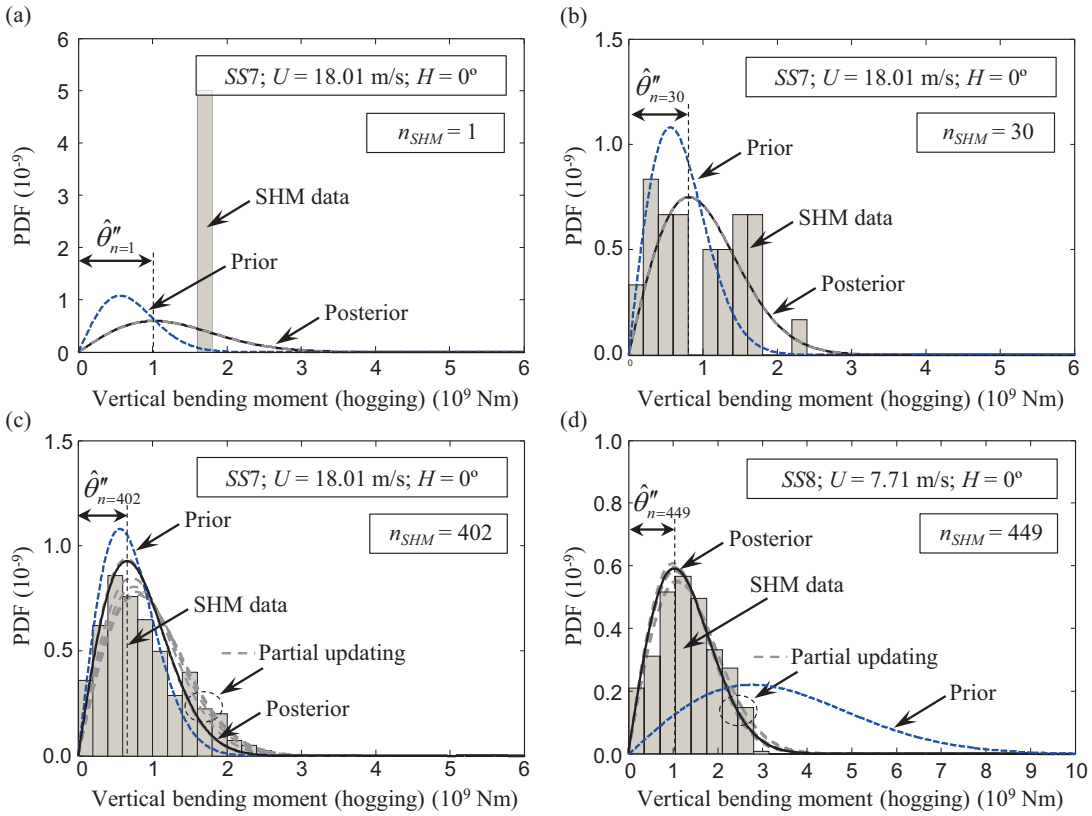

Figure 7.4 Updating process including prior distributions, SHM histograms, and posterior distributions for the VBMs of (a,b,c) signal 1 and (d) signal 2, where *SS* indicates the sea state, *S* is the ship speed and *H* is the heading angle. Partial distribution for VBM signal 1 with $n_{SHM} = 1$ and $n_{SHM} = 30$ are shown in (a) and (b), respectively.

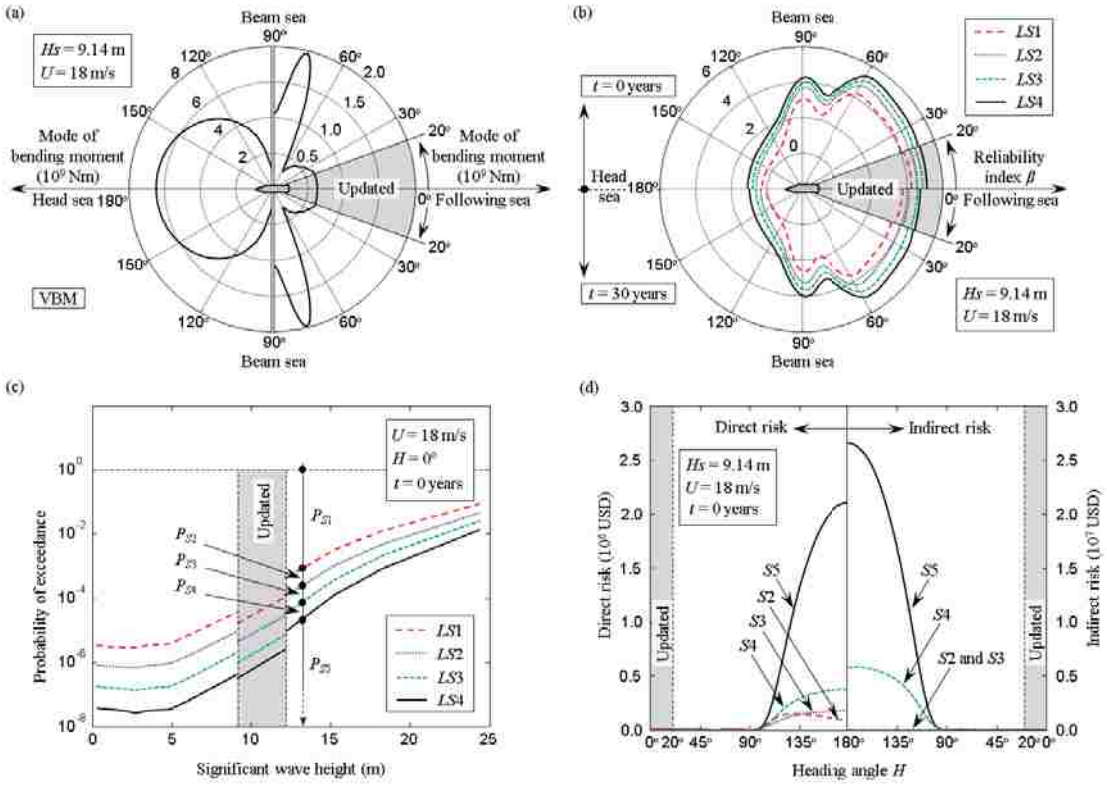

Figure 7.5 Initially predicted and updated profiles (indicated with a light gray shaded region) of (a) VBM, (b) reliability index (intact ship t = 0 years and aged ship t = 30 years), (c) probability of exceedance (intact ship t = 0), and (d) direct and indirect risk (intact ship t = 0).

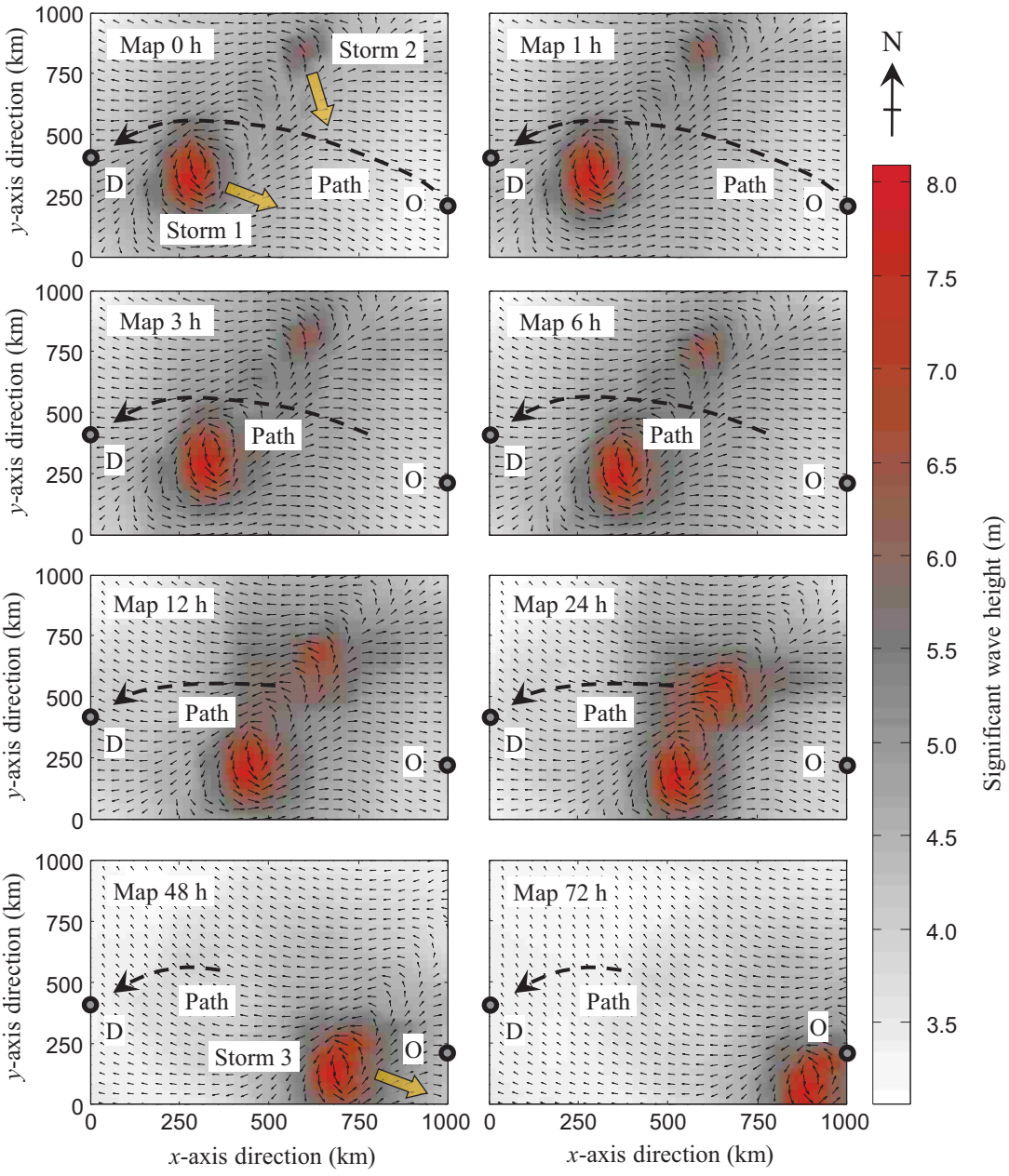

Figure 7.6 Assumed sea weather maps associated with the current sea weather (0 h) and prediction for time frames of 1 h, 3 h, 6 h, 12 h, 24 h, 48 h, and 72 h. The variation of the significant wave height is reported in the scale on the right-hand side of the figure, and the vector field within the maps indicates the wave direction. Three moving storms are also reported in the maps. Trip origin point O and destination point D are also shown.

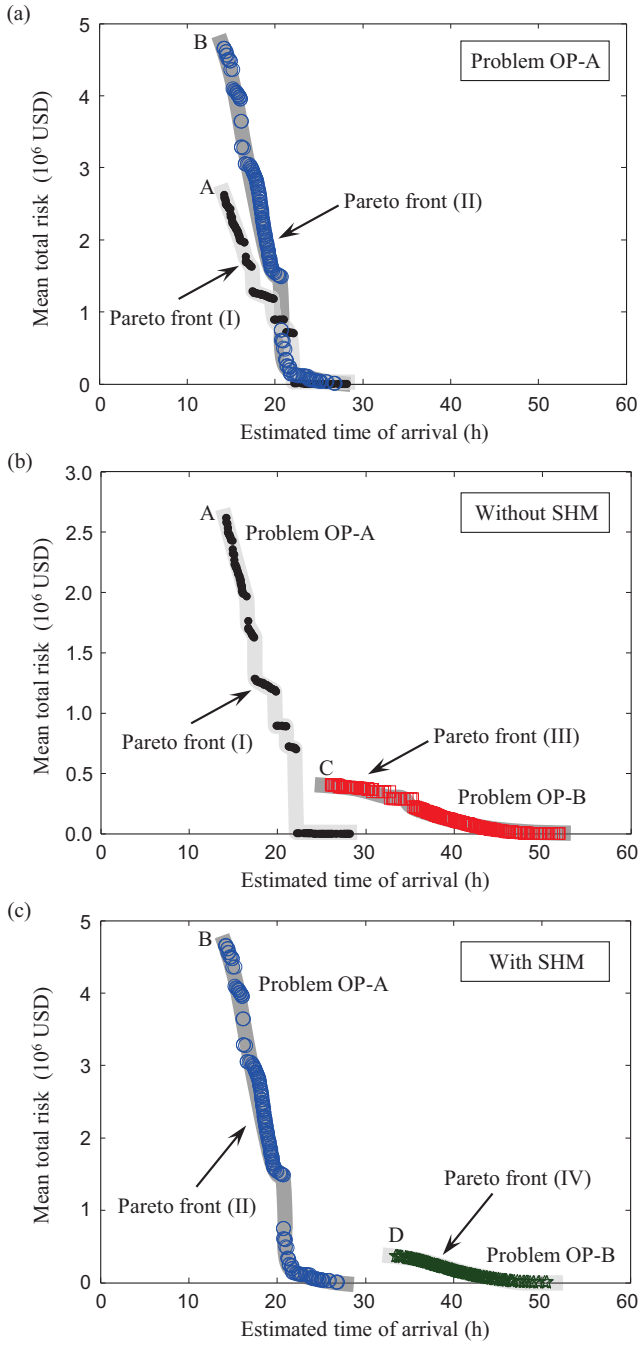

Figure 7.7 (a) Pareto fronts (I) and (II) of Table 7.2, obtained by solving OP-A. (b) Pareto fronts (I) and (III) of Table 7.2, without considering SHM and assuming $\beta_{threshold}$ and $R_{threshold}$ equal to 2.5 and 8×10^6 USD for front (III). (c) Pareto fronts (II) and (IV) of Table 7.2, considering SHM and assuming $\beta_{threshold}$ and $R_{threshold}$ equal to 2.5 and 8×10^6 USD for front (IV). Points A, B, C and D represent the fastest routes within the Pareto fronts (I), (II), (III), and (IV), respectively.

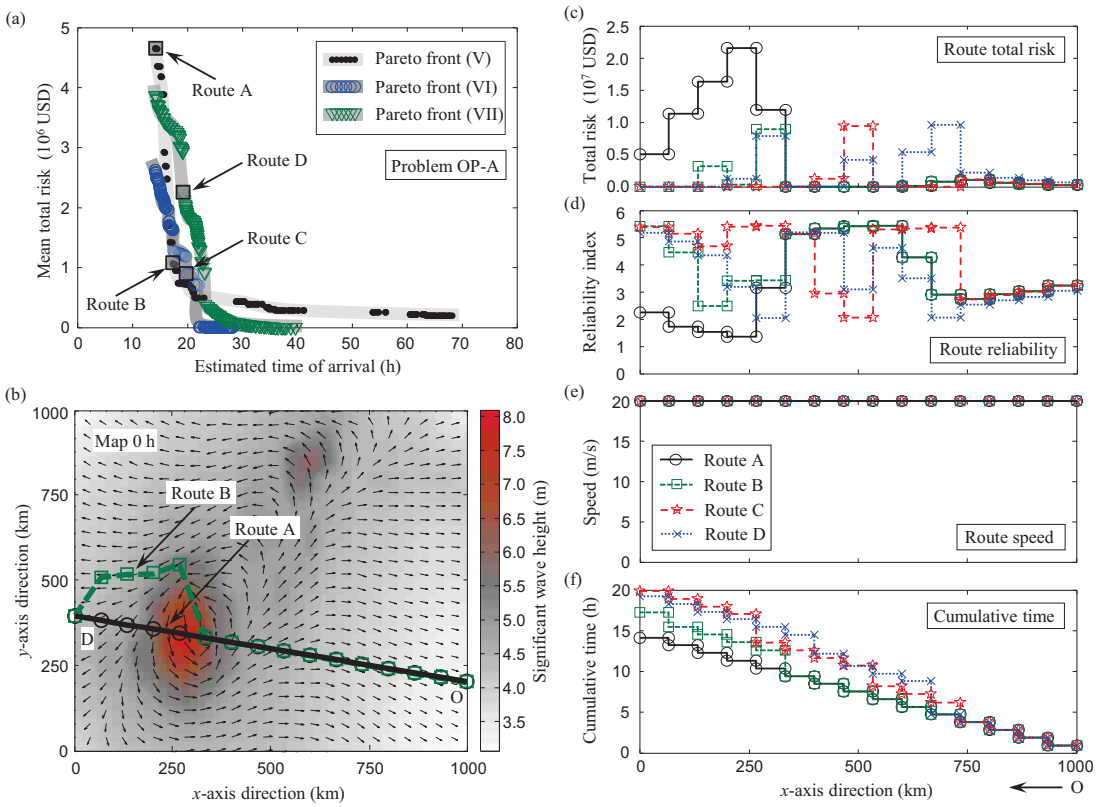

Figure 7.8 (a) Pareto fronts (V), (VI), and (VII) (in accordance with Table 7.2), obtained by solving OP-A. Four optimal routes called routes A, B, C, and D are selected. (b) Paths of the four selected routes A, B, C, and D. represented in the current sea map (0 h). Profiles of the four solutions, reporting on (c) route total risk (USD), (d) route reliability index associated with ultimate failure (*LS*4), (e) ship speed (m/s), and cumulative time from departure (h).

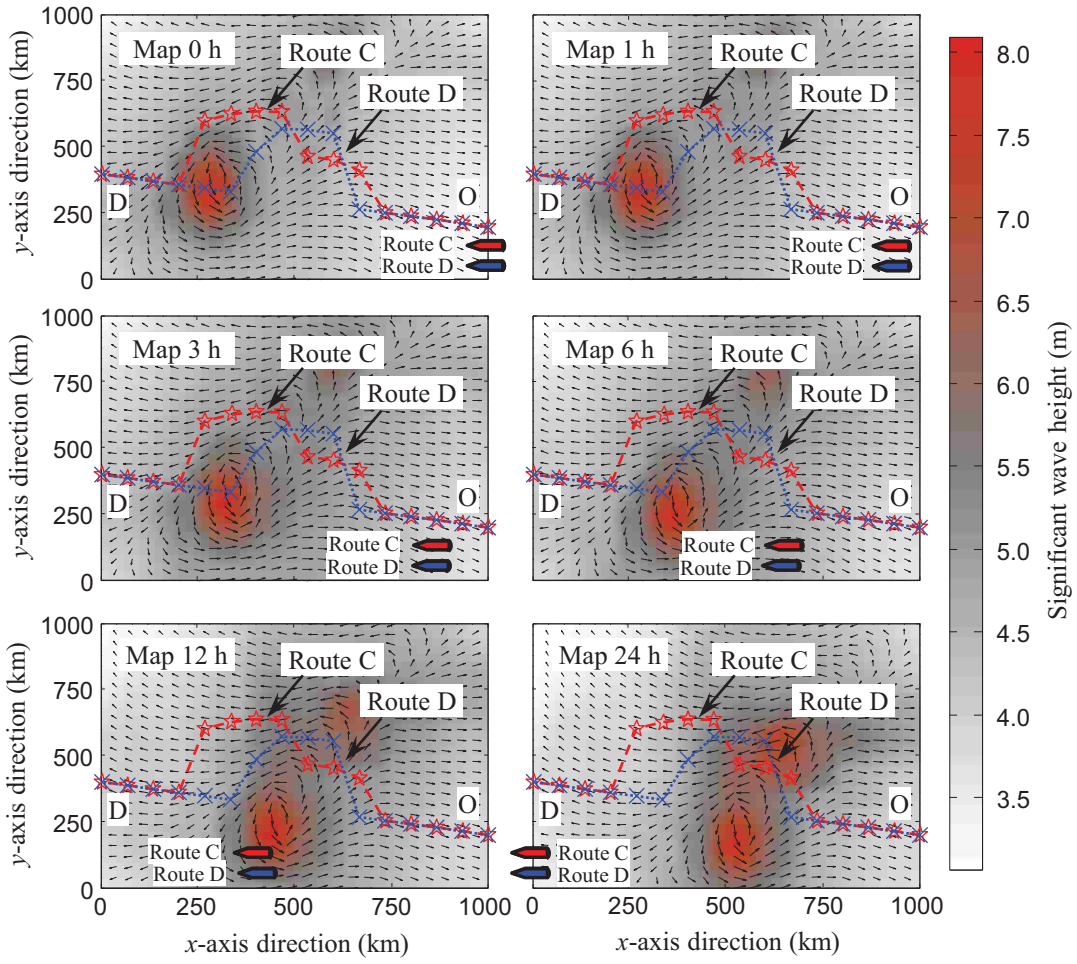

Figure 7.9 Paths associated with the selected optimal routes C and D of Figure 7.8(a). The two ship shaped symbols indicatively show the location of the ship with respect to the x-axis for the two considered routes.

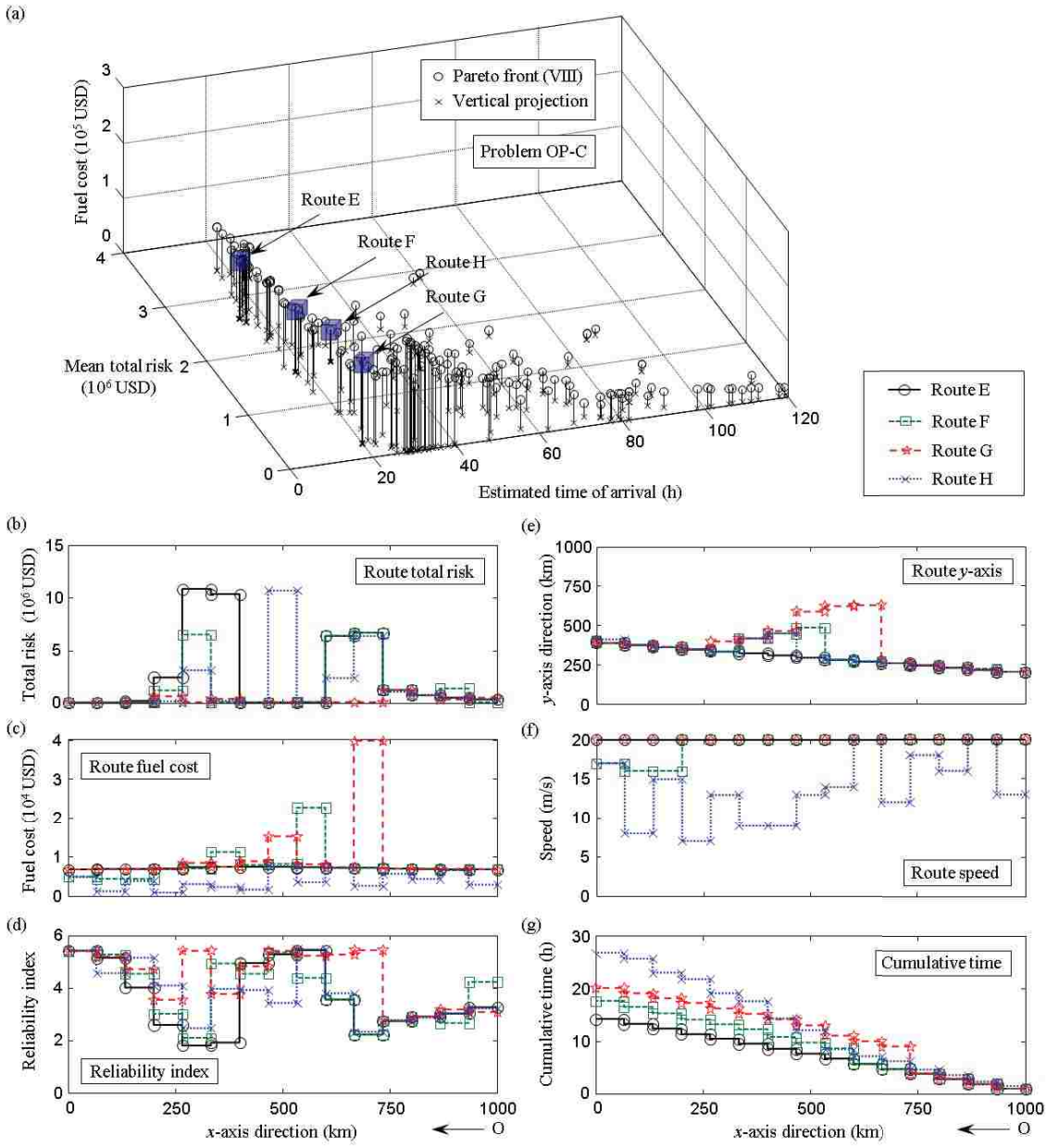

Figure 7.10 (a) Pareto fronts (VIII) of Table 7.2, obtained by solving OP-C. Four optimal routes called routes E, F, G, and H are selected. Profiles of the four solutions, reporting on (b) route total risk (USD), (c) fuel cost (USD), (d) route reliability index associated with ultimate failure (*LS*4), (e) route *y*-axis value (km), (f) ship speed (m/s), and cumulative time from departure (h).

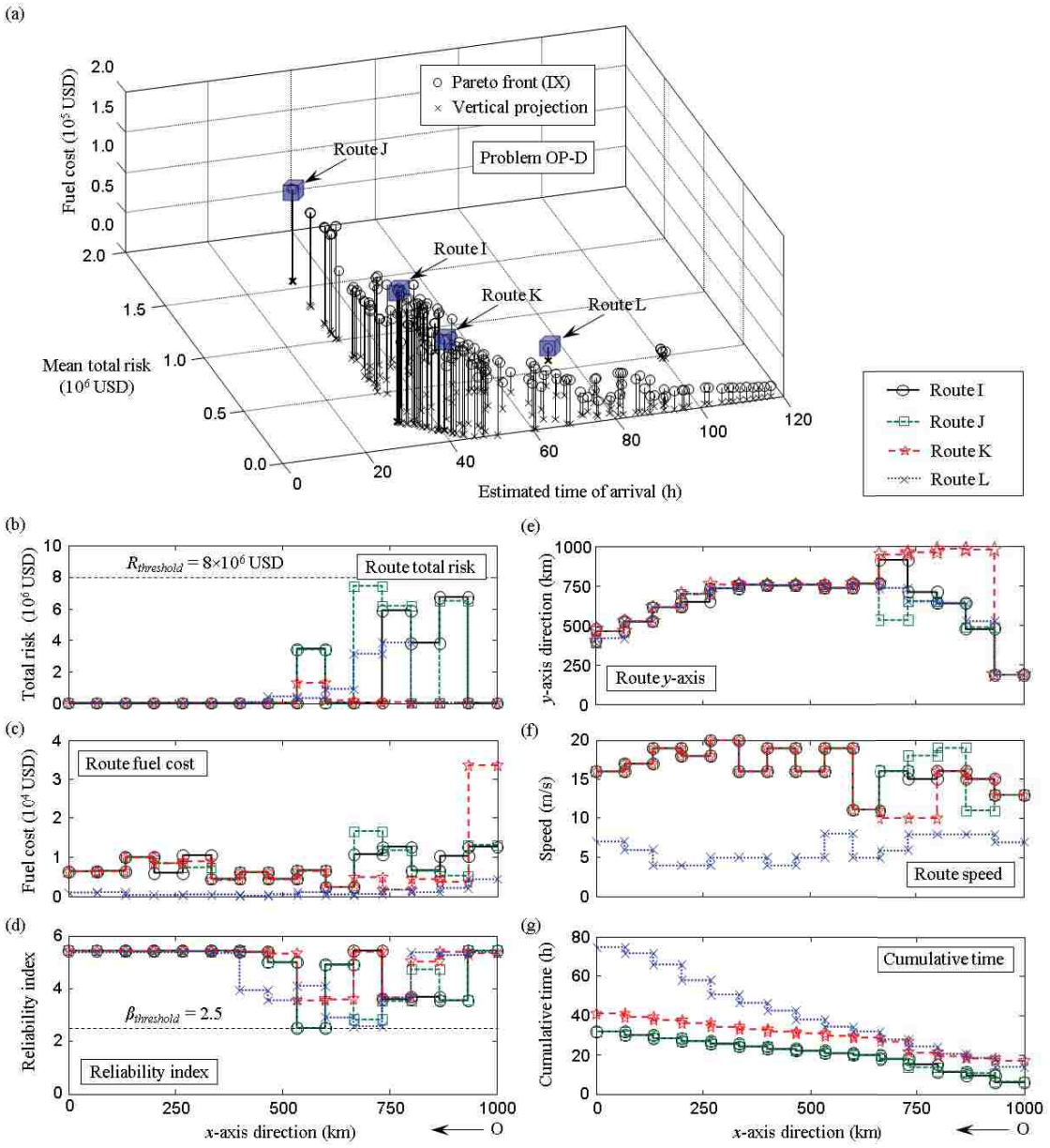

Figure 7.11 Pareto fronts (IX) of Table 7.2, obtained by solving OP-D and assuming $\beta_{threshold}$ and $R_{threshold}$ equal to 2.5 and 8×10^6 USD, respectively. Four optimal routes called routes I, J, K, and L are selected. Profiles of the four solutions, reporting on (b) route total risk (USD), (c) fuel cost (USD), (d) route reliability index associated with ultimate failure (*LS*4), (e) route y-axis value (km), (f) ship speed (m/s), and cumulative time from departure (h).

CHAPTER 8

SUMMARY, CONCLUSIONS AND RECOMMENDATIONS

8.1 SUMMARY

This study has developed a risk-informed approach for the life-cycle assessment and management of civil and marine structures with emphasis on single highway bridges, groups of bridges, and ship structures. The study is composed of two parts. Part I deals with the life-cycle management of single bridges and bridge groups based on risk, in which also a probabilistic tool for the prediction of resilience to disaster is presented. Part II proposes an optimality-based approach for the management of aging ship structures under different operational conditions and integrating structural health monitoring (SHM), considering reliability, redundancy, and risk as performance indicators.

In Chapter 2, a comprehensive computational approach for assessing the time-dependent risk as an indicator of the life-cycle performance has been presented. The effects of several hazards, including live loads, environmental attacks, scour, and earthquakes, on time-dependent structural failure probabilities and their associated consequences have been investigated. Moreover, redundancy has been considered into risk assessment by introducing a risk modifier coefficient. Epistemic and aleatory

uncertainties have been accounted for within quantitative risk assessment of structural systems and have been modeled for each step of risk assessment, including structural performance evaluation, analysis of the probability of occurrence of different types of hazards, and evaluation of the associated consequences due to the inadequacy of the structural system.

In Chapter 3, some important issues emerging from the life-cycle risk assessment of spatially distributed aging bridges within a transportation network have been investigated. The time-dependent effects of traffic and seismic hazards, for a group of aging bridges contained into an earthquake-prone region have been investigated. A detailed consequence analysis has been performed in order to evaluate the effects associated with different bridge limit states.

Chapter 4 has extended the existing deterministic model of resilience to disaster towards an approach for the probabilistic prediction of seismic resilience. The social impact in terms of direct and indirect costs has also been investigated. A spectrum of restoration strategies are studied based upon a model that describes the variation of functionality over time with emphasis on single highway bridges and bridge highway segments affected by earthquakes.

In Chapter 5 an efficient approach for the evaluation of ship reliability and redundancy including the effects of corrosion, allowing to investigate different operational conditions, has been presented. The strip method was used for the assessment of the response amplitude operator (RAO) of vertical bending moment (VBM) for three ship cross-sections and the probabilistic analysis of structural

responses for natural sea is conducted by investigating specific sea states, ship speeds and heading angles.

Chapter 6 has developed an approach for risk assessment, accounting for the consequences induced by different limit states. Risk has been used as a performance indicator with the purpose of evaluating the optimal routing of ships. Direct risk assessment of ships has been performed with respect to discrete hull damage states and for a large spectrum of operational conditions. Mission parameters such as ship speed and heading angle, structural reliability, estimated time of arrival (ETA), and traveled distance are assessed for the case of a ship traveling between two points given a sea weather map. Optimization has been performed in order to obtain the paths that minimize both risk and ETA for the case in which the ship is intact and when the effects due to corrosion are considered.

Chapter 7 has developed a comprehensive risk-based approach for near real-time optimal routing of ships integrating structural health monitoring data and considering weather prediction. Bayesian statistics have been used in order to update the prior information by using the collected SHM data, obtaining an improved (posterior) prediction. Both closed-form solution and simulation-based technique have been developed for the updating process. Moreover, different sea weather maps were integrated within the developed optimization framework. Two-objective and three-objective optimization problems were solved by minimizing (a) ETA and total risk, and (b) ETA, total risk, and fuel costs, respectively.

8.2 CONCLUSIONS

Among the specific conclusions drawn from each chapter of this thesis, only the most important are summarized in this section. From Part I (i.e. framework involving bridge structures), the following conclusions are drawn:

- The interpretation of the results given by the probability density function (PDF) of the time-to-failure associated with each considered hazard represents a valuable tool for the identification of the importance of hazards (i.e. from the highest to the lowest effects) affecting the bridge under investigation.
- While assessing risk, the level of detail in modeling the effects of a potential hazard must fit the importance of such hazard with respect to total risk. A highly detailed model is needed only for those hazards with significant contributions to the total risk.
- Bridge risk assessment is a process that carries significant epistemic and aleatory uncertainties generated by multiple sources such as the assessment of the bridge vulnerability and the consequences associated with bridge failure or malfunction. The treatment of such uncertainties in modeling the bridge performance over time requires exceptional care. It has been found that the dispersion of the time-dependent total risk increases over time.
- The investigation of the normalized indirect risk index provides useful information about the importance of the considered bridge. The effect of a potential failure mode may have great impact on the economy of the surrounding areas, causing indirect losses to be much greater than the direct ones over time.

- When life-cycle risk is assessed under multiple hazards, the predominant hazard must be adequately modeled in order to achieve reliable estimates of total risk. Therefore, if the investigated group of bridges is located within an earthquake-prone region, it is crucial to model the seismic hazard (earthquake scenarios) with a powerful tool such as the probabilistic ground motion and associated fragility analysis. It has been found that the only inclusion of risk induced by traffic hazard provides an incomplete analysis that may lead to a wrong decision process.
- As expected, it has been found that the risk induced by seismic hazard increases over time due to structural aging consideration and the predicted increment of the average daily traffic (ADT) over time. It has been found that the dispersion of seismic risk increases over time. The inclusion of epistemic uncertainties enhances the probabilistic model, but adds dispersion to the initial sample.
- According to the proposed framework, it is found that expected rehabilitation costs are greater than expected rebuilding costs. Whilst this is true in this case, this observation may change depending on the extent of damage and on the method of computation.
- The assessment of seismic resilience can be conducted in a probabilistic way by including uncertainty affecting both bridge vulnerability and recovery phase. The proper use of the parameters, within the used model, allows investigating several recovery processes associated with different levels of damage. The average functionality recovery heavily depends on the gain obtained by the rehabilitations associated with extensive and complete damages.

From Part II (i.e. framework involving ship structures), the following conclusions are drawn:

- The proposed polar representation for reliability and redundancy improves the interpretation of the structural safety level under specific operational conditions, helping the ship operator make appropriate decisions.
- It has been found that the impact of corrosion effects (ship aging) on reliability and redundancy is in general limited compared with the effects of specific critical operations.
- When the structural performance reaches critical threshold, the ship operations must be modified according to the residual structural safety by reducing the forward speed, or by changing the heading angle according to the obtained polar profiles.
- The results obtained from the optimization show that several solutions can be adopted depending on the acceptable risk and on the allowable ETA. All the solutions, except for the shortest and fastest one, provide directions that avoid the assumed storm in order to reduce direct risk.
- Aging effects lead to higher risk and optimal routes can be different than those made for intact ships. Different Pareto-optimal sets are obtained for two cases, highlighting the importance of this aspect in the decision making process.
- The developed closed-form solution for the updating process, based on the assumption that the peak responses follow the Rayleigh distribution, provides results that perfectly match those obtained by numerical simulation using the slicer

sampling. The profiles of load effects in terms of VBM and horizontal bending moment (HBM), reliability index, and risk have been consequently updated.

- It is found that near real-time decision making can be achieved by integrating SHM data with the prior performance information. If a permanent SHM system is installed, the proposed updating process would yield to real-time decision making.
- It is found that the optimization of three objectives (minimization of ETA, total risk, and fuel cost) provides a comprehensive set of optimal solutions. A higher fuel cost is generally associated with low risk, whereas the opposite is not always true. Moreover, solutions with high ETA are generally associated with low risk, due to longer routes necessary to avoid dangerous situations.
- It is also found that the Pareto fronts when weather prediction is considered have lower risk than those based on the current sea map only.

8.3 RECOMMENDATIONS FOR FUTURE WORK

The recommendations for future work related to Part I (involving bridge structures) are as follows:

- This study mainly focused on the assessment and prediction of the performance of existing structures. The developed approaches for risk assessment and resilience to disaster should be extended to new structures in order to achieve performance-based design.
- The proposed approach for the assessment of life-cycle risk of single highway bridges and bridge groups needs to be extended to bridge transportation networks

by including the effects of traffic redistribution in order to consider a more realistic network performance.

- The need of opinions and input from experts working in different fields are critical in order to provide the community with valuable and applicable research. Interdisciplinary research teams covering aspects related to transportation engineering, structural engineering, and economics, must be formed and interdisciplinary research teams incentivized.
- It is important to develop specific approaches for combining hazards (only if they are relevant) by evaluating their simultaneous or sequential effects on single bridges.
- For the prediction of seismic resilience, a comprehensive calibration of recovery curves covering different bridge classes and different rural and metropolitan areas is still missing in the existing literature. Only an extensive focus of future research can fill this lack of information leading to more accurate evaluations resilience.
- The probabilistic approach for resilience, applied to single highway bridges and bridge highway segments, has to be extended to existing transportation networks by considering real case studies.

For Part II (involving ship structures), the recommendations for future work are summarized as follows:

- Detailed analyses of dynamic effects induced by waves are not explicitly included into the reliability analysis of ship structures of this study because of computational limitations. Therefore, research is needed for the implementation of

dynamic effects such as whipping and springing through FE and Response Surface analyses.

- The proposed approach for optimal ship routing, that minimize risk, ETA, and fuel cost, must be extended in order to account for several other objectives such as ship movements, wave resistance, and other operating costs.
- Uncertainties associated with weather prediction are not considered in this study; therefore, they can be accounted for by developing an extension of the proposed approach for optimal ship routing.
- Although it is recognized that the flexural failure mode of the hull midship section is the critical mode, time-variant redundancy and risk should be investigated also for different failure modes such as shear and torsional moments.

REFERENCES

AASHTO (2003). *A Manual of User Benefit Analysis for Highways*. 2nd Edition, American Association of State Highway and Transportation Officials (AASHTO), Washington, DC, 288p

AASHTO (2007). *LRFD Bridge Design Specifications*. 4th Edition, American Association of State Highway and Transportation Officials (AASHTO), Washington, DC.

ABS (2010). *Guidance Notes on Springing Assessment for Container Carriers*. American Bureau of Shipping (ABS), Houston, TX.

Adey, B., Hajdin, R. and Brühwiler, E. (2003). Risk-Based Approach to the Determination of Optimal Interventions for Bridges Affected by Multiple Hazards. *Engineering Structures*, Elsevier, 25(7), 903–912.

Akgül, F. (2002). *Lifetime System Reliability Prediction for Multiple Structure Types in a Bridge Network*. PhD Thesis, University of Colorado at Boulder, Boulder, CO.

Akiyama, M., Frangopol, D.M. and Matsuzaki, H. (2011). Life-Cycle Reliability of RC Bridge Piers under Seismic and Airborne Chloride Hazards. *Earthquake Engineering & Structural Dynamics*, John Wiley & Sons, 40(15), 1671–1687.

Akpan, U.O., Koko, T.S., Ayyub, B. and Dunbar, T.E. (2002). Risk Assessment of Aging Ship Hull Structures in the Presence of Corrosion and Fatigue. *Marine Structures*, Elsevier, 15(3), 211–31.

Albrecht, P. and Naeemi, A. (1984). *Performance of Weathering Steel in Bridges*. NCHRP Report 272, Washington, DC.

Ang, A. H-S and Tang, W.H. (1984). *Probability Concepts in Engineering Planning and Design: Decision, Risk and Reliability*. Vol. II, John Wiley & Sons, New York City, NY, 562p.

Ang, A. H-S, (2010). Significance of Uncertainty in the Calculation of Risk and Reliability – Emphasis on Decisions for Protection against Natural Hazards. *International Symposium on Reliability Engineering and Risk Management (ISRERM2010)*, Sept. 23–26, 2010, Shanghai, China. CD-ROM.

Ang, A.H-S and de Leon, D. (2005). Modeling and Analysis of Uncertainties for Risk-Informed Decisions in Infrastructures Engineering. *Structure and Infrastructure Engineering*, Taylor & Francis, 1(1), 19–31.

Ang, H-S. A. and Tang, W.H. (2007). *Probability Concepts in Engineering: Emphasis on Applications to Civil and Environmental Engineering*. 2nd Edition, Wiley and Sons, New York City, NY, 406p.

Anscombe, F.J. (1961). Bayesian Statistics. *American Statistician*, Taylor & Francis, 15(1), 21–24.

Arora, J.S. (2004). *Introduction to Optimum Design*. Elsevier Academic Press, 728p.

ATC (1985). *Earthquake Damage Evaluation Data for California*. Technical Report ATC-13, Applied Technology Council (ATC), Redwood City, CA.

Ayyub, B.M., Akpan, U.O., Rushton, P.A. and Koko, T.S. (2002). *Risk-Informed Inspection of Marine Vessels*. Ship Structure Committee: SSC-421.

Ayyub, B.M., Assakkaf, I.A. and Atua, K.I. (2000). Reliability-Based Load and Resistance Factor Design (LRFD) of Hull Girders for Surface Ships. *Naval Engineers Journal*, John Wiley & Sons, 112(4), 279–296.

Ayyub, B.M., Assakkaf, I.A., Atua, K.I., Engle, A., Hess, P.E., Karaszewski, Z., Kihl, D., Melton, W., Sielski, R.A., Sieve, M., Waldman, J. and White, G.J. (1998). *Reliability-Based Design of Ship Structures: Current Practice and Emerging Technologies*. Research Report to the US Coast Guard, SNAME, T&R Report R-53.

Bai, Y. (2003). *Marine Structural Design*. Elsevier, Amsterdam, The Netherlands, 626p.

Baker, J.W., Schubert, M. and Faber, M.H. (2008). On the Assessment of Robustness. *Structural Safety*, Elsevier, 30(3), 253–267.

Basöz, N., and Mander, J. (1999). *Enhancement of the Highway Transportation Lifeline Module in HAZUS*, National Institute of Building Sciences (NIBS), Washington, DC.

Basu, R.I., Kirkhope, K.J. and Srinivasan, J. (1996). *Guideline for Evaluation of Finite Elements and Results*. Ship Structure Committee: SSC-387.

Bea, R.G. (2001). Risk Assessment and Management of Offshore Structures. *Progress in Structural Engineering and Materials*, John Wiley & Sons, 3(2), 180–187.

Bertram, V., Söding, H. and Graf, K. (2006). *PDSTRIP* – A strip method for ship and yacht seakeeping. *9th Numerical Towing Tank Symposium*, 1–3 October, 2006, Le Croisic, France.

Bidlot, J.R., Janssen, P. and Abdalla, S. (2006). Extreme Waves in the ECMWF Operational Wave Forecasting System. *9th International Workshop on Wave Hindcasting and Forecasting*, September 24-29, 2006, Victoria, Canada.

Blockley, D.I. (1999). Risk Based Structural Safety Methods in Context. *Structural Safety*, Elsevier, 21(4), 335–48.

Bocchini, P. and Frangopol, D.M. (2011a). Generalized Bridge Network Performance Analysis with Correlation and Time-Variant Reliability. *Structural Safety*, Elsevier, 33(2), 155–164.

Bocchini, P. and Frangopol, D.M. (2011b). Resilience-Driven Disaster Management of Civil Infrastructure. *In Computational Methods in Structural Dynamics and Earthquake Engineering (M. Papadrakakis, M. Fragiadakis, V. Plevris eds.)*, Third International Conference on Computational Methods in Structural Dynamics and Earthquake Engineering COMPDYN 2011, May 26-28, Corfu, Greece, 2011.

Bocchini, P. and Frangopol, D.M. (2012a). Optimal Resilience- and Cost-Based Post-Disaster Intervention Prioritization for Bridges along a Highway Segment. *Journal of Bridge Engineering*, ASCE, 17(1), 117–129.

Bocchini, P. and Frangopol, D.M. (2012b). Restoration of Bridge Networks After an Earthquake: Multi-Criteria Intervention Optimization. *Earthquake Spectra*, EERI, 28(2), 426–455.

Bocchini, P. and Frangopol, D.M. (2013). Connectivity-Based Optimal Scheduling for Maintenance of Bridge Networks. *Journal of Engineering Mechanics*, ASCE, 139(6), DOI: 10.1061/(ASCE)EM.1943-7889.0000271.

Bocchini, P., Decò, A. and Frangopol, D.M. (2012). Probabilistic Functionality Recovery Model for Resilience Analysis. *In Bridge Maintenance, Safety, Management, Resilience and Sustainability (Biondini F and Frangopol, DM eds.)*, IABMAS'12, July 8–12, 2012, Stresa, Italy, Taylor and Francis, Abingdon, UK, pp. 1920–1927.

Brown, G.G., Graves, G.W. and Ronen, D. (1987). Scheduling Ocean Transportation of Crude Oil. *Management Science*, INFORMS, 33(3), 335–346.

Bruneau, M. and Reinhorn, A. (2007). Exploring the Concept of Seismic Resilience for Acute Care Facilities. *Earthquake Spectra*, EERI, 23(1), 41–62.

Bruneau, M., Chang, S.E., Eguchi, R.T., Lee, G.C., O'Rourke, T.D., Reinhorn, A.M., Shinozuka, M., Tierney, K., Wallace, A.W. and von Winterfeldt, D. (2003). A Framework to Quantitatively Assess and Enhance the Seismic Resilience of Communities. *Earthquake Spectra*, EERI, 19(4), 733–752.

Bucher, C. (2009). *Computational Analysis of Randomness in Structural Mechanics*. Vol. 3, Structures & Infrastructures Series, Frangopol, D.M., editor, Taylor & Francis, Leiden, The Netherlands.

Bucher, C.G. and Bourgund, U. (1990). A Fast and Efficient Response Surface Approach for Structural Reliability Problems. *Structural Safety*, Elsevier, 7, 57–66.

Bureau of Public Roads (1964). *Traffic Assignment Manual*. U.S. Department of Commerce, Urban Planning Division, Washington DC.

Caltrans (2009). *California Life-Cycle Benefit/Cost Analysis Model (Cal-B/C)*. Volume 3, California Department of Transportation, Sacramento, CA.

Caltrans (2010). *Comparative Bridge Costs*. California Department of Transportation, Sacramento, CA.

Campbell, K.W. and Bozorgnia, Y. (2007). *Campbell-Bozorgnia NGA Ground Motion Relations for the Geometric Mean Horizontal Component of Peak and Spectral Ground Motion Parameters*. Report 2007/02, Pacific Earthquake Engineering Research Center (PEER), University of California, Berkeley, CA.

CCS (2005). *Guidelines for Direct Strength analysis of Container Ship*. GD05-2005, China Classification Society (CCS), Beijing, China, 41p.

Cesare, M., Santamarina, J.C., Turkstra, C.J. and Vanmarcke, E. (1993). *Risk-Based Bridge Management*. *Journal of Transportation Engineering*, ASCE, 119(5), 742–750.

Chang, L., Peng, F., Ouyang, Y., Elnashai, A.S. and Spencer, B.F. Jr. (2012). Bridge Seismic Retrofit Program Planning to Maximize Postearthquake Transportation Network Capacity. *Journal of Infrastructure Systems*, ASCE, 18(2), 75–88.

Chang, S.E. and Shinozuka, M. (2004). Measuring Improvements in the Disaster Resilience of Communities. *Earthquake Spectra*, EERI, 20(3), 739–755.

Chang, S.E., Shinozuka, M. and Moore, J.E. (2000). Probabilistic Earthquake Scenarios: Extending Risk Analysis Methodologies to Spatially Distributed Systems. *Earthquake Spectra*, EERI, 16(3), 557–572.

Chopra, A.K. (2006). *Dynamics of Structures*, 3rd Edition, Prentice Hall, Upper Saddle River, NJ, 912p.

CIB (2001). *Risk Assessment and Risk Communication in Civil Engineering*. Report 259, TG 32, International Council for Research and Innovation in Building and Construction (CIB), Rotterdam, The Netherlands.

Cimellaro, G.P., Reinhorn, A.M. and Bruneau, M. (2010). Seismic Resilience of a Hospital System. *Structure and Infrastructure Engineering*, Taylor & Francis, 6(1-2), 127–144.

Coles, S.G. and Powell, E.A. (1996). Bayesian Methods in Extreme Value Modelling: a Review and New Developments. *International Statistical Review*, John Wiley & Sons, 64(1), 119–136.

Cornell, C.A. (1967). Bounds on the Reliability of Structural Systems. *Journal of Structural Division*, ASCE, 93(ST1), 171–200.

Cornell, C.A. (1968). Engineering Seismic Risk Analysis. *Bulletin of Seismological Society of America*, SSA, 58(5), 1583–1606.

Cosentino, P., Ficara, V. and Luzio, D. (1977). Truncated Exponential Frequency-Magnitude Relationship in the Earthquake Statistics. *Bulletin of Seismological Society of America*, SSA, 67(6), 1615–1623.

CSI (2009). *SAP2000 Educational 14.1.0 – Analysis Reference*. Computers and Structures Inc. (CSI), Berkeley, CA.

Das, P.C. and Pardi, L. (2001). Optimum Maintenance Strategies for Trunk Road Bridges in England and Italy. In *Current and future trends in bridge design, construction and maintenance 2*, Das PC, Frangopol DM and Nowak AS (eds). Thomas Telford Ltd, London, UK, 341–348.

Dassault Systèmes Simulia (2011). *ABAQUS/Standard Version 6.11 User's Manuals*. Dassault Systèmes Simulia Corp., Providence, RI.

Deb, K. (2001). *Multi-Objective Optimization Using Evolutionary Algorithms*. John Wiley & Sons, New York City, NY, 518p.

Decò, A. and Frangopol, D.M. (2010). Deterioration and Maintenance of RC Bridge Decks under Uncertainty: Condition and Reliability Indicators. *In Bridge Maintenance, Safety and Management, IABMAS'10 (Frangopol, Sause and Kusko Eds.)*, Proceedings of the Fifth International IABMAS Conference, Philadelphia, PA, July 11–15, 2010, CRC Press (CD-ROM, 3133–3140).

Decò, A. and Frangopol, D.M. (2011). Risk Assessment of Highway Bridges under Multiple Hazards. *Journal of Risk Research*, Taylor & Francis, 14(9), 1057–1089.

Decò, A. and Frangopol, D.M. (2012). Lifetime Risk Assessment of Bridges Affected by Multiple Hazards. *In Bridge Maintenance, Safety, Management, Resilience and Sustainability (Biondini F and Frangopol, DM eds.)*, Taylor and Francis, London, UK, CD-ROM, pp. 2922-2929. Sixth International Conference on Bridge Maintenance, Safety and Management, IABMAS, July 8–12, 2012, Stresa, Italy.

Decò, A. and Frangopol, D.M. (2013a). Life-Cycle Risk Assessment of Spatially Distributed Aging Bridges under Seismic and Traffic Hazards. *Earthquake Spectra*, EERI, 29(1), 127–153.

Decò, A. and Frangopol, D.M. (2013b). Risk-Informed Optimal Routing of Ships Considering Different Damage Scenarios and Operational Conditions. *Reliability Engineering and System Safety*, Elsevier, 19, 126–140.

Decò, A. and Frangopol, D.M. (2013c). Near Real-Time Multi-Criteria Optimal Ship Routing Integrating Risk and Structural Health Monitoring, (submitted).

Decò, A., Bocchini, P. and Frangopol, D.M. (2013). A Probabilistic Approach for the Prediction of Seismic Resilience of Bridges. *Earthquake Engineering & Structural Dynamics*, John Wiley & Sons, DOI: 10.1002/eqe.2282 (in press).

Decò, A., Frangopol, D.M. and Bocchini, P. (2013). Pre-Event Probabilistic Assessment of Seismic Resilience of Bridge Highway Segments. In *Safety, Reliability, Risk and Life-Cycle Performance of Structures and Infrastructures (G. Deodatis, B.R. Ellingwood, D. M. Frangopol eds.)*, CRC Press, Taylor and Francis Group, London, UK. *11th International Conference on Structural Safety & Reliability*, June 16–20, 2013, New York City, NY.

Decò, A., Frangopol, D.M. and Okasha, N.M. (2011). Time-Variant Redundancy of Ship Structures. *Journal of Ship Research*, SNAME, 55(3), 208–219.

Decò, A., Frangopol, D.M. and Okasha, N.M. (2012). *Time-Variant Redundancy of Ship Structures*. Transactions of SNAME, Vol. 119, 28–47.

Decò, A., Frangopol, D.M. and Zhu, B. (2012). Reliability and Redundancy Assessment of Ships under Different Operational Conditions. *Engineering Structures*, Elsevier, 42, 457–471.

Deschamps, L. and Greenwell, C. (2009). *Integrating Cost Estimating with the Ship Design Process*. SPAR Associates, Inc., Annapolis, MD.

Devine, E.A. (2009). *An Overview of the Recently-Completed JHSS Monohull and Trimaran Structural Seaways Loads Test Program*. Naval Surface Warfare Center,

Carderock Division (NSWCCD), West Bethesda, MD, PowerPoint Briefing, 30 October, 2009.

Dinovitzer, A. (2003). *Life Expectancy Assessment of Ship Structures*. Ship Structure Committee: SSC-427.

Ditlevsen, O. (1979). Narrow Reliability Bounds for Structural Systems. *Journal of Structural Mechanics*, ASCE, 7(4), 453–472.

Dolinskaya, I.S., Kotinis, M., Parsons, M.G. and Smith, R.L. (2009). Optimal Short-Range Routing of Vessels in a Seaway. *Journal of Ship Research*, SNAME, 53(2), 1–9.

DOT-FL (2009). *Transportation Costs Report*. State of Florida - Department of Transportation (DOT-FL), Tallahassee, FL.

Drummen, I., Wu, M. and Moan, T. (2009). Experimental and Numerical Study of Containership Responses in Severe Head Seas. *Marine Structures*, Elsevier, 22(2), 172–193.

ECMWF (2013). *European Centre for Medium-Range Weather Forecasts (ECMWF)*, Reading, UK. Website: http://www.ecmwf.int/, (accessed March 2013).

Ellingwood, B.R. (2001). Acceptable Risk Bases for Design of Structures. *Progress in Structural Engineering and Materials*, John Wiley & Sons, 3(2), 170–179.

Ellingwood, B.R. (2005). Risk-Informed Condition Assessment of Civil Infrastructure: State of Practice and Research Issues. *Structure and Infrastructure Engineering*, Taylor & Francis, 1(1), 7–18.

Ellingwood, B.R. and Wen, Y.K. (2005). Risk-Benefit Based Design Decisions for Low Probability/High Consequence Earthquake Events in Mid-America. *Progress in Structural Engineering and Materials*, John Wiley & Sons, 7(2), 56–70.

Engius (2002). *Case Study: Interstate 40 Bridge Reconstruction*. Webbers Falls, Oklahoma. Engius, Stillwater, OK, 2002. Webpage: http://www.engius.com.

Estes, A.C. (1997). *A System Reliability Approach to the Lifetime Optimization of Inspection and Repair of Highway Bridges*. PhD Thesis, University of Colorado, Boulder, CO.

Estes, A.C. and Frangopol, D.M. (1998). RELSYS: A Computer Program for Structural System Reliability Analysis. *Structure Engineering and Mechanics*, Techno Press, 6(8), 901–919.

Estes, A.C. and Frangopol, D.M. (1999). Repair Optimization of Highway Bridges using System Reliability Approach. *Journal of Structural Engineering*, ASCE, 125(7), 766–775.

Fagerholt, K., Laporte, G. and Norstad, I. (2010). Reducing Fuel Emissions by Optimizing Speed on Shipping Routes. *Journal of the Operational Research Society*, Macmillan Publishers, 61, 523–529.

Faltinsen, O.M. (1990). *Sea Loads on Ships and Offshore Structures*. Cambridge University Press, Cambridge, UK, 328p.

FEMA (2009a). *HAZUS-MH MR4 - Earthquake Model User Manual*. Department of Homeland Security, Federal Emergency Management Agency, Washington, DC.

FEMA (2009b). *HAZUS-MH MR4 - Earthquake Model Technical Manual*. Department of Homeland Security, Federal Emergency Management Agency, Washington, DC.

FHWA (1995). *Recording and Coding Guide for the Structure Inventory and Appraisal of the Nation's Bridges*. Report No. FHWA-PD-96-001, U.S. Department of Transportation, Federal Highway Administration (FHWA), Washington, DC.

FHWA (2009). *National Bridge Inventory (NBI) Database*. U.S. Department of Transportation, Federal Highway Administration (FHWA), Washington, DC. Webpage: www.fhwa.dot.gov/bridge/nbi.htm.

FHWA (2010). *National Bridge Inventory (NBI) Database*. U.S. Department of Transportation, Federal Highway Administration (FHWA), Washington, DC. Webpage: www.fhwa.dot.gov/bridge/nbi.htm.

FHWA (2011a). *Deficient Bridges by State and Highway System 2011 - National Bridge Inventory (NBI) database*. Federal Highway Administration (FHWA), Washington, DC. Webpage: http://www.fhwa.dot.gov/bridge/nbi/defbr11.cfm.

FHWA (2011b). *Additional Guidance on NS 23 CFR, Part 650 D*. Federal Highway Administration (FHWA), Washington, DC. Webpage: http://www.fhwa.dot.gov/bridge/0650dsup.cfm.

Fink D. (1997). *A Compendium of Conjugate Priors*. In Progress Report: Extension and enhancement of methods for setting data quality objectives, DOE contract 95-831.

Frangopol, D.M. (2011). Life-Cycle Performance, Management, and Optimization of Structural Systems under Uncertainty: Accomplishments and Challenges. *Structure and Infrastructure Engineering*, Taylor & Francis, 7(6), 389–413.

Frangopol, D.M. and Bocchini, P. (2011). Resilience as Optimization Criterion for the Rehabilitation of Bridges Belonging to a Transportation Network Subject to Earthquake. *Proceedings of the ASCE 2011 Structures Congress SEI 2011 (Ames, Droessler and Hoit Eds.)*, Las Vegas, NV, 2011, 2044–2055.

Frangopol, D.M. and Bocchini, P. (2012). Bridge Network Performance, Maintenance and Optimization under Uncertainty: Accomplishments and Challenges, *Structure and Infrastructure Engineering*, Taylor & Francis, 8(4), 341–356.

Frangopol, D.M. and Curley, J.P. (1987). Effects of Damage and Redundancy on Structural Reliability. *Journal of Structural Engineering*, ASCE, 113(7), 1533–1549.

Frangopol, D.M. and Liu, M. (2007). Maintenance and Management of Civil Infrastructure Based on Condition, Safety, Optimization, and Life-Cycle Cost. *Structure and Infrastructure Engineering*, Taylor & Francis, 3(1), 29–41.

Frangopol, D.M. and Nakib, R. (1991). Redundancy in Highway Bridges. *Engineering Journal*, AISC, 28(1), 45–50.

Frangopol, D.M. and Okasha, N.M. (2008). Probabilistic Measures for Time-Variant Redundancy. *Proceedings of Inaugural International Conference of the Engineering Mechanic Institute EM08*, ASCE, May 18–21, University of Minnesota, Minneapolis, MN, (CD-ROM).

Frangopol, D.M., Bocchini, P., Decò, A., Kim, S., Kwon, K., Okasha, N.M. and Saydam, D. (2011a). Integrated Life-Cycle Framework for Maintenance, Monitoring, and Reliability of Naval Ship Structures. *Proceedings of Fleet Maintenance & Modernization Symposium FMMS 2011*, San Diego, CA, August 30–31, 2011.

Frangopol, D.M., Bocchini, P., Decò, A., Kim, S., Kwon, K., Okasha, N.M., Saydam, D. and Salvino, L.W.. (2011b). Life-Cycle Ship Reliability Assessment, Damage Detection, and Optimization. *Proceeding of the eleventh international conference on fast sea transportation FAST 2011 (Peltzer Ed.)*, ASNE, September 26–29, 2011, Honolulu, HI, 555–560.

Frangopol, D.M., Bocchini, P., Decò, A., Kim, S., Kwon, K., Okasha, N.M. and Saydam, D. (2012). Integrated Life-Cycle Framework for Maintenance, Monitoring, and Reliability of Naval Ship Structures. *Naval Engineers Journal*, ASNE, 124(1), 89–99.

Frangopol, D.M., Kallen, M-J and van Noortwijk, J.M. (2004). Probabilistic Models for Lifecycle Performance of Deteriorating Structures: Review and Future Directions. *Progress in Structural Engineering and Materials*, John Wiley & Sons, 6(4), 197–212.

FREE!ship (2006). *FREE!ship Manual – Version 2.6*. Webpage: http://www.freeship.org [accessed October 2011].

Gelman, A., Carlin, J., Stern, H. and Rubin, D. B. (2003). *Bayesian Data Analysis*. 2nd edition. Chapman & Hall/CRC, Boca Raton, FL, 696 p.

Ghosh, J. and Padgett, J.E. (2010). Aging Considerations in the Development of Time-Dependent Seismic Fragility Curves. *Journal of Structural Engineering*, ASCE, 136(12), 1497–1511.

Ghosn, M., Moses, F. and Frangopol, D.M. (2010). Redundancy and Robustness of Highway Bridge Superstructures and Substructures. *Structure and Infrastructure Engineering*, Taylor & Francis, 6(1–2), 257–78.

Gibbons, A.M. (1985). *Algorithmic Graph Theory*. Cambridge University Press, Cambridge, UK, 514p.

Glen, I.F., Paterson, R.B. and Luznik, L. (1999). *Sea Operational Profiles for Structural Reliability Assessment*. Ship Structure Committee: SSC-406.

Goldberg, D.E. (1989). *Genetic Algorithms in Search, Optimization, and Machine Learning*. Addison-Wesley, Boston, MA, 432p.

Golroo, A., Mohaymany, A.S. and Mesbah, M. (2010). Reliability Based Investment Prioritization in Transportation Networks. *Proceedings of the 89th annual meeting of the Transportation Research Board of the National Academies*, Washington, DC, 10–14 January, 2010, (CD-ROM).

Google Inc. (2011). *Google Earth, release 6.1.0.5001*. Keyhole Inc. & Google Inc., Menlo Park, CA.

Gordo, J.M. and Guedes Soares, C. (1996). Approximate Methods to Evaluate the Hull Girder Collapse Strength. *Marine Structures*, Elsevier, 9(3), 449–470.

Gordo, J.M. and Guedes Soares, C. (1997). Interaction Equation for the Collapse of Tankers and Containership under Combined Bending Moments. *Journal of Ship Research*, SNAME, 41(3), 230–240.

Guedes Soares, C. (1992). Combination of Primary Load Effects in Ship Structures. *Probabilistic Engineering Mechanics*, Elsevier, 7(2), 103–111.

Guedes Soares, C. and Garbatov, Y. (1999). Reliability of Maintained Ship Hulls Subjected to Corrosion and Fatigue under Combined Loading. *Journal of Constructional Steel Research*, Elsevier, 52(1), 93–115.

Guedes Soares, C. and Teixeira, A.P. (2000). Structural Reliability of two Bulk Carrier Designs. *Marine Structures*, Elsevier, 13(2), 107–128.

Hinnenthal, J. (2008). *Robust Pareto – Optimum Routing of Ships utilizing Deterministic and Ensemble Weather Forecasts*. PhD Thesis, Berlin Institute of Technology, Berlin, Germany.

Hørte, T., Wang, G. and White, N. (2007). Calibration of the Hull Girder Ultimate Capacity Criterion for Double Hull Tankers. *Proceeding of the 10th International Symposium on Practical Design of Ships and Other Floating Structures*, American Bureau of Shipping ABS, Houston, Texas, Vol. 1, pp. 553–564.

Hu, Y., Cui, W. and Pedersen, P.T. (2004). Maintained Ship Hull Girder Ultimate Strength Reliability Considering Corrosion and Fatigue. *Marine Structures*, Elsevier, 17(2), 91–123.

Hughes, O.F. (1983). *Ship Structural Design: A Rationally-Based, Computer-Aided, Optimization Approach*. John Wiley & Sons, New York City, NY, 582p.

Hussein, A.W. and Guedes Soares, C. (2009). Reliability and Residual Strength of Double Hull Tankers Designed According to the New IACS Common Structural Rules. *Ocean Engineering*, Elsevier, 36(17-18), 1446–1459.

IACS (2008). *Common Structural Rules for Double Hull Oil Tankers*. International Association of Classification Societies (IACS), London, UK.

IMO (1997). *Interim Guidelines for the Application of Formal Safety Assessment (FSA) to the IMO Rule-Making Process*. MSC/Circ. 829 and MEPC/Circ. 335, International Maritime Organization (IMO), London, UK.

IMO (2006). *Goal-Based New Ship Construction Standards. Submitted by the International Association of Classification Societies (IACS)*. MSC 81/INF.6, International Maritime Organization (IMO), London, UK.

IUMI (2012). *Hull Fact Sheet*. IUMI Facts & Figures Committee, International Union of Marine Insurance (IUMI), Hamburg, Germany.

JCSS (2008). *Risk Assessment in Engineering - Principles, system representation & risk criteria*. Edited by Faber, M.H., Joint Committee on Structural Safety (JCSS).

Jones, T., Middelmann, M. and Corby, N. (2005). *Natural Hazard Risk in Perth, Western Australia*. GeoCat No. 63527, Geoscience Australia, Canberra, Australia.

Journée, J.M.J. and Meijers, J.H.C. (1980). *Ship Routeing for Optimum Performance. Transactions IME*. Conference on Operation of Ships in Rough Weather, The Institute of Marine Engineering, Science & Technology, London, UK, 56p

Kattell, J. and Eriksson, M. (1998). *Bridge Scour Evaluation: Screening, Analysis, & Countermeasures*. United States Department of Agriculture (USDA) - Forest Service, Washington, DC.

Kay, S.M. (1993). *Fundamentals of Statistical Signal Processing*. Prentice Hall, Upper Saddle River, NJ, 672p.

Kim, S. and Frangopol, D.M. (2011). Optimum Inspection Planning for Minimizing Fatigue Damage Detection Delay of Ship Hull Structures. *International Journal of Fatigue*, Elsevier, 33(3), 448–459.

Korvin-Kroukowski, B.V. and Jacobs, W.R. (1957). *Pitching and Heaving Motions of a Ship in Regular Waves*. Transactions of SNAME, Vol. 65, 590–632.

Kwon, K. and Frangopol, D.M. (2012). System Reliability of Ship Hull Structures under Corrosion and Fatigue. *Journal of Ship Research*, SNAME, 56(4), 234–251.

Kwon, K., Frangopol, D.M. and Kim, S. (2013). Fatigue Performance Assessment and Service Life Prediction of High-Speed Ship Structures based on Probabilistic Lifetime Sea Loads. *Structure and Infrastructure Engineering*, Taylor & Francis, 9(2), 102–115.

Kyriakidis, P.C. (2005). Sequential Spatial Simulation using Latin Hypercube Sampling. *Geostatistics Banff 2004: Seventh International Geostatistics Congress (Leuangthong and Deutsch Eds.)*, Quantitative Geology and Geostatistics, Kluwer Academic Publishers, Dordrecht, The Netherlands, 14(1), 65–74.

Leemis, L.M. (1995). *Reliability, Probabilistic Models and Statistical Methods*. Prentice Hall, Englewood Cliffs, NJ, 384p.

Liu, M. and Frangopol, D.M. (2005). Time-Dependent Bridge Network Reliability: Novel Approach. *Journal of Structural Engineering*, ASCE, 131(2), 329–337.

Liu, M. and Frangopol, D.M. (2006). Probability-Based Bridge Network Performance Evaluation. *Journal of Bridge Engineering*, ASCE, 11(5), 633–641.

Liu, P.L., Lin, H.Z. and Der Kiureghian, A. (1989). *CALREL User Manual*. Department of Civil Engineering, University of California, Berkeley, CA.

Lua, J. and Hess, P.E. (2003). Hybrid Reliability Predictions of Single and Advanced Double-Hull Ship Structures. *Journal of Ship Research*, SNAME, 47(2), 155–176.

Lua, J. and Hess, P.E. (2006). First-Failure-Based Reliability Assessment and Sensitivity Analysis of a Naval Vessel under Hogging. *Journal of Ship Research*, SNAME, 50(2), 158–70.

Luís, R.M., Teixeira, A.P. and Guedes Soares, C. (2009). Longitudinal Strength Reliability of a Tanker Hull Accidentally Grounded. *Structural Safety*, Elsevier, 31(3), 224–33.

Mackie, K.R. and Stojadinović, B. (2006). *Post-Earthquake Functionality of Highway Overpass Bridges*. *Earthquake Engineering & Structural Dynamics*, John Wiley & Sons; 35(1), 77–93.

Mahmoud, H.N., Connor, R.J. and Bowman, C.A. (2005). *Results of the Fatigue Evaluation and Field Monitoring of the I-39 Northbound Bridge over the Wisconsin River*. ATLSS Report No. 05-04, Lehigh University, Bethlehem, PA.

Mander, J.B. (1999). *Fragility Curve Development for Assessing the Seismic Vulnerability of Highway Bridges, Research Progress and Accomplishments: 1997–1999*, Multidisciplinary Center for Earthquake Engineering Research (MCEER), Buffalo, NY.

Mansour, A.E. (1997). *Assessment of Reliability of Ship Structures*. Ship Structure Committee: SSC-398.

Mansour, A.E. and Hovem, L. (1994). Probability Based Ship Structural Safety Analysis. *Journal of Ship Research*, SNAME, 38(4), 329–339.

Mansour, A.E. and Thayamballi, A. (1994). *Probability Based Ship Design; Loads and Load Combinations*. Ship Structure Committee: SSC-373.

Mansour, A.E., Jan, H.Y., Zigelman, C.I., Chen, Y.N. and Harding, S.J. (1984). *Implementation of Reliability Methods to Marine Structures*. Transactions of SNAME, Vol. 92, 353–382.

Martin, W.A. and McGuskin, N.A. (1998). *Travel Estimation Techniques for Urban Planning*. National Cooperative Research Program (NCHRP) Report 365, Transportation Research Board, National Research Council, Washington, DC.

Maunsell Ltd. (1999). *Serviceable Life of Highway Structures and Their Components*. Final report, Birmingham (UK), Highways Agency, London, UK.

McKay, M.D., Conover, W.J. and Beckman, R.J. (1979). A Comparison of three Methods for Selecting Values of Output Variables in the Analysis of Input from a Computer Code. *Technometrics*, Taylor & Francis, 21(2), 239–245.

Michel, W.H. (1999). Sea Spectra Revisited. *Marine Technology*, SNAME, 36(4), 211–227.

Miles, S.B. and Chang, S.E. (2006). Modeling Community Recovery from Earthquakes. *Earthquake Spectra*, EERI, 22(2), 439–458.

Miroyannis, A. (2006). *Estimation of Ship Construction Costs*. B.S. Thesis, Department of Mechanical Engineering, Massachusetts Institute of Technology, Boston, MA.

Myers, R.H. and Montgomery, D.C. (2002). *Response Surface Methodology: Process and Product Optimization using Designed Experiment*. John Wiley & Sons, New York City, NY, 704p.

Neal, R.M. (2003). Slice Sampling. *Annals of Statistics*, Institute of Mathematical Statistics, 31(3), 705–741.

Neves, L.C., Frangopol, D.M. and Cruz, P.J. (2006a). Probabilistic Lifetime-Oriented Multiobjective Optimization of Bridge Maintenance: Single Maintenance Type. *Journal of Structural Engineering*, ASCE, 132(6), 991–1005

Neves, L.C., Frangopol, D.M. and Petcherdchoo, A. (2006b). Probabilistic Lifetime-Oriented Multiobjective Optimization of Bridge Maintenance: Combination of Maintenance Types. *Journal of Structural Engineering*, ASCE, 132(11), 1821–1834.

Nielson, B.G. and DesRoches, R. (2007). Analytical Seismic Fragility Curves for Typical Bridges in the Central and Southeastern United States, *Earthquake Spectra*, EERI, 23(3), 615–633.

NOAA (2013). *National Data Buoy Center*. National Oceanic and Atmospheric Administration (NOAA), Washington, DC. Website: http://www.ndbc.noaa.gov/, (accessed March 2013).

Okasha, N.M. and Frangopol, D.M. (2009). Lifetime-Oriented Multi-Objective Optimization of Structural Maintenance Considering System Reliability, Redundancy and Life-Cycle Cost using GA. *Structural Safety*, Elsevier, 31(6), 460–474.

Okasha, N.M. and Frangopol, D.M. (2010a). Time-Variant Redundancy of Structural Systems. *Structure and Infrastructure Engineering*, Taylor & Francis, 6(1–2), 279–301.

Okasha, N.M. and Frangopol, D.M. (2010b). Efficient Method Based on Optimization and Simulation for the Probabilistic Strength Computation of the Ship Hull. *Journal of Ship Research*, SNAME, 54(4), 1–13.

Okasha, N.M. and Frangopol, D.M. (2010c). Redundancy of Structural Systems with and without Maintenance: an Approach based on Lifetime Functions. *Reliability Engineering and System Safety*, Elsevier, 95(5), 520–533.

Okasha, N.M. and Frangopol, D.M. (2010d). Novel Approach for Multi-Criteria Optimization of Life-Cycle Preventive and Essential Maintenance of Deteriorating Structures. *Journal of Structural Engineering*, ASCE, 136(8), 1009–1022.

Okasha, N.M., Frangopol, D.M. and Decò, A. (2010). Integration of Structural Health Monitoring in Life- Cycle Performance Assessment of Ship Structures under Uncertainty. *Marine Structures*, Elsevier, 23(3), 303–321.

Olsson, A., Sandberg, G. and Dahlblom, O. (2003). On Latin Hypercube Sampling for Structural Reliability Analysis. *Structural Safety*, Elsevier, 25(1), 47–68.

Özgüc, Ö., Das, P.K. and Barltrop, N. (2006). The New Simple Equations for the Ultimate Compressive Strength of Imperfected Stiffened Plates. *Ocean Engineering*, Elsevier, 34(7), 970–986.

Padgett, J.E. and DesRoches, R. (2007). Bridge Functionality Relationships for Improved Seismic Risk Assessment of Transportation Networks. *Earthquake Spectra*, EERI, 23(1), 115–130.

Padgett, J.E., DesRoches, R. and Nilsson, E. (2010). Regional Seismic Risk Assessment of Bridge Network in Charleston, South Carolina. *Journal of Earthquake Engineering*, Taylor & Francis, 14(6), 918–933.

Paik, J.K. and Frieze, P.A. (2001). Ship Structural Safety and Reliability. *Progress in Structural Engineering and Materials*, John Wiley & Sons, 3(2), 198–210.

Paik, J.K., Kim, S.K. and Lee, S.K. (1998). Probabilistic Corrosion Rate Estimation Model for Longitudinal Strength Members of Bulk Carriers. *Ocean Engineering*, Elsevier, 25(10), 837–860.

Paik, J.K., Thayamballi, A.K. and Che, J.S. (1996). *Ultimate Strength of Ship Hulls under Combined Vertical Bending, Horizontal Bending, and Shearing Forces*. Transactions of SNAME, Vol. 104, 31–59.

Paik, J.K., Thayamballi, A.K., Kim, S.K. and Yang, S.H. (1998). Ship Hull Ultimate Strength Reliability Considering Corrosion. *Journal of Ship Research*, SNAME, 42(2), 154–165.

Paik, J.K., Wang, G., Kim, B.J. and Thayamballi, A.K. (2002). *Ultimate Limit State Design of Ship Hulls*. Transactions of SNAME, Vol. 110, 285–308.

Palladino, F., Bouscasse, B., Lugni, C. and Bertram, V. (2006). Validation of ship motion functions of PDSTRIP for some standard test cases. *9th Numerical Towing Tank Symposium*, 1–3 October 2006, Le Croisic, France.

Papatzanakis, G.I., Papanikolaou, A.D. and Liu, S. (2012). Optimization of Routing with Uncertainties. *Journal of Marine Science and Application*, Springer, 11(1), 10–17.

Papoulis, A. (1984). *Probability, Random Variables, and Stochastic Processes*. 2nd Ed., McGraw-Hill, New York City, NY, 576p.

Park, J., Nojima, N. and Reed, D. (2006). Nisqually Earthquake Electric Utility Analysis. *Earthquake Spectra*, EERI; 22(2), 491–509.

PDSTRIP (2006). *Program PDSTRIP: Public Domain Strip Method – User Manual*. Webpage : http://sourceforge.net/projects/pdstrip. [accessed October 2011].

Resolute Weather (2011). *Pierson-Moskowitz Sea Spectrum*. Website: http://www.eustis.army.mil/weather (accessed May 2012).

Robert, C.P. (2007). *The Bayesian Choice. Springer*, New York City, NY, 602p.

Rose, A. (2004). Defining and Measuring Economic Resilience to Disasters. *Disaster Prevention and Management*, Emerald Group Publishing, 13(4), 307–314.

Rudko, D.D. (2003). *Logistical Analysis of the Littoral Combat Ship*. MS Thesis, Naval Postgraduate School, Monterey, CA.

Sánchez-Silva, M. and Rackwitz, R. (2004). Socioeconomic Implications of Life Quality Index in Design of Optimum Structures to Withstand Earthquakes. *Journal of Structural Engineering*, ASCE, 130(6), 969–977.

Seville, E. and Metcalfe, J. (2005). *Developing a Hazard Risk Assessment Framework for the New Zealand State Highway Network*. Land Transport New Zealand Research Report 276.

Shinozuka, M., Feng, M.Q., Lee, J. and Naganuma, T. (2000). Statistical Analysis of Fragility Curves. *Journal of Engineering Mechanics*, ASCE, 126(12), 1224–1231.

Shinozuka, M., Zhou, Y., Kim, S-H, Murachi, Y., Banerjee, S., Cho, S. and Chung, H. (2005). *Socio-Economic Effect of Seismic Retrofit Implemented on Bridges in Los Angeles Highway Network*. Final report to the California Department of Transportation, University of California, Irvine, CA.

Sikora, J. and Brady, T. (1989). *Cumulative Lifetime Load Criteria for Surface Ships*. DTRC-SSPD-173-35, David Taylor Research Center, Bethesda, MD.

Skjong, R. (2002). Risk Acceptance Criteria: Current Proposals and IMO Position. *Surface Transport Technologies for Sustainable Development*, 4–6 June, 2002, Valencia, Spain.

Skjong, R. and Bitner-Gregersen, E.M. (2002). Cost Effectiveness of Hull Girder Safety. *Proceedings of OMAE 2002*, 21st Offshore Mechanics and Arctic Engineering (OMAE) Conference, 23–28 June, 2002, Oslo, Norway.

Smith, C.S. (1977). Influence of Local Compressive Failure on Ultimate Longitudinal Strength of a Ship's Hull. *Proceeding International Symposium on Practical Design in Shipbuilding (PRADS)*, October 1977, Tokyo, Japan, pp. 73–80.

Spicer, R.S. and Miller, T.R. (2010). *Final Report to the National Highway Traffic Safety Administration: Uncertainty Analysis of Quality Adjusted Life Years Lost*. Pacific Institute for Research and Evaluation, Calverton, MD.

Stein, S.M., Young, G.K., Trent, R.E. and Pearson, D.R. (1999). Prioritizing Scour Vulnerable Bridges Using Risk. *Journal of Infrastructure Systems*, ASCE, 5(3), 95–101.

The MathWorks (2011). *MATLAB Version 7.13*. The MathWorks Inc., Natick, MA.

Thoft-Christensen, P. (1998). Assessment of the Reliability Profiles for Concrete Bridges. *Engineering Structures*, Elsevier, 20(11), 1004–1009.

TRB (2000). *Highway Capacity Manual*. Special Report 209, Transportation Research Board (TRB), National Research Council, Washington, DC.

USDOT (2011). *Treatment of the Value of Preventing Fatalities and Injuries in Preparing Economic Analyses - 2011 Revision*. U.S. Department of Transportation (USDOT), Washington, DC.

USGS (2003). *Water-Resources Investigations - Flood-Frequency Characteristics of Wisconsin Streams*. Report 03-4250, Department of the Interior, U.S. Geological Survey, Reston, VA.

USGS (2009). *Earthquake Search Tool*. Department of the Interior, U.S. Geological Survey, Reston, VA. Webpage: http://geohazards.usgs.gov/eqprob/2009/index.php.

USGS (2010). *Water data for the Nation*. Department of the Interior, U.S. Geological Survey, Reston, VA. Webpage: http://waterdata.usgs.gov.

USGS (2011). *Earthquake Search Tool*. Department of the Interior, U.S. Geological Survey (USGS), Reston, VA. Webpage: http://earthquake.usgs.gov/earthquakes/eqarchives/epic/.

van Noortwijk, J.M. and Klatter, H.E. (2004). The Use of Lifetime Distributions in Bridge Maintenance and Replacement Modelling. *Computers and Structures*, Elsevier, 82(13-14), 1091–1099.

Wang, G. and Wiernicki, C.J. (2004). Using Nonlinear Finite Element Method to Design Ship Structures for Ice Loads. *SNAME Annual Meeting*, September 29 - October 1, 2004, Washington, DC.

Wang, G., Boon, B., Brennan, F.P., Garbatov, Y., Ji, C., Parunov, J., Rahman, T.A., Rizzo, C., Rouhan, A., Shin, C.H. and Yamamoto, N. (2009). *Condition Assessment of Aged Ships and Offshore Structures*. Volume 2, 17th International Ship and Offshore Structures Congress, 16–21 August 2009, Seoul, Korea.

Wang, Z. (2007). Seismic Hazard and Risk Assessment in the Intraplate Environment: the New Madrid Seismic Zone of the Central United States. *Geological Society of America Special Papers*, GSA, 425, 363–374.

Wells, D.L. and Coppersmith, K.J. (1994). New Empirical Relationships among Magnitude, Rupture Length, Rupture Width, and Surface Displacement, *Bulletin of the Seismological Society of America*, SSA, 84(4), 974–1002.

Wijnolst, N. and Wergeland, T. (1996). *Shipping*. Delft University Press, Delft, Netherlands, 591p.

Wolfram Research (2010), *Mathematica - Version 8.0*. Wolfram Research Inc., Champaign, IL.

WSC (2008). *Record Fuel Prices Place Stress on Ocean Shipping*. World Shipping Council (WSC), Washington, DC.

Xu, N., Guikema, S.D., Davidson, R.A., Nozick, L.K., Çağnan, Z. and Vaziri, K. (2007). Optimizing Scheduling of Post-Earthquake Electric Power Restoration Tasks. *Earthquake Engineering and Structural Dynamics*, John Wiley & Sons, 36(2), 265–284.

Yang, S-I, Frangopol, D.M. and Neves, L.C. (2004). Service Life Prediction of Structural Systems using Lifetime Functions with Emphasis on Bridges. *Reliability Engineering & System Safety*, Elsevier, 86(1), 39–51.

Zheng, Y. and Das, P.K. (2000). Improved Response Surface Method and its Application to Stiffened Plate Reliability Analysis. *Engineering Structures*, Elsevier, 22, 544–551.

Zobel, C.W. (2011). Representing Perceived Tradeoffs in Defining Disaster Resilience. *Decision Support Systems*, Elsevier, 50(2), 394–403.

APPENDIX A

PERFORMANCE INDICATORS, PROBABILISTIC METHODS AND OPTIMIZATION

A.1 PERFORMANCE INDICATORS

Several deterministic and probabilistic performance indicators have been investigated over the last decades. These indicators serve as measure of structural performance of both undamaged and damaged structures. In life-cycle analysis, indicators commonly used include: safety margin, probability of failure, reliability index, lifetime distributions, redundancy index, vulnerability, damage tolerance, risk, robustness, and resilience. Most of these performance indicators are usually time dependent because they are affected by progressive and/or sudden deterioration processes. In the reminder of this Appendix, reliability and redundancy indices, lifetime distributions, risk, and resilience, which are the most used indicators in this study, are reviewed.

A.1.1 RELIABILITY INDEX

Ang and Tang (1984) define reliability as "the probabilistic measure of assurance of performance". Therefore, the problems of reliability of structural systems may be represented as the problem of "supply" versus "demand". In other words, reliability measures the capacity of components/systems to withstand to the applied load, related

to the capacity through a performance function that takes into account the relevant uncertainty of the reliability problem.

The indicator of the performance governing the problem of supply and demand is generally governed by the following performance function (Ang and Tang 1984)

$$g(\mathbf{X}) = g(X_1, X_2, ..., X_n) \tag{A.1}$$

where $\mathbf{X} \equiv \{X_1, X_2, \ldots, X_n\}$ is the vector of the random variables and the performance function $g(\mathbf{X})$ determines the states

$$[g(\mathbf{X}) > 0] \qquad \text{“safe state”} \tag{A.1}$$

$$[g(\mathbf{X}) = 0] \qquad \text{“limit state”} \tag{A.2}$$

$$[g(\mathbf{X}) < 0] \qquad \text{“failure state”} \tag{A.3}$$

Equation (A.1) can be expressed through a simplified and more intuitive form that includes the capacity C and demand D

$$g(C, D) = C - D \tag{A.4}$$

The relevant random variables are then included into the terms C and D of Equation (A.5). Figure A.1 shows the schematic representation of a linear limit state function that separates the safe and failure domains. Based on the performance functions of Equations (A.1) and (A.5), the probabilities of the safe state P_s and failure state P_f are defined as (Ang and Tang 1984)

$$P_s = P[g(\mathbf{X}) \geq 0] = P[C \geq D] \tag{A.5}$$

$$P_f = P[g(\mathbf{X}) < 0] = P[C < D] \tag{A.6}$$

Thus, if the joint probability density function (PDF) of the random variables $\{X_1, X_2, \ldots, X_n\}$ is $f_{\mathbf{X}}(\mathbf{x}) = f_{X_1, X_2, \ldots, X_n}(x_1, x_2, \ldots, x_n)$, the probability of failure P_f is analytically computed as

$$P_f = P[g(\mathbf{X}) < 0] = \int_{\mathbf{F}} f_{\mathbf{X}}(\mathbf{x}) d\mathbf{x} \tag{A.7}$$

where

$$\mathbf{F} \equiv \{g(\mathbf{X}) < 0\} \tag{A.8}$$

is the failure domain. Usually, the integral of Equation (A.8) cannot be solved with a closed-form solution; therefore, approximate methods must be used such as the First-Order Reliability Method (FORM), the Second-Order Reliability Method (SORM), or through simulations. The reliability index β is usually assumed to be associated with the probability of failure as follows

$$\beta = -\Phi^{-1}(P_f) \tag{A.9}$$

where $\Phi^{-1}(\cdot)$ is the inverse standard normal cumulative distribution function (CDF).

If C and D of Equation (A.5) are statistically independent normally distributed random variables with mean values μ_C and μ_D, respectively, and standard deviations σ_C and σ_D, respectively, the probability distribution of the safety margin $M = C - D$ is also normal with mean value μ_M and standard deviation σ_M given as

$$\mu_M = \mu_C - \mu_D \tag{A.10}$$

$$\sigma_M = \sqrt{\sigma_C^2 + \sigma_D^2} \tag{A.11}$$

Consequently, the reliability index and the associated probability of failure are computed as

$$\beta = \frac{\mu_M}{\sigma_M} = \frac{\mu_C - \mu_D}{\sqrt{\sigma_C^2 + \sigma_D^2}} \tag{A.12}$$

$$P_f = \Phi\left(-\frac{\mu_M}{\sigma_M}\right) = \Phi\left(\frac{\mu_D - \mu_C}{\sqrt{\sigma_C^2 + \sigma_D^2}}\right) \tag{A.13}$$

Figure A.2 shows qualitatively the normal distributions of the capacity *C*, demand *D*, and safety margin *M*. As shown, the reliability index β is the ratio of the mean of the safety margin and its standard deviation.

When multiple failure modes and/or multiple components being part of a system are analyzed, system reliability is performed. In this case, *k* multiple failure modes and/or multiple components have different performance functions represented as (Ang and Tang 1984)

$$g_i(\mathbf{X}) = g_i(X_1, X_2, ..., X_n) \qquad i = 1, 2, ..., k \tag{A.14}$$

such that the individual failure events are

$$E_i = [g_i(\mathbf{X}) < 0] \qquad i = 1, 2, ..., k \tag{A.15}$$

Therefore, the probability of failure of the system is expressed as

$$P_f = \int_{(E_1 \cup E_2 \cup ... \cup E_k)} \cdots \int f_{X_1, X_2, ..., X_n}(x_1, x_2, ..., x_n) dx_1 dx_2 \cdots dx_n \tag{A.16}$$

The overall system performance can be evaluated by modeling multiple failure modes and/or multiple components with classical theory of series and parallel system reliability. For instance, a series system will fail if any one of its component fails, whereas a parallel systems will fail only if all its components fail. The failure domain $\mathbf{\Omega}$ of series and parallel systems is then defined as (Ang and Tang 1984)

$$\mathbf{\Omega} \equiv \bigcup_{i=1}^{k} \{g_i(\mathbf{X}) < 0\} \qquad i = 1,2,...,k \tag{A.17}$$

$$\mathbf{\Omega} \equiv \bigcap_{i=1}^{k} \{g_i(\mathbf{X}) < 0\} \qquad i = 1,2,...,k \tag{A.18}$$

For series-parallel systems, composed by a series systems of Q parallel subsystems with N_i components, the failure domain $\mathbf{\Omega}$ becomes (Ang and Tang 1984)

$$\mathbf{\Omega} \equiv \bigcup_{i=1}^{Q} \bigcap_{j=1}^{N_i} \{g_{ij}(\mathbf{X}) < 0\} \tag{A.19}$$

The probability of failure of the systems depends upon the correlation among the safety margins of the single components. Figure A.3 shows the schemes of series, parallel, and series-parallel systems. Because of the complexity of the problem, generally, closed-form solutions are not available; therefore, approximated solutions in the form of bounds have been developed. Cornell (1967) provided first-order bounds, whereas Ditlevsen (1979) refined these bounds by proposing tighter second-order bounds. For practical purposes, FORM and SORM can also be used. In this study reliability problems have been solved by using the software RELSYS (Estes and

Frangopol 1998) and CALREL (Liu *et al.* 1989). Reliability analysis is extensively performed throughout this study.

A.1.2 LIFETIME FUNCTIONS

This section reviews three lifetime functions, including the CDF of the time-to-failure, survivor function, and hazard function, that are used in Chapters 2 and 3 of this study.

The first reviewed lifetime distribution is the CDF of the time-to-failure $F(t)$ that represents the probability that the time-to-failure of a component/system is less than time t. Okasha and Frangopol (2010c) define $F(t)$ as

$$F(t) = P[T \le t] = \int_0^t f(u)du \qquad t,u \ge 0 \tag{A.20}$$

where $f(u)$ is the PDF of the time-to-failure. This indicator is also called time-dependent reliability within some research groups.

The survivor function $S(t)$ is complementary to the CDF of the time-to-failure $F(t)$, therefore, $S(t)$ is defined as the probability that a component/system is still functioning at time t (Leemis 1995)

$$S(t) = P[T > t] = 1 - F(t) = \int_t^\infty f(u)du \qquad t \ge 0 \tag{A.21}$$

Figure A.4 shows the qualitative relationship among the PDF of the time-to-failure $f(t)$, the CDF of the time-to-failure $F(t)$, and the survivor function $S(t)$. It can be noticed that the area to the left of time t_0 is $F(t_0)$ and the area to the right of t_0 is $S(t_0)$.

The last indicator to be reviewed is the hazard function $h(t)$ that represents the frequency with which components/systems fail. Its definition is as follows (Leemis 1995)

$$h(t) = \frac{f(t)}{S(t)} \qquad t \geq 0 \tag{A.22}$$

A.1.3 REDUNDANCY INDEX

Besides reliability index and lifetime functions redundancy is also a useful performance indicator that provides warnings of partial failure. A redundant system has enough resources to survive even though one component within itself fails; the structural system will collapse only if the failure pattern propagates throughout multiple components. A high level of redundancy can contribute to the mitigation of unexpected actions generated by potential hazard-induced events. Several definitions were investigated by Frangopol and Curley (1987) in order to relate redundancy to the meaning of "warning provider," including:

1. Reserve capacity factor

$$Red_1 = \frac{L_{intact}}{L_{design}} \tag{A.23}$$

in which L_{intact} is the load carrying capacity of the intact structure and L_{design} is the design load.

2. Residual capacity factor

$$Red_2 = \frac{L_{damaged}}{L_{intact}} \tag{A.24}$$

where $L_{damaged}$ is the load carrying capacity of the damaged structure.

3. Normalized capacity factor

$$Red_3 = \frac{L_{intact}}{L_{intact} - L_{damaged}} \tag{A.25}$$

If a probabilistic approach is used, and the time-dependent reliability indices associated with the yielding limit state for the components and with the ultimate collapse for the system are evaluated, the time-variant redundancy index may alternatively be defined by (Frangopol and Okasha 2008)

$$Red_4(t) = \beta_{f(sys)}(t) - \beta_{y(sys)}(t) \tag{A.26}$$

$$Red_5(t) = \frac{\beta_{f(sys)}(t) - \beta_{y(sys)}(t)}{\beta_{f(sys)}(t)} \tag{A.27}$$

where $\beta_{f(sys)}(t)$ and $\beta_{y(sys)}(t)$ are the reliability indices with respect to the occurrence of first yielding and system failure at time t, respectively. Analogously, time-variant redundancy indices can be calculated by using the probabilities of exceedance of the above mentioned limit states (Frangopol and Okasha 2008, Okasha and Frangopol 2010a)

$$Red_6(t) = P_{y(sys)}(t) - P_{f(sys)}(t) \tag{A.28}$$

$$Red_7(t) = \frac{P_{y(sys)}(t) - P_{f(sys)}(t)}{P_{f(sys)}(t)} \tag{A.29}$$

in which $P_{y(sys)}(t)$ and $P_{f(sys)}(t)$ are the probabilities of first yielding and system failure at time t, respectively. Lastly, Okasha and Frangopol (2010d) introduced a redundancy measure based on lifetime functions, defined as

$$Red_8(t) = \frac{F_{wc}(t) - F_s(t)}{F_s(t)} \tag{A.30}$$

where $F_s(t)$ and $F_{wc}(t)$ are the CDF of the time-to-failure of the system and weakest component, respectively. The evaluation of the time-variant redundancy index is included in Chapters 2 and 5 of this study.

A.1.4 RISK

Risk is defined as the combination of chances and consequences of events generated by different hazards in a given context. Therefore, a major task in risk assessment is the identification of a spectrum of hazards, which affects the structure under investigation, based on the location of the structure and other factors. The outcome of such analysis is a list of all the hazards which may affect the structural system. Hazards are situations or circumstances that cause a level of danger to the structural system leading to potential occurrence of structural failures or malfunctioning. Accordingly, the hazard scenario is a sequence of possible events producing undesirable results in terms of consequences (CIB 2001). The prediction of hazard-induced events and the quantification of their caused consequences are aspects of essential relevance for risk assessment. In general, the instantaneous total risk R of a structural system can be expressed as follows (CIB 2001):

$$R = \int \cdots \int \delta(x_1, x_2, ..., x_n) f_{X_1, X_2, ..., X_n}(x_1, x_2, ..., x_n) dx_1 dx_2 \cdots dx_n \quad \text{(A.31)}$$

where δ represents the consequences, and $f_{\mathbf{X}}(\mathbf{x}) = f_{X1},_{X2},\ldots,_{Xn}(x_1,x_2,\ldots,x_n)$ is the joint PDF containing the considered random variables $\mathbf{X} \equiv \{X_1,X_2,\ldots,X_n\}$. The solution of the above-multiple integral is not obvious and in most cases it cannot be obtained numerically. Therefore, some assumptions must be introduced in order to separate the effects induced by different hazards (e.g. assuming that hazards are mutually exclusive and collectively exhaustive). Concepts related to risk assessment are included in several chapters because they represent the backbone of this study. Time-dependent risk has been evaluated for both highway bridges and ship structures.

A.1.5 RESILIENCE

According to Bruneau *et al.* (2003), resilience is a performance indicator that "measures the ability of a community to mitigate the effects of an extreme event, to contain the effects of the event when it occurs, and to efficiently recover". This definition can be adapted to several structural and infrastructural systems, such as bridge transportation networks (Bocchini and Frangopol 2012a, Bocchini and Frangopol 2012b) and hospital networks (Cimellaro, Reinhorn and Bruneau 2010), among others. Generally, resilience *Res* can be defined as (Cimellaro, Reinhorn and Bruneau 2010)

$$Res = \int_{t_0}^{t_h} Q(t) dt \quad \text{(A.32)}$$

where $Q(t)$ is the time-dependent functionality, t is the time, t_0 is the time at which the extreme event occurs, and t_h is the investigated time horizon. The schematic representations of resilience and time-dependent functionality are shown in Figure A.5. It is assumed that, when the extreme event occurs, the pre-event functionality drops, leading to a residual functionality. Subsequently, recovery activities restore the functionality. Resilience is proportional to the shaded area in Figure A.5.

Moreover another aspect of resilience is described by means of 'rapidity', which is defined as the derivative of the time-dependent functionality with respect to the recovery time (Cimellaro, Reinhorn and Bruneau 2010)

$$Rap = \frac{dQ(t)}{dt} \qquad t_0 \le t \le t_h \tag{A.33}$$

Resilience and rapidity are discussed in Chapter 4.

A.2 PROBABILISTIC METHODS AND OPTIMIZATION

This section covers some of the probabilistic methods and the optimization technique used in this study. A brief review of the fundamentals of Latin Hypercube sampling, slice sampling, and the basics of Bayesian updating is provided herein. Notions of optimization are also provided.

A.2.1 LATIN HYPERCUBE SAMPLING

Latin Hypercube is sampling technique that belongs to the family of the stratified sampling methods. It provides a more representative distribution of the outputs for the same number of simulated input samples than the standard Monte Carlo sampling

(Kyriakidis 2005). A square grid containing sample positions represents a Latin square only if there is only one sample in each row and each column. The generalization of this concept leads to the Latin Hypercube (McKay, Conover and Beckman 1979). A simulation based on this sampling technique allows to save computational time and computer resources with respect to a crude Monte Carlo simulation because requires a less number of samples in order to reach a specific confidence level (Neves, Frangopol and Cruz 2006, Neves, Frangopol and Petcherdchoo 2006). Based on Olsson, Sandberg and Dahlblom (2003), the algorithm for the generation of realizations of correlated and uncorrelated random variables, through Latin Hypercube sampling, is summarized as follows:

1. Generate an $N \times K$ matrix **P**, where N is the number of samples, and K is the number of random variables, in which each of the K columns is a random permutation of 1,..,N.
2. Generate an $N \times K$ matrix **R** of independent random numbers from the uniform distribution (0,1).
3. Generate the elements y_{ij} of the matrix **Y**, such that the elements of **P** are divided by the number of samples $N + 1$ and mapped on the standard Gaussian distribution

$$y_{ij} = \Phi^{-1}\left(\frac{p_{ij}}{N+1}\right) \tag{A.34}$$

4. Obtain the covariance matrix of **Y** that is estimated by using the Cholesky decomposition as follows

$$\bar{\mathbf{L}}\bar{\mathbf{L}}^{T} = \mathrm{cov}(\mathbf{Y}) \tag{A.35}$$

where $\overline{\mathbf{L}}$ is the lower triangular.

5. Evaluate a new matrix **Y*** with a sample covariance equal to the identity

$$\mathbf{Y}^* = \mathbf{Y}\left(\overline{\mathbf{L}}^{-1}\right)^T \tag{A.36}$$

if the random variables are uncorrelated, and

$$\mathbf{Y}^* = \mathbf{Y}\left(\overline{\mathbf{L}}^{-1}\right)^T \mathbf{L}^T \tag{A.37}$$

if they are correlated, where **L** is the lower triangle matrix from the Cholesky decomposition of the target correlation matrix.

6. Obtain the matrix **P***, where its elements are the ranks of the elements of the columns of **Y***.

7. Generate the matrix **S** as

$$\mathbf{S} = \frac{1}{N}\left(\mathbf{P}^* - \mathbf{R}\right) \tag{A.38}$$

8. Obtain the matrix **X**, in which each element of **S** is mapped on the selected marginal distribution of each random variables as

$$x_{ij} = F_j^{-1}\left(s_{ij}\right) \tag{A.39}$$

where $F_j^{-1}(\cdot)$ is the inverse CDF of random variable x_j.

This sampling algorithm has been coded with the software MATLAB (The MathWorks 2011) and extensively used throughout this study for those analyses that have required simulations.

A.2.2 SLICE SAMPLING

The slice sampling algorithm is a kind of Markov chain Monte Carlo algorithm for the generation of pseudo-random numbers from a statistical distribution (Neal 2003). This sampling algorithm is used in this study for the obtaining the posterior distribution of the Bayesian statistics treated in Chapter 7. The algorithm has been implemented by forcing the specific mapping distribution in accordance to the posterior distribution. Briefly, the algorithm is summarized as follows (The MathWorks 2011):

1. Assume an initial value $x(s)$ within the domain of $d(x)$.
2. Draw a uniformly distributed value y from $(0, d(x(s)))$, defining a horizontal "slice" as $S = \{x: y < d(x)\}$.
3. Find an interval $I = (L, R)$ around $x(s)$ that contains all, or much of the "slice" S.
4. Draw the new point $x(s+1)$ within this interval.
5. Increment $s \rightarrow s+1$ and repeat steps 2 through 4 until the desired number of samples is reached.

A.2.3 BAYESIAN UPDATING

Bayesian approach makes it possible to use the additional monitoring information in conjunction with the already available initial information (Kay 1993). Briefly, the Bayesian approach mainly deals with the parameters θ_j, which are described by their associated PDF called "prior PDF" $f'(\theta)$. In turns, the prior PDF has parameters itself, that are often called "hyperparameters" in order to distinguish them from the basic parameters of the underlying random variable X (Fink 1997). Assuming that

$x_1, x_2, \ldots x_j, \ldots, x_n$ are the stored observations, then the likelihood function $L(\theta)$ assuming a given parameter θ is (Ang and Tang 2007)

$$L(\theta) = \prod_{j=1}^{n} f_X\left(x_j \mid \theta\right) \tag{A.40}$$

where $f_X(x_j|\theta)$ is the PDF of the random variable X evaluated with the SHM data value x_j, given the PDF parameter θ. Based on the Bayes' theorem, the posterior PDF $f''(\theta)$, i.e. the updated PDF of the parameters θ_j, is obtained by combining the prior PDF with the likelihood of the available observations as follows (Ang and Tang 2007)

$$f''(\theta) = k_n L(\theta) f'(\theta) \tag{A.41}$$

where k_n is the normalizing constant given as follows

$$k_n = \frac{1}{\int_{-\infty}^{\infty} L(\theta) f'(\theta) d\theta} \tag{A.42}$$

The expected value of parameter θ is commonly used as Bayesian estimator; therefore, by using the method of moments, the updated parameter θ is given by (Ang and Tang 2007)

$$\hat{\theta}'' = \int_{-\infty}^{\infty} \theta f''(\theta) d\theta \tag{A.43}$$

Figure A.6 shows the qualitative representation of the distribution associated with collected SHM data, and of the prior distribution $f'(\theta)$ and posterior distribution $f''(\theta)$. The implementation of SHM observation through Equation (A.41) and the closed-form solution for Equation (A.42) are not always achievable. Therefore, numerical

based techniques, such as Markov chain Monte Carlo (Coles and Powell 1996), Metropolis-Hastings algorithm (Robert 2007), and slice sampling algorithm (Neal 2003), among others, may be used. Both closed-form solution and simulation-based method are covered in Chapter 7.

A.2.4 OPTIMIZATION

Optimization is an important tool that allows making optimal decisions within life-cycle management of bridges and ship structures. For instance, optimization has been used for the management of civil structures and infrastructures (Estes and Frangopol 1999, Neves, Frangopol and Cruz 2006, Neves, Frangopol and Petcherdchoo 2006, Okasha and Frangopol 2009, Okasha and Frangopol 2010d, Frangopol and Bocchini 2011, Kim and Frangopol 2011, Bocchini and Frangopol 2012a, Bocchini and Frangopol 2012b), and for the management of ship structures (Journée and Meijers 1980, Papatzanakis, Papanikolaou and Liu 2012). The general formulation of a multi-objective minimization problem is provided by (Arora 2004):

Given: system properties (e.g. values of performance indicators, maintenance costs, sea elevation map)

Find: the design vector

$$\mathbf{Z} \equiv \{Z_1, Z_2, ..., Z_n\} \tag{A.44}$$

To minimize: the objective functions

$$\min \mathbf{o}(\mathbf{Z}) = (o_1(\mathbf{Z}), o_2(\mathbf{Z}), ..., o_k(\mathbf{Z})) \tag{A.45}$$

Subjected to: the equality constraints

$$a_i(\mathbf{Z}) = 0 \quad i = 1,...p \tag{A.46}$$

and inequality constraints

$$b_j(\mathbf{Z}) \leq 0 \quad j = 1,...m \tag{A.47}$$

where k is the number of objective functions, p is the number of equality constraints, and m is the number of inequality constraints.

Figure A.7 shows the schematic representation of qualitative solutions of a bi-objective optimization problem (both the objective have to be minimized), in which there are non-Pareto solutions, and Pareto points included within the Pareto front. For instance, typical objective functions to be optimized within the life-cycle management framework may be reliability index, redundancy index, risk, resilience, total travel time of ships, life-cycle costs, retrofit costs, among others, considering design variables, such as the interval time of maintenance actions, material properties, geometrical dimensions of structures, ship traveling speed, and ship direction while traveling, among others.

The solution of single-objective optimization problems can be found by using, for instance, sequential quadratic programming, which is an implemented tool of the optimization function *fmincon* of MATLAB (The MathWorks 2011). Alternatively, Genetic Algorithm (GA) may be used. GA is a search heuristic method that mimics the process of natural evolution generating solutions by using techniques inspired by natural evolution, such as inheritance, mutation, selection, and crossover. The solution of single-objective optimization problems through GA is implemented in MATLAB in the tool *ga*, in which linear and non-linear constraints can be considered. The solution

of a single-objective optimization problem is unique. However, the solution of multi-objectives optimization problems required more advanced algorithm, in order to obtain results in the form of a Pareto front (Arora 2004). The MATLAB software includes a tool for this purpose called *gamultiobj*. Although this is a powerful tool, non-linear constraint cannot be explicitly input, therefore, penalty functions must be used. When the objectives to be optimized are at least two, decision makers are provided with a spectrum of optimal solutions (Pareto front) that are useful when the decision must be made considering for instance economic constraints and time constraints, among others. In this study, optimization has been used in Chapters 6 and 7, in which optimal ship routing is performed.

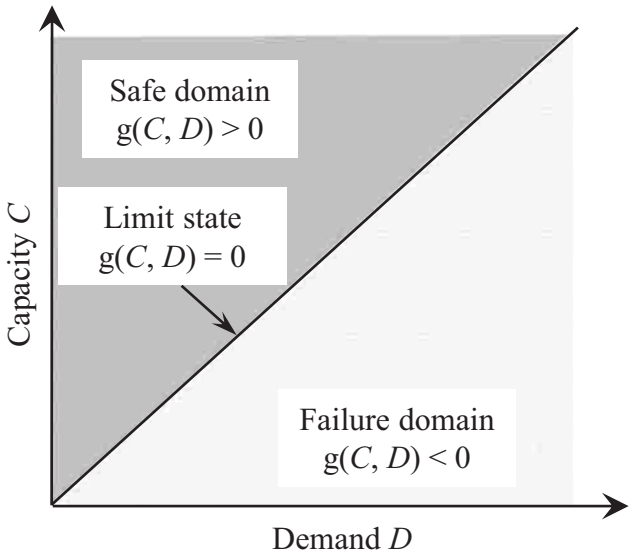

Figure A.1 Schematic representation of the safe, failure, and the limit state.

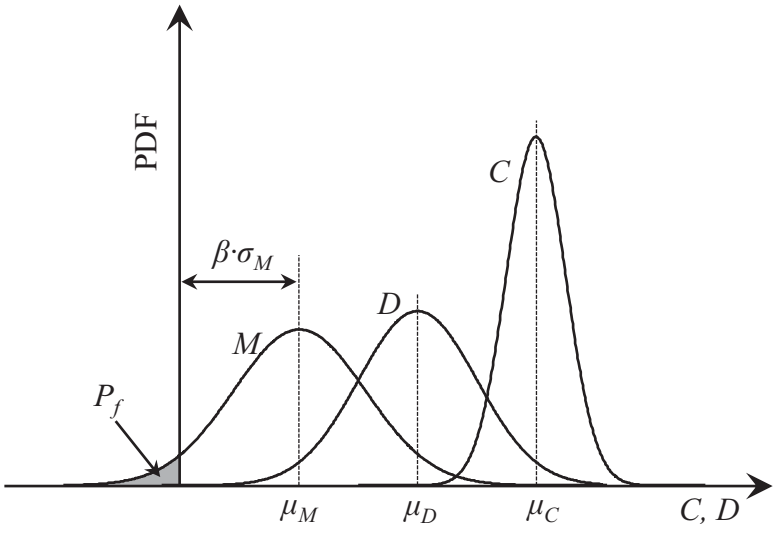

Figure A.2 Qualitative representation of the normal distributions of the capacity *C*, demand *D*, and safety margin *M*.

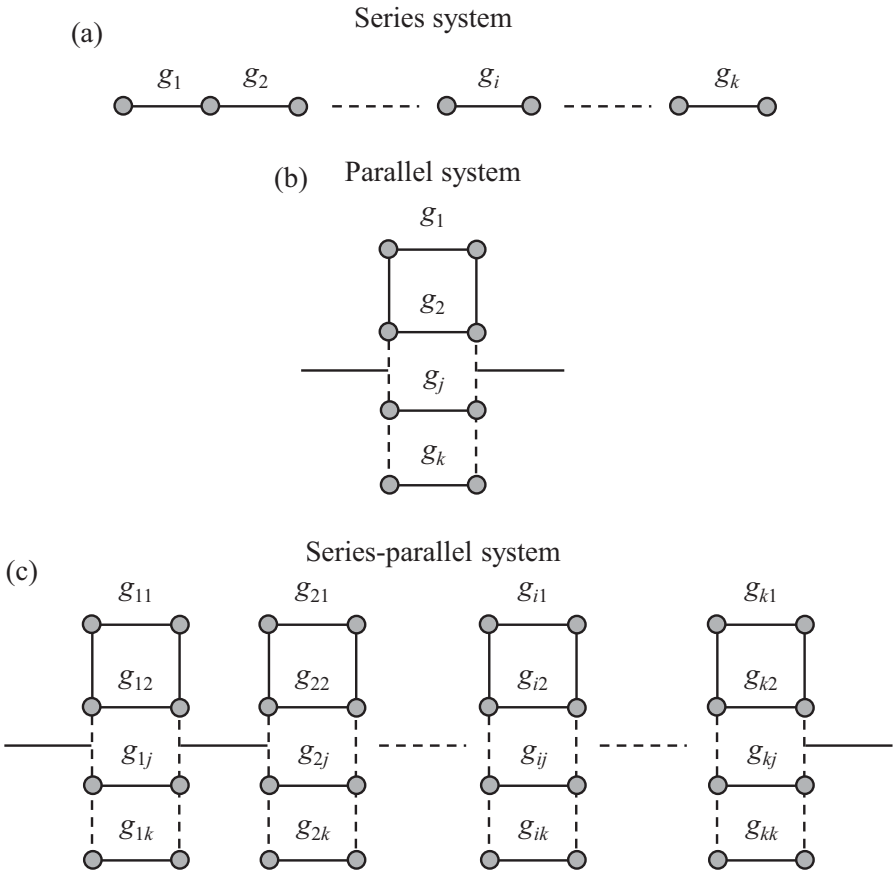

Figure A.3 Schemes of series, parallel, and series-parallel systems.

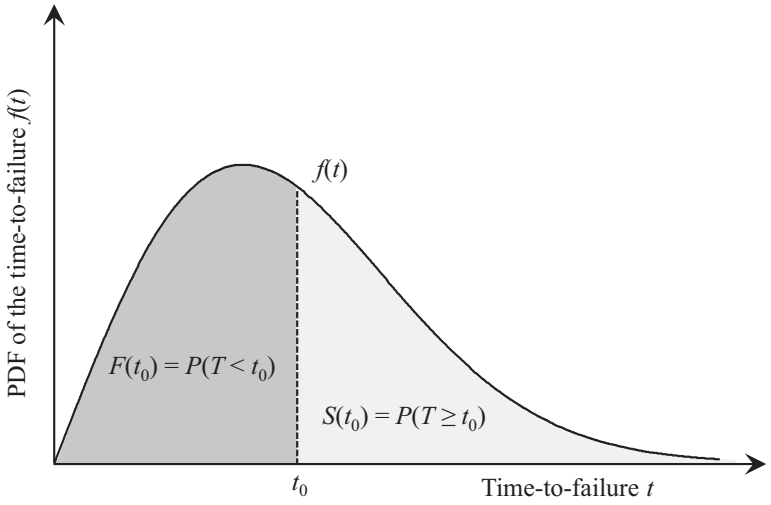

Figure A.4 Qualitative relationship among the PDF of the time-to-failure $f(t)$, CDF of the time-to-failure $F(t)$, and the survivor function $S(t)$.

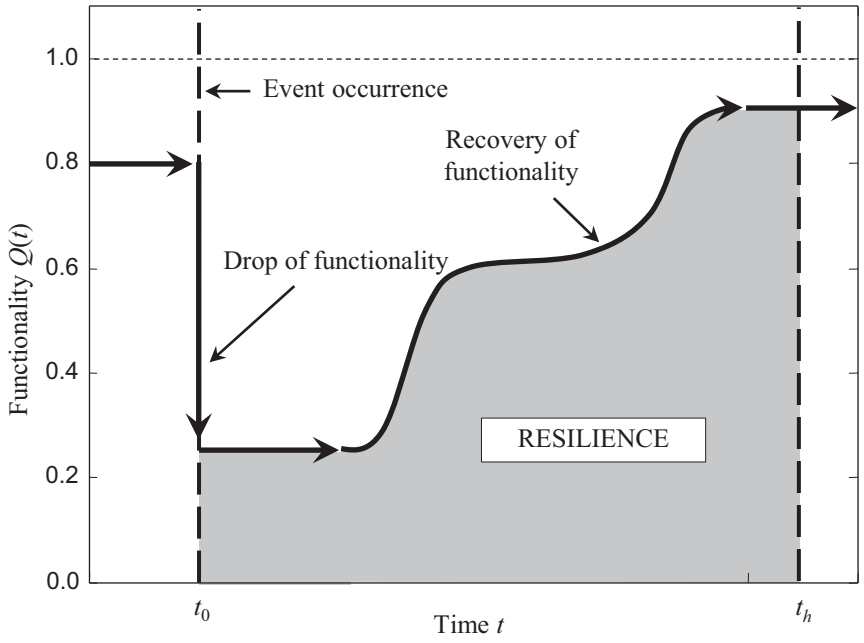

Figure A.5 Schematic representation of resilience and time-dependent functionality.

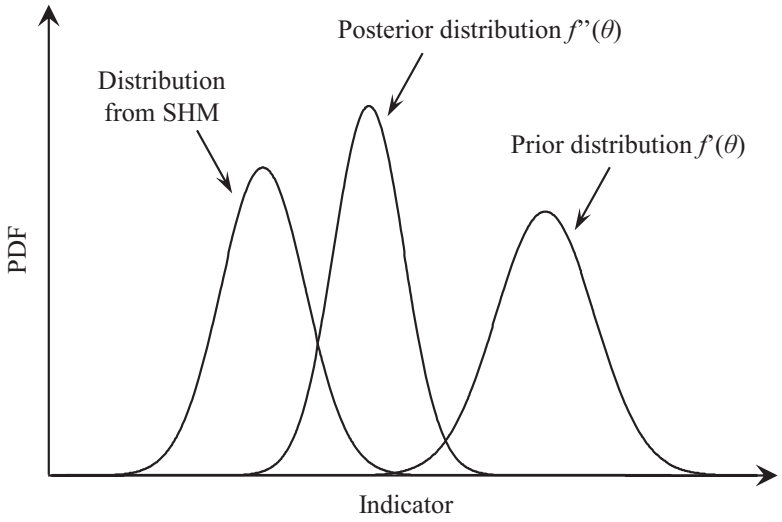

Figure A.6 Qualitative representation of the distribution associated with collected SHM data, prior distribution $f'(\theta)$, and posterior distribution $f''(\theta)$.

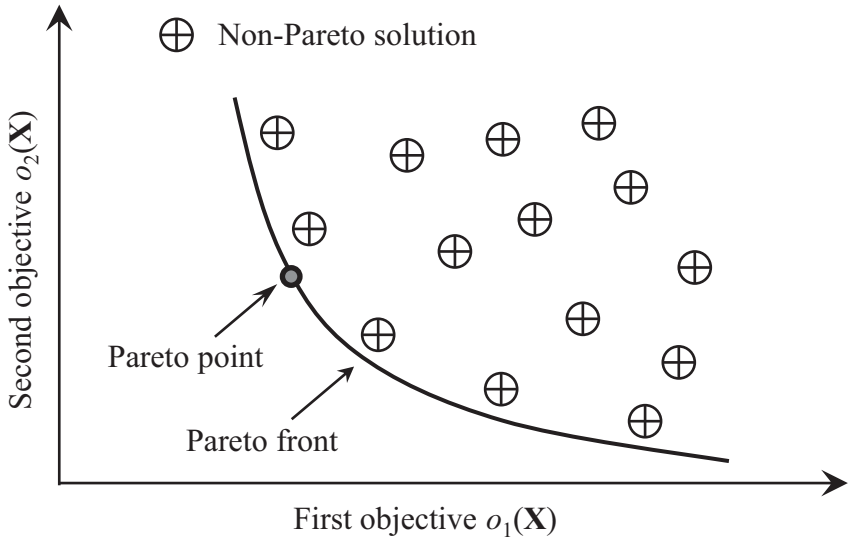

Figure A.7 Schematic representation of qualitative solutions of a bi-objective optimization problem.

APPENDIX B

COMPUTATIONAL FRAMEWORK FOR THE MANAGEMENT OF AGING SHIP STRUCTURES

This appendix describes the developed computational framework for the management of aging ship structures based on the several papers published (Decò, Frangopol and Okasha, 2011, Decò, Frangopol and Zhu 2012, Decò, Frangopol and Okasha 2012b) or submitted for possible publication (Decò and Frangopol 2013b, Decò and Frangopol 2013c). Figure B.1 shows the developed framework that is composed by four modules.

Briefly, Module (1) evaluates the loads effects on the hull, due to still water and waves and by considering different ship operational conditions (see Figure B.2). The body of the ships is modeled with the software FREE!ship (2006). Then, based on the ship geometry, the hydrodynamic software PDSTRIP (2006) is used to evaluate the structural response of a given hull section under regular wave. By considering the sea spectrum for natural sea, the statistical descriptors of the response can be evaluated. These lasts operation are implemented into a MATALB code that also account for different ship operational conditions. This framework is used in Chapters 5, 6, and 7. Module (2) covers the assessment and prediction of the flexural capacity of critical ship sections (see Figure B.3). Two frameworks are developed. The first framework, which is used in Chapter 5, is based on a self-developed MATALB (The MathWorks

2011) code that basically evaluates the vertical flexural capacities associated with the failure of the first stiffened panel and ultimate failure of a hull section. The second framework is used in Chapters 6 and 7. A hull section is modeled with the finite element (FE) software ABAQUS (Dassault Systèmes Simulia 2011) and FE analyses are performed for evaluating the contours that accounting for the combined effects of vertical and horizontal flexural capacities. Then, by applying the response surfaces method, it is possible to obtain the statistical descriptors of vertical and horizontal flexural capacities associated with different level of plastification of the hull section. Module (3) performs reliability analysis for the accounted limit states and different ship operational conditions (see Figure B.4). In this module, performance indicators, including reliability, redundancy, and risk are assessed. Moreover, in order to assess risk, economic losses are also quantified. Reliability analysis is performed by using the software RELSYS (Estes and Frangopol 1998). This module is used in Chapters 5, 6, and 7. Finally, Module (4) describes the approach for the optimal routing of ships as management tool (see Figure B.5). The optimization is solved by using the Genetic Algorithm that is implemented into a MATLAB toolbox (The MathWorks 2011). The optimization problem is based upon the quantification of reliability and risk associated with a wide spectrum of ship operational conditions, and upon assumed weather maps, reporting the significant wave heights and wave directions. The design variables are the ship speed and direction, and the objectives to be minimized are the ship estimated time of arrival, risk, and fuel consumption. This module is used in Chapters 6 and 7.

Figure B.6 shows the interaction between the software used within the developed framework. Their interconnection is handled by self-developed MATLAB codes that

automatically interact with other software by writing input files and reading output files.

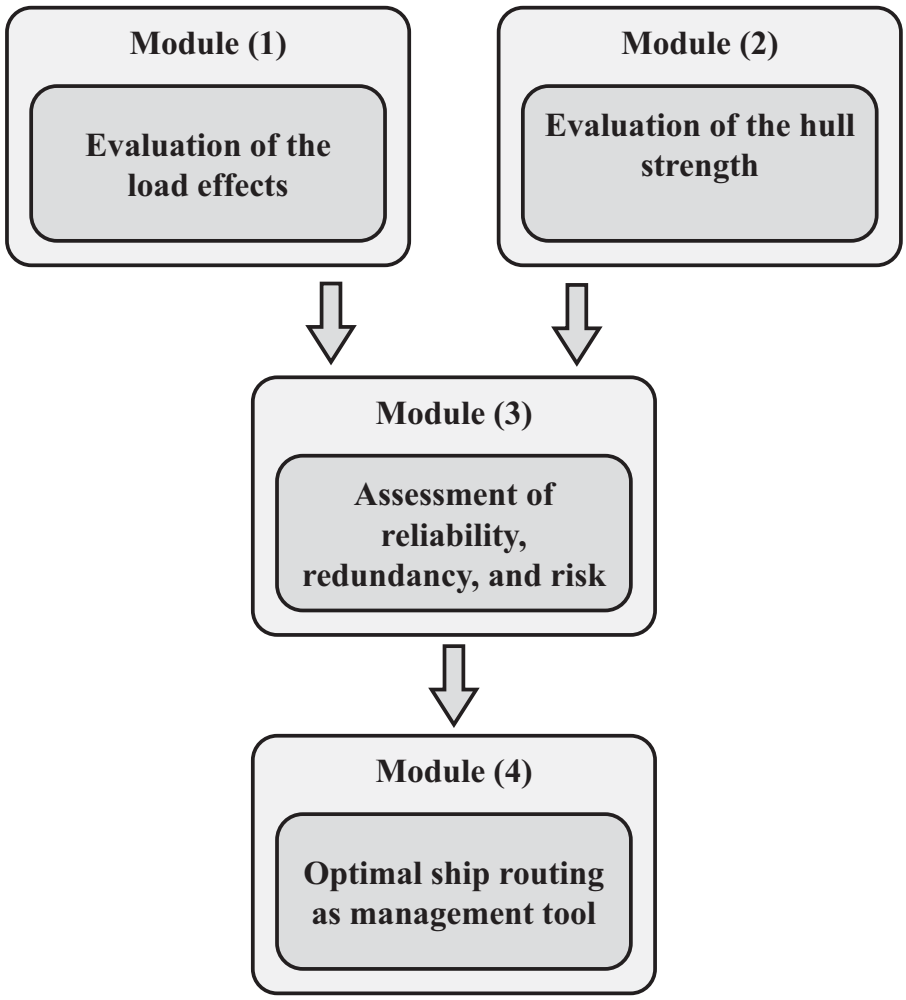

Figure B.1 Computational framework for the management of aging ship structures composed by four modules.

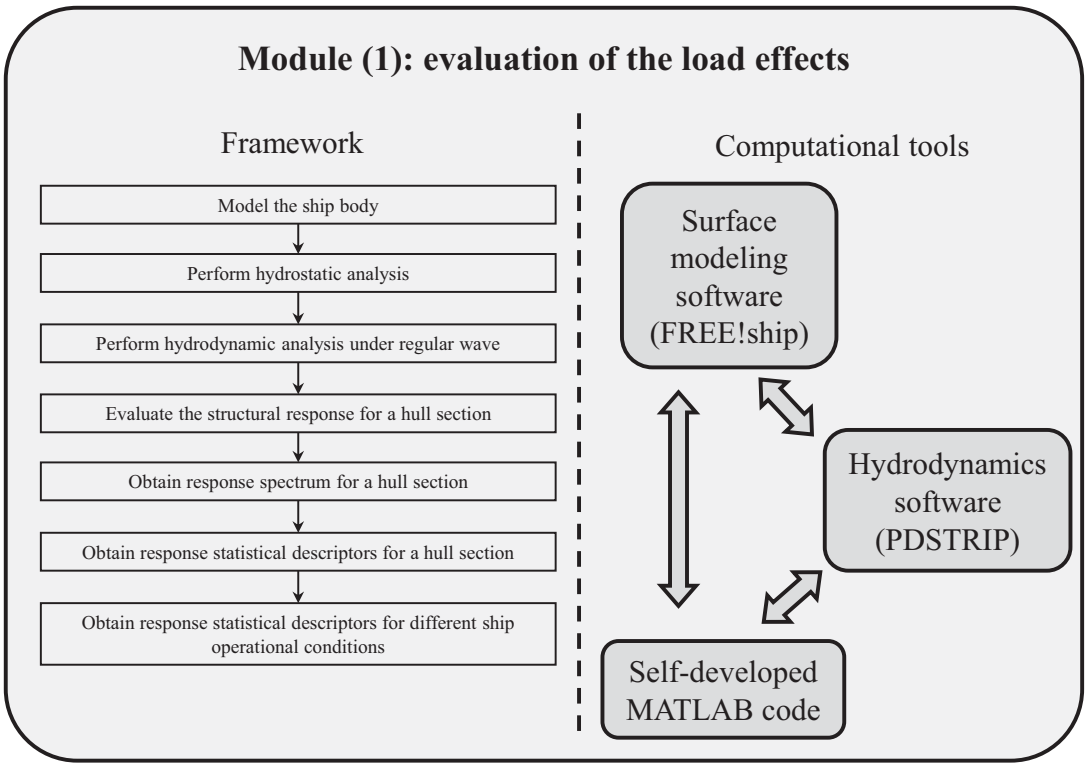

Figure B.2 Module (1) evaluates the loads effects on the hull.

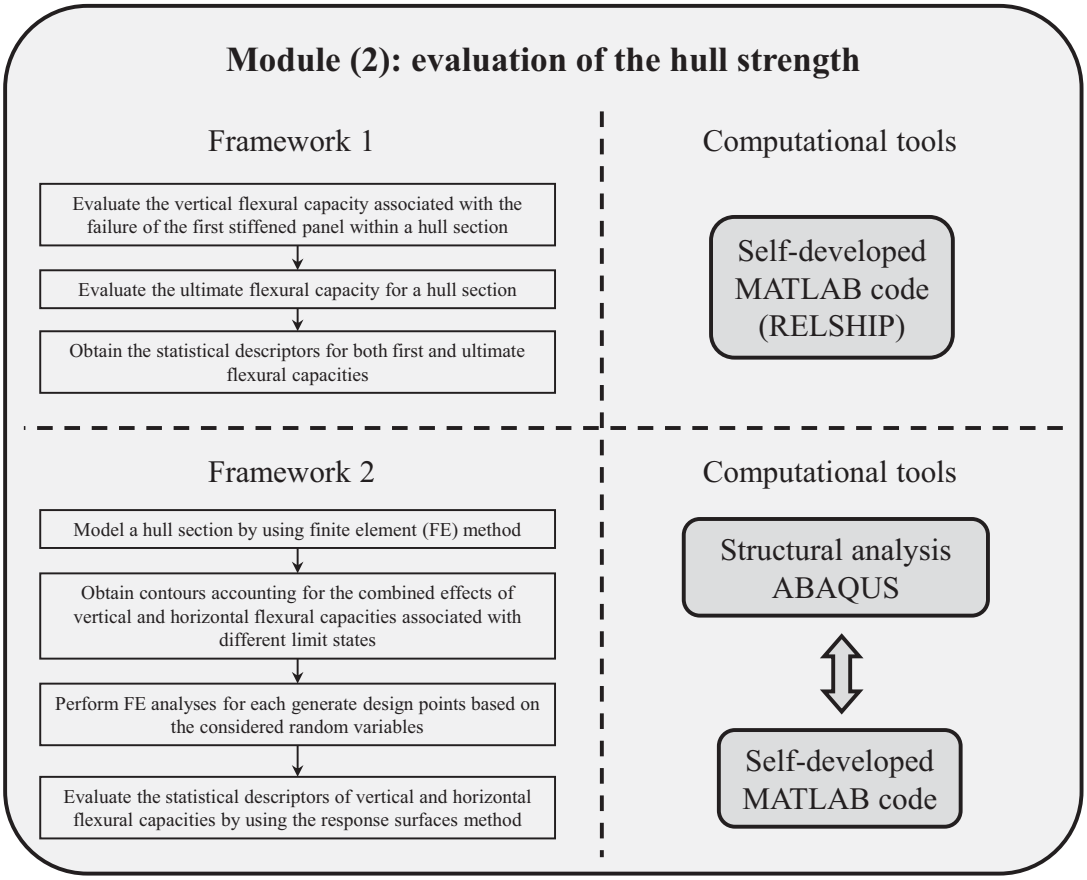

Figure B.3 Module (2) assesses and predicts the flexural capacity of critical ship sections.

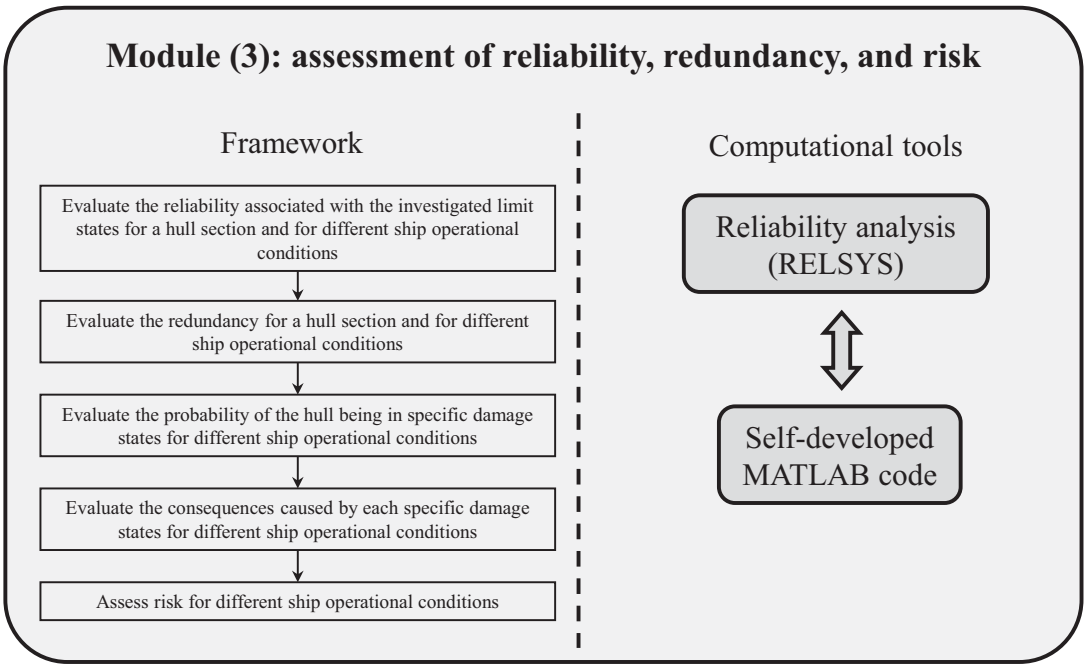

Figure B.4 Module (3) includes reliability analysis for the accounted limit states and different ship operational conditions.

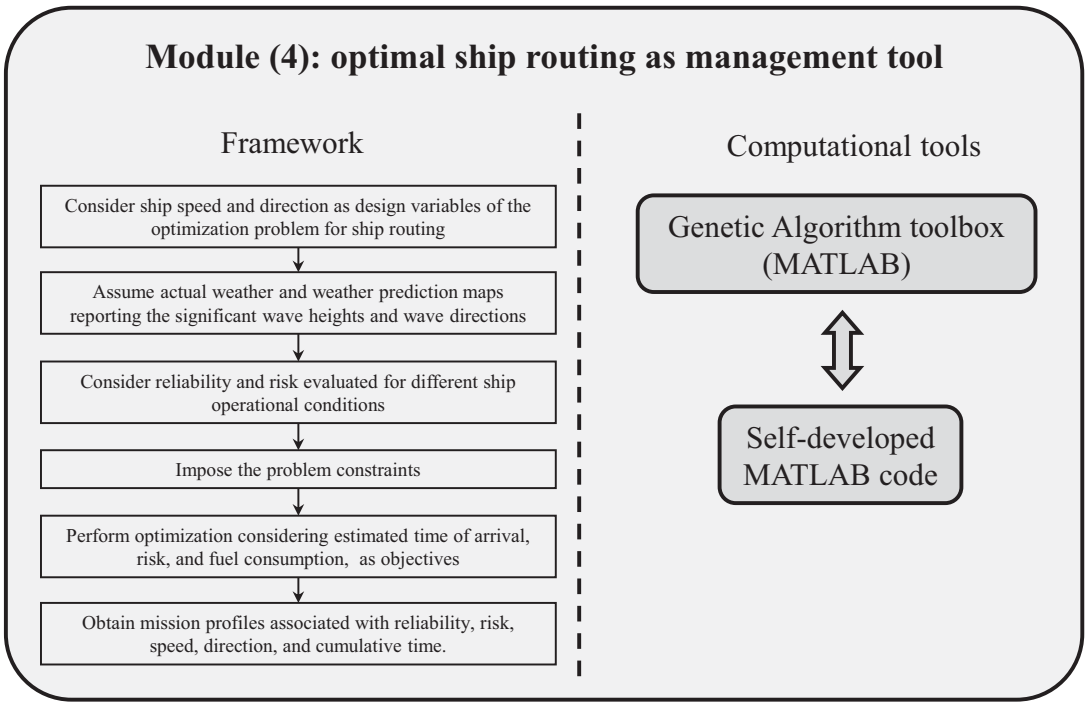

Figure B.5 Module (4) includes the approach for the optimal routing of ships.

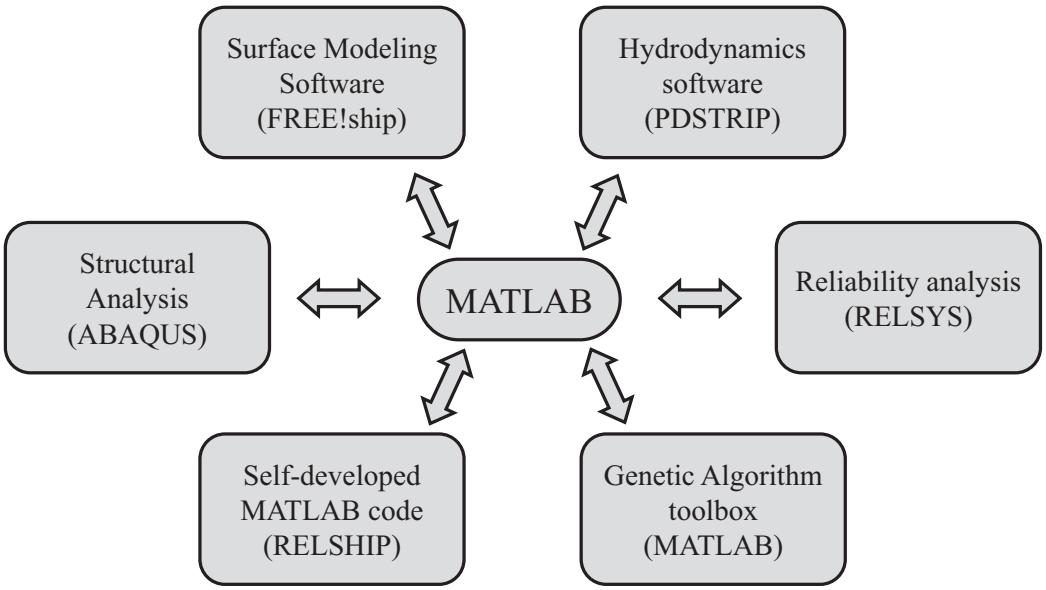

Figure B.6 Interaction between the software used within the developed framework.

APPENDIX C

LIST OF NOTATIONS

C.1 NOTATIONS OF CHAPTER 2

$A(t)$	=	average daily traffic referred to year t
A_{DS}	=	median spectral acceleration associated with the occurrence of the damage state DS
$A_s(t)$	=	time-variant top transversal tensile steel reinforcement area
B	=	parameters based on the environment aggressivity
c_{ATC}	=	average total compensation per hour
c_{AW}	=	average wage per hour
C_c	=	monetary value associated with the consequences
C_{corr}	=	corrosion coefficient
C_D	=	monetary values associated with direct consequences
c_{goods}	=	time value of the goods transported in a cargo
$C_i(t)$	=	instantaneous capacity associated with failure mode i
C_{ID}	=	monetary values associated with indirect consequences
$C_p(t)$	=	corrosion penetration
c_{Reb}	=	rebuilding cost per square meter
C_{Reb}	=	rebuilding costs
C_{Run}	=	running costs
$c_{Run,car}$	=	average costs for running cars per kilometer
$c_{Run,truck}$	=	average costs for running trucks per kilometer
C_{TL}	=	time loss costs
D	=	depth
d	=	duration of the detour

D_0 = initial top reinforcement diameter

DD = dimensionless depth ranges of the stream

D_f = depth at full flow

D_{fm} = distribution factor for moments

D_l = net length of the detour

DS = damage state

F = failure

f = full flow

$f_{ttf}(t)$ = PDF of the time-to-failure

$FV(t)$ = future monetary value referred to year t

$f_{\mathbf{X}}(\mathbf{x})$ = joint PDF of the vector of the random variables $\mathbf{X} = \{X_1,\ldots,X_j,\ldots,X_m\}$

$g_i(t)$ = instantaneous performance functions associated with failure mode i

H = hazard

$h(t)$ = hazard function

HQ = seismic event

i_{corr} = corrosion parameter

L = bridge length

M = earthquake Richter magnitude

M_{DL} = dead load applied moment

M_{LL} = live load applied moment

M_n = flexural moment capacity of the reinforced concrete deck

M_u = ultimate girder moment capacity

M_y = yielding girder moment capacity

n = number of the considered hazards

n_b = number of top transversal steel bars

N_C = epistemic uncertainty coefficient referring to the consequences

N_{FC} = epistemic uncertainty coefficient associated with the flexural moment capacities

NR_{ID}	=	normalized indirect risk index
N_S	=	epistemic uncertainty coefficient associated with the applied moments
O_{Car}	=	average vehicle occupancies for cars
O_{Truck}	=	average vehicle occupancies for trucks
$P(SS_i)$	=	probability of occurrence of the *i*-th seismic scenario
$P_{CD}(t)$	=	annual probability of structural failure associated with complete damage
P_f	=	annual failure probability
$P_{f,SC}$	=	annual failure probability due to scour
$P_{f,sys}$	=	system probability of failure
$P_{f,sys}(t)$	=	annual system failure probability
PSA	=	spectral acceleration amplitude for a period of 1 sec
PV	=	present monetary value
$P_{y,sys}(t)$	=	annual probability of exceeding the yielding limit state
Q	=	discharge
Q_{100}	=	flood discharge associated with the selected recurrence interval
Q_f	=	discharge at full flow
r	=	annual discount rate of money
R	=	risk
R_D	=	direct risk
RI	=	redundancy index
R_{ID}	=	indirect risk
RMC	=	risk modifier coefficient
s	=	sum of squared residuals
$S_i(t)$	=	instantaneous load effect associated with failure mode *i*
Sp	=	average detour speed
SS	=	seismic scenario
SV	=	scour vulnerability
T	=	average daily truck traffic percentage

t	=	time
$TDP_f(t)$	=	time-dependent failure probability
T_i	=	corrosion initiation time
TS	=	considered time span
W	=	bridge width
XY	=	latitude and longitude of the earthquake epicenter
α	=	dynamic allowance
β_c	=	normalized composite log-normal standard deviation
β_{sys}	=	system reliability index
δ	=	consequences
η_R	=	load modifier coefficient
κ	=	shape parameter of the Weibull distribution
λ	=	scale parameter of the Weibull distribution
ρ	=	radius of the considered region area
Φ	=	standard normal CDF
Φ^{-1}	=	inverse standard normal CDF

C.2 NOTATIONS OF CHAPTER 3

$A(t)$	=	average daily traffic referred to year t
$A[k]$	=	average daily traffic referred to year k
A_{DS}	=	median spectral acceleration associated with the occurrence of the damage state DS
$A_{DS}[0]$	=	original median spectral acceleration associated with the occurrence of the damage state DS
a_l and b_l	=	coefficients depending on the earthquake characteristics associated with rupture length
a_w and b_w	=	coefficients depending on the earthquake characteristics associated with rupture width
B	=	total number of bridges within the network

c_0	=	costs that do not depend on the level of damage
$C_D(t)$	=	time-dependent direct consequences
$C_{ID}(t)$	=	time-dependent indirect consequences
c_{Inj}	=	cost associated with injuries
c_{Inv}	=	inventory cost
$c_{Op,car}$	=	operating costs of cars
$c_{Op,truck}$	=	operating costs of trucks
c_{Reb}	=	rebuilding cost per square meter
c_{Reb}	=	rebuilding cost per square meter
$c_{S,car}$	=	car salvage value
$c_{S,cargo}$	=	value of the cargo
$c_{S,truck}$	=	truck salvage value
c_{TC}	=	total compensation per hour
c_{VSL}	=	value of a statistical life
c_W	=	wage per hour
D	=	directional factor
d	=	duration of the detour
D_l	=	bypass detour length
DS	=	damage state
E_{Inj}	=	factor accounting for epistemic uncertainties associated with time-injury costs
E_{LHL}	=	factor accounting for epistemic uncertainties associated with time-loss of human lives
E_{MD}	=	factor accounting for epistemic uncertainties associated with material damaged in a vehicular accident
E_{Op}	=	factor accounting for epistemic uncertainties associated with operating costs
E_{Reb}	=	factor accounting for epistemic uncertainties associated with rebuilding costs

E_{Reh} = factor accounting for epistemic uncertainties associated with rehabilitation costs

E_{TL} = factor accounting for epistemic uncertainties associated with time-loss costs

F = total traffic flow

F_C = bridge traffic flow capacity

f_{dis} = distance term

f_{flt} = style-of-faulting term

f_{hng} = hanging-wall term

f_{mag} = magnitude term

f_{sed} = deep site response term

f_{site} = shallow site response term

F_{ttf} = CDF of the time-to-failure of the superstructure

f_{ttf} = PDF of the time-to-failure of the superstructure

$FV(t)$ = future monetary value referred to year t

K_1 and K_1 = percentages of traffic associated with the portion of ADT during the peak and off-peaks hours

L = bridge length

M = earthquake Richter magnitude

M_0 = threshold magnitude value

M_p = maximum regional finite magnitude value

n_L = number of lanes carried by the bridge

O_{Car} = vehicle occupancy for cars

O_{Truck} = vehicle occupancy for trucks

$P[ND](t)$, $P[SL](t)$, $P[MOD](t)$, $P[EXT](t)$, and $P[COM](t)$ = time-dependent probabilities of no damage *ND*, slight damage *SD*, moderate *MOD*, extensive damage *EXT*, and complete damage *COM*

$P[S1|Surv](t)$, $P[S2|Surv](t)$, and $P[S3|Surv](t)$ = time-dependent of being in service states $S1$, $S2$, and $S3$ given that the bridge survives

$P_{E,S1}(t)$, $P_{E,S2}(t)$, $P_{E,S3}(t)$, and $P_{E,S4}(t)$ = time-dependent probabilities of the bridge being in service state $S1$, $S2$, $S3$, and $S4$ due to seismic hazard

PSA = response spectra accelerations

$P_{T,f}$ = annual failure probability due to traffic hazard

$P_{T,S1}(t)$, $P_{T,S2}(t)$, $P_{T,S3}(t)$, and $P_{T,S4}(t)$ = time-dependent probabilities of the bridge being in service state $S1$, $S2$, $S3$, and $S4$ due to traffic hazard

PV = present monetary value

r = annual discount rate of money

R_l = rupture length

R_{Net} = life-cycle total risk for the network

$R_{Tot}(t)$ = life-cycle total risk

R_w = rupture width

S = traveling speed

S_0 = free-flow traffic speed

t = time

T_m = marginal travel time

W = bridge width

$\hat{Y}$ = median value of the peak ground acceleration

Y_{unc} = predicted value of the median value of the peak ground acceleration accounting for epistemic uncertainties

α_{Inj} = percentage of expected injuries

α_{LHL} = percentage of expected human losses

β = distribution parameter of the truncated exponential distribution

β_c = normalized composite log-normal standard deviation

γ = aging coefficient

δ = coefficient accounting for the level of damage

$\Delta \ln \hat{Y}$ = incremental value of the median ground motion due to epistemic uncertainties

κ = shape parameter of the Weibull distribution

λ = scale parameter of the Weibull distribution

ρ = percentage of traffic increment between two available ADTs spaced 10 years apart

τ = average daily truck traffic percentage

Φ = standard normal CDF

C.3 NOTATIONS OF CHAPTER 4

$A'_l(t)$ and $A'_d(t)$ = time-dependent post-event ADTs of link and detour

A_d = detour ADT before the seismic event

A_l, and A_{tot} = link and total ADTs

A_t = average daily traffic

b = bridge

B = the total number of considered bridges

b_r = bypass cost ratio

C_b = total cumulative costs for bridge b of the network

c_c = correlation coefficient

c_{dis} = correlation coefficient associated with the relative distance between two bridges

c_{imp} = correlation coefficient associated with the importance of the carried link within the network

c_L = correlation coefficient associated with the bridge length

$C_{net,s}$ = total direct cost for the entire bridge transportation network, given network recovery scenario s

$c_{op,car}$ = operating costs of cars per kilometer

$c_{op,truck}$ = operating costs of trucks per kilometer

c_{reb} = rebuilding cost per square meter

c_{rem} = debris removal cost per square meter

c_{tc} = total compensation per hour

c_{typ}	=	correlation coefficient associated with the bridge type
c_w	=	wage per hour
D	=	directional factor
dis	=	relative distance between two bridges
D_l	=	additional travel distance
d_r	=	damage ratio
F_C	=	bridge traffic flow capacity
$F_{C,l}$ and $F_{C,d}$	=	link and detour traffic flow capacities
i	=	restoration strategy
imp	=	importance of the carried link within the network
j	=	strategy outcome
K_1 and K_1	=	percentages of traffic associated with the portion of ADT during the peak and off-peaks hours
L	=	bridge length
L_l	=	link length
n_l	=	number of lanes carried by the bridge
$n_{l,l}$ and $n_{l,d}$	=	number of lanes of link and detour
O_{car}	=	vehicle occupancy for cars
O_{truck}	=	vehicle occupancy for trucks
P_{DS}	=	probability of damage state DS
$Q(t)$	=	time-dependent functionality
Q_r	=	residual functionality
r	=	rapidity
R	=	resilience
s	=	network recovery scenario
$S'_l(t)$ and $S'_d(t)$	=	time-dependent traffic traveling speeds of link and detour after the seismic event
S_0	=	free-flow traffic speed
$S_l(t)$ and $S_d(t)$	=	time-dependent traffic traveling speeds of link and detour before the seismic event

t	=	time
t_0	=	time at which the seismic event occurs
t_h	=	investigated time horizon
t_r	=	time at which the recovery process ends
$TTD(t)$	=	time-dependent total travel distance of the users within the network
$TTT(t)$	=	time-dependent total travel time of the users within the network
typ	=	bridge type
V_c	=	velocity coefficients for costs
V_t	=	velocity coefficients for duration
W	=	bridge width
α_j, β_j, and γ_j	=	coefficients
γ_D	=	relative weight of importance associated with the travel distance
γ_{dis}	=	relative weight of importance associated with the relative distance between two bridges
γ_{imp}	=	relative weight of importance associated with the importance of the carried link within the network
γ_L	=	relative weight of importance associated with the bridge length
γ_T	=	relative weight of importance associated with the travel time
γ_{typ}	=	relative weight of importance associated with the bridge type
δ_i	=	idle time interval
δ_r	=	recovery duration
δ_r'	=	updated recovery duration
ρ_{Qr}	=	correlation coefficient of the residual functionality
$\rho_{\delta i}$	=	correlation coefficient of the idle time
$\rho_{\delta r}$	=	correlation coefficient of the recovery duration
τ	=	average daily truck traffic percentage
$\Gamma(t)$	=	time-dependent network performance
Γ^0	=	network performance in the cases in which all the bridges are out of service

Γ^{100} = network performance in the cases in which all the bridges are in service

C.4 NOTATIONS OF CHAPTER 5

a = acceleration component of the undisturbed wave field

A = added mass coefficient

A_w = wave amplitude

B = damping coefficient

b = ship breadth

b_w = web width

C = restoring coefficient

C_1 = annual corrosion rate

C_2 = corrosion constant

C_b = block coefficient

CS = ship cross-section

C_{wv} = wave coefficient

d = stiffener depth

E = elastic modulus

F = complex amplitudes of the exciting force and moment

F_D = diffraction forces

FF = first failure

F_{FK} = Froude-Kriloff forces

FFM = first failure moment

f_{sw} = factor for the variation of still water vertical bending moment along the vessel length

g = gravitational acceleration

G = performance function

H = ship heading angle

h = ship height

$H_{1/3}$	=	significant wave height
hog	=	hogging
i	=	complex unit
j	=	reference axis
k	=	matrix index
l	=	ship length
M_c	=	flexural capacity
M	=	mass matrix
m_0	=	area under the spectral density function
M_{sw}	=	still water vertical bending moment
M_w	=	wave-induced vertical bending moment
n	=	unit vectors normal to the body surface
p	=	pressure over the section contour
P_f	=	failure probability
r	=	thickness loss
RI_1 and RI_2	=	redundancy indices
S	=	ship wetted surface
s	=	variable of integration
sag	=	sagging
S_M	=	response spectrum
SS	=	sea state
S_W	=	wave spectrum
S_X	=	spectral density function of the input
S_Y	=	spectral density function of the output
t	=	time
t_0	=	corrosion initiation time
T_1	=	wave mean period
t_f	=	flange thickness
t_p	=	plating thickness
t_w	=	web thickness

U	=	forward ship speed
UF	=	ultimate failure
UFM	=	ultimate failure moment
X	=	input
x_R	=	model uncertainty associated with the resistance determination
x_{sw}	=	model uncertainty associated with the still water bending moment prediction
x_w	=	model uncertainty associated with the wave-induced bending moment prediction
Y	=	output
α	=	mode of the Rayleigh distribution
β	=	reliability index
$\ddot{\eta}$	=	acceleration of the rigid body
$\dot{\eta}$	=	velocity of the rigid body
η	=	displacement of the rigid body
κ	=	curvature
μ	=	mean value
σ	=	standard deviation
σ_{Yp}	=	plating yielding stresses
σ_{Ys}	=	stiffener yielding stresses
Φ	=	transfer function
Φ^{-1}	=	inverse standard normal CDF
ω	=	circular frequency
ω_e	=	circular encounter frequency

C.5 NOTATIONS OF CHAPTERS 6 AND 7

b	=	ship breadth
$c_{1,LSi}$ and $c_{2,LSi}$	=	parameters of the contour limit state equation
C_b	=	ship block coefficient

C_{Con}	=	construction costs
$C_{D,si}$	=	total direct cost
CF	=	complexity factor
$C_{fat,Si}$	=	losses due to fatalities associated with specific states *Si*
c_{fuel}	=	fuel cost per liter
C_{fuel}	=	fuel cost rate
$C_{ID,si}$	=	total indirect cost
$C_{inj,Si}$	=	losses due to injuries associated with specific states *Si*
C_{Reh}	=	rehabilitation costs
C_{Si}	=	total consequences associated with specific states *Si*
$C_{tot,fuel}$	=	total fuel costs
c_{VSL}	=	value of a statistical life
$DISPL$	=	ship full load displacement
d_r	=	damage ratio
ETA	=	estimated time of arrival
$f(t,\mathbf{X})$	=	joint PDF of the considered random variables $\mathbf{X} = x_1, x_2,\ldots,x_k$ at a given time t
$f'(\theta)$	=	prior distribution of the parameter θ
$f''(\theta)$	=	posterior distribution of the parameter θ
f_{Si}	=	percentage of fatalities associated with specific states *Si*
$f_X(x_j\|\theta)$	=	PDF of the random variable X evaluated with the SHM data value x
$G_{LSi,SE,U,H}(t)$	=	time-dependent performance function associated with a *LSi* and for different operational conditions
H	=	ship heading angle
h	=	ship height
Hs	=	significant wave height
i	=	complex unit
k	=	travel segment index
k_n	=	normalizing constant

k_1, k_2, k_3, and k_4	=	coefficients for fuel estimation
k_D	=	correlation factor between wave-induced and dynamic bending moments
k_W	=	correlation factor for the wave-induced bending moment
l	=	total number of random variables
$L(\theta)$	=	likelihood function
LBP	=	length between the perpendiculars of the ship
LS	=	limit states
$m_{0,Hs,U,H}$	=	zero-*th* moment of the associated response spectrum for a given set of Hs, U, and H
M_h	=	horizontal bending moment due to sea load effects
$M_{h,LSi}$	=	horizontal flexural capacity associated with a specific limit state LSi
$M_{high,Hs,U,H}$	=	high-frequency VBM
$M_{low,Hs,U,H}$	=	updated low-frequency VBM
M_{sw}	=	still water bending moment
M_v	=	vertical bending moment due to sea load effects
$M_{v,LSi}$	=	vertical flexural capacity associated with a specific limit state LSi
M_{WH}	=	whipping bending moment
$M_{wh,Hs,U,H}$	=	horizontal wave-induced bending moment
$M_{wv,Hs,U,H}$	=	vertical wave-induced bending moment
N	=	number of segments
O	=	ship occupancy
$p(t)$	=	excitation function
$P(\omega)$	=	Fourier transform
$P[Hs,U,H]$	=	occurrence probability of encountering determinate sea states under different operational parameters
$P_{LSi,Hs,U,H}(t)$	=	time-dependent exceedance probability associated with a LSi and for different operational conditions

$P_{Si,Hs,U,H}(t)$	=	time-dependent probabilities of the hull being in a specific state *Si* for different operational conditions
$R(t)$	=	time-dependent risk
$R_{,Hs,U,H}(t)$	=	time-dependent total risk for a given set of *Hs*, *U*, and *H*
$r'_{fuel,Hs}$	=	design fuel consumption rate for a specific sea state
$R_{D,Hs,H}(t)$	=	time-dependent direct risk for a given set of *Hs*, *U*, and *H*
Re	=	real part of the complex quantity
r_{inj}	=	the ratio of costs due to injuries and fatalities
$R_{k,Hs,U,H}$	=	total risk associated with the *k*-th route segment
R_{mean}	=	mean total risk
RS	=	response
$R_{threshold}$	=	maximum thresholds of the total risk
S	=	state
SF	=	size factor
STF	=	ship type factor
$S_W(\omega)$	=	sea spectrum
t	=	time
T_k	=	time necessary for the ship to cover the *k*-th route segment
U	=	ship speed
U'	=	design speed
U_{max}	=	maximum allowable ship speed
U_{min}	=	minimum allowable ship speed
WGT_{100}	=	weight of the SWBS 100
x_i and x_j	=	random variables
x_R	=	parameters accounting for the model uncertainties associated with the resistance determination
x_{sw}	=	parameters accounting for the model uncertainties associated with still water bending moment prediction
x_w	=	parameters accounting for the model uncertainties associated with wave-induced bending moment prediction

y	=	ordinate
y_{min} and y_{max}	=	bounds of y coordinate
α	=	mode of the Rayleigh distribution (hyperparameter)
α_0, α_i, α_{ij}, and α_{ii}	=	polynomial coefficients
$\beta_{k,LS4,Hs,U,H}$	=	reliability index of *LS*4 associated with the *k*-th route segment
$\beta_{LSi,Se,U,H}(t)$	=	time-dependent reliability index associated with a *LSi* and for different operational conditions
$\beta_{threshold}$	=	minimum thresholds of the reliability index
δ	=	parameter of the contour limit state equation
$\delta(t,\mathbf{X})$	=	consequences
θ	=	parameter
$\lambda_{Hs,U,H}$	=	mean of VBM for a combination of *Hs*, *U*, and *H*
σ_{HBM}	=	standard deviation of HBM
σ_{VBM}	=	standard deviation of VBM
$\Phi^*_{HBM}(\omega)$	=	complex conjugate of the transfer function of HBM
$\Phi_{VBM}(\omega)$	=	transfer function of VBM
ω	=	frequency

C.6 NOTATIONS OF APPENDIX A

C	=	capacity
D	=	demand
$\mathbf{F}$	=	failure domain
$F(t)$	=	CDF of the time-to-failure
$f(t)$	=	PDF of the time-to-failure
$f'(\theta)$	=	prior distribution of the parameter θ
$f''(\theta)$	=	posterior distribution of the parameter θ
$F_j^{-1}(\cdot)$	=	inverse CDF
$F_s(t)$	=	CDF of the time-to-failure of the system
$F_{wc}(t)$	=	CDF of the time-to-failure of the weakest component

$f_{\mathbf{X}}(\mathbf{x})$	=	joint PDF of the random variables
$f_X(x_j\|\theta)$	=	PDF of the random variable X evaluated with the SHM data value x
$g(\mathbf{X})$	=	performance function including the vector of the random variables $\mathbf{X} \equiv \{X_1, X_2, \ldots, X_n\}$
$h(t)$	=	hazard function
k	=	failure modes and/or multiple components
K	=	number of random variables
k_n	=	normalizing constant
$L(\theta)$	=	likelihood function
$L_{damaged}$	=	load carrying capacity of the damaged structure
L_{design}	=	design load
L_{intact}	=	load carrying capacity of the intact structure
M	=	safety mrgin
N	=	number of samples
$P_{f(sys)}(t)$	=	time-dependent probability associated with the system failure
$P_{y(sys)}(t)$	=	time-dependent probability associated with the occurrence of first yielding
Q	=	number of parallel subsystems with N_i components
$Q(t)$	=	time-dependent functionality
R	=	risk
Res	=	resilience
$S(t)$	=	survivor function
t	=	time
t_0	=	time at which the extreme event occurs
t_h	=	investigated time horizon
β	=	reliability index
$\beta_{f(sys)}(t)$	=	time-dependent reliability index with respect to the occurrence of first yielding
$\beta_{y(sys)}(t)$	=	time-dependent reliability index with respect to system failure

θ	=	parameter
μ_C	=	mean values of the capacity
μ_D	=	mean values of the demand
μ_M	=	mean values of the safety margin
σ_C	=	standard deviation of the capacity
σ_D	=	standard deviation of the demand
σ_M	=	standard deviation of the safety margin
Φ^{-1}	=	inverse standard normal CDF
$\mathbf{\Omega}$	=	failure domain of series or parallel systems

VITA

Alberto Decò was born in Casalmaggiore, Italy, to Amedeo Decò and Daniela Zanella.

In October 2005, he earned his Degree in Civil Engineering (equivalent to Bachelor + Master of Science) from the University of Bologna, Bologna, Italy. In 2005, he was awarded with a Scholarship for conducting research towards the development of the Graduation Thesis abroad. From February to August 2005, he visited the University of Colorado, Boulder CO, and conducted research under the supervision of Prof. Dan M. Frangopol, developing most of his Graduation Thesis. In the August of 2008, his started his Ph.D. program at Lehigh University, Bethlehem PA, working under the supervision of Prof. Dan M. Frangopol.

Prior to join Lehigh University, he worked as Structural Engineer with CAIREPRO, society of Architects and Civil Engineers, Reggio Emilia, Italy and with SAIPEM (ENI), Milan, Italy.

From February 2006, he is also a licensed Civil Engineer in Italy (District of Mantua), and in October 2011, he earned the Fundamental Engineering (FE) Certification in the USA.